THEORETICAL STUDIES OF HIGH-POWER ULTRAVIOLET AND INFRARED MATERIALS

M. Sparks, et al

Xonics, Incorporated

Prepared for:

Defense Supply Service
Defense Advanced Research Projects Agency

30 June 1975

Unclassified

SECURITY CLASSIFICATION OF THIS PAGE (When Data Entered)

REPORT DOCUMENTATION PAGE		READ INSTRUCTIONS BEFORE COMPLETING FORM
1. REPORT NUMBER	2. GOVT ACCESSION NO.	3. RECIPIENT'S CATALOG NUMBER
4. TITLE (and Subtitle) THEORETICAL STUDIES OF HIGH-POWER ULTRAVIOLET AND INFRARED MATERIALS		5. TYPE OF REPORT & PERIOD COVERED Fifth Technical Report, 6 Dec. 1974 through 30 June 1975 6. PERFORMING ORG. REPORT NUMBER
7. AUTHOR(s) M. Sparks and C. J. Duthler		8. CONTRACT OR GRANT NUMBER(s) DAHC15-73-C-0127
9. PERFORMING ORGANIZATION NAME AND ADDRESS Xonics, Incorporated 6849 Hayvenhurst Avenue Van Nuys, California 91406		10. PROGRAM ELEMENT, PROJECT, TASK AREA & WORK UNIT NUMBERS
11. CONTROLLING OFFICE NAME AND ADDRESS Defense Supply Service Room 1D245 - The Pentagon Washington, D.C. 20310		12. REPORT DATE 30 June 1975 13. NUMBER OF PAGES 253
14. MONITORING AGENCY NAME & ADDRESS (if different from Controlling Office) Defense Advanced Research Projects Agency 1400 Wilson Boulevard Arlington, Virginia 22209		15. SECURITY CLASS. (of this report) Unclassified 15a. DECLASSIFICATION DOWNGRADING SCHEDULE

16. DISTRIBUTION STATEMENT (of this Report)

This document may be further distributed only with specific prior approval of the Defense Supply Service, Washington, D.C.

17. DISTRIBUTION STATEMENT (of the abstract entered in Block 20, if different from Report)

18. SUPPLEMENTARY NOTES

Research sponsored by Defense Advanced Research Projects Agency under ARPA Order No. 1969, No. 7, Program Code 6D10

19. KEY WORDS (Continue on reverse side if necessary and identify by block number)

ultraviolet absorption, laser damage, nonlinear index of refraction, optical properties, infrared absorption, laser materials, enhanced stimulated Raman scattering, theory, electron avalanche, two-photon absorption, optical distortion

20. ABSTRACT (Continue on reverse side if necessary and identify by block number)

(1) It is shown that current theories of electron-avalanche breakdown suffer such difficulties as: Theoretical values of the ionization frequencies are too small, by tens of orders of magnitude in some cases, to explain experimental damage results even when the large conduction-electron densities below are assumed. The explanation for the disagreement of the experimental frequency dependence of the breakdown electric field E_B with the predicted dependence $E_B \sim (1 + \omega^2\tau^2)^{1/2}$ as an anomalously small value of the electron relaxation time τ is inconsistent with the value of τ required to

DD FORM 1 JAN 73 1473 EDITION OF 1 NOV 65 IS OBSOLETE

Unclassified

SECURITY CLASSIFICATION OF THIS PAGE (When Data Entered)

explain the magnitude of E_B, with the calculated value of τ, and with experiments. The temperature dependence of E_B is incorrect. Assumed electron densities of 10^8-10^{10} cm^{-3} required to initiate the avalanche conflict with photoconductivity measurements, and electronic-conductivity estimates give $< 10^{-6}$ probability of avalanche initiation. The theories are not predictive. These serious difficulties are removed by a theory in which starting electrons are generated by thermal and tunnel emission from the cathode (in dc experiments) and from imperfections, field-induced emission from imperfections, including multiphoton ionization, and multiphoton excitation from the valence band. Mechanisms for initiating and sustaining the avalanche include the Holstein photon-electron-phonon interaction, inter-conduction-band transitions, and at dc, Seitz lucky-electron excitation over a barrier plus a self-sustaining mechanism. Preliminary results with no adjusted parameters agree well with pulse-length and frequency experiments. (2) Calculated failure intensities for vuv xenon-laser window materials are 60 MW/cm^2 (impurity) to 0.14 GW/cm^2 (intrinsic) for electron-plasma defocusing, 0.74 GW/cm^2 for fracture, 1.6 GW/cm^2 for melting, and 2 GW/cm^2 (or 0.15 GW/cm^2) for preself-focusing (i.e., nonlinear refractive index n_2) with a normal resonance enhancement (or anomalously large enhancement for special conditions). Joule heating by the generated conduction electrons, which is greater than the direct heating by the absorption process, and electron-avalanche multiplication of the conduction electrons were included. Electron-plasma-induced optical distortion is greater than thermally induced optical distortion. Two heating processes involving F centers are shown to be potentially important at other frequencies. In the n_2 optical distortion, which occurs at powers below the threshold for self focusing beam collapse, the enhancement results from the resonances in the electronic oscillators. (3) A scheme of obtaining a set of tight-binding electronic wave functions is presented and applied to the problems of calculating the large corrections to the Hartree-Fock band structure of alkali halides and of calculating the surface electronic states in the gap. (4) At the measured impurity absorption (0.15 cm^{-1}), electron-plasma defocusing can possibly give rise to the lowest failure threshold (60 MW/cm^2) calculated to date. Excitation of valence electrons into gap states associated with dislocations is shown to be a candidate impurity-absorption mechanism. (5) An experimental infrared absorption peak at the sum of three optical-phonon frequencies in several alkali halides is explained by a theory that also simplifies reliable multiphonon absorption calculations. (6) Well known difficulties with commutation relations and noise sources in damped quantum systems are resolved for the case of enhanced stimulated Raman scattering.

TABLE OF CONTENTS

TABLE OF CONTENTS (Cont'd)

TABLE OF CONTENTS (Cont'd)

LIST OF ILLUSTRATIONS

LIST OF ILLUSTRATIONS (Cont'd)

PREFACE

This Fifth Technical Report describes the work performed on Contract Number DAHC15-73-C-0127 on Theoretical Studies of High-Power Ultraviolet and Infrared Window Materials during the period from December 6, 1974 through June 30, 1975. The work on the current contract is a continuation of that of the previous Contract Number DAHC15-72-C-0129.

The following investigators contributed to this report:

Dr. C. J. Duthler, principal research scientist

Dr. T. D. Holstein, consultant, University of California, Los Angeles

Dr. A. A. Maradudin, consultant, University of California, Irvine, California

Dr. D. L. Mills, consultant, University of California, Irvine, California

Dr. L. J. Sham, consultant, University of California, San Diego, California

Dr. M. Sparks, principal investigator.

Previously reported results are not repeated in the present report, with the exception of Sec. H, Enhanced Stimulated Raman Scattering and General Three-Boson Parametric Instabilities, which is expanded from a previous version to include effects of damping and relaxation to thermal equilibrium, and their effects on the commutation relations in the quantum treatment.

A. INTRODUCTION AND SUMMARY

This report includes the new results of ongoing theoretical studies of mechanisms by which dielectric solids fail as a result of the coupling to high-intensity ultraviolet and infrared radiation. An investigation of electrical breakdown in dielectrics was initiated when it was discovered that current theories could not afford estimates of the values of the breakdown electric field in the ultraviolet region.

Defocusing of the optical beam by the conduction electrons generated in absorption and avalanche processes and by the nonlinear index n_2 before strong self focusing occurs are analyzed.

The lack of a satisfactory understanding of the basic optical properties of even the alkali halides continues to introduce uncertainties in a number of areas under investigation. Some early results of a program to obtain the needed information are described.

Vestiges of the problems of enhanced stimulated Raman scattering and infrared multiphonon absorption are included in the present report. Results of these studies are as follows:

Theory of Electrical Breakdown in Dielectrics. Evidence is presented that current theories of electron-avalanche breakdown in dielectrics are inadequate to explain existing data or to be predictive, and a theory with encouraging preliminary results is presented. The motivation for the study of electron-avalanche breakdown was an attempt to predict the magnitude of the breakdown electric field E_B and its temperature and frequency dependence and to predict whether the effect

would be intrinsic or extrinsic, all in the vacuum ultraviolet region. It was found that current theories could not afford this information, and that these theories suffer from serious difficulties.

At least part of an apparent disagreement in the literature and among investigators in the field as to how good the current theories are, stems from what is expected of the theory. If the goal of the theory is to explain the magnitude of the breakdown field E_B within an order of magnitude or so, then any one of many theories that have been proposed will suffice. This is in fact to be expected since small changes in the value of the electric field give rise to large changes in the values of the physical quantities of interest, such as the ionization frequency. The electric field E appears in an exponent in most theories, and even a factor-of-two change in E can change the probability for damage by tens of orders of magnitude in some cases. This situation is analogous to the fact that the value of the temperature must be known more accurately than within a factor of ten in most cases, as in thermal emission over a barrier or in the human body, where a one percent change is large and a factor of two is intolerable.

If, on the other hand, the goal of the theory is to explain the magnitude of avalanche ionization frequency ω_c in the expression for the conduction-electron density, $n_c = n_{c0} \exp(\omega_c t)$, to within an order of magnitude at the observed value of E_B or to explain the dependence of E_B on the laser frequency ω, temperature T, laser-pulse duration t_p, or material parameters, or to be predictive, then current theories are inadequate. The problem is more serious than simply an inability to calculate the values of ω_c or E_B to within some required accuracy, as it was found in our early attempts to understand the existing

experimental data that even in being overly generous with the values of all parameters, current theories still failed. If a theory cannot explain the experimental results to within the estimated errors of the experimental and theoretical results, the theory will be considered as unsatisfactory. A factor of three to ten difference in E_B simply is not sufficient.

Specific difficulties with current theories of electron-avalanche breakdown include the following: (1) Ionization rates obtained from dc and laser measurements are not explained by the theories. Even with the large number of initial conduction electrons discussed in (4) below, the theoretical ionization rates are too small, by tens of orders of magnitude in some cases, to explain the damage results. (2) The increase in the value of E_B from the first 10.6 μm laser experiment over the dc value was attributed to the predicted frequency dependence $E_B \sim (1 + \omega^2\tau^2)^{1/2}$, where τ is the electron relaxation time. It was then surprising that there was little additional increase in E_B first at 1.06 μm, then at 0.694 μm. The explanation that no additional frequency dependence was observed as a result of τ having an anomalously small value τ_s for some unknown reason leaves the difference between the dc and 10.6 μm results unexplained. What is more serious, with the value of τ required to explain the magnitude of E_B, there should be a large frequency dependence according to the relation $E_B \sim (1+ \omega^2\tau^2)^{1/2}$. Finally, calculated values of τ are two orders of magnitude greater than τ_s.

(3) The temperature dependence of E_B is incorrect. (4) The assumed value of the electron density $n_c = 10^8 - 10^{10}\,cm^{-3}$ required to initiate the avalanche is unreasonably large. Such high densities are in conflict with results of photoconductivity measurements. Bounds on n_c set by estimates of the value of the

electronic conductivity indicate that the probability of finding an electron in the focal volume during the pulse is less than 10^{-6}, possibly much less, in some cases.

Preliminary results of a new theory of electrical breakdown in dielectrics agree well in magnitude and shape with experimental results for the pulse-length dependence and frequency dependence of the breakdown electric field with no adjusted parameters. The difficulties of the previous theories are removed by the present theory, which includes mechanisms for generating starting electrons and for initiating and sustaining an avalanche. Mechanisms of generating the starting electrons include thermal and tunnel emission from the cathode (in dc experiments) and from imperfections, field-induced emission from imperfections, including multiphoton ionization, and multiphoton excitation from the valence band. Mechanisms for initiating and sustaining the avalanche include the Holstein photon-electron-phonon interaction, inter-conduction-band transitions, and at dc, the Seitz lucky-electron process with free acceleration at high electron energy plus a self-sustaining mechanism. Although the preliminary results are encouraging, results of additional work in progress are needed to determine the validity of the theory.

VUV Window Failure by Multiphoton Absorption and Electron Defocusing, Avalanche, and Absorption. Rough estimates of the values of the intrinsic intensity limits at which a window material fails at the xenon-laser frequency are 0.14 GW/cm^2 for electron-plasma defocusing, 0.74 GW/cm^2 for fracture, and 1.6 GW/cm^2 for melting. A potentially lower value of 60 MW/cm^2 from impurity absorption and subsequent electron-plasma defocusing may not be applicable if

the quantum efficiency for generating conduction electrons is low or if the impurity absorption saturates. The Joule heating by the conduction electrons that are generated by the two-photon-absorption and the electron-avalanche processes is greater than the direct heating by the two-photon-absorption process. Electron-plasma-induced optical distortion by these conduction electrons is greater than thermally induced optical distortion for the cases considered, in which approximately one conduction electron is generated for every photon absorbed. Electron-avalanche multiplication increases the conduction-electron density above the two-photon value, the effect being greater at higher intensities. Ordinary F-center absorption and a new F-center heating process are shown to be negligible here, but important at other frequencies and at higher F-center concentrations.

Precollapse Self Focusing. Self focusing is known to be a major factor that limits the power that can be transmitted through a transparent optical element. The optical distortion that occurs at power levels below the value at which the beam collapses to a small self-focused spot can limit the effectiveness of a system. Changes in the refractive index $\delta n = n_2 E^2$ result in optical distortion for the usual case in which E^2 is not constant across the profile of the beam. Using the figure-of-merit type failure criterion of $\lambda / 8$ optical distortion, the failure intensity for a typical value of the nonlinear index $n_2 = 10^{-13}$ esu is $I_f \cong 7.5$ GW/cm^2. A resonance enhancement of n_2 should reduce the threshold to $I_f \cong 2.5$ GW/cm^2 in lithium fluoride at $\hbar\omega = 7.21$ eV, which is slightly greater than one half the electronic band gap E_g. It is estimated that precollapse self focusing will be negligible with respect to electron-plasma defocusing as a

failure mechanism in LiF at 7.2 eV. However, there are two cases where optical distortion from the nonlinear index may be dominant. At higher frequencies near E_g in LiF, the nonlinear index may become large and negative (that is, defocusing). Other materials may have strong, sharp two-photon-absorption bands which may yield a considerably enhanced nonlinear index in the vicinity of these bands. The remote possibility of avoiding self focusing by operating at the frequency at which n_2 changes sign appears to exist, but has not been considered carefully.

Fundamental Optical Properties of Alkali Halides. It is surprising that there is a lack of understanding of even the most fundamental optical properties of the alkali halides, which are perhaps the simplest of all materials. There is even recent debate on the origin of the fundamental absorption edge, with some investigators believing that it is excitonic and others believing that it is direct-gap absorption. Theoretical values of the band gap are calculated to within a small fraction of an electron volt in involved numerical calculations, then approximate corrections of several electron volts are added to account for electronic polarization effects. There still is discussion on whether extreme tight binding or nearly free electron behavior is more appropriate for the conduction band. Such problems, which will be discussed when the current status of theory is considered in detail in a subsequent report, hinder a number of other studies including multiphoton absorption, the self-focusing enhancement, the Holstein photon-electron-phonon process, inter-conduction-band transitions, and other aspects of electrical breakdown in insulators. Very early results related to a program to understand the optical properties are included. To perform the theoretical quantitative calculations of the properties under study, one requires knowledge not only of the electronic energy bands, but also the Bloch functions associated

with the bands. An interpolation scheme based on a set of tight-binding wave functions is used. The scheme reproduces the band structure calculated by the Hartree-Fock method and provides wave functions that are simple to generate and to apply to the variety of theoretical studies already mentioned.

These wave functions are being used in a scheme of calculating the corrections to the Hartree-Fock band structure. This is an important problem since sophisticated Hartree-Fock schemes are in very poor agreement with experiment, to the point where it is argued that there are corrections to the Hartree-Fock band gap from electron-correlation effects that amount to ~ 30 percent of the band gap. With such serious questions regarding the magnitude and even the source of the absorption edge besieging the current theoretical picture, there is little hope of proceeding further until these problems are resolved.

The wave functions are also being used in a study of surface electronic states in the gap. It is anticipated that the wave functions, or perhaps suitably improved ones, will be used in the other studies, as already mentioned. Additional optical studies underway, which concern local field corrections, values of various matrix elements, exchange effects, and impurity states, will be discussed in subsequent reports.

Impurity Absorption. The impurity-absorption study has been somewhat low on the priority list, but deserves further investigation directed toward studies of optical effects of impurity absorption and determining the source of the large extrinsic absorption of order 10^{-1} to $10\,cm^{-1}$ in the ultraviolet region. Estimates discussed above indicate that electron-plasma defocusing by the electrons generated by linear absorption by imperfections could give rise to the lowest failure

threshold, I_f = 60 MW/cm^2, compared to the two-photon threshold of 140 MW/cm^2. This result would require the generation of approximately one conduction electron for each photon absorbed and would require that the absorption not saturate. Both conditions are possible, but not certain, the probability for such a low threshold being somewhat less than 50 percent. This process, being extrinsic, can in principal be removed. The possibility of two-photon creation of defects that in turn absorb linearly may cause a further limitation of vuv materials.

An impurity-absorption mechanism in which valence electrons are excited into electronic states associated with dislocations is shown to be a candidate for explaining the large observed impurity absorption.

Theory of Multiphonon Absorption. An extension of the Sparks and Sham theory of multiphonon absorption has simplified the first principles calculation of the absorption coefficient from the phonon spectrum in alkali-halide crystals. In addition to making the calculations simpler, new physical effects are predicted.

Recent experiments by J. A. Harrington and M. Hass show a well-defined peak in the low-temperature, infrared absorption coefficient at a frequency corresponding to the sum of three optical phonons. This peak is most pronounced in alkali-halide crystals such as KrBr and NaI which have a frequency gap in their phonon spectra. An n-phonon quasiselection rule (transition matrix elements small, but not zero), similar to the previous two-phonon quasiselection rule derived by Duthler and Sparks, is obtained by an extension of the Sparks and Sham theory of multiphonon absorption. The n-phonon quasiselection rule states that the fundamental, reststrahl phonon, created by the absorption of an infrared photon, splits more strongly into final states having an odd number of optical phonons than into

final states having an even number of optical phonons. This rule is expected to be valid for absorption by the higher-order dipole moment mechanism as well as for the explicitly considered anharmonic lattice process. The further realization that the matrix elements for decay of the fundamental, reststrahl phonon depend primarily on the branches of the final-state phonons with dependence on the phonon wave vectors being weak, greatly simplifies the calculation of the absorption coefficient from the phonon spectrum. With this approximation, the absorption coefficient is calculated using an average, branch-dependent matrix element and a multiphonon density of states in which the phonon branches are kept distinct.

Enhanced Stimulated Raman Scattering. In previous reports it was shown that there was a parametric instability in the Raman scattering process that explained previously anomalous results and had important practical consequences. It was also shown that the previous theories had missed the instability by either neglecting the increase in the vibrational amplitudes above their thermal equilibrium values or linearizing the mode-amplitude equations by a scheme that precluded the instability. In our treatments, damping and relaxation to thermal equilibrium were introduced formally. There are well known difficulties, such as non-satisfied commutation relations, that result from these procedures. As stated in the previous treatments, these difficulties were not believed to be serious. A treatment of these problems in the present report supports this view. By enlarging the system to include the modes responsible for the damping (for a simple two-Boson damping mechanism), the problems are avoided and the meaning of the previous results becomes clearer.

B. CURRENT STATUS OF ELECTRON-AVALANCHE-BREAKDOWN THEORIES

M. Sparks
Xonics, Incorporated, Van Nuys, California 91406

It is argued that current theories of electron-avalanche breakdown in dielectrics are inadequate to explain existing data or to be predictive. Specific difficulties include the following: (1) The theoretical values of the ionization frequencies are too small, by tens of orders of magnitude in some cases, to explain the experimental damage results even when the large initial conduction electron densities in (4) below are assumed. (2) The theoretical result for the frequency dependence of the breakdown electric field $E_B \sim (1 + \omega^2 \tau^2)^{1/2}$ disagrees with experimental results. The explanation in terms of an anomalously small electron relaxation frequency is inconsistent with the value of τ required to explain the magnitude of E_B, with calculated values of τ (by two orders of magnitude), and with the difference between the dc and 10.6 μm experimental values of E_B. (3) The temperature dependence of E_B is incorrect. (4) The assumed value of the electron density $n_c = 10^8 - 10^{10}$ cm^{-3} required to initiate the avalanche is in conflict with results of photoconductivity measurements. Bounds on n_c set by estimates of the value of the electronic conductivity indicate that the probability of finding an electron in the focal volume during the pulse is less than 10^{-6}, possibly much less, in some cases.

I. INTRODUCTION

The motivation for the study of electron-avalanche breakdown was an attempt to predict the magnitude of the breakdown electric field E_B and its temperature and frequency dependence and to predict whether the effect would be intrinsic or extrinsic, all in the vacuum-ultraviolet region. It was found that current theories could not afford this information. The rather serious problems with current theories are discussed in the present section. In the following section, a tentative theory of avalanche breakdown that appears to alleviate these difficulties is presented. In Sec. D, high-field breakdown in the vacuum-ultraviolet region is discussed. In the vuv region, a broader view than electron-avalanche breakdown must be taken.

The practical importance of breakdown in limiting the performance of material in numerous applications and fundamental interest in the subject have stimulated enormous interest in electrical breakdown in dielectrics. The laser studies of avalanche breakdown in the last five years have supplied invaluable new experimental data. No attempt is made to review the literature on electron-avalanche breakdown, which extends from the early studies of A. von Hippel[1] in 1931 to the present. In fact, in the first volume of Annalen der Physik in 1799, A. Van Marum[2] reported the laboratory observation of electrical breakdown in glass. There are a number of textbooks and reviews. The newer of J. J. O'Dwyer's[3] books, the reviews by N. Bloembergen[4] and N. Klein,[5] and the report by D. Fradin[6] should lead the reader into the literature.

At least part of an apparent disagreement in the literature and among investigators in the field as to how good the current theories of electrical breakdown in

solids are, stems from what is expected of the theory. If the goal of the theory is to explain the magnitude of the breakdown field E_B within an order of magnitude or so, then any one of many theories that have been proposed will suffice. This is in fact to be expected since small changes in the value of the electric field give rise to large changes in the values of the physical quantities of interest, such as the ionization frequency. The electric field appears in an exponent in most theories, and even a factor-of-two change in E can change the probability for damage by tens of orders of magnitude in some cases. For example, see Fig. 2 in Sec. III. This situation is analogous to the fact that the value of the temperature must be known more accurately than within a factor of ten in most cases, as in thermal emission over a barrier or in the human environment, where a one percent change is large, a ten percent change is intolerable, and a factor of two is exocrematory.

If, on the other hand, the goal of the theory is to explain the magnitude of avalanche ionization frequency ω_c in the expression for the conduction-electron density, $n_c = n_{c0} \exp(\omega_c t)$, to within an order of magnitude at the observed value of E or to explain the dependence of E_B on the laser frequency ω, temperature T, laser pulse duration t_p, or material parameters, or to be predictive, then current theories are inadequate. The problem is more serious than simply an inability to calculate the values of ω_c or E_B to within some required accuracy, as it was found in the early attempts to understand the existing experimental data that even in being overly generous with the values of all parameters, current theories still failed. If a theory cannot explain the experimental results to within the estimated errors of the experimental and theoretical results, the theory will be considered as unsatisfactory. A factor of three to ten difference in E_B is not sufficient.

II. THE AVALANCHE PROCESS

The simplest current explanation of electron-avalanche breakdown is as follows. In the presence of an electric field $\underset{\sim}{E}$ and electron-phonon collisions, an electron drifts in the direction of $\underset{\sim}{E}$, gaining energy $\mathcal{E}$ as it goes. The electron absorbs energy $\mathcal{E}$ from the electric field E, as illustrated schematically in Fig. 1a. The rate of energy gain from the field is given by the well known relation

$$\left(\frac{d\mathcal{E}}{dt}\right)_E = \frac{e^2 \tau_k E^2}{m(1+\omega^2 \tau_k^2)} \tag{2.1}$$

where ω is the frequency of the electric field and τ_k is the electron relaxation frequency for large-angle scattering. When the electron attains sufficient energy $\mathcal{E}_I$, it can excite another conduction across the electronic energy gap from the valence band. Repetition of this multiplication process continues to increase the number of electrons until breakdown occurs. Breakdown has been assumed to occur when this process increases the electron density n_c from an initial value of $10^8 - 10^{10}\ cm^{-3}$ to $10^{18}\ cm^{-3}$, as discussed at the end of Sec. III.

For the dc case illustrated in Fig. 1, electron-phonon collisions prevent the electron from accelerating very rapidly to high energies by changing its direction of travel every τ_k seconds on the average. If the electron were to go without suffering a collision for a long time, its energy would be increased more efficiently. Such a "lucky" event, shown at L in Fig. 1a, is discussed in Sec. VI. Small-angle collisions are less effective in inhibiting the rapid build up of energy. However, both small-angle and large-angle collisions reduce the

electron energy since phonons (having energies $\hbar\omega_q$) are excited in the scattering process. In Fig. 1, the build up of energy, impeded by the large-angle scattering and the energy loss are visualized individually in the (a) and (b) parts of the figure. In passing, notice that the electron drift velocity $v_d = \mu E$, where $\mu = e\tau_k/m$ is the mobility, is determined by the increase in the component k_z of wave vector $\underset{\sim}{k}$ in the direction of $\underset{\sim}{E}$, which is related to the curvature of the trajectory in Fig. 1a.

The rate of loss of energy to the lattice phonons is

$$(d\mathcal{E}/dt)_L = \hbar\omega_p/\tau_L \tag{2.2}$$

where $\hbar\omega_p$ is an average phonon energy and τ_L is the time constant that includes small- and large-angle scattering. The time constants τ_k and τ_L are calculated in Sec. C-VIII. Equating (2.1) and (2.2) and solving for $E = E_{EL}$ gives the value

$$E_{EL} = \left(\frac{m\hbar\omega_p}{e^2} \frac{1+\omega^2\tau_k^2}{\tau_k\tau_L} \right)^{1/2} \tag{2.3}$$

of E at which the net rate of change of $\mathcal{E}$ is zero. For $E > E_{EL}$, the electron gains energy on the average, and vice versa. If the electron gains energy on the average at each collision, it will accelerate until $\mathcal{E} = \mathcal{E}_I$. Thus, the simplest criterion for breakdown is that $E \geq E_B$ with

$$E_B = E_{EL} \quad . \tag{2.4}$$

The energy dependence of the relaxation frequencies will be considered in Sec. VIII. Values of E_B calculated from (2.4) and (2.3) typically are a factor of

three to ten times greater than observed values. For example, at 1.06 μm with $\tau_k = 1.36 \times 10^{-15}$ sec and $\tau_L = 8.77 \times 10^{-16}$ sec, for sodium chloride at room temperature from Sec. C-VIII, (2.3) and (2.4) give

$$E_B = 9.0 \text{ MV/cm}$$

which is a factor of 4.3 times greater than the experimental value[6] of 2.1 MV/cm.

III. IONIZATION FREQUENCY

Current theories do not explain the experimentally determined values of the ionization frequency ω_c, as will now be shown. The ionization frequency can be obtained from the model in Sec. II by integrating

$$\frac{d\mathcal{E}}{dt} = \left(\frac{d\mathcal{E}}{dt}\right)_E - \left(\frac{d\mathcal{E}}{dt}\right)_L \quad , \tag{3.1}$$

for $\mathcal{E} = 0$ to $\mathcal{E}_I$, which corresponds to $t = 0$ to t_I, where t_I is the time required for the electron to gain energy $\mathcal{E}_I$ in the presence of the field and of phonon collisions. The values of $(d\mathcal{E}/dt)_E$ and $(d\mathcal{E}/dt)_L$ in (3.1) are given by (2.1) and (2.2). Assuming that τ_k and τ_L are constants, the integration gives

$$\mathcal{E}_I = \frac{e^2 \tau_k}{m(1+\omega^2 \tau_k^2)} (E^2 - E_{EL}^2)\, t_I \quad . \tag{3.2}$$

Since the number of conduction electrons doubles every t_I seconds, n_c is equal to

$$n_c = n_{c0}(2)^{t_p/t_I} \quad ,$$

which can be written as

$$n_c = n_{c0}\, e^{\omega_c t_p} \quad , \tag{3.3}$$

with

$$\omega_c = 0.693\, \frac{\hbar\omega_p}{\mathcal{E}_I \tau_L}\, \frac{E^2 - E_{EL}^2}{E_{EL}^2} \qquad \text{for } E > E_{EL} \tag{3.4}$$

and $\omega_c = 0$ for $E < E_{EL}$. For $\hbar\omega_p = 1/40\,eV$, $\mathcal{E}_I = 8\,eV$, $\tau_L = 8.77 \times 10^{-16}$ sec, $\tau_k = 1.36 \times 10^{-15}$ sec (from Sec. C-VIII), and $\lambda = 1.06\,\mu m$, (2.3) gives $E_{EL} = 9.04\,MV/cm$. With these values and $E = 1.1\,E_{EL}$, (3.4) gives $\omega_c = 5.19 \times 10^{11}\,sec^{-1}$. The agreement with experiment is poor, as illustrated in Fig. 2 and discussed below.

In comparing the result (3.4) for ω_c with experimental results of the dependence of E_B on the laser-pulse duration t_p, the relation between ω_c and t_p is needed. This is commonly obtained[6] by assuming that n_c is increased from an initial value of 10^8–$10^{10}\,cm^{-3}$ to a final value of $10^{18}\,cm^{-3}$, as already mentioned. Taking the logarithm of (3.3) with $n_{c0} = 10^9\,cm^{-3}$, and $n_c(t_p) = 10^{18}\,cm^{-1}$ gives the required expression

$$\omega_c = t_p^{-1}\,\ell n\,(n_c/n_{c0}) \cong 20.7\,t_p^{-1} \tag{3.5}$$

The experimental values[6] of t_p^{-1} for sodium chloride at room temperature and $1.06\,\mu m$ are shown in Fig. 2. The dc results, which will be discussed in Sec. VI, are included here for comparison with the $1.06\,\mu m$ results. The theoretical result for t_p^{-1} from (3.4) and (3.5) is plotted as a single curve. The theoretical results of Holway and Fradin[7] obtained from a numerical solution of a transport equation, with one parameter adjusted, also are shown in Fig. 2. The agreement between experiment and either theory is poor. At $E_B \cong 2\,MV/cm^2$, (3.4) gives $t_p^{-1} = 0$, compared with the experimental value of $\sim 10^8\,sec^{-1}$. Extrapolating the Holway-Fradin curve to $E = 2\,MV/cm$ (which surely gives an inaccurate value for such a great extrapolation) gives a value

of t_p^{-1} that is 18 orders of magnitude smaller than the experimental value. The relatively smaller factor of ~3.7 between the lowest experimental point and the Holway-Fradin curve illustrates the assertion made in Sec. I, that order-of-magnitude accuracy in the value of E_B is very weak testimony at best for the validity of a theory of avalanche breakdown. It is perhaps worth mentioning that ω_c appears in an exponent in (3.3); thus a factor of 10^{18} error in ω_c makes a factor of

$$(10^9)^{10^{18}}$$

error in n_c.

Finally, consider the criterion for damage. The one used above

$$n_c/n_{c0} = 10^9 \tag{3.6}$$

is one of the commonly used criteria. Seitz[8] introduced the "40 generation" criterion in which an electron starting at the cathode must undergo 40 multiplications before reaching the anode. This corresponds to

$$n_c/n_{c0} = (2)^{40}$$

on the average. With

$$(2)^{30} = 10^9 \quad ,$$

the criterion (3.6) corresponds to 30 generations during the laser-pulse duration. Another commonly used criterion[5, 9, 10] is that the sample temperature must be raised to the melting temperature. There are many other possible criteria, some of which are discussed in Sec. D.

IV. FREQUENCY DEPENDENCE OF THE BREAKDOWN FIELD

It will be shown in this section that current theories give a much stronger frequency dependence of E_B than observed experimentally. It is currently believed that the frequency dependence of E_B should be given by

$$E_B \sim (1+\omega^2 \tau_k^2)^{1/2} \tag{4.1}$$

which follows from (2.4) and (2.3). The increase in the value of E_B from the first 10.6 μm laser experiments over the dc values was attributed to this frequency factor in (4.1). It was then surprising that there was little additional increase in E_B first at 1.06 μm, then at 0.694 μm.

At $\lambda = 0.694\,\mu m$, the value of $1/\omega$ is 3.69×10^{-16} sec. According to (4.1) and the experimental result that E_B changes little between 10.6, 1.06, and 0.694 μm, the value of τ would have to satisfy

$$\tau_k < 2.10 \times 10^{-16} \text{ sec} \tag{4.2}$$

(even for a 15-percent increase in E_B from 10.6 to 0.694 μm) for values of $\mathcal{E}$ between ~1/40 eV and ~8 eV. It is extremely unlikely that τ_k is this small. The calculations in Sec. C-VIII indicate that τ_k is an order of magnitude greater than 2×10^{-16} sec for all values of $\mathcal{E}$ on this range, and that τ_k is two orders of magnitude greater than the value in (4.2) at $\mathcal{E} \cong 8$ eV.

Furthermore, the values of τ_k required to explain the observed values of E_B are inconsistent with (4.2). At 10.6 μm, the experimental value of E_B is[11] 1.95 MV/cm for NaCl. From (2.4) and (2.3) with $\tau_k = \tau_L$ and $\hbar\omega_p = 1/40$ eV,

the value of τ_k required to give this experimental value of E_B is

$$\tau_k = 2.00 \times 10^{-15}\,\text{sec}^{-1} \quad . \tag{4.3}$$

The frequency dependence of E_B calculated from (2.3) with this value of τ_k is in poor agreement with experiment, as seen in Fig. 3. For example, even though the theoretical curve was fit to the experimental result at 10.6 μm, the theoretical value of E_B = 11.1 MW/cm at 0.694 μm is much greater than the experimental value of 2.3 MV/cm. If the difference between τ_k and τ_L is included, the agreement is even poorer. Including the energy dependence of τ_k and τ_L makes little difference in this result.

V. INITIAL ELECTRON DENSITY

In this section it will be shown that the initial density of conduction electrons is so small that the probability of finding an electron in a typical focal volume is much less than unity. This is in disagreement with current theories, in which the initial density of electrons n_{c0} in (3.3) required to start the avalanche is usually assumed to have the value

$$n_{c0} = 10^8 - 10^{10}\,\mathrm{cm}^{-3} \quad . \tag{5.1}$$

It is also assumed that the avalanche process must increase the value of n_c to $10^{18}\,\mathrm{cm}^{-3}$. From (3.3), the ionization frequency $\omega_c = t_p^{-1} \ell n\,(n_c / n_{c0})$ is rather weakly dependent on the initial electron density n_{c0}. With $n_c = 10^{18}$ cm^{-1}, changing the value of n_{c0} from $10^9\,\mathrm{cm}^{-3}$ to $10^4\,\mathrm{cm}^{-3}$ changes ω_c by 56 percent. However, there is the more serious problem with small electron densities that the probability of an electron being in the focal volume during the pulse becomes negligibly small for the small values of n_{c0}, as discussed below.

The assumed value of n_{c0} in (5.1) would at first appear to be a reasonable density, which could result from thermal ionization of impurity levels, for example. Under closer examination, this density is seen to be unreasonably large. First, with $10^8 - 10^{10}$ conduction electrons per cubic centimeter, previous observations of photocurrents would have been impossible.

It is not difficult to see why lower densities are expected. For F centers in sodium chloride for the best case of the chemical potential having the value

$\frac{1}{2}\mathcal{E}_F$ (below the conduction band), where $\mathcal{E}_F \cong 2\,eV$ is the energy of the F center below the conduction band, the theoretical value of n_c at room temperature is[12]

$$n_c = (5 \times 10^{13}\, 2.41 \times 10^{19})^{1/2} \exp\left[-\tfrac{1}{2}(2)(40)\right]$$

$$= 10^{-1}\,cm^{-3}$$

which is negligibly small. The density $5 \times 10^{13}\,cm^{-3}$ of F centers is the greatest value the crystal can have without being colored, as shown in Sec. D. Shallower imperfection levels could contribute more electrons, but it is currently believed that there is not a sufficient density of shallow levels, and $10^8 - 10^{10}$ cm^{-3} from shallow levels is inconsistent with photoconductivity experiments.

Measurements of the dc conductivity σ would afford sufficiently accurate estimates of the value of n_c. However, room-temperature values of σ were not found in the literature. In the absence of experimental values, a simple estimate further suggests that $n_c = 10^8 - 10^{10}\,cm^{-3}$ is unlikely. Values of σ in $(ohm\,cm)^{-1}$ are[12] 10^6 for a good conductor, 10^2 to 10^9 for semiconductors, 10^{-14} to 10^{-22} for insulators, and 10^{-26} for extrapolation from high-temperature ionic conductivity values. For $n_c = 10^8 - 10^{10}\,cm^{-3}$, σ lies in the semiconductor range rather than the insulator range, which is not reasonable for alkali halides.

For σ in the insulator range, that is $\sigma \leq 10^{-14}\,(ohm\,cm)^{-1} = 9 \times 10^{-3}\,sec^{-1}$, the conductivity relation[12]

$$n_c = m\sigma / e^2 \tau_k$$

gives

$$n_c \leq 2 \times 10^4 \text{ cm}^{-3} \quad . \tag{5.2}$$

For this limit of n_c, the probability of finding an electron in the focal volume can be estimated as follows. Since the electron-avalanche process is highly nonlinear, only the region of the focal volume with E near the maximum is effective, and the diameter d_f and length ℓ_f of the high-field region are less than the $1/e^2$ or $1/e$ values. Reasonable values for 1.06 μm experiments,[13] which also correspond to the damage volume, are $d_f = 2\,\mu\text{m}$ and $\ell_f = 50\,\mu\text{m}$. With $V_f \cong 2 \times 10^{-10}\,\text{cm}^3$ and (5.2), the value of $n_c V_f$ is

$$n_c V_f < 4 \times 10^{-6} \quad .$$

This negligibly small probability of finding an electron in the focal volume indicates that there is not a sufficient electron density to initiate the avalanche. Furthermore, the value of n_c from (5.2) is at least eight orders of magnitude too small to explain the number of nucleation centers reported by Smith, Bechtel, and Bloembergen.[13]

This problem of an insufficient prepulse electron density is one of the less serious difficulties with current theories since there are mechanisms for generating the starting electrons, as discussed in Sec. C. However, the source of the starting electrons can determine the value of E_B; then assuming that $n_{c0} = 10^8 - 10^{10}\,\text{cm}^{-3}$ would give an incorrect value of E_B.

VI. LUCKY-ELECTRON AVALANCHE AT DC

Several of the attempts to alleviate the difficulties in the simple theory discussed in the previous sections will be considered here and in the following two sections. In the present section it will be shown that current lucky-electron theories do not explain the experimental values of E_B. The value of τ_k is the average time between collisions, with each individual time between collisions being different from τ_k in general. Seitz[8] and Shockley[14] considered the effects of the deviations from the average in dc experiments. In the discussion of Fig. 1 in Sec. II, it was pointed out that collisions limit the rate of energy absorption from the field in the dc case. Thus, a few "lucky" electrons that have collision times much greater than the average value can gain energy $\mathcal{E}_I$ even when $(d\mathcal{E}/dt)_E < (d\mathcal{E}/dt)_L$ is satisfied on the average. Thus E_B can be less than the value of E_{EL} in (2.3).

A simple demonstration of the large energy gained by the lucky electrons is obtained from the equation of motion between collisions for the component k_z of the electron wave vector $\underset{\sim}{k}$ along the direction of the dc field $\underset{\sim}{E} = \hat{z}E$

$$dk_z/dt = eE/\hbar \quad . \tag{6.1}$$

The solution between collisions is

$$k_z = k_{z0} + eEt/\hbar \quad .$$

The corresponding electron energy is

$$\mathcal{E} = \frac{\hbar^2}{2m}\left[k_x^2 + k_y^2 + \left(k_{z0} + \frac{eEt}{\hbar}\right)^2\right]$$

which shows that the greater the value of t between collisions, the greater the value of $\mathcal{E}$. In passing, notice that the energy gained

$$\Delta\mathcal{E} = \frac{\hbar e E t}{m}\left(k_{z0} + \frac{e E t}{2\hbar}\right) \tag{6.2}$$

is large for small-angle collisions, for which k_{z0} is large on the average. Also, for isotropic scattering, for which $k_{z0} = 0$ on the average, (6.2) with $t = \tau_{iso}$ and $(d\mathcal{E}/dt)_E = \Delta\mathcal{E}/\tau_{iso}$ give

$$\left(\frac{d\mathcal{E}}{dt}\right)_E = \frac{e^2 \tau_{iso} E^2}{2m} \quad , \tag{6.3}$$

in agreement with (2.1) for $\frac{1}{2}\tau_{iso} = \tau_k$ and $\omega = 0$.

In Sec. C-XII it is shown that the probability that the electron goes for time t without undergoing a collision is

$$P_\tau(t) = e^{-t\langle 1/\tau_k \rangle} \quad , \tag{6.4}$$

where $\langle 1/\tau_k \rangle$ is the time average of $1/\tau_k$. The time t_{nc} required for an electron to gain energy $\mathcal{E}_I \cong 8\,eV$ in the absence of collisions is, from (6.2) with k_{z0} negligible

$$t_{nc} = \frac{(2m\mathcal{E}_I)^{1/2}}{eE} = \left(\frac{1\,MV/cm}{E}\right) 9.54 \times 10^{-14}\ sec \quad . \tag{6.5}$$

The time average $\langle 1/\tau_k \rangle$ can be approximated by the average over the electron wave vector k, as shown in Sec. C-XIII. From Fig. 7 of Sec. C-VIII, the

average from $\mathcal{E} = k_B T = 1/40\,\text{eV}$ to $\mathcal{E} = \mathcal{E}_I = 8.1\,\text{eV}$ is $\langle 1/\tau_k \rangle = 3 \times 10^{14}\,\text{sec}^{-1}$. Thus, (6.4) and (6.5) give

$$P_\tau(t_{nc}) = \exp\left[-28.6 \left(\frac{1\,\text{MV/cm}}{E} \right) \right] \quad . \tag{6.6}$$

This small probability of ionization per "try" of 3.8×10^{-13} for $E = 1\,\text{MV/cm}$ must be multiplied by the number of "tries," which can be estimated as follows. Seitz[8] has argued that 40 multiplications, which results in $(2)^{40} = 10^{12}$ electrons in a small volume, is a typical value for breakdown. In other words, the electron must undergo 40 multiplications before being swept into the anode by the field. Thus, for a sample 3.2×10^{-2} cm thick[15] and electrons with average drift velocity[3] $v = \mu E = 20(\text{cm}^2/\text{V sec})\, 10^{16}\,\text{V/cm}$, the electron energy must reach $\mathcal{E}_I$ (in the presence of collisions) in time

$$t_I = \frac{1}{40} \frac{3.2 \times 10^{-2}\,\text{cm}}{2 \times 10^{7}\,\text{cm/sec}} \left(\frac{1\,\text{MV/cm}}{E} \right) = \left(\frac{1\,\text{MV/cm}}{E} \right) 4.00 \times 10^{-11}\,\text{sec} \quad .$$

During this time t_I, the electron makes $t_I/\tau_k = 2.93 \times 10^4$ collisions on the average. After each collision, it has another try to accelerate without a collision. Thus, the number of tries is t_I/τ_k. The probability of ionization P_I is the product of the probability of ionization per try times the number of tries:

$$P_I = \frac{t_I}{\tau_k} P_\tau(t_{nc}) = 1.1 \times 10^{-8} \ll 1 \quad . \tag{6.7}$$

This small value of P_I at the experimental value of $E = 1\,\text{MV/cm}$ shows that the lucky-electron mechanism of avalanche is clearly inadequate in this example.

The ionization frequency ω_c is approximately equal to the product of the number of tries per unit time $1/\tau_k$ and the probability of ionization per try

$$\omega_c \cong \frac{1}{\tau_k} e^{-t_{nc}/\langle 1/\tau_k \rangle} \tag{6.8}$$

where the coefficient $1/\tau_k$ is the thermal equilibrium value. Thus, from (6.6) and (6.8)

$$\omega_c = 7.33 \times 10^{14} \exp\left[-28.6 \left(\frac{1\,\mathrm{MV/cm}}{E}\right)\right] \mathrm{sec}^{-1} \quad . \tag{6.9}$$

The comparison in Fig. 4 of this ionization frequency ω_c in (6.9) with experimental values[15] illustrates the poor agreement with theory. The experimental dc results are obtained by converting the sample length ℓ to the time t_ℓ required for the electron to drift across the sample by using the expression

$$t_\ell = \ell/\mu E$$

where μ is the electron mobility. The ionization frequency ω_c is then obtained from (3.5) with $t_p = t_\ell$. Values of t_ℓ for the curve marked "μ const" were calculated using the constant, low field experimental value of[3] $\mu = 20\,\mathrm{cm}^2/\mathrm{V}$ sec for the mobility. For the $\mu = \mu(E)$ curve, the theoretical expression for the field dependence of mobility is given on p. 122 of Ref. 3. In the variable-μ result used in Ref. 16 it was assumed that the mobility decreases with increasing field, as it should for nonpolar solids. In the theoretical result used here, the mobility increases with increasing field. The physical reason is that $\mu = e\tau_k/m$ and increasing the field increases the average value of τ_k by forcing the electrons

into the higher k region in Fig. 7 of Sec. C-VIII where the relaxation frequency $1/\tau_k$ is smaller. Thus, the lower curve in (d) of Fig. 1 in Ref. 16 appears to be a reasonable lower limit in general, but it apparently is not approached in the alkali halides. In Fig. 2, only the constant μ curve was shown for clarity in comparing the dc and 1.06 μm results.

VII. LUCKY REVERSING-ELECTRON AVALANCHE AT LASER FREQUENCIES

It will be shown that the lucky reversing-electron theory[17] cannot explain 0.694 μm breakdown results. The mechanism probably is important only at frequencies below the CO_2-laser frequency, and then only with the modifications discussed in Sec. C-III.

If an electron in an ac electric field does not undergo collisions, its wave vector oscillates with some peak value k_{pk}, rather than increasing continuously as in the dc case. Thus, the wave vector can be increased between two collisions by the peak-to-peak value $2k_{pk}$, at most. The value of

$$2k_{pk} = \frac{2\sqrt{2}eE}{\hbar\omega} = \frac{E}{2.2\ \mathrm{MVcm^{-1}}}\ \frac{\lambda}{0.694\ \mu\mathrm{m}}\ 3.50\times 10^{6}\mathrm{cm^{-1}} \tag{7.1}$$

is easily obtained by integrating (6.1) with $E(t) = E_{pk}\exp(i\omega t)$ and using $E_{pk} = \sqrt{2}\,E_{RMS}$ with $E \equiv E_{RMS}$.

According to the lucky-reversing-electron theory, the electron must suffer a backscattering collision during the time the value of k is near k_p. Then the electron is traveling in the same direction as $\underset{\sim}{E}$ during two successive half cycles. It is therefore accelerated, rather than deaccelerated as it would be if its direction had not been reversed. This process must be repeated until $k = k_I$, where k_I is the value of k required to generate a second electron, as before. The sequence is so unlikely that a very rough estimate is sufficient to demonstrate that it is negligible.

For an electron that has a lucky reversing collision when $k_z = -k_{pk}$, the next lucky reversing collision must occur at $k = +k_{pk}$. For the case of

$\omega\tau_k \gg 1$, the electron makes several oscillations before suffering a collision, on the average. Thus the probability of a collision during the time $t_{pk} - \frac{1}{2}\Delta t$ to $t_{pk} + \frac{1}{2}\Delta t$, where $t = t_{pk}$ at $k = +k_{pk}$, is approximately equal to $\nu\Delta t \equiv \omega\Delta t/2\pi$. Here $1/\nu$ is the period of oscillation. For $\omega\tau_k \ll 1$ it can be shown that the probability is even lower.

Selecting Δt to make $k = 0.8\,k_{pk}$ at the two ends of the time interval Δt and using $2\cos^{-1} 0.8 = 73.7°$ gives $\nu\Delta t = 0.205$. A generous estimate of the effective fractional solid angle $\Delta\Omega/4\pi$ for backscatter near 180° is 1/5, which gives

$$P_B = \frac{1}{5}\nu\Delta t = 4 \times 10^{-2}$$

for the probability of the backscattering collision.

The number N_C of such collisions required to make $k = k_I$ is greater than $k_I/2k_{pk}$. The inequality results from the fact that the change in k between the reversing collision is less than $2k_{pk}$ since the collisions were assumed to occur at $|k| > 0.8\,k_{pk}$ and collisions with scattering angle $\theta \neq 180°$ are less effective. Thus an overestimate is obtained by using $N_C = k_I/2k_{pk}$. The value of k_I is $\sim 1.46 \times 10^8\ \mathrm{cm}^{-1}$ for $\mathcal{E}_I \cong 8\,\mathrm{eV}$ and $2k_p \cong 3.50 \times 10^6\ \mathrm{cm}^{-1}$ according to (7.1). Thus $N_C = 41.9$.

The probability for k reaching k_I is therefore

$$\left(P_B\right)^{N_C} = (4 \times 10^{-2})^{41.9} = 2.67 \times 10^{-59} \quad . \tag{7.2}$$

Multiplying by the number of tries $t_p/\tau_k = 5 \times 10^6$ during the pulse duration t_p, which is again an overestimate since $\omega\tau_k \gg 1$, gives $P_s\ 1.3 \times 10^{-52}$ for the probability of success of attaining $k = k_I$, which is negligible as stated.

A previous estimate[17] used much smaller values of the number of reversing collisions N_C (M in the reference), which appears in the exponent in (7.2). Values of N_C = 1 to 7 for various materials, apparently obtained from a fit to experimental results, are much smaller than our lower limit of $N_C = 42\,(0.694/1.06) = 27$. Also, the tacit assumption that $\omega\tau_k \ll 1$ is satisfied appears to have been made in one part of the previous calculation. These two differences account for tens of orders of magnitude difference in the two results.

VIII. ENERGY DEPENDENCE OF ELECTRON RELAXATION FREQUENCIES

At the early stages of the electron-avalanche-breakdown investigation reported in Sec. C, a number of modifications of the existing theories were tried in hopes of solving the problems of these theories. Only slight improvements could be made. For example, consider the effects of including the energy dependence of the relaxation frequencies. A calculation in Sec. C-VIII of the values of τ_k and τ_L gives the results in Fig. 7 of Sec. C.

Including this energy dependence of τ_k and τ_L in (2.1) and (2.2) gives the results sketched in Fig. 5. Increasing the value of E raises the curve $(d\mathcal{E}/dt)_E \sim E^2$ and leaves $(d\mathcal{E}/dt)_L$ unchanged. For sufficiently great values of E, the curve $(d\mathcal{E}/dt)_E$ lies above $(d\mathcal{E}/dt)_L$ at all values of k as marked "greater E" in Fig. 5, and breakdown surely would occur in most cases of interest.

For the value of E in Fig. 5, electrons with $k_\ell < k < k_{EL}$ lose energy on the average, while those with $k < k_\ell$ and $k > k_{EL}$ (for $\omega\tau \ll 1$) gain energy on the average. Thus, the lucky-electron process must take the electron across the barrier between k_ℓ and k_{EL}, shown shaded in Fig. 5. This is considerably more probable in general than making $k = k_I$ as discussed in Secs. VI and VII. However, even this easier process has a probability that is too low to explain the experimental results. In Sec. C-III it will be shown that if the electrons generated in the avalanche process have $k > k_{EL}$, then the lucky-electron mechanism, with the starting electrons supplied by cathode or impurity emission, can explain the dc data.

For the case of laser frequencies, the factor $(1 + \omega^2 \tau_k^2)^{-1}$ in (2.1) reduces the value of $(d\mathcal{E}/dt)_E$, the reduction being especially great at large k where τ_k is large. There is typically another barrier, or region of $(d\mathcal{E}/dt)_E < (d\mathcal{E}/dt)_L$, at high values of k, as illustrated in Fig. 5. At 10.6 μm with E = 2 MV/cm, this second barrier starts at $k \cong k_I = 1.6 \times 10^8 \text{ cm}^{-1}$. At higher frequencies, the value of $(1 + \omega^2 \tau_k^2)^{-1}$ becomes so small that the two barriers merge, and all electrons with $k > k_\ell$ lose energy on the average. The lucky-electron process then must carry k all the way to k_I, which is very unlikely as already shown.

REFERENCES

1. A. von Hippel, Z. Physik 67, 707 (1931); J. Appl. Phys. 8, 815 (1937).
2. M. Van Marum, Ann. Physik 1, 68 (1799).
3. J. J. O'Dwyer, The Theory of Electrical Conduction and Breakdown in Solid Dielectrics (Clarendon, Oxford, 1973).
4. N. Bloembergen, IEEE J. Quantum Elect. QE-10, 375 (1974).
5. N. Klein, Adv. in Elect. and Elect. Phys. 26, 309 (1969).
6. D. W. Fradin, Harvard University Technical Report No. 643, Contract No. N00014-67-A-0298-0006, May (1973); D. W. Fradin, E. Yablonovitch, and M. Bass, Appl. Opt. 12, 700 (1973).
7. L. H. Holway and D. W. Fradin, J. Appl. Phys. 46, 279 (1975).
8. F. Seitz, Phys. Rev. 76, 1376 (1949).
9. P. F. Braunlich, Bendix Research Laboratories Final Report, Contract No. F19628-73-C-0032, August (1974); P. Braunlich, A. Schmid, and P. Kelly, Appl. Phys. Lett. 26, 150 (1975).
10. M. Sparks and C. J. Duthler, J. Appl. Phys. 44, 3038 (1973).
11. E. Yablonovitch, Appl. Phys. Lett. 19, 495 (1971).
12. C. Kittel, Introduction to Solid State Physics, 4th ed. (Wiley, New York, 1971).
13. W. L. Smith, J. H. Bechtel, and N. Bloembergen, Phys. Rev., in press, and in Proc. of 7th NBS-ONR-ASTM Symposium on Damage in Laser Materials, Boulder, Colorado, July, 1975 (to be published).
14. W. Shockley, Czech. J. Phys. B11, 81 (1961) and Sol. St. Elect. 2, 35 (1961).
15. D. B. Watson and W. Heyes, J. Phys. Chem. Solids 31, 2531 (1970).
16. E. Yablonovitch and N. Bloembergen, Phys. Rev. Lett. 29, 907 (1972).
17. M. Bass and H. H. Barrett, IEEE J. Quant. Elect. QE-8, 338 (1971).

Figure Captions

Fig. 1. Schematic representation of an electron's path in the presence of an electric field $\underset{\sim}{E}$ and collisions with phonons: Part (a) illustrates the increase in the electron's energy by a dc electric field and (b) shows the energy loss to phonons. At L in (a), the electron is "lucky," that is it does not suffer a collision for a long time, thereby gaining great energy from the field.

Fig. 2. Comparison of 1.06 μm[6] (points ⊙) and dc[15] (dashed curve) experimental values of the inverse pulse duration t_p^{-1} with two solid theoretical curves showing poor agreement for both. The preliminary present results (points ⊡ and dotted curve) are discussed in Sec. C.

Fig. 3. Comparison of the experimental results[6] with the theoretical results (2.4) and (2.3) fit at 10.6 μm showing poor agreement for the frequency dependence of the breakdown electric field. The preliminary present theory (points ⊡) is discussed in Sec. C.

Fig. 4. Comparison of the experimental results[15] with the result Eq. (6.9) of the lucky-electron theory. The agreement is improved from that of Eq. (3.4) for the average electron, but is still poor. The present theory (points ⊡) is discussed in Sec. C.

Fig. 5. Wave-vector dependence of the electron energy gain and loss showing the shaded energy barriers of net average loss.

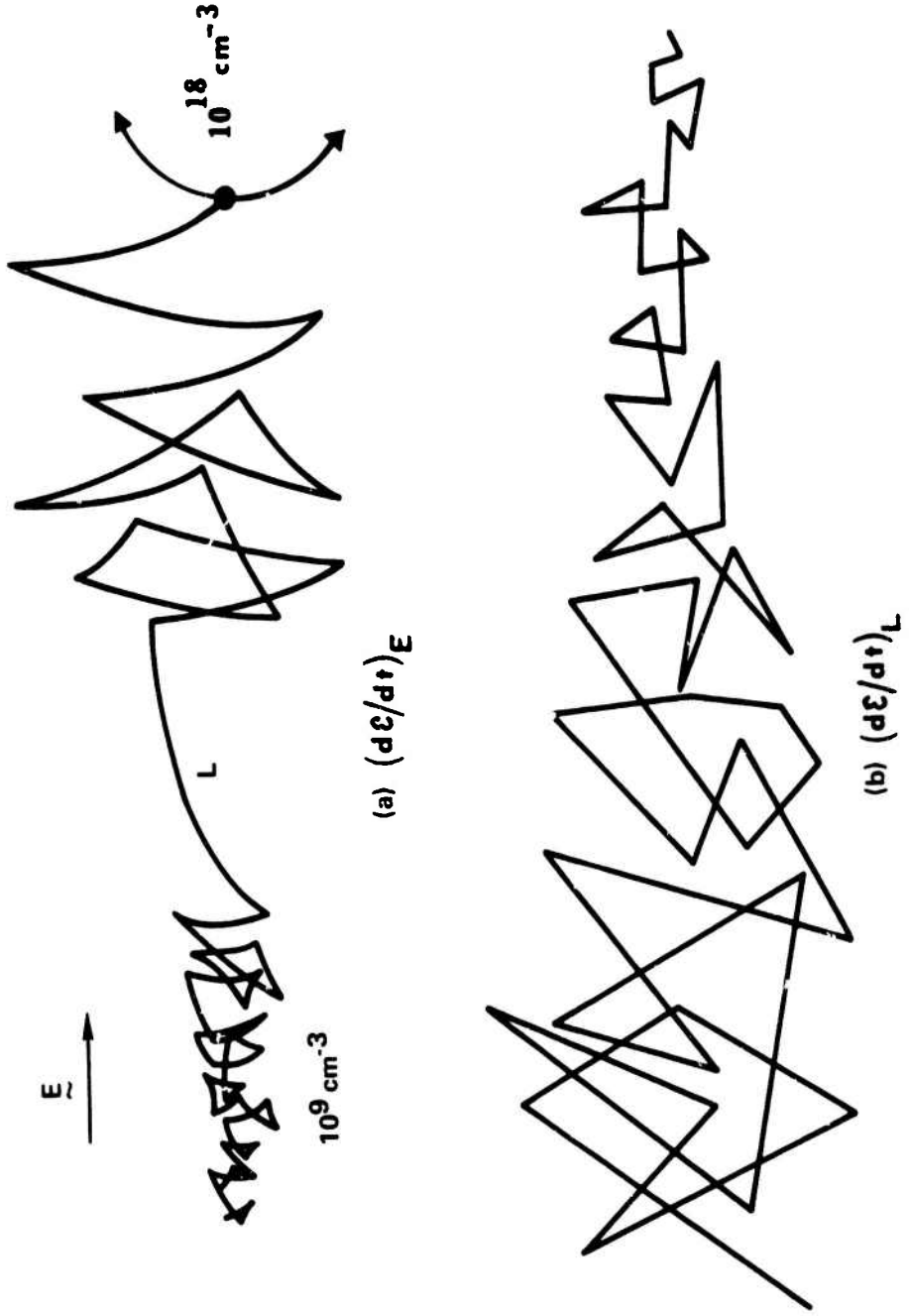
10^{18} cm^{-3}
L
10^{9} cm^{-3}
E
(a) $(d\mathcal{E}/dp)_E$
(b) $(dE/dp)_L$

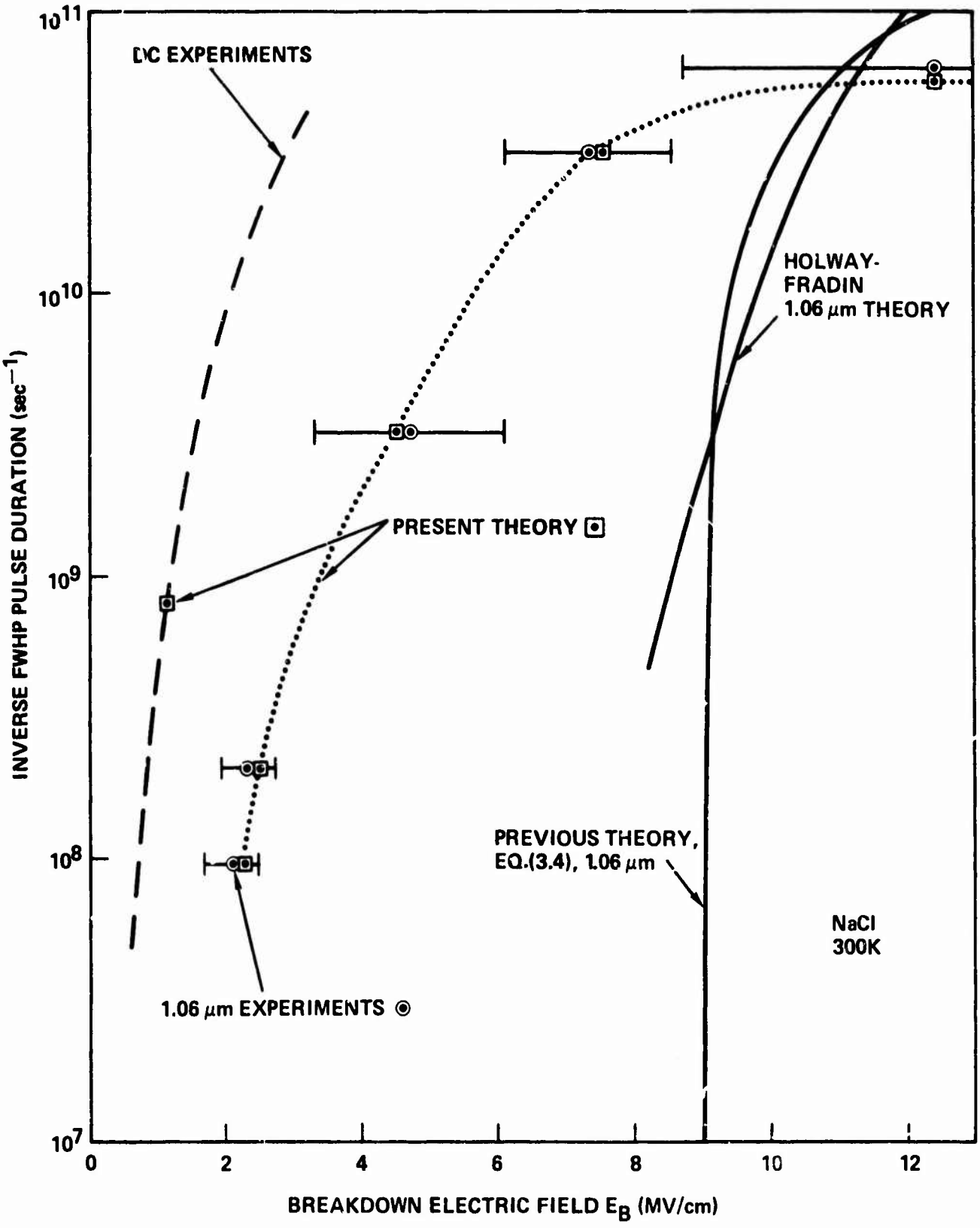
DC EXPERIMENTS
HOLWAY-
FRADIN
1.06 μm THEORY
PRESENT THEORY
PREVIOUS THEORY,
EQ.(3.4), 1.06 μm
NaCl
300K
1.06 μm EXPERIMENTS
INVERSE FWHP PULSE DURATION (sec⁻¹)
BREAKDOWN ELECTRIC FIELD E_B (MV/cm)
10^11
10^10
10^9
10^8
10^7
0
2
4
6
8
10
12

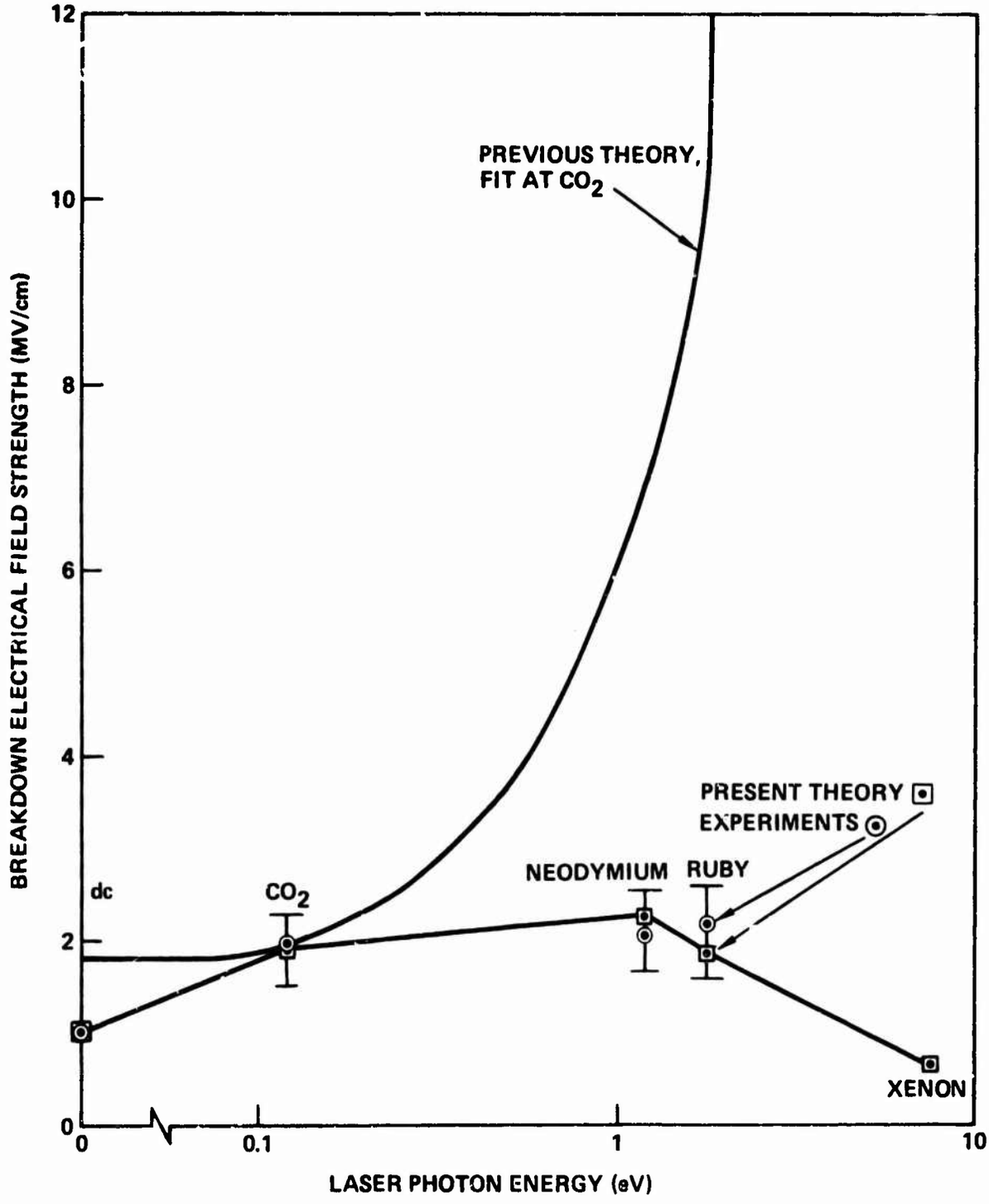
12
10
8
6
4
2
0
BREAKDOWN ELECTRICAL FIELD STRENGTH (MV/cm)
PREVIOUS THEORY,
FIT AT CO_2
PRESENT THEORY
EXPERIMENTS
dc
CO_2
NEODYMIUM
RUBY
XENON
0
0.1
1
10
LASER PHOTON ENERGY (eV)

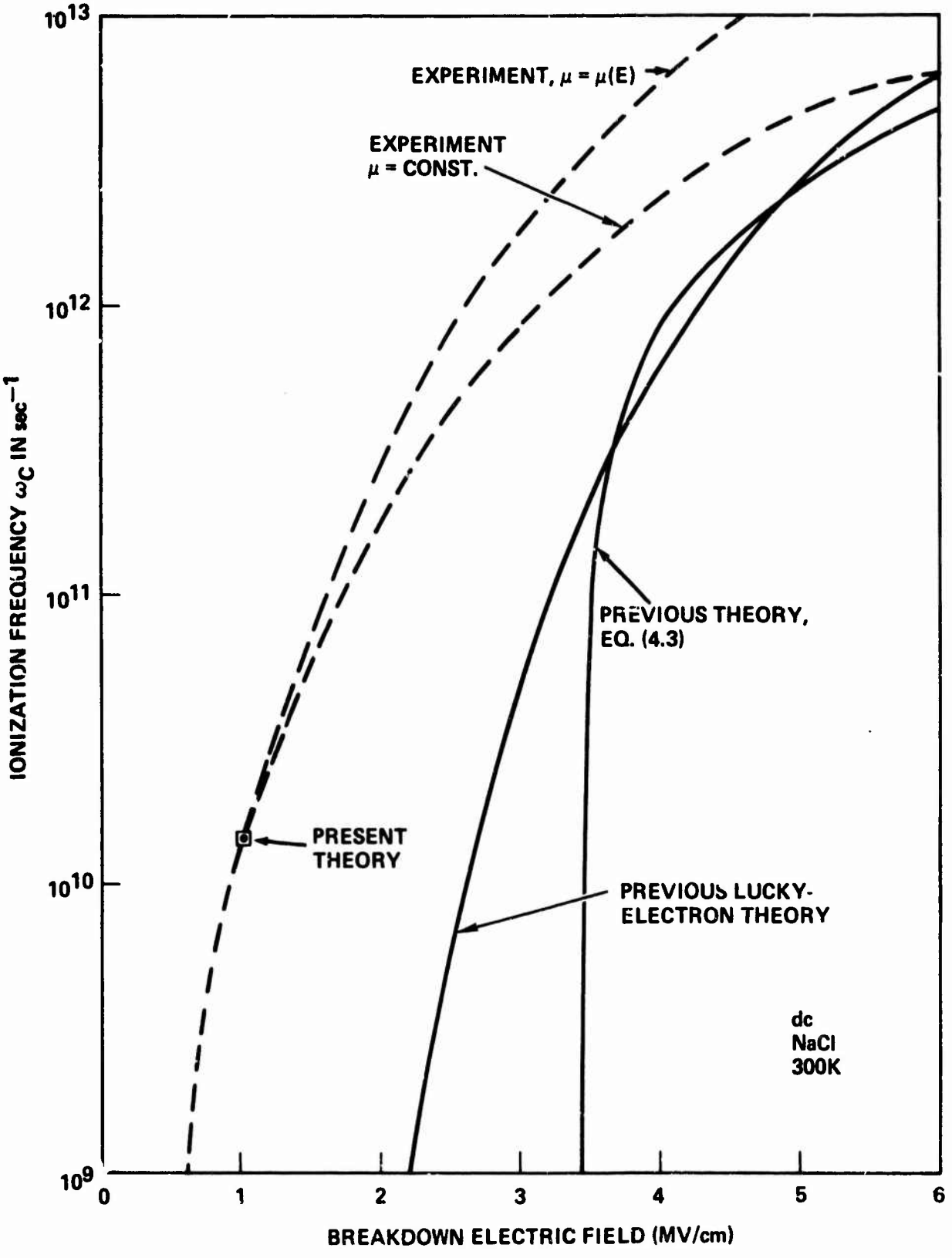
EXPERIMENT, μ = μ(E)
EXPERIMENT
μ = CONST.
PREVIOUS THEORY,
EQ. (4.3)
PRESENT
THEORY
PREVIOUS LUCKY-
ELECTRON THEORY
dc
NaCl
300K
IONIZATION FREQUENCY ω_C IN sec^-1
BREAKDOWN ELECTRIC FIELD (MV/cm)
10^13
10^12
10^11
10^10
10^9
0
1
2
3
4
5
6

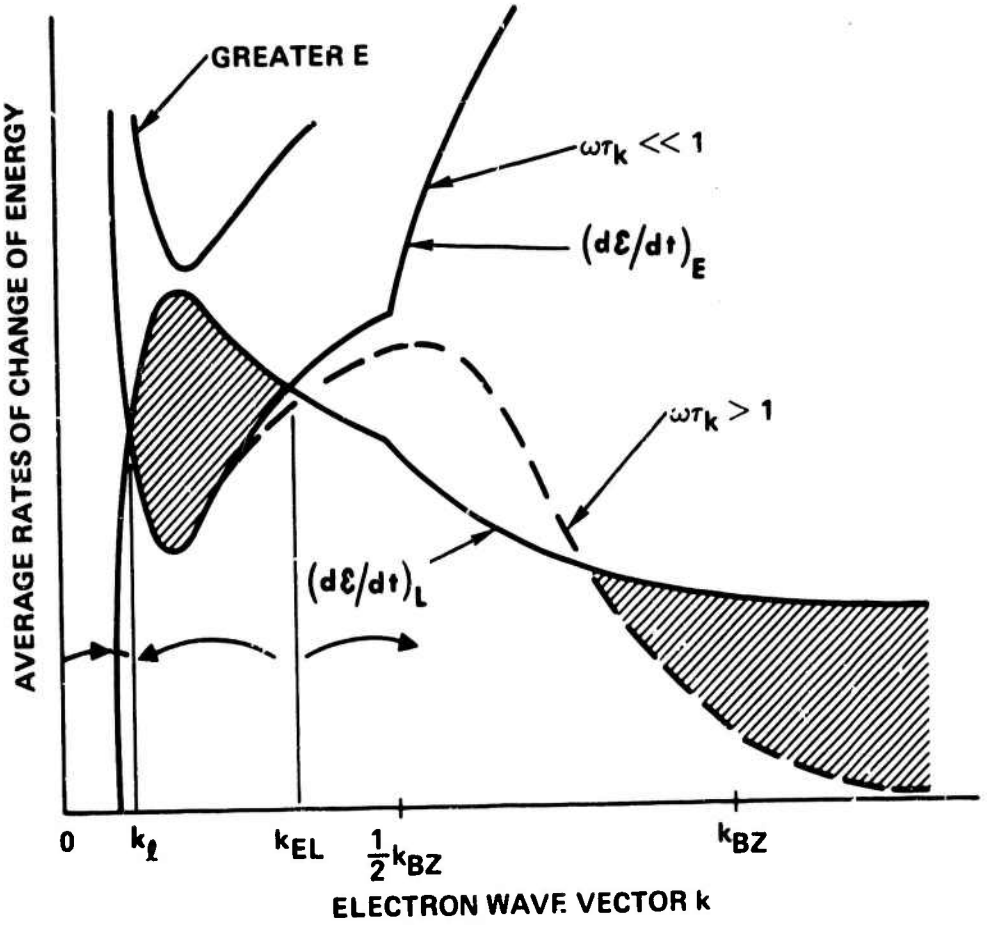
GREATER E
$\omega\tau_k \ll 1$
$(d\mathcal{E}/dt)_E$
$\omega\tau_k > 1$
$(d\mathcal{E}/dt)_L$
AVERAGE RATES OF CHANGE OF ENERGY
0
k_ℓ
k_{EL}
$\frac{1}{2}k_{BZ}$
k_{BZ}
ELECTRON WAVE VECTOR k

C. PRELIMINARY THEORY OF ELECTRON-AVALANCHE BREAKDOWN IN DIELECTRICS BY LASER AND DC FIELDS

M. Sparks
Xonics, Incorporated, Van Nuys, California 91406

Preliminary results of a theory of electrical breakdown in dielectrics agree well in magnitude and shape with experimental results for the pulse-length dependence and frequency dependence of the breakdown electric field with no adjusted parameters. The difficulties of previous theories, which were recently shown to be serious, are removed by the present theory, which includes mechanisms for generating starting electrons and for initiating and sustaining an avalanche. Mechanisms of generating the starting electrons include thermal and tunnel emission from imperfections and from the cathode (in dc experiments), field-induced emission from imperfections, including multiphoton ionization, and multiphoton excitation from the valence band. Mechanisms for initiating and sustaining the avalanche include the Holstein photon-electron-phonon interaction, inter-conduction-band transitions, and at dc, the Seitz lucky-electron process with free acceleration at high electron energy plus a self-sustaining mechanism. Although the preliminary results are encouraging, results of additional work in progress are needed to determine the validity of the theory.

I. INTRODUCTION

Damage of dielectric materials by high electric fields, which has been the subject of numerous experimental and theoretical investigations over a period of years,[1,2] has received renewed attention in recent years as a result of laser damage experiments.[2b] Electrical breakdown of dielectrics by lightning was one of the first known electrical phenomena, and laboratory experiments of electrical breakdown in glass were made in 1799.[1] In spite of the vast literature on the subject, previous theories of electron-avalanche breakdown are inadequate to be predictive or even to explain existing data. Difficulties with previous theories were reviewed in Sec. B.

The general features of the present theory, which assuages these difficulties, are as follows: There must be a mechanism to generate enough electrons to start the avalanche, then there must be a mechanism to increase their energy to the threshold $\mathcal{E}_I$ for ionization. This "ionization" energy $\mathcal{E}_I$ is the energy at which additional electrons are excited from the valence band to the conduction band. Mechanisms of generating the starting electrons include thermal and tunnel emission from the cathode (in dc experiments) and from imperfections, field-induced emission from imperfections, including multiphoton ionization, and multiphoton excitation from the valence band. In uncolored sodium chloride, for which most of our calculations to date have been performed, the only known impurity center that is likely to contribute a sufficient number of starting electrons is the F center, which lies 1.94 eV below the conduction band. There are no known shallow bulk levels in the alkali halides.

The possibility of other imperfections contributing to the starting electron density is unlikely but apparently cannot be ruled out entirely. Surface states are not expected to be important in current experiments since electrons from the surface would not have time to reach the focal volume during the pulse. The possibility that starting electrons are freed from numerous very small inclusions apparently has not been completely ruled out. However, experimental results indicated that this process, as well as other damage mechanisms involving very small inclusions, is unlikely. It has been established that large inclusions lower the damage threshold, of course.

Mechanisms of increasing the electron energy to the ionization value $\mathcal{E}_1$ include the lucky-electron process,[3,4] average-electron acceleration,[3] the Holstein photon-electron-phonon processes,[5] and vertical inter-conduction-band transitions. The last two processes, which are important because the electron can absorb a full quantum of energy $\hbar\omega$ with high probability, are two of the key features of the theory for the laser experiments. In the Holstein process, illustrated schematically in Fig. 1, the large phonon wave vector allows wave-vector conservation so that the large photon energy $\hbar\omega$ can be absorbed by the electron. Energy and wave-vector conservation are not possible at a single electron-photon vertex (first vertex in Fig. 1a).

Damage to the crystal occurs when a sufficient number of conduction electrons have been generated. Several damage mechanisms are discussed. It is shown that excessive temperature rise caused by the Joule (σE^2) heating of the generated electrons is sufficient to explain the dc experiments. At optical frequencies the Holstein process of absorption by the generated electrons and Joule heating are sufficient to explain the experimental results.

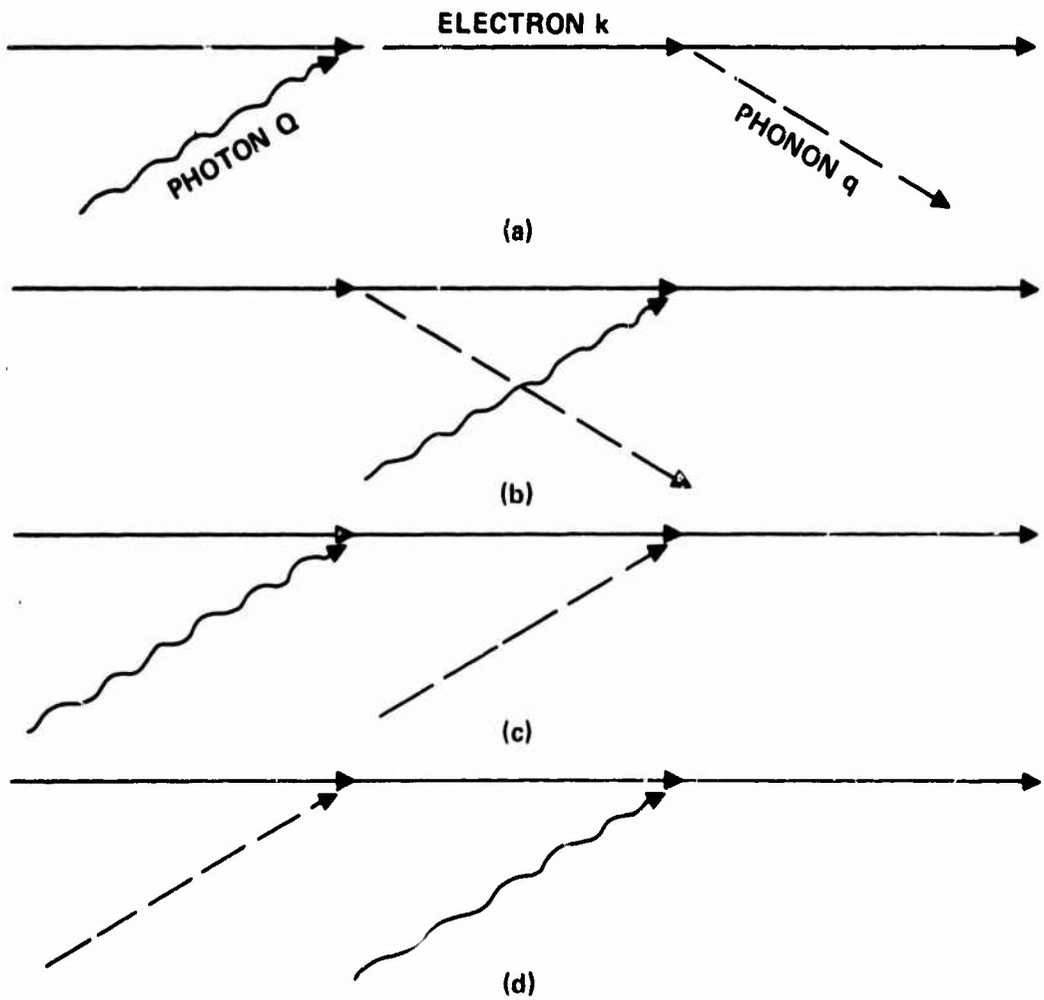

Fig. 1. Schematic illustration of the Holstein process for photon absorption showing the various combinations of phonon absorption and emission. The photon arrows are reversed for photon emission.

In the present theory, the thesis[6, 2b] that the same mechanism is responsible for breakdown from dc through 0.694 μm has been abandoned, although there are still common threads for all mechanisms. Each involved mechanics for generating starting electrons and for increasing their energies to the threshold for ionization. It is not surprising that different mechanisms are operative at different frequencies and different pulse durations since small changes in the value of E_B typically give rise to large changes in the electron ionization rate, as discussed in Sec. B. The factor of two range in E_B as a function of frequency (see Sec. XIV) is in fact quite large. The overall range of E_B reported in the literature for the alkali halides is well over an order of magnitude, which is enormous.

The results of the theory are summarized in Sec. XIV. The agreement in magnitude and shape of the pulse-duration t_p dependence of the breakdown field E_B with the experimental results at 1.06 μm are very good for the three decades change in t_p with no adjusted parameters. The theoretical frequency dependence of E_B from dc through the ruby-laser frequency also agrees well with experimental values. The single dc value of ω_c calculated to date lies on the experimental curve of $\omega_c(E_B)$.

The good agreement with the experimental results is encouraging, especially in view of the facts that no parameters were adjusted to obtain the agreement and that previous theoretical values of ω_c with adjusted parameters disagreed with experimental values, by tens of orders of magnitude in some cases.

Nevertheless, it must be emphasized that the results are preliminary. First, the theory involves a number of physical processes, most of which have received little or no theoretical or experimental attention. These include: the Holstein process,[5] the interband transitions between various conduction bands, the cross

sections for electron ionization of impurities, electron-electron ionization cross sections, effect of excitons on the electron processes, reliable values of the electron relaxation frequencies, details of the melting, fracture, and possibly other mechanisms of the final stages of the damage process, a number of mechanisms that could generate electrons needed to initiate the multiplication process, and a calculation that includes the processes which change the electron energy by large amounts in a transport equation. None of these processes are understood sufficiently well for accurate calculation of the value of E_B.

Second, most of the results are obtained from rather rough estimates. Dr. T. Holstein has suggested a transport-equation formalism that incorporates the features of the theories and will apply this new approach to the problem. Furthermore, in some cases the breakdown depends on the values of electron-relaxation frequencies τ for which there are no experimental values, and theoretical estimates of the values of τ are expected to be accurate to within a factor of two or so at best.

The good agreement between the experimental and theoretical results is in fact better than had been expected in view of these uncertainties. Finally, the theory is in such an early stage of development that it is possible that major changes could evolve. Thus, it is likely that we now have a satisfactory understanding of electron-avalanche breakdown over a wide range of experimental conditions, but there is a definite possibility that the theory of avalanche breakdown is still incomplete.

The results of the present report indicate that there are a number of areas in which additional investigations, both experimental and theoretical, would be useful. The lack of knowledge of the band structure, including the energy levels

and wave functions, of the alkali halides is a serious limitation to the accuracy of the calculations. Some of the same matrix elements appearing in the two-photon absorption calculations also appear in the electron-avalanche calculations. The band-structure information is needed in still other studies, including self focusing, frequency doubling, luminescence, photoelectric emission, and ordinary one-photon absorption. Accurate values of the electron-relaxation frequencies are needed. Other areas were discussed above.

All ac electric-field values are RMS, and the values of the damage field correspond to the intensity I_0 at the peak of the laser pulse in the focal plane, where $I = I_0 \exp(-r/w_1)^2 \exp(-0.83\ t/t_p)^2$, with t_p the full-width-half-maximum pulse duration and w_1 the beam waste, that is, the radius r at which the intensity drops to $1/e$ of the on-axis value. The relation between E and I is $I = n_r c E^2/4\pi$.

Important results are denoted by underscored equation numbers.

II. AVERAGE-ELECTRON MODEL

In the average-electron model the average energy loss to the lattice $(d\mathcal{E}/dt)_L$ and the average energy gained from the electric field $(d\mathcal{E}/dt)_E$ are considered. Breakdown occurs when

$$(d\mathcal{E}/dt)_E > (d\mathcal{E}/dt)_L \tag{2.1}$$

for all $\mathcal{E} < \mathcal{E}_I$, where $\mathcal{E}_I$ is the so-called ionization energy at which the electron generates a second conduction electron by excitation across the electronic energy gap. This model, which is now believed to be inadequate to explain breakdown since (2.1) is too stringent a requirement, as discussed in Sec. B, is introduced here as a base for the calculations to follow.

The rate at which the field E adds energy to the electron is obtained from the wave-vector equation

$$\hbar(dk_z/dt + k_z/\tau_k) = eE \tag{2.2}$$

where $\underset{\sim}{E}$ is along the z axis and k_z is the z component of the electron wave vector $\underset{\sim}{k}$. With $\underset{\sim}{E} = \underset{\sim}{E}_{0k} \exp(i\omega t)$, the steady-state solution is

$$k_z = \frac{e\tau}{\hbar(1 + i\omega\tau_k)} E \quad . \tag{2.3}$$

With current $\underset{\sim}{J} = e\underset{\sim}{v}$, where the velocity v_z is equal to $\hbar k_z/m$, the rate at which the field puts energy into the electron is

$$(d\mathcal{E}/dt)_E = \frac{1}{2} \mathrm{Re} \underset{\sim}{J} \cdot \underset{\sim}{E}^* = \frac{1}{2} \mathrm{Re} \hbar e k_z E^*/m \quad .$$

Substituting (2.3) into this equation and using $E^2 \equiv \frac{1}{2} E_{pk}^2$, where E is the root-mean-square value of the field, gives

$$\left(\frac{d\mathcal{E}}{dt}\right)_E = \frac{e^2 \tau_k E^2}{m(1+\omega^2 \tau_k^2)} \tag{2.4}$$

which is the well known conductivity result σE^2 for a single electron.

The rate at which the electron loses energy to the lattice is

$$(d\mathcal{E}/dt)_L = \hbar\omega_p/\tau_L \tag{2.5}$$

where ω_p is a phonon frequency, and the relaxation frequency τ_L is different from τ_k in (2.4) as discussed in Sec. B and below. Equating (2.4) and (2.5) gives the threshold value E_{EL} above which the electrons gain energy from the field:

$$E_{EL} = E_> f_{EL} \tag{2.6}$$

where

$$E_> \equiv \left(\frac{m\hbar\omega_p\omega^2}{e^2}\right)^{1/2} = 6.72 \text{ MV/cm}$$

$$f_{EL} = \left(\frac{1+\omega^2\tau_k^2}{\omega^2\tau_k^2} \quad \frac{\tau_k}{\tau_L}\right)^{1/2}$$

The numerical value of $E_>$ is for $m = m_f$ (free electron mass), $\hbar\omega_p = 1/40$ eV (for NaCl) and $\omega = 1.78 \times 10^{15}$ sec (for $\lambda = 1.06\mu$m). Values of parameters are listed and discussed in Sec. XIII.

A zeroth-order approximation to the breakdown field E_B is obtained by setting $\tau_k = \tau_L \equiv \tau$, where τ is independent of electron energy $\mathcal{E}$, as discussed in Sec. B. In considering the avalanche process in greater detail, the wave-vector dependence of the gain $(d\mathcal{E}/dt)_E$ and loss $(d\mathcal{E}/dt)_L$ is important. This wave-vector dependence arises from the wave-vector dependence of the electron relaxation frequencies τ_k and τ_L, whose values are determined by the electron-phonon interaction. Electron-electron scattering is negligible since there are so few electrons in insulators, and the electron-phonon scattering is so strong that scattering by impurities can be neglected.

Consider the interaction of the electrons with the longitudinal-optical phonons. If the electron energy $\mathcal{E}$ is less than the phonon energy $\hbar\omega_p$, the emission process in Fig. 2a cannot conserve energy, and the rate $1/\tau_e$ for the emission process is zero. Thus, the low-energy electrons, with $\mathcal{E} < \hbar\omega_p$, gain energy by the phonon absorption processes in Fig. 2b. At zero temperature, the rate $1/\tau_a$ for the absorption process (b) is zero since there are no thermally excited phonons to absorb. At very high temperatures ($k_B T \gg \hbar\omega_p$), $1/\tau_e \cong 1/\tau_a$ for $\mathcal{E} > 2.2\,\hbar\omega_p$. The general case is considered in Sec. VIII.

The rate at which the electron loses energy to the lattice is

$$d\mathcal{E}_L/dt = \hbar\omega_p(1/\tau_e - 1/\tau_a) \equiv \hbar\omega_p/\tau_L \quad . \tag{2.7}$$

The relation between $1/\tau_L \equiv 1/\tau_e - 1/\tau_a$ and the relaxation time τ_k, which is the time required for k_z to relax to 1/e times its original value and is the relaxation time in $d\mathcal{E}_E/dt$, is

$$\frac{1}{\tau_L} = \frac{G(k)}{(2n_p + 1)} \frac{1}{\tau_k} \tag{2.8}$$

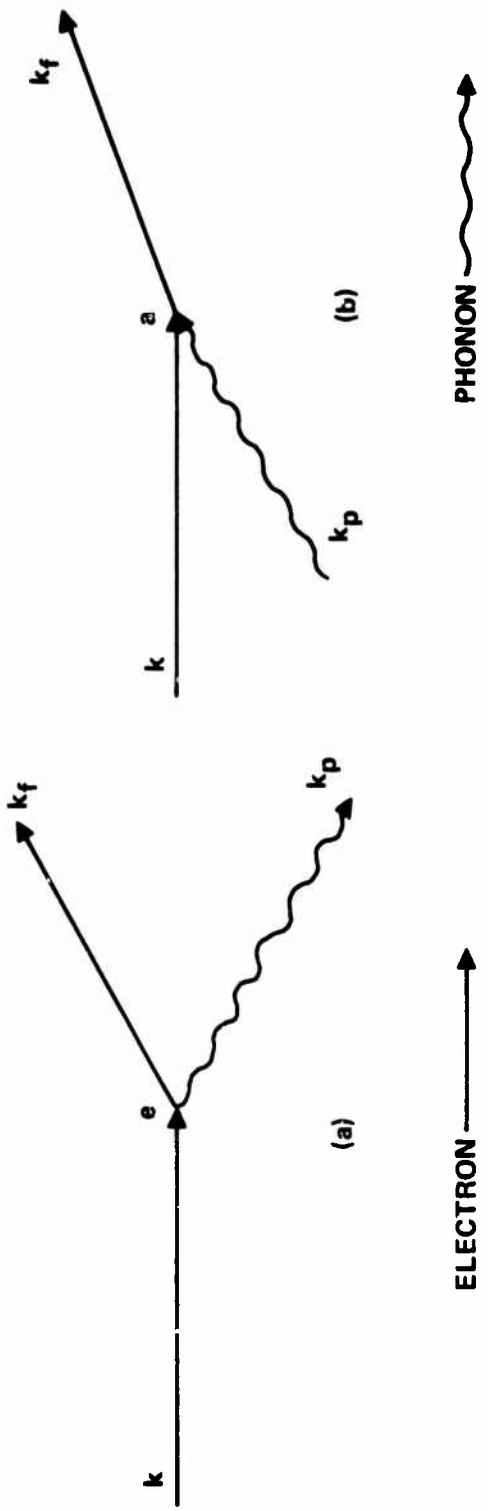

Fig. 2. Electron scattering processes. In (a) the electron loses energy $\hbar\omega$ and in (b) it gains energy $\hbar\omega_p$. The wave-vector direction $\hat{k}$ changes in both cases in general.

where

$$n_p = [\exp(\hbar\omega_p / k_B T) - 1]^{-1} \tag{2.9}$$

is the phonon occupation number, and

$$G(k) = \ell n(4k^2/k_p^2) \quad , \qquad \text{for } k < \tfrac{1}{2} k_{BZ}$$

$$= (2k/k_{BZ})^2 \ell n(2k k_{BZ}/k_p^2), \qquad \text{for } k > \tfrac{1}{2} k_{BZ} \quad .$$

This result (2.8), which is derived in Sec. VIII, is valid for $k \gtrsim 2k_p$.

The relaxation frequency τ_k, which determines the decay of a component of the electron wave vector $\underset{\sim}{k}$, is related to large scattering angles, while τ_L determines the energy transfer to the lattice, which occurs in both large- and small-angle scattering. In general, the large-angle process is slower, that is, $\tau_k > \tau_L$. The relaxation frequency $1/\tau_\Lambda \equiv 1/\tau_a + 1/\tau_e$, which is the relaxation frequency with both small- and large-angle scattering included, will not be needed here.

The calculations of the relaxation frequencies in Sec. VIII are based on perturbation theory, the conditions for the validity of which are valid for $\mathcal{E} \gg \hbar\omega_p$, but are known[7] not to be satisfied for $\mathcal{E} \cong 2\hbar\omega_p$ since the electron-phonon coupling is so strong. For example, the electron is scattered in a distance that is shorter than its wavelength. Thornber and Feynman[8] have shown that the rate of energy transfer to lattice is extremely large for $\mathcal{E} \cong 2\hbar\omega_p$. Refining the calculations of the relaxation frequencies in the region $\mathcal{E} \cong 2\hbar\omega_p$

would be of interest, but of lower priority than a number of other calculations discussed below. For the present report, the perturbation-theory calculations are used without modification. Fortunately, the resulting values of the breakdown field are not too sensitive to the values of the relaxation frequencies at $\mathcal{E} \cong 2\hbar\omega_p$ in most cases, assuming that using reasonable values of τ_k and τ_L has meaning.

In addition to the scattering by longitudinal-optical phonons, the scattering by acoustical phonons appears to be nonnegligible, as pointed out by Seitz.[3] The value of the relaxation frequency for this latter process has a peak near $k = k_{BZ}$, where k_{BZ} is the value of k at the Brillouin zone boundary, where its value is of the same order of magnitude as the perturbation-theory value of the longitudinal-optical peak. The theoretical results of Sec. VIII are displayed as plots of $1/\tau_k$ and $1/\tau_L$ as functions of k.

From these plots of the relaxation frequencies, curves of $(d\mathcal{E}/dt)_E$ and $(d\mathcal{E}/dt)_L$ are sketched in Fig. 3 and discussed in Sec. B. For the present purpose, a brief review of the case of $\omega\tau_k \ll 1$ will suffice. If E is sufficiently great, as marked "greater E" in the figure, then $(d\mathcal{E}/dt)_E$ is greater than $(d\mathcal{E}/dt)_L$ for all $\mathcal{E}$, and avalanche occurs if there is sufficient time and starting electron density. It will be shown below that the breakdown requirement that $(d\mathcal{E}/dt)_E$ be greater than $(d\mathcal{E}/dt)_L$ is too stringent in general, and that breakdown can occur at lower values of E, as already mentioned. For the lower value of E shown in Fig. 3, $(d\mathcal{E}/dt)_E$ is greater than $(d\mathcal{E}/dt)_L$ for $k > k_{EL}$, but is less for $k_\ell < k < k_{EL}$.

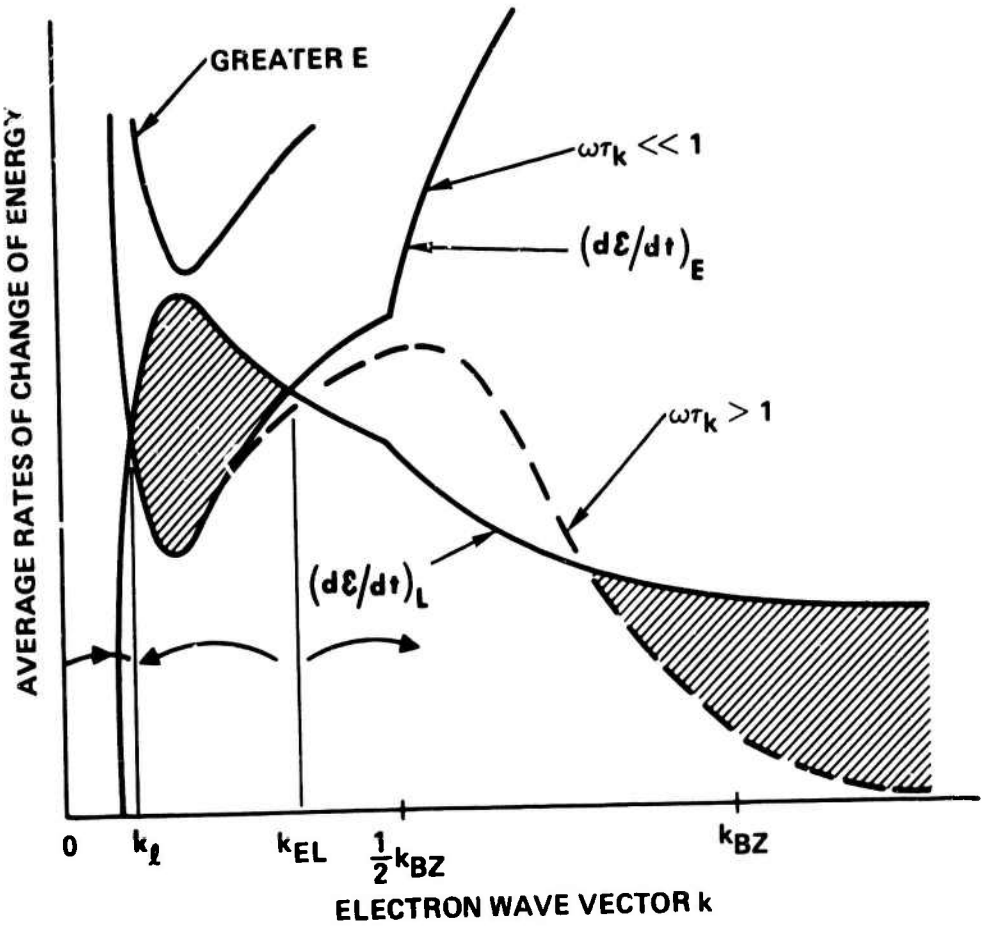

Fig. 3. Wave-vector dependence of the electron energy gain and loss showing the shaded energy barriers of net average loss.

Determining how the electron gets through this barrier, shown as the shaded region between k_{EL} and k_ℓ in the figure, i.e., how the wave vector k is increased from k_ℓ to k_{EL}, is one of the tasks of the theory. The case of $\omega\tau_k > 1$ illustrated in the dashed curve is discussed in Sec. IV.

In passing it is mentioned that the explicit temperature dependence of E_{EL} in (2.6) is different in two limits of $\omega^2\tau_k^2 \gg 1$ and $\omega^2\tau_k \ll 1$. In the high-temperature limit of $2n_p + 1 \cong 2k_BT/\hbar\omega_p$, using $1/\tau_k \sim 2n_p + 1$ and the fact that $1/\tau_L$ is not an explicit function of temperature in (2.6) gives

$$E_{EL} \sim (1/\tau_k)^{1/2} \sim T^{1/2} \qquad \text{for } \omega^2\tau_k^2 \ll 1$$

$$E_{EL} \sim (\tau_k)^{1/2} \sim T^{-1/2} \qquad \text{for } \omega^2\tau_k^2 \gg 1 \quad .$$

In considering the temperature dependence of E_B, the temperature dependence of a_{nn}, N_+, and ω_p must be included. What is even more important, the temperature dependence of the various processes, such as thermal emission from the cathode and from impurities, and the Holstein process must be included.

III. BREAKDOWN AT DC

It will be shown for dc electron-avalanche breakdown that the starting electrons are thermally emitted from the cathode and that the "lucky electron" process of collisionless acceleration carries these electrons across the barrier to wave vector $k_{EL} \cong 0.67\, k_{BZ} = 7.4 \times 10^{7}\ cm^{-1}$ ($\mathcal{E}_{EL} \cong 2.5\,eV$).

Any theory which is to survive as tenable must explain all of the available data, a large fraction of which is at dc[2a] in the case of electron-avalanche breakdown. Thus dc breakdown will be considered even though it is not of direct interest in the present study. The treatment is brief, and space-change effects are neglected. It appears that they could be included without difficulty, but this would carry us too far afield in this preliminary report. The possibility that the usual mechanism of space-change lowering of the value of E_B does not strongly affect results below should be considered in a complete treatment of dc breakdown.

According to (2.6) with $\omega = 0$ and $1.28\,\tau_L \cong \tau_k \cong 1.39 \times 10^{-15}$ sec at $k \cong 2k_p$, the values of E required for electrons with any energy to be accelerated is $E = 3.07$ MV/cm. For lower values of E, electrons with wave vector k on the range $k_\ell < k < k_{EL}$ lose energy on the average, as discussed in Sec. II. The value of k_{EL} is determined by (2.6) with τ_k and τ_L functions of k. For example, for $\mathcal{E}_{EL} = 1.5\,eV$ (or $k_{EL} \cong \frac{1}{2} k_{BZ}$), the values of τ_k and τ_L are $1.28\,\tau_L = \tau_k = 2.04 \times 10^{-15}$ sec from (8.38) and (8.39). With these values, (2.6) gives $E_{EL} = 2.09$ MV/cm. Electrons with $k < k_{EL}$ are said to be in the barrier.

For the experimental value of $E = 1$ MV/cm, the barrier extends to $k_{EL} = 0.67\, k_{BZ}$. Some electrons with $k < k_{EL}$ are accelerated to $k = k_{EL}$ by the

"lucky electron" process of acceleration by the field without undergoing large-angle collisions. Recall from Sec. B that the electron-phonon collisions limit the energy absorbed by the field and that τ_k is an average time between collisions. An electron that happens to suffer no large-angle collision for a long time may absorb sufficient energy to bring k up to the value k_{EL}. Then for $k > k_{EL}$ the electron is accelerated to $k = k_I$, at which wave vector another conduction electron is generated across the gap.

We have shown that the four processes of thermal and tunnel electron emission from the cathode and from impurities, with the barrier lowered by the field, are potential sources of the starting electrons. At room temperature in NaCl, thermionic emission from the cathode is the strongest of these processes.

The thermionic-emission current from the cathode is given by the well known result[9,2a]

$$J = J_0 e^{-\phi_{red}/k_B T} \quad , \tag{3.1}$$

where

$$J_0/e = \left(\frac{T}{300\,K}\right)^2 \left(\frac{m}{m_f}\right) \; 6.83 \times 10^{25} \text{ electrons/cm}^2 \text{ sec} \quad ,$$

$$\phi_{red} = \phi - \Delta\phi \quad ,$$

and

$$\Delta\phi = e^{3/2} n_r^{-1} E^{1/2} = \left(\frac{1.5}{n_r}\right)\left(\frac{E}{1\,MV/cm^{-1}}\right)^{1/2} 0.253 \text{ eV} \quad .$$

For emission into a solid rather than a vacuum, the free-electron mass m_f has been replaced by an effective mass m, and the zero-field barrier height ϕ is

determined by requiring the chemical potential μ to be continuous at the metal-dielectric interface, as illustrated in Fig. 4. The continuity of μ is required since the electron flow is proportional to the gradient of μ so that a discontinuity in μ would imply a δ function in the electron flow. It is assumed that $\phi = -\mu$ is equal to one-half the ground state energy E_F of the F center, or $\phi = 0.7$ eV in NaCl. See the discussion on p. 313 of Ref. 9, where it is shown that $-\mu = \frac{1}{2}E_F + \frac{1}{2}k_BT\,\ell n(n_0/n_F)$ where $n_0 \equiv 2(2\pi m k_B T/\hbar^2)^{3/2} = 5.98 \times 10^{21}\,\mathrm{cm}^{-3}$, n_F is the density of F centers, and μ is chemical potential measured with respect to the bottom of the conduction band. The numerical value of n_0 is for $m = m_f$ and room temperature. The term $\frac{1}{2}k_BT\,\ell n(n_0/n_F)$ is marginally negligible at room temperature if $n_F = 5 \times 10^{13}\,\mathrm{cm}^{-1}$, as discussed in Sec. D. At higher temperatures, this term increases, thereby increasing the barrier height ϕ. The possible increase in the breakdown field from this effect is not realized in typical cases since other temperature effects are stronger. Notice, for example, the factor $1/k_BT$ in (3.1). However, it is possible in principle to reduce the value of E_B by increasing the impurity F-center concentration.

Next, the probability $P_\tau(t)$ that an electron with relaxation time $\tau = \tau_k$ will go for time t without making a collision is, from Sec. XII,

$$P_\tau(t) = e^{-t\langle 1/\tau\rangle} \tag{3.2}$$

where

$$\langle 1/\tau\rangle = t^{-1}\int_0^t dt'(1/\tau) \equiv R/\tau_{1/2} \tag{3.3}$$

with $\tau_{1/2}$ defined as the value of τ_k at $k = \frac{1}{2}k_{BZ}$. Values of R are calculated in Sec. XII. The value of t of interest here is the time required for an electron to

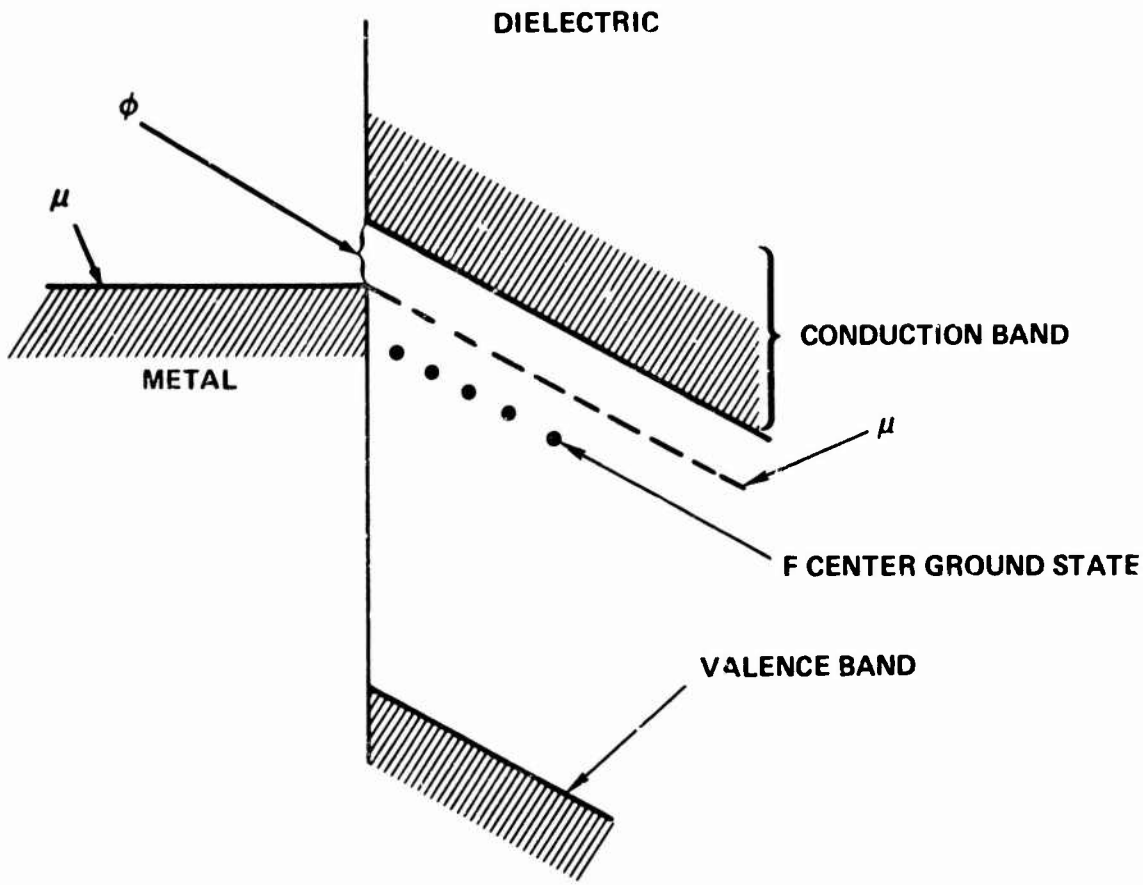

Fig. 4. Energy levels at the metal-dielectric interface showing the barrier ϕ. The barrier reduction $e^{3/2} n_r^{-1} E^{1/2}$ is not shown on the figure.

acquire energy $\mathcal{E}_{EL}$ (or $k = k_{EL}$). The relation between k and t for the time between collisions is determined by the equation of motion

$$dk_z/dt = e\,\mathrm{Re}\,E_{pk}\,e^{i(\omega t+\theta)}$$

where Re denotes the real part, and the general case of arbitrary ω is considered for additional use in Sec. IV. The solution with $k_z = 0$ at $t = 0$ is

$$k_z = \mathrm{Re}(e E_{pk}/i\hbar\omega)\, e^{i\theta}\left(e^{i\omega t} - 1\right)$$

$$= (e E_{pk}/\hbar\omega)\,[\sin(\omega t+\theta) - \sin\theta] \quad . \tag{3.4}$$

For the dc case, setting $\omega = \theta = 0$ and $E_{pk} = E$ gives $k_z = eEt/\hbar$. Substituting this result and (3.3) into (3.2) gives

$$P_\tau(k_{EL}) = \exp(-\hbar R k_{EL}/e\tau_{1/2}E) \quad . \tag{3.5}$$

After every collision, an electron has another "try" to gain the required wave vector k_{EL}. Thus, an electron makes t_ℓ/τ_{th} tries in time t_ℓ on the average, where t_ℓ is the time required for the electron to traverse the sample of length ℓ and τ_{th} is the value of τ_k for the electrons in thermal equilibrium. The value of $\ell = 3.2 \times 10^{-2}$ cm, which corresponds to $E_B = 1$ MV/cm in the experiments of Watson and coworkers,[10,2a] will be used here. The value of t_ℓ is related simply to the mobility μ by the relation

$$t_\ell = \ell/\mu_{th}E \tag{3.6}$$

where the subscript th denotes that the appropriate mobility is that of the electrons in thermal equilibrium (in the presence of the field). The number of electrons

that traverse the sample in time t is $(J/e)\,\mathcal{A}t$ where $\mathcal{A}$ is the area of cathode. The total number of tries N_t in time t is therefore

$$N_t = (J/e)\, V_s t / \tau_{th}\, \mu_{th} E$$

where $V_s = \mathcal{A}\ell$ is the volume of the sample exposed to the high field.

Setting the probability of success $N_t P_\tau(k_{EL})$ equal to one half[5] and using (3.1) and (3.5) gives

$$\frac{(J_0/e) V_s t}{\mu_{th} \tau_{th} E} \exp\left[- \left(\frac{\phi_{red}}{k_B T} + \frac{h R k_{EL}}{e \tau_{1/2} E} \right) \right] = \frac{1}{2} \qquad (3.7)$$

which is a transcendental equation for E, with k_{EL}, ϕ_{red}, and R functions of E according to (2.6), (3.1), and (3.3). A convenient form of (3.7) is obtained by taking the logarithm and using $(k_{EL}/\frac{1}{2}k_{BZ}) \cong 1.35\,(1\,\mathrm{MV\,cm^{-1}}/E)^{1/2}$, which is derived from (2.6), (8.38), and (8.39) with the small variation from the logarithm term neglected. The result is

$$\left(\frac{E}{1\,\mathrm{MV/cm}}\right) = \left[\frac{30.0 \left(\frac{R}{1.25}\right) \left(\frac{2.04 \times 10^{-15}\,\mathrm{sec}}{\tau_{1/2}} \right)}{14.6\,B - \ell n \left(\frac{E}{1\,\mathrm{MV/cm}}\right) + 10.12 \left(\frac{E}{1\,\mathrm{MV/cm}}\right)^{1/2} \left(\frac{1.5}{n_r}\right) \left(\frac{300\,K}{T}\right)} \right]^{2/3} \qquad (3.8)$$

for $E \gtrsim 1.97$ MV/cm (in other words, $k_{EL} > \frac{1}{2}k_{BZ}$). Here B is defined as

$$14.6\,B \equiv 53.4 + \ell n \left(\frac{T}{300\,K}\right)^2 \left(\frac{m}{m_f}\right)^2 \left(\frac{V_s}{6.6 \times 10^{-5}\,\mathrm{cm^3}}\right) \left(\frac{t}{10^{-6}\,\mathrm{sec}}\right) \left(\frac{20\,\mathrm{cm^2/V\,sec}}{\mu_{th}}\right)^2$$

$$- 38.8 \left(\frac{\phi_{red}}{0.97}\right) \left(\frac{300}{k_B T}\right) \quad . \qquad (3.9)$$

The simple numerical solution of (3.8) with R given by (12.7) and (12.8) gives E_B = 1.0 MV/cm for the NaCl case, which agrees with the experimental value[10,2a] of E = 1.0 MV/cm. There are no adjustable parameters in the theoretical result.

In setting the probability $N_t P_\tau(k_{EL})$ equal to 1/2 in (3.7), it is tacitly assumed that once an avalanche is started by getting one electron with $k = k_{EL}$, it will be sustained. The validity of this assumption is not known. However, it does seem plausible that the assumption is valid since the electron with $\mathcal{E} = \mathcal{E}_I$ is being accelerated rapidly because $(d\mathcal{E}/dt)_E >> (d\mathcal{E}/dt)_L$ at such high energy. In fact, it is shown at the end of the present section that it is likely that an electron with $\mathcal{E} = \mathcal{E}_I$ will be accelerated to $\mathcal{E} \cong \mathcal{E}_I + 4\,eV$ without suffering a τ_k collision. Hence, it is likely that its energy will be greater than $\mathcal{E}_I$ by more than a fraction of an electron volt at the time of the ionization process. If, for example, the energy is $\mathcal{E}_I + \delta\mathcal{E}$ with $\delta\mathcal{E} > 2\mathcal{E}_{EL}$, the excess energy $\delta\mathcal{E}$ will be shared by the original and newly generated conduction electrons. Then one or both of these electrons will have $k > k_{EL}$, depending on the value of $\delta\mathcal{E}$ and on what fraction of $\delta\mathcal{E}$ each electron receives. Notice that all that is required to sustain the avalanche is that more than one of the two electrons attain $k > k_{EL}$ on the average. It is important that this assumption of a sustaining avalanche be satisfied. If both electrons have $k << k_{EL}$ on the average, then E_B will be closer to the value E_{EL} = 3.07 MV/cm than to the smaller value of E = 1.0 MV/cm from (3.8).

The value of $t = 10^{-6}$ sec was chosen in (3.9) as a reasonable number. Fortunately, the value of E_B is insensitive to the value of t. For example, increasing t from 10^{-6} sec to one minute reduces E_B from 1.0 MV/cm to 0.82 MV/cm.

Another tacit assumption made in the derivation of (3.8) is that the sample is sufficiently thick for the avalanche to produce the required number of conduction electrons before the electrons are swept into the anode by the field. It can be shown that this condition is fulfilled in the present case in which $\ell = 3.2 \times 10^{-2}$ cm^{-1}. For thin samples, the condition is not satisfied, and the required time for the avalanche contributes to the increase in E_B with decreasing sample length, in addition to the contribution from $V_s = \alpha \ell$ in (3.8).

The dependence of the breakdown field E_B on temperature, sample length ℓ, and material parameters will be discussed in a subsequent report. Cursory investigations indicate that the present theory affords a satisfactory explanation of the experimental obs: vations. In particular, the theory appears to afford the first explanation o: .he increase in E_B with increasing temperature at low temperature followed by a decrease in E_B wi. increasing temperature at high temperature use.

Consider the probability that an electron with initial energy $\mathcal{E}_I$ will be accelerated to $\mathcal{E}_I + 4\,eV$ without collisions. From (3.2), the probability is

$$P = e^{-t_{nc}\langle 1/\tau_k \rangle} \tag{3.10}$$

where t_{nc} is the time required to increase $\mathcal{E}$ from $\mathcal{E}_I$ to $\mathcal{E}_I + 4\,eV$ in the absence of collisions. From (3.4) with k_I along the z axis and $E = 1\,MV/cm$

$$t_{nc} = \frac{\hbar(k - k_I)}{eE} = 2.13 \times 10^{-14}\ sec \tag{3.11}$$

where $k \equiv k_I + k_\delta = 1.78 \times 10^{18}\ cm^{-1}$ is the wave vector for $\mathcal{E} = \mathcal{E}_I + 4\,eV$ $= 12.1\,eV$. From (12.4) and (8.38)

$$\left\langle \frac{1}{\tau_k} \right\rangle = \frac{1}{\tau_I} \frac{1}{k_\delta} \int_{k_I}^{k_I + k_\delta} dk (k_I/k)^3$$

$$= \frac{1}{\tau_I} \frac{k_I}{2k_\delta} \left[1 - \frac{1}{(1+k_\delta/k_I)^2} \right] \quad . \tag{3.12}$$

With $\tau_I \equiv \tau_k(k = k_I) = 2.84 \times 10^{-14}\ \text{sec}^{-1}$ and $k_\delta/k_I = 0.222$, this gives

$$\langle 1/\tau_k \rangle = (3.82 \times 10^{-14}\ \text{sec})^{-1} \quad . \tag{3.13}$$

Substituting (3.11) and (3.13) into (3.10) gives

$$P = 0.572$$

which is large, as mentioned above.

It remains to be verified that $(d\mathcal{E}/dt)_L$ is negligible during this time:

$$\left(\frac{d\mathcal{E}}{dt}\right)_L t_{nc} = \frac{\hbar\omega_p t_{nc}}{\tau_L}$$

$$= 0.174\,\text{eV} \quad .$$

This value of 0.174 eV is negligible with respect to the 4 eV gained.

IV. BREAKDOWN AT 10 μm

In this section it will be shown that for electron-avalanche breakdown at the CO_2 laser frequency, the starting electrons are excited from F centers by multiphoton absorption and that the Holstein process, and possibly the lucky-reversing-electron process, are sufficient to accelerate the electron to $k_{EL} \cong \frac{1}{2} k_{BZ} \equiv k_{1/2}$ (or $\mathcal{E}_{EL} \cong 1.5\,eV$). It appears that the value of E_B at 10.6 μm at room temperature and below may be more accurate than other calculated values since the former depends only on the ratio τ_k / τ_L, rather than on the values of τ_k.

First consider the effect of the dependence of the relaxation frequencies on the electron wave vector. The value $E_{EL}(k)$ of E at which $(d\mathcal{E}/dt)_E = (d\mathcal{E}/dt)_L$ for a particular wave vector k is given by (2.6). The following values of parameters in (2.6) will be used: $\hbar\omega_p = 1/40$ eV, $\omega = 1.78 \times 10^{14}$ sec^{-1}, and, for $k > k_{1/2}$, $\omega^2 \tau_k^2 = 0.132\,(k/k_{1/2})^6$ and

$$\omega^2 \tau_k^2 = 0.132 \left(\frac{k}{k_{1/2}}\right)^6 \left(\frac{2.16}{2n_p+1}\right)^2 ,$$

and

$$\frac{\tau_k}{\tau_L} = 1.28 \frac{5.53}{5.53 + \ell n\, k/k_{1/2}} \left(\frac{2.16}{2n_p+1}\right) \left(\frac{k}{k_{1/2}}\right)^2 \qquad (4.1)$$

where the values of τ_k and τ_L are from Sec. VIII. With these values, (2.6) gives

$$E_{EL} = \left(\frac{1 + 0.132\,(k/k_{1/2})^6}{0.132\,(k/k_{1/2})^6} \frac{m}{m_f} \frac{5.53}{5.53 + \ell n\, k/k_{1/2}} \frac{2.16}{2n_p+1} \right)^{1/2}$$

$$\times \frac{k}{k_{1/2}}\ 0.760\ \text{MV/cm} \quad . \qquad (4.2)$$

The values of E_{EL} from (4.2) for $k > k_{1/2}$ and from (2.6) for $k = k_p$ at several values of k are: $E_{EL} = 5.71\,MV/cm$ at $k = k_p$; $E_{EL} = 1.93\,MV/cm$ at $k = k_{1/2}$; $E_{EL} = 1.52\,MV/cm$ at $k = k_{BZ}$; and $E_{EL} = 1.87\,MV/cm$ at $k = k_I = 1.46 \times 10^8\,cm^{-1} = 2.64\,k_{1/2}$. From these values it is seen that for $E_B = E_{EL}(k_I) = 1.87\,MV/cm$, E is greater than E_{EL} for $k_I > k > k_{EL} \cong k_{1/2}$. Thus, an average electron with $k \gtrsim k_{1/2}$ is accelerated to $k = k_I$, where it generates another conduction electron.

For this value of $E_B = 1.87\,MV/cm$, and $t_p \cong \frac{1}{3} 10^{-8}$ sec, there appears to be no difficulty in getting electrons across the barrier to $k_{EL} = k_{1/2}$ by any one of several processes. For example, the average values on the interval k_p to k_{EL} of the frequency for the Holstein process, in which an electron gains energy $\hbar\omega = 0.117\,eV$ is, from Sec. IX,

$$\omega_H = \left(\frac{E}{1.87\,MV/cm^{-1}} \right)^2 2.61 \times 10^{15}\,sec^{-1} \quad . \tag{4.3}$$

The time constant t_{1eV} for an electron with $\mathcal{E} = 1.5\,eV$ to lose its energy to the lattice is obtained by integrating (2.5), which gives

$$t_{1eV} = \frac{1.5\,eV}{\hbar\omega_p \langle 1/\tau_L \rangle} \quad . \tag{4.4}$$

Replacing the time average of $1/\tau_L$ by the average of k, as in Sec. XII, and using $1/\tau_L$ from Fig. 7 of Sec. VIII, gives, for the average on the interval k_p to $k_{1.5eV} \cong k_{1/2}$

$$\langle 1/\tau_L \rangle = 9.2 \times 10^{14}\,sec^{-1} = (1.09 \times 10^{-15}\,sec)^{-1} \quad . \tag{4.5}$$

Substituting (4.5) into (4.4) and using $\hbar\omega_p = 1/40$ eV gives

$$t_{1eV} = 6.52 \times 10^{-14} \text{ sec} \quad .$$

Since $t_{1.5\,eV}$ is greater than $13/\omega_H = 4.98 \times 10^{-15}$ sec, this estimate suggests that the Holstein process is sufficient to generate electrons with $k = k_{1/2}$.

The generation rate is $dn_c/dt = \omega_c n_c$, where $\omega_c \cong \omega_H/13 = 2.01 \times 10^{14}$ sec^{-1}, very roughly. This value of ω_c is well above the value $\omega_{c\,rqd}$ $= \ell n(n_c/n_{c0})/t_p \approx 10^9\ \text{sec}^{-1}$ (from Sec. XI) required to cause failure.

The lucky-reversing-electron process discussed in Sec. B also may be sufficient to take the electrons from k_p to $k_{1/2}$, although the result is marginal and the estimate is crude. Very briefly, the maximum value of k an electron can gain between collisions is the peak-to-peak value

$$2k_{pk} = \frac{2\sqrt{2}\,eE}{\hbar\omega} = \left(\frac{E}{1.87\ \text{MV/cm}}\right) \quad 4.53 \times 10^7\ \text{cm}^{-1} \tag{4.6}$$

from (3.4) with $E_{pk} = \sqrt{2}\,E_{RMS} \equiv \sqrt{2}\,E$. The value of $k_{1/2} - k_p$ is $5.55 \times 10^7 - 7.04 \times 10^6 = 4.85 \times 10^7\ \text{cm}^{-1}$. Thus, one process of gaining $k = 2p_k$ is sufficient to make $k = k_{EL}$, very roughly.

From (3.10) the probability of the electron going one-half cycle ($t = 1/2\nu$ $= \pi/\omega$) without a collision is

$$P_{\tau_k}(\pi/\omega) = e^{-(\pi/\omega)\langle 1/\tau_k\rangle} = 1.98 \times 10^{-5} \tag{4.7}$$

where the numerical values are for $\pi/\omega = 1.76 \times 10^{-14}$ sec and $\langle 1/\tau_k\rangle$ $= (1.63 \times 10^{-15}\ \text{sec})^{-1}$. For $\omega\tau_k \gg 1$, so that the electron makes at least

a complete cycle or two, the probability of scattering when E is near a peak ($|E| > 0.9\, E_{pk}$) is $2\cos^{-1}(0.9)/\pi = 0.287$. The number of tries in time t is $t/\tau_k = t/1.39\times10^{-15}$ sec. Setting the probability of success equal to one

$$0.287\ \frac{t_{p1}}{1.39\times10^{-15}}\ 1.98\times10^{-5} = 1$$

and solving for t gives $t_{p1} = 2.45\times10^{-10}$ sec. With

$$n_c = n_{c0}(2)^{t/t_{p1}}$$

$$= n_{c0}\, e^{\omega_c t}$$

the value of the ionization frequency ω_c is

$$\omega_c = 0.69/t_{p1} = 2.83\times10^{9}\ \text{sec}^{-1} \qquad (4.8)$$

which is approximately equal to the required value $\omega_{c\,rqd} = \ell n(n_c/n_{c0})/t_p$ $\cong \ell n\,(10^{18}/10^{7})/10^{-8} = 2.5\times10^{9}$ sec for $t_p = 10^{-8}$ sec.

It is not known if there will be a sufficient number of starting electrons. In the absence of this information, a rough estimate suggests that the number will be sufficient. The theoretical value for the two-photon ionization rate ω_{F2} in the expression

$$(dn_c/dt)_{F2} = \omega_{F2}\, n_F$$

where n_F is the F-center density is[11]

$$\omega_{F2} = \left(\frac{2\pi r_0 c f I}{\hbar\omega^2 n_r}\ \frac{m_f}{m}\right)^2 \frac{2\pi}{\Delta\omega}\, G(\omega) = 6.90\times10^{14}\ \text{sec} \qquad (4.9)$$

where $r_0 \equiv e^2/m_f c^2 = 2.82 \times 10^{-13}$ sec, f is an oscillator strength usually assumed to have the value $f \cong 1$, I is the intensity, n_r the index of refraction, $\Delta\omega \cong 0.46$ eV the line width, and $G(\omega)$ is the line-shape factor normalized to $G(\omega) = 1$ at the absorption peak. The numerical value displayed in (4.9) is for the case of I = 13.0 GW/cm (or E = 1.87 MV/cm), f = 1, $\omega = 1.78 \times 10^{14}$, $n_r = 1.5$, $m = \frac{1}{2} m_f$, $\Delta\omega = 0.46\,\text{eV} = 7.01 \times 10^{14}$ sec, and $G(\omega) = 1$.

For three-, four-, and higher-order photon processes, each additional order introduces a factor α of order

$$\alpha = \left(\frac{|\langle i|\mathcal{H}|j\rangle|}{\mathcal{E}_{ij}} \right)^2$$

$$= \left| \frac{eE}{im\omega} \right|^2 \frac{3}{2} \frac{f_{ij} m}{\mathcal{E}_{ij}} \qquad (4.10)$$

where the "$\underset{\sim}{A} \cdot \underset{\sim}{p}$" Hamiltonian is $\mathcal{H} = (e/mc)\, \underset{\sim}{p} \cdot \underset{\sim}{A} = (eE/m\omega)\, \hat{E} \cdot (-i\hbar\nabla)$ and f_{ij} is the oscillator strength for the transition from states $|i\rangle$ to $|j\rangle$. For a hydrogenic F center with[9] 2.7 eV between the first two levels, the spacing between levels two and three is $\mathcal{E}_{23} \cong 2.7 \left(\frac{1}{4} - \frac{1}{9}\right) \left(1 - \frac{1}{4}\right)^{-1} = 0.50$ eV. Approximating $\mathcal{E}_{ij}$ by $\mathcal{E}_{23}$ in (4.10) gives

$$\alpha = \left(\frac{E}{1.78\,\text{MV/cm}} \right)^2 \left(\frac{m}{\frac{1}{2} m_f} \right) \left(\frac{f_{23}}{0.25} \right) 0.29 \quad .$$

The value of the oscillator strength f_{23} for the 2-3 transition, which is expected to be slightly smaller than that of the 1-2 transition,[12] is assumed to have the value $f_{23} = 0.25$. For absorption to the value 2.2 eV in the NaCl F band (where $G(\omega) \cong 1/10$),[9] the number of photons is 2.2/0.117 = 19. Thus

$$\omega_{F19} \cong \omega_{F2} (\alpha)^{19-2} = 5.01 \times 10^{4}\ \text{cm}^{-1} \quad .$$

The number of carriers generated in time $t_p = \frac{1}{3} 10^{-8}$ sec is

$$n_c \cong n_F \omega_{F19} t_p = 8.34 \times 10^{9}\ \text{cm}^{-3}$$

which is a sufficient starting density.

It must be verified that there are starting electrons in the focal volume V_f. For

$$V_f = \frac{\pi}{4} \left(\frac{1}{3} 70 \times 10^{-4} \right)^3 10 = 1.0 \times 10^{-7}\ \text{cm}^{-3}$$

there are $nV_f = 834$ electrons in the focal volume, which is of course sufficient.

It should be mentioned that ω_{F19} is proportional to E^{38}; thus, a small reduction in E causes a great reduction in n_c. For example, a 20 percent reduction in E causes a factor of 2.1×10^{-4} reduction in n_c. Finally, when the electric field is so high that the higher-order processes have approximately the same values of ω_F as in the present case, the perturbation-theory results cannot be taken as exact, but only as an indication that the higher-order processes do have large values of ω_F.

The theoretical value of $E_B = 1.87$ MV/cm, obtained from the condition $E_B = E_{EL}$ at $\mathcal{E} = \mathcal{E}_I$, is in excellent agreement with the experimental value[13] of 1.95 ± 0.20 MV/cm.

V. BREAKDOWN AT 1.06 μm

It will be shown that the starting electrons are generated by two-photon absorption by the F centers and that these electrons gain energy $\mathcal{E} > \mathcal{E}_I$ by the Holstein process plus vertical inter-conduction-band transitions.

Consider the starting electrons. The case of a 10 nanosecond pulse length t_p is considered first; then the effect of changing t_p will be considered. The rate of generation of conduction electrons by the two-photon ionization of ground-state F centers is

$$(dn_c/dt)_{F2} = \omega_{F2} n_F \tag{5.1}$$

where n_F is the number of F centers per unit volume in the ground state and ω_{F2} from (4.8) can be written as

$$\omega_{F2} = \frac{f^2}{0.25} \left(\frac{E}{2.1\,MV/cm} \right)^4 \left(\frac{1.5}{n_r} \right)^2 \left(\frac{\lambda}{1.06\,\mu m} \right)^4 \left(\frac{m_f}{2\,m} \right)^2$$

$$\times \left(\frac{0.46\,eV}{\Delta\omega} \right) G(\omega)\ 2.74 \times 10^{10}\,sec^{-1} \quad . \tag{5.2}$$

where the product f^2 of the two oscillator strengths is taken as (1)(0.25) as discussed in Sec. IV. With $n_c + n_f = n_{c0} + n_{F0}$ from conservation of electrons, where the subscript zero denotes the time $t = 0$ at which the laser is turned on, (5.1) gives, with subscript F2 on dn_c/dt dropped

$$\frac{dn_c}{dt} = \omega_{F2} (n_{F0} + n_{c0}) - \omega_{F2} n_c \quad .$$

The solution

$$n_c \cong n_c - n_{c0} = n_{F0} \left(1 - e^{-\omega_{F2} t}\right) \qquad (5.3)$$

shows that n_c approaches n_{F0} exponentially with time constant $1/\omega_{F2}$, which has value $3.65 \times 10^{-10} (2.1\ \mathrm{MV\,cm^{-1}}/E)^4$ sec for the present example, with $G(\omega) = 1/10$ for NaCl at 300 K. Since this value of 3.65×10^{-10} sec is short with respect to the laser pulse duration of 10^{-8} sec, most of the F centers are ionized early in the pulse. Similarly, at $E = 12$ MV/cm, $1/\omega_c = 3.42 \times 10^{-13}$ sec is short with respect to the pulse duration of 1.5×10^{-11} sec. Thus, the number of starting electrons can be taken as the number of F centers n_{F0}.

In the subsequent multiplication process, the n_{F0} conduction electrons are assumed to be in thermal equilibrium (in the presence of the electric field). It can be shown that the electrons have energy $\mathcal{E} \ll \hbar\omega = 1.17$ eV, except for a few electrons in the tail of the distribution. These electrons gain the required ionization energy $\mathcal{E}_I$ as follows. For energies greater than ~3 eV, the vertical inter-conduction-band process discussed in Sec. X appears to be sufficient to increase $\mathcal{E}$ to $\mathcal{E}_I$. The value of 3 eV is attained by the Holstein process acting three times. These two processes are illustrated schematically in Fig. 5, where H denotes the Holstein process and V the vertical interband process. The phonon scattering P changes the direction of $\underset{\sim}{k}$ rapidly. The energy change $\hbar\omega_{L0}$ at each phonon scattering event is small with respect to $\hbar\omega = 1.17$ eV.

The first Holstein process generates electrons with $\mathcal{E} \cong \hbar\omega$ at the rate

$$dn_{\hbar\omega}/dt = \omega_H(k_B T)\, n_c \quad , \qquad (5.4)$$

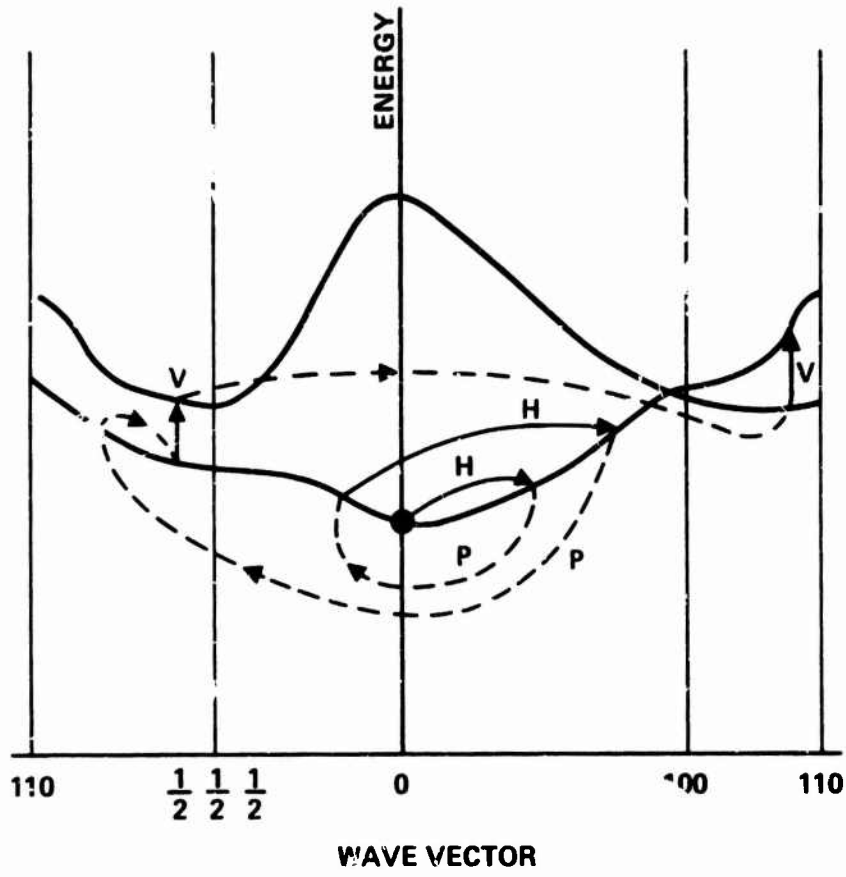

Fig. 5. Schematic illustration of the processes in which an electron gains energy $\mathcal{E} > \mathcal{E}_I$ by Holstein collisions H, vertical inter-conduction-band collisions V, and phonon collisions P.

where $\omega_H(k_BT)$ is the value of ω_H at $\mathcal{E} = k_BT = 1/40\,eV$, as considered in Sec. IX. These electrons with energy $\mathcal{E} \cong \hbar\omega$ have probability P_{+2} of being accelerated to $\mathcal{E} = 3\,eV$ by two subsequent Holstein events, where the value of P_{+2} can be estimated as follows. By integrating the probability $P_+ \equiv P_+^{(\tau)}(t) = 1 - \exp(-t/\tau) \cong t/\tau$ that an electron having collision frequency τ will have a collision in time $t \ll \tau$, it can be shown that

$$P_{+2} = 1 - (1 + t/\tau)\, e^{-t/\tau} \cong \frac{1}{2}(t/\tau)^2 \quad . \tag{5.5}$$

In general, $P_{+n} = (t/n)^n/n!$ is the probability that the electron will have n collisions in time $t \ll \tau$.

The value of t in (5.4) must be sufficiently short that the electron does not lose its energy to the lattice more rapidly than it gains the energy $n\hbar\omega$ in the Holstein collision process. In the initial and two subsequent Holstein processes the electron gains energy $3\hbar\omega = 3.5\,eV$. Thus, the value of t is chosen as the time $t_{1/2}$ required to lose $\frac{1}{2}\,eV$.

Combining (5.4) and (5.5), with $\tau = 1/\omega_H$ and $t = t_{1/2}$, gives

$$dn_c/dt = \omega_c n_c \tag{5.6}$$

with

$$\omega_c \cong \frac{1}{2}\,\omega_H(k_BT)\,\omega_H^2\,E_{1/2}^2 \tag{5.7}$$

An approximation to $t_{1/2}$ is obtained as for t_{1eV} in (4.4) by integrating the energy loss to the lattice, $(d\mathcal{E}/dt)_L$, in (2.5) to obtain

$$t_{1/2} = \frac{\frac{1}{2}\,eV}{\hbar\omega_{LO}\langle 1/\tau_L\rangle} \quad . \tag{5.8}$$

The average of $\langle 1/\tau_L\rangle$ on the interval $\mathcal{E} = 0.5$ to $2.5\,eV$, which is easily obtained from a numerical integration of the $1/\tau_L$ curve in Fig. 7 of Sec. VIII, is

$$\langle 1/\tau_L\rangle_{0.5\text{-}2.5\,eV} = 7.6 \times 10^{14}\,sec^{-1} \quad .$$

With $\hbar\omega_{LO} = 1/40\,eV$ in (5.8), this gives

$$t_{1/2} = 2.63 \times 10^{-14}\,sec \quad . \tag{5.9}$$

The average value of ω_H on the interval 0-2 eV is used, where the shift in the interval from that of $\langle 1/\tau_L\rangle$ is to account for the fact that the phonon collisions reduce the value of $\mathcal{E}$ after the increase by the Holstein process. (In a more rigorous treatment in progress, such arguments are taken into account automatically.) A numerical integration using the values given in Sec. IX gives

$$\langle \omega_H\rangle_{0\text{-}2\,eV} = \left(\frac{E}{2\,MV/cm}\right)^2 1.7 \times 10^{12}\,sec^{-1} \quad .$$

With these values and with $\omega_H(k_BT) = (E/2\,MV\,cm^{-1})^2\,1.43 \times 10^{12}\,sec^{-1}$, (5.7) gives

$$\omega_c = \left(\frac{E}{2\,MV/cm}\right)^6 1.43 \times 10^{9}\,sec^{-1} \quad . \tag{5.10}$$

Substituting (5.10) into (11.4) and solving for E_B gives

Sec. C

$$E_B = \left(\frac{10.9 + 4\,\ell n\,(E/2\ \mathrm{MV\,cm^{-1}})}{1.43 \times 10^9\, t_p} \right)^{1/6} . \qquad (5.11)$$

In obtaining (5.11), the following value of σ_{tot} from (11.2) and (11.5) was used:

$$\sigma_{tot} = \sigma_1 + \sigma_H = 1.01 \times 10^{-7} + 6.02 \times 10^{-8} = 1.61 \times 10^{-7}\ \mathrm{cm^3/sec} .$$

With $t_p = \frac{1}{3} \times 10^{-8}$ sec, where the factor of 1/3 is discussed in Sec. XIII, (5.11) gives $E_B = 2.30$ MV/cm, in good agreement with the experimental value[14] of 2.1 ± 0.4 MV/cm^2. Plots of this result along with results below are given in Sec. XIV.

The dependence of E_B on the laser pulse duration t_p can be obtained as follows. For $t_p = \frac{1}{3}\,(4.7 \times 10^{-9}\ \mathrm{sec})$, (5.11) gives

$$\frac{E_B(4.7 \times 10^{-9}\ \mathrm{sec})}{E_B(10^{-8}\ \mathrm{sec})} = 1.11$$

in agreement with the experimental value[14] of 1.1 ± 0.05.

For $t_p = \frac{1}{3}\,(3 \times 10^{-10}\ \mathrm{sec})$, (5.11) gives

$$E_B = 4.3\ \mathrm{MV/cm}$$

again in good agreement with the experimental value[15] of 4.7 ± 0.4 MV/cm.

At $t_p = \frac{1}{3}\,(3.0 \times 10^{-11}\ \mathrm{sec})$, (5.11) gives

$$E_B = 6.41\ \mathrm{MV/cm}$$

compared with $E_B = 7.35$ MV/cm from experiment.[16] Finally, at $t_p = \frac{1}{3}(1.5 \times 10^{-11}\,\text{sec})$, (5.11) gives

$$E_B = 7.24 \text{ MV/cm}$$

which is in poor agreement with the experimental value[14] of 12.4 ± 3.7.

There are a number of possible reasons for the poor agreement at the shortest pulse duration of 15 psec. The most likely reason at present appears to be that the value of ω_c becomes limited by the inter-conduction-band processes. The number p_I of electron-phonon collisions (τ_L collisions) that the electron undergoes during the time required for its energy to be increased from 3 eV to $\mathcal{E}_i \cong 8$ eV is equal to the number of inter-conduction-band transitions

$$\frac{(8-3)\text{eV}}{1.17\,\text{eV}} \quad \frac{1}{1-r}$$

times the number of collisions per inter-conduction-band transition

$$\frac{1.17\ \text{eV}}{(1/40)\text{eV}}\ r$$

where r is the fraction of the gained energy $\hbar\omega$ that is lost to the phonons between two vertical transitions, on the average. Thus

$$p_I = \frac{200\,r}{(1-r)} \quad . \tag{5.12}$$

The time $1/\omega_{cV}$ required to make these p_I collisions is $p_I \langle \tau_L \rangle_{3\text{-}8}$ with $\langle \tau_L \rangle_{3\text{-}8} = 2.13 \times 10^{-15}$ sec:

$$\frac{1}{\omega_{cV}} = \frac{4.26 \times 10^{-13}\,r}{(1-r)} \quad . \tag{5.13}$$

Since the Holstein and interband processes are in series, the inverse relaxation frequencies are added:

$$\frac{1}{\omega_{c\,net}} = \frac{1}{\omega_{cH}} + \frac{1}{\omega_{cV}} \tag{5.14}$$

where ω_c in (5.10) has now been written as ω_{cH}. Substituting (5.14) into (11.4) gives

$$\frac{1}{1.43\times10^{9}\,t_p}\left(\frac{2\,MV/cm}{E_B}\right)^{6} + \frac{4.26\times10^{-13}\,r}{t_p(1-r)} = \ell n\left[\frac{CT}{n_{c0}\sigma_{tot}E_B^2(1/\omega_{c\,net})}\right] . \tag{5.15}$$

Unfortunately, the value of r is unknown. In the absence of this value, it will be assumed that $r = \frac{1}{2}$. This value appears to be reasonable. An electron then loses half the energy gained in an inter-conduction-band collision before it suffers another such collision.

A simple numerical solution of (5.15) with $r = \frac{1}{2}$ shows that E_B becomes very large as t_p approaches a value slightly less than $\frac{1}{3}(1.5\times10^{-11})$ sec, and that

$$E_B = 7.9\ MV/cm$$

for $t_p = (3.0\times10^{-11})$, and

$$E_B = 4.45\ MV/cm$$

for $t_p = \frac{1}{3}(3\times10^{-10})$ sec. For the smaller values of t_p considered above, E_B is unchanged. The agreement between these theoretical and experimental results is excellent, as seen in Fig. 9 of Sec. XIV.

VI. BREAKDOWN AT 0.694 μm

At the ruby-laser frequency, the starting electrons are generated by five-photon absorption across the gap, which is a faster process than two-photon absorption by F centers. The starting electrons are accelerated to $\mathcal{E} \cong 3\,\text{eV}$ by the Holstein process acting twice. Then the vertical inter-conduction-band process accelerates the electrons to $\mathcal{E} = \mathcal{E}_I$, as at 1.06 μm.

Braunlich and coworkers[17] made a computer calculation of the number of conduction electrons generated in NaCl at the ruby-laser and doubled-ruby-laser frequencies with $10^{10}\,\text{cm}^{-3}$ starting-electron density and compared their results to data[14] obtained at 1.06 μm. Starting with the semiempirical curve of $1/t_p(E)$ obtained[14] from a fit to the data, they showed that t_p^{-1} was increased by including multiphoton ionization and decreased by using the damage criterion that the temperature be raised to the melting point rather than that n_c be increased to $10^{18}\,\text{cm}^{-3}$. The net result was a curve of $1/t_p(E)$ that fit the data as well as the original semiempirical curve. The significance of the work was in showing that including multiphoton absorption decreased the value of E_B by approximately $\sqrt{2}$.

The analysis below suggests that had the initial electron density been set equal to zero, there would have been little change in the value of E_B. In the present theory the major role of the multiphoton process is this generation of starting electrons.

A simple estimate below indicates that the two-photon absorption by F centers is not sufficiently rapid to ionize a substantial fraction of the F centers during a 10 nsec pulse. Thus, (5.1) can be approximated by

$$(dn_c/dt)_{F2} \cong \omega_{F2} n_{F0} \tag{6.1}$$

where n_{F0} is the number of F centers at time $t = 0$. With this two-photon generation process, the five-photon generation process, and the two-Holstein-plus-vertical avalanche process, the rate of change of n_c is

$$dn_c/dt = \dot{n}_5 + \omega_c n_c \tag{6.2}$$

where

$$\omega_c \cong \omega_H(k_B T)\, \omega_H(1.79\text{eV})\, t_{1/2}(1.79\text{eV}) \tag{6.3}$$

and

$$\dot{n}_5 \equiv \omega_{F2} n_{F0} + \frac{1}{5} \omega_5 n_v$$

where the five-photon term has the value[17,18] $\frac{1}{5}\omega_5 n_v = \frac{1}{5} 1.12 \times 10^{-119} (I/\hbar\omega)^5$ $= 1.20 \times 10^{24} (E/2\ \text{MV/cm}^{-1})^{10}$. From (5.2) with $G(\omega) \approx \{1 + [2(1.786)/1.94]^4\}$ $= 4.33 \times 10^{-4}$, where 1.94 eV is the depth of the F center in NaCl, and n_{F0} $= 5 \times 10^{13}\ \text{cm}^{-3}$ from Sec. D, the value of $\omega_{F2} n_{F0}$ is $2.04 \times 10^{22} (E/2\ \text{MV/cm}^{-1})^4$. Thus

$$\dot{n}_5 = [1.20 \times 10^{24} (E/2\ \text{MV cm}^{-1})^{10} + 2.04 \times 10^{20} (E/2\ \text{MV cm}^{-1})^4]\ \text{cm}^{-3}\text{sec}^{-1}. \tag{6.4}$$

The second (F center) term in (6.4) is negligible with respect to the first (five-photon ionization) term for values of E of interest.

The solution to (6.2) with $n_c = 0$ at $t = 0$ is

$$n_c = (n_5/\omega_c)\left(e^{\omega_c t} - 1\right) \quad . \tag{6.5}$$

Replacing $n_c = n_{c0}\exp(\omega_c t)$ in Sec. XI by (6.5) and repeating the simple integration gives

$$\omega_c t_p = \ell n\left(\frac{CT\omega_c^2}{\dot{n}_5 \sigma_{tot} E^2} + 1 + \omega_c t_p\right) \quad . \tag{6.6}$$

The factors 1 and $\omega_c t_p$ in the logarithm usually are negligible. Setting ω_c from (6.3) equal to ω_c in (6.6) and using $\omega_H(k_B T) = 3.32\times10^{11}\,(E/2\ \mathrm{MV\,cm^{-1}})^2\ \mathrm{sec^{-1}}$ and $\omega_H(1.79) = 4.46\times10^{11}\,(E/2\ \mathrm{MV\,cm^{-1}})\,\mathrm{sec^{-1}}$ from (9.19) and (9.27) and $t_{1/2}(1.79\,\mathrm{eV}) = 3.26\times10^{-14}$ sec from (5.10) and $\sigma_{tot} = \sigma_1 + \sigma_H = 4.72\times10^{-8} + 2.14\times10^{-8} = 6.86\times10^{-8}\ \mathrm{cm^3/sec}$ from (11.2) and (11.5) and $t_p = \frac{1}{3}\times10^{-8}$ sec gives

$$\omega_c = (E/2\ \mathrm{MV\,cm^{-1}})^4\ 4.82\times10^9\ \mathrm{sec^{-1}}$$

and

$$E = \left(\frac{11.4 - 4\,\ell n\,(E/2)}{16.1}\right)^{1/4} \tag{6.7}$$

which has the solution $E_B = 1.85$ MV/cm. The agreement with the experimental value of $2.2 + 0.44$ MV/cm is satisfactory.

VII. BREAKDOWN AT 172 nm (7.21 eV)

The electron-avalanche breakdown process and other failure mechanisms in lithium fluoride at the xenon-laser frequency are considered in Sec. D. The results for avalanche breakdown are, very briefly, as follows. The starting electrons are generated by two-photon absorption across the gap. The electron energy is increased to $\mathcal{E} \geq \mathcal{E}_I$ by one Holstein event plus one vertical inter-conduction-band transition. The resulting value of E_B is

$$E_B = 0.56 \text{ MV/cm}$$

which corresponds to intensity

$$I = 1.6 \text{ GW/cm}^2 \quad .$$

The result is shown on the same figure with the NaCl results in the following section. However, the difference in material parameters of the two materials, as well as the frequency difference, contributes to the difference in the value of E_B.

VIII. ELECTRON-PHONON RELAXATION FREQUENCIES

The electron-phonon interaction will be considered in somewhat greater detail than in previous treatments.[19,20] In a polar crystal the interaction between the electrons and the longitudinal-optical phonons is quite strong.[19] Seitz[3] has pointed out that the coupling to coustical phonons probably is not negligible, especially for electrons with energy[3] $\mathcal{E} \cong \frac{1}{4}\mathcal{E}_{BZ}$, where $\mathcal{E}_{BZ}$ is the average electron energy for wave vectors at the Brillouin-zone boundary. Both of these processes will be considered, and both the relaxation frequency $1/\tau_\Lambda$, which determines the electron mean free path (for any scattering angle), and $1/\tau_k$, which is the large-scattering angle or transport relaxation frequency, will be calculated. The value of the relaxation time τ_L, which determines the energy transfer to the lattice, is related to τ_Λ by the simple relation $\tau_L = (2n_p + 1)\tau_\Lambda$.

In Ref. 3, the maximum values of the acoustical-phonon relaxation frequencies occurred at $\mathcal{E}_{BZ}$ rather than $\frac{1}{4}\mathcal{E}_{PZ}$. The arithmetic in Ref. 3 appears to be the same as that below. Thus, the source of the factor of four difference is unknown. The difference is rather important since extending the peak to $\mathcal{E}_{BZ}$ increases the value of $1/\tau_k$ in the region $\mathcal{E} > \frac{1}{4}\mathcal{E}_{BZ}$, which causes substantial changes in the value of E_B in some cases.

The coupling of the electrons to the longitudinal-optical phonons arises from the energy of the electron in the electric field of these phonons resulting from the relative longitudinal displacement of the positive and negative charges. Only the longitudinal component of the ion motions generates an electric field

because the source term $-4\pi \nabla \cdot \underset{\sim}{P}$ in the equation for the field $\nabla \cdot \underset{\sim}{E}_p = -\nabla^2 \phi = -4\pi \nabla \cdot \underset{\sim}{P}$, where $\underset{\sim}{P}$ is the dipole moment per unit volume, does not vanish for these modes. The Hamiltonian is

$$\mathcal{H} = e\phi(r) \tag{8.1}$$

where the scalar field $\phi(r)$ is determined by the relations

$$\underset{\sim}{E}_p = -\nabla\phi \tag{8.2}$$

$$\nabla \cdot (\underset{\sim}{E} + 4\pi \underset{\sim}{P}) = 0 \tag{8.3}$$

and

$$\underset{\sim}{P} = e(\underset{\sim}{u}_+ - \underset{\sim}{u}_-) N_+ \tag{8.4}$$

where $\underset{\sim}{u}_\pm$ are the displacements of the positive and negative ions and N_+ is the number of ion pairs per cubic centimeter.

The solution to (8.3) for longitudinal modes, for which $\nabla \cdot \underset{\sim}{P} \neq 0$ as already mentioned, is easily shown to be

$$\underset{\sim}{E} = -4\pi \underset{\sim}{P} \quad . \tag{8.5}$$

The well known phonon expansion of the displacements is

$$\underset{\sim}{u}_\pm(\underset{\sim}{r}) = \sum_{\underset{\sim}{q}} (\hbar / 2 N_+ V M_\pm \omega_q)^{1/2} \, \underset{\sim}{u}_{\pm q} A_q e^{i \underset{\sim}{q} \cdot \underset{\sim}{r}} \tag{8.6}$$

where $\underset{\sim}{q}$ is the phonon wave vector, $M_\pm$ are the ion masses, $A_q = a_q + a^\dagger_{-q}$ with the a's and $a^\dagger$'s phonon annihilation and creation operators, and ω_q are the phonon frequencies. Substituting (8.1) and (8.4) into (8.5) gives $\underset{\sim}{E}$. Then, since all of the spatial dependence of the n's is in the factors $\exp(i \underset{\sim}{q} \cdot \underset{\sim}{r})$ and the

modes are longitudinal ($\hat{u}_{\pm q} = \hat{q}$, where $\hat{}$ denotes unit vector), ϕ is obtained from E_{p} simply by replacing $\hat{u}_{\pm q}$ in each term by $(iq)^{-1}$, which gives

$$\mathcal{K} = \sum_{q} B_q A_q e^{i\underset{\sim}{q} \cdot \underset{\sim}{r}} \tag{8.7}$$

where

$$B_q \equiv -i4\pi e^2 N_+ (\hbar/2 N_+ V M q^2 \omega_q)^{1/2} U_q$$

and $U_q M^{-1/2}$ is defined by the relation

$$\left| M_+^{-1/2} \underset{\sim}{u}_{+q} - M_-^{-1/2} \underset{\sim}{u}_{-q} e^{i\underset{\sim}{q} \cdot \underset{\sim}{\delta}} \right| \equiv M^{-1/2} \quad . \tag{8.8}$$

Here $\underset{\sim}{\delta}$ is the basis vector. For $q\delta \ll 1$, $\underset{\sim}{u}_{\pm q} = (M_r / M_{\pm})^{1/2} \hat{u}_{+q}$, where M_r is the reduced mass, $M_r^{-1} = M_+^{-1} + M_-^{-1}$. Then $M^{-1/2} = M_r^{-1/2}$. At the zone edge along (111) for the optical modes, $|\underset{\sim}{u}_{\pm q}|$ is equal to unity for the smaller mass M_s and zero for the greater mass M_g. Then $M^{-1/2} = M_s^{-1/2}$. In general M is of the order of an atomic mass of the crystal.

As discussed in Sec. II, the two processes in which the electron scattering is accompanied by emission and absorption of phonons must be considered. The relaxation frequencies $1/\tau_e$ and $1/\tau_a$ for the two processes, that is the probabilities per unit time that the processes will occur, are

$$1/\tau_{a,e} = 2\pi\hbar^{-1} \sum_{q} \sum_{k_f} |\langle n_q \mp 1 | \mathcal{K} | n_q \rangle|^2 \delta(\mathcal{E}_{a,e}) \tag{8.9}$$

where n_q are the phonon occupation numbers, k_f is the wave vector of the final electron, and $\mathcal{E}_{a,e} = \mathcal{E} - \mathcal{E}_f \pm \hbar\omega_q$, with $\mathcal{E}$ and $\mathcal{E}_f$ the initial and final electron

energies. The electron wave vectors were not written out in the matrix elements. The integrals in the matrix elements vanish unless wave vector is conserved, as usual, thus eliminating the sum on $\underset{\sim}{k}_f$. There are no factors of two from electron spin in (8.9) since the interest is in the electron. In calculating the total energy flow into the lattice, a factor of two would arise because the contribution from all electrons (having both spins) must be included. In either case, the matrix elements are diagonal in spin. The numerical factor agrees with that of Frölich,[19] where $N_+ = 1/2\ a_{nn}^3$ for the rocksalt structure.

The delta function in (8.9) can be cast into a useful form as follows:

$$\mathcal{E}_{a,e} = \mathcal{E}(k) - \mathcal{E}(k_f) \pm \hbar\omega_{LO}$$

where ω_{LO} is the average of ω_q (which varies only slightly with q) in the sum on q in (8.9). Since k_f is a function of u, where u is defined as the cosine of the angle θ between $\underset{\sim}{k}$ and $\underset{\sim}{q}$, then $\mathcal{E}_{a,e} = f(u)$, and

$$\delta[f(u)] = \frac{1}{\left|df/du\right|_{u_0}}\,\delta(u - u_0) \quad , \tag{8.10}$$

where $df/du = d\mathcal{E}_{a,e}/du = -d\mathcal{E}(k_f)/du$, with

$$\frac{d\mathcal{E}(k_f)}{du} = \frac{dk_f}{du}\,\frac{d\mathcal{E}(k_f)}{dk_f} \quad . \tag{8.11}$$

With $k_f = \left|\underset{\sim}{k} \pm \underset{\sim}{q}\right| = (k^2 \pm 2kqu + q^2)^{1/2}$, (8.10) and (8.11) give

$$\delta(\mathcal{E}_{a,e}) = \frac{m_k}{\hbar^2 kq}\,\delta(u - u_{a,e}) \tag{8.12}$$

where m_k is defined by the relation

$$\frac{1}{k}\ \frac{d\mathcal{E}(k)}{dk} \equiv \frac{\hbar^2}{m_k}$$

and $u_{a,e}$ are the roots of

$$\mathcal{E}(k) - \mathcal{E}[k_f(u)] \pm \hbar\omega_{LO} = 0 \quad . \tag{8.13}$$

For electrons whose energies near the center of the Brillouin zones, $\mathcal{E} = \hbar^2 k^2/2m_k$, and the roots of (8.13) are easily found to be

$$u_{a,e} = \frac{k_p^2 \mp q^2}{2kq} \quad , \qquad k_p^2 \equiv 2m_k\omega_{LO}/\hbar \tag{8.14}$$

Notice that u_e is always positive; thus the emission process scatters only in the forward hemisphere. Also, an electron with $k = k_p$ has energy $\mathcal{E} = \hbar\omega_{LO}$.

For electrons with $\mathcal{E} \gg \hbar\omega_p$, define $k_f = k + \Delta k$, then

$$\mathcal{E}(k_f) = \mathcal{E}(k + \Delta k) \cong \mathcal{E}(k) + \Delta k\, d\mathcal{E}/dk \quad .$$

Then

$$\mathcal{E}_{a,e} = -\Delta k\, d\mathcal{E}/dk \pm \hbar\omega_p \quad . \tag{8.15}$$

Since $\Delta k \ll k$ for $\mathcal{E} \gg \hbar\omega_p$, the approximation

$$k_f = (k^2 \pm 2kqu + q^2)^{1/2} \cong k + \Delta k$$

where

$$\Delta k = \pm qu + \frac{1}{2} q^2/k \tag{8.16}$$

is well satisfied. Substituting (8.16) into (8.15) and solving for $u_{a,e}$ gives (8.14) again. Since one of the approximations $\mathcal{E} \cong \hbar^2 k^2 / 2 m_k$ or $\mathcal{E} >> \hbar\omega_p$ is always satisfied in the current case, (8.14) can be used everywhere.

Substituting (8.12) and (8.7) into (8.9) and assuming that $\omega_q \equiv \omega_{LO}$ = constant and that M is constant gives, for this case of optical phonons

$$\frac{1}{\tau_{a,e}} = \frac{4\pi e^4 m_k N_+ n_{a,e} F_{a,e}}{\hbar^2 \omega_{LO} M k} \qquad (8.17)$$

where $n_a \equiv n_p$, $n_e \equiv n_p + 1$, and

$$F_{a,e} = \int_0^{k_{BZ}} dq\, q^{-1} \int_{-1}^{1} du\, \delta(u - u_{a,e})$$

where the first Brillouin zone has been approximated by a sphere of radius k_{BZ}.

Using

$$\int_{-1}^{1} du\, \delta(u - u_{a,e}) = 1 \qquad \text{for } |u_{a,e}| < 1$$

$$= 0 \qquad \text{for } |u_{a,e}| > 1$$

gives

$$F_{a,e} = \int_{q_{a,e}^{(\ell)}}^{q^{(u)}} dq\, q^{-1} \quad , \qquad (8.18)$$

where

$$q^{(u)} \equiv \text{lesser of } \left(k_{BZ},\ q_{a,e}^{(u)} \right) \quad . \qquad (8.19)$$

With $u_a = \pm 1$, (8.14) gives

$$u_a^{(u)}/k = (1+x)^{1/2} \pm 1 \quad , \tag{8.20a}$$

where $x \equiv k_p^2/k^2$ and the two roots of (8.14) for $u_e = +1$ are

$$u_e^{(u)}/k = 1 \pm (1-x)^{1/2} \tag{8.20b}$$

For $k^2 \gg k_p^2$, (8.20a) and (8.20b) give the same result

$$q^{(u)} \cong \text{lesser of } (2k, k_{BZ}) \qquad q^{(\ell)} \cong k_p^2/2k \quad . \tag{8.21}$$

Then,

$$F_a \cong F_e \cong \ell n\, 4k^2/k_p^2 \quad , \qquad \text{for } k < \tfrac{1}{2} k_{BZ} \quad , \tag{8.22}$$

and

$$F_a = F_e = \ell n\,(2k\, k_{BZ}/k_p^2) \quad . \qquad \text{for } k > \tfrac{1}{2} k_{BZ} \quad . \tag{8.23}$$

Next consider the relaxation time τ_k, which is the average time required for the component of $\underset{\sim}{k}$ along $\underset{\sim}{E}$ to be reduced by a factor of $1/e$. The values of $1/\tau_a$ and $1/\tau_e$ above are important in determining the value of $(d\mathcal{E}/dt)_L$ and the collision rates $1/\tau_a \pm 1/\tau_e$. The field can put energy into the electrons more rapidly for forward scattering than for isotropic scattering. Thus, the angle dependence of the scattering must be considered, which leads to this

transport collision frequency $1/\tau_k$. Before considering Frölich's treatment of $1/\tau_k$, a simple argument is instructive. From the expression

$$\left(\frac{d\mathcal{E}}{dt}\right)_E = \left(\frac{dk_z}{dt}\right)_E \frac{dk}{dk_z} \frac{d\mathcal{E}}{dk}$$

with $dk/dk_z = k_z/k$, $k^{-1}d\mathcal{E}/dk \equiv \hbar^2/m_k$, and $dk_z/dt = eE/\hbar$, where the electric field is along the z direction, and $dk_z/dt = eE/\hbar$, there results

$$(d\mathcal{E}/dt)_E = (e\hbar E/m_k)k_z \quad . \tag{8.24}$$

For isotropic scattering, $k_z = 0$ on the average after each collision; thus the average value of k_z is the average value $eE\tau_{iso}/2\hbar$ between collisions, and (8.24) gives the well known result $(e^2\tau_k/m_k)E^2$ with $\tau_k = \frac{1}{2}\tau_{iso}$. If the collisions are not isotropic, the component of momentum δk_z gained between collisions is not entirely lost in the collision. In the extreme case of an electron traveling along the z axis with absolutely forward scattering ($\underset{\sim}{k}$ remaining along z), $k_z = k$, where $k >> eE\tau/2\hbar$ in general. With absolutely forward scattering, an electron not originally traveling in the z direction will approach the z direction since the momentum gained from the field between collisions is in the z direction.

The following treatment, which is equivalent to that of Frölich,[19] accounts for nonisotropic scattering by calculating the relaxation frequency $1/\tau_k$ for the z component k_z of $\underset{\sim}{k}$. If the previous expression (8.17) for $1/\tau_{a,e}$ is written as

$$1/\tau_{a,e} = \int d\underset{\sim}{q}\, \Phi_{a,e}(q)$$

where $\Phi_{a,e} \equiv \Phi n_{a,e}\, \delta(u - u_{a,e})$, with

$$\Phi \equiv \frac{2e^4 m_k N_+}{\hbar^2 \omega_{LO} M k q^3}$$

then

$$(dk_z/dt)_{coll} \equiv -k_z/\tau_k = \int d\underset{\sim}{q}\, (\Delta k_{za} \Phi_a + \Delta k_{ze} \Phi_e) \tag{8.25}$$

where $\Delta k_{z\,a,e}$ are the mean changes in k_z in a collision. Since $\underset{\sim}{k}_f = \underset{\sim}{k} \pm \underset{\sim}{q}$, the change $\Delta \underset{\sim}{k}_{a,e}$ in $\underset{\sim}{k}$ is $\pm \underset{\sim}{q}$. The polar axis in $\underset{\sim}{q}$ space is chosen along $\underset{\sim}{k}$. Since $\Phi_{a,e}$ is independent of ϕ, the integral of $\Delta k_{z\,a,e}$ over ϕ can be performed independently of $\Phi_{a,e}$. As illustrated in Fig. 6 for the case of absorption, the average $\langle \underset{\sim}{q} \rangle_\phi = q \cos\theta \hat{k}$, and the z component is $\langle q_z \rangle_\phi = (q k_z/k) \cos\theta$. This result also can be obtained from the identity

$$\hat{q} \cdot \hat{E} \equiv \cos\theta_{qE} = \cos\theta_{qk} \cos\theta_{Ek} + \sin\theta_{qk} \sin\theta_{Ek} \cos(\phi_{qk} - \phi_{Ek})$$

since the integral over $\phi = \phi_{qk}$ of $\cos(\phi_{qk} - \phi_{Ek})$ vanishes.

For the case of current interest in which $k \gtrsim 2k_p$, the integrands $\Phi_{a,e}$ become equal, apart from the factors $n_p + 1$ and n_p, and (8.25) gives

$$1/\tau_k = 2\pi \int_{-1}^{1} du \int_0^{k_{BZ}} dq\, q^2 \Phi [(-qu/k)\, n_p\, \delta(u + u_a)$$

$$+ (+qu/k)(n_p + 1)\, \delta(u + u_e)] \tag{8.26}$$

where

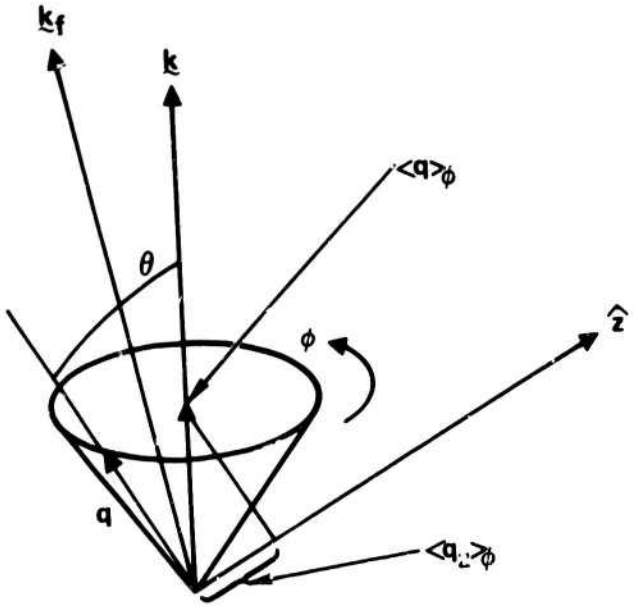

Fig. 6. Construction illustrating the average value of $\langle \underset{\sim}{q} \rangle_\phi = \hat{k}\, q \cos\theta$.

$$u_{a,e} = \mp \frac{q}{2k} + \frac{k_p^2}{2kq}$$

from (8.14). Since $k_p^2 \ll k_{BZ}^2$ and the extra factor of q^2 weights the large value of q, the second term in (8.27) can be neglected, and (8.26) gives

$$1/\tau_{k0} = 2\pi \int_{q^{(\ell)}}^{q^{(u)}} dq\, q^2\, (q^2/2k^2)\,(2n_p + 1)\,\Phi$$

$$= \frac{C(2n_p + 1)\, k_{BZ}}{2k^3} \left[\left(q^{(u)}\right)^2 - \left(q^{(\ell)}\right)^2 \right] \qquad (8.28)$$

where the subscript 0 was added to $1/\tau_k$ to denote the optical-mode interaction, and

$$C = \frac{8\pi e^4 m_k N_+}{\hbar^2 \omega_{LO} M k_{BZ}} \equiv 1.13 \times 10^{14}\ \text{sec}^{-1} \quad . \qquad (8.29)$$

The numerical value is for the case of $m_k = 0.75\, m_f$, $M = M_s = 3.84 \times 10^{-23}$ g, $N_+ = 2.23 \times 10^{22}\ \text{cm}^{-3}$, and $\hbar\omega_p = 1/40$ eV. The extra factor q^2/k^2 in (8.28) accounts for the nonisotropic scattering. With $\left(q^{(\ell)}\right)^2 \ll \left(q^{(u)}\right)^2$ and $q^{(u)}$ = lesser of $(2k, k_{BZ})$, (8.28) gives for the optical-mode interaction

$$1/\tau_{k0} = C(2n_{LO} + 1)\, k_{BZ}/2k \qquad \text{for } k < \tfrac{1}{2} k_{BZ}$$

$$= C(2n_{LO} + 1) = (4.08 \times 10^{-15}\ \text{sec})^{-1} \qquad \text{for } k = \tfrac{1}{2} k_{BZ}$$

$$= C(2n_{LO} + 1)\, k_{BZ}^3/(2k)^3 \qquad \text{for } k > \tfrac{1}{2} k_{BZ} \quad . \qquad (8.30)$$

This can be compared with the previous results (8.17), (8.22), (8.23), and $\tau_L^{-1} = \tau_a^{-1} - \tau_e^{-1}$, which can be written as

$$
\begin{aligned}
1/\tau_{LO} &= 2C \ln(2k/k_{LO})\, k_{BZ}/2k && \text{for } k < \tfrac{1}{2}k_{BZ} \\
&= 2C \ln(k_{BZ}/k_{LO})(1.60\times 10^{-15}\ \text{sec})^{-1} && \text{for } k = \tfrac{1}{2}k_{BZ} \\
&= C \ln(2k\,k_{BZ}/k_{LO}^2)\, k_{BZ}/2k && \text{for } k > \tfrac{1}{2}k_{BZ} \qquad (8.31)
\end{aligned}
$$

where the numerical value is for NaCl with the same parameters used for (8.30). For small k, the scattering is fairly isotropic, and (8.30) and (8.31) give approximately the same result for τ_k and $\tau_\Lambda = \tau_{LO}(2n_{LO}+1)^{-1}$ (within a factor of ~ 3). For $k > \frac{1}{2}k_{BZ}$, the scattering is more in the forward direction, and τ_k becomes considerably longer than τ_Λ (by the factor $(k/k_{BZ})^2 \ln(2k\,k_{BZ}/k_p^2)$). For forward scattering, it takes longer to turn $\underset{\sim}{k}$, that is to reduce $\mathcal{E}$ by $\hbar\omega_{LO}$.

The corresponding results for the acoustical-mode interaction can be obtained as follows. The deformation-interaction Hamiltonian[7] is taken as $\mathcal{H} = \mathcal{E}_1 \nabla \cdot \underset{\sim}{u}$, where $\mathcal{E}_1$ is a constant with dimensions of energy that is believed to be of order of a few electron volts and $\underset{\sim}{u}$ is the lattice displacement. In the small wave-vector limit $qa \ll 1$, $\underset{\sim}{u}_{\pm q}$ in (8.6) are well approximated by $u_{\pm q} = (M_\pm/M_{dp})^{1/2}\,\hat{u}q$, where $M_{dp} = M_\Sigma \equiv M_+ + M_- = M_s + M_g$. Then (8.6) reduces to the well known result

$$
u = u_+ = u_- = \sum_q (\hbar/2N_+ V M_{dp}\omega_{LA})^{1/2}\, \hat{u}_q A_q e^{i\underset{\sim}{q}\cdot\underset{\sim}{r}} \qquad (8.32)
$$

which shows that the two masses M_s and M_g oscillate with equal amplitudes that are determined by the total mass M_Σ. Here ω_{LA} is the longitudinal-

acoustical phonon frequency. From (8.31) and (8.32)

$$\mathcal{H}_{dp} = \sum_q B_{dq} A_q \, e^{i \underset{\sim}{q} \cdot \underset{\sim}{r}} \tag{8.33}$$

where, with $\hat{q} \cdot \hat{u}_q = 1$ for longitudinal modes

$$B_{dq} = i e_1 \, q \, (\hbar / 2 N_+ V M_{dp} \omega_{LA})^{1/2} \quad . \tag{8.34}$$

The deformation potential is commonly applied to low-energy electrons, which interact with phonons having small q. In the absence of information about the deformation potential at large values of q, (8.34) will be used formally with M_{dp} replaced by the greater mass M_g for large k, where q is large. The relation between the two electron-phonon processes can be seen by comparing (8.7) and (8.33), which shows that

$$e_1^2 \rightarrow (4\pi e^2 N_+)^2 \; \frac{M_{dp}}{M} \; \frac{\omega_{LA}}{\omega_{LO}} \; \frac{1}{q^4} \quad . \tag{8.35}$$

Making this replacement in (8.28) and reevaluating the integral gives

$$\begin{aligned} 1/\tau_{kA} &= C_1 (2 n_{LA} + 1) \, 2k / k_{BZ} && \text{for } k \leq \tfrac{1}{2} k_{BZ} \\ &= C_1 (2 n_{LA} + 1) = (4.08 \times 10^{-15} \text{ sec})^{-1} && \text{for } k = \tfrac{1}{2} k_{BZ} \\ &= C_1 (2 n_{LA} + 1) \, k_{BZ}^3 / 2k)^3 && \text{for } k \geq \tfrac{1}{2} k_{BZ} \end{aligned} \tag{8.36}$$

where

$$C_1 = \frac{e_1^2 \, m_k \, k_{BZ}^3}{4\pi \hbar^2 \omega_{LA} M_{dp} N_+} = 1.13 \times 10^{14} \text{ sec}^{-1}$$

and the numerical values are for the values of parameters listed in Sec. XIII. If $1/\tau_{kA}$ from (8.36) is formally equated to $1/\tau_{k0}$ from (8.30) at $k = \frac{1}{2} k_{BZ}$, it is found that

$$\varepsilon_1 \rightarrow \frac{4\pi e^2 N_+}{k_{BZ}^2} \left(\frac{2 M_{dp}}{M} \frac{\omega_{LA}(2 n_{L0} + 1)}{\omega_{L0}(2 n_{LA} + 1)} \right) = 4.54 \text{ eV} \quad .$$

It is shown in Sec. XIII that this value of ε_1 which corresponds to equal values of $1/\tau_{k0}$ and $1/\tau_{kA}$ at the maximum of $1/\tau_{kA}$ is well within the accuracy of an estimated value of ε_1; thus $\varepsilon_1 = 4.54 \text{eV}$ will be used.

Repeating the same procedure for $1/\tau_{LA}$ gives

$$\begin{aligned} 1/\tau_{LA} &= C_1 \, 2k/k_{BZ} && \text{for } k \leq \tfrac{1}{2} k_{BZ} \\ &= C_1 && \text{for } k = \tfrac{1}{2} k_{BZ} \\ &= C_1 \, k_{BZ}/2k && \text{for } k \geq \tfrac{1}{2} k_{BZ} \quad . \end{aligned} \qquad (8.37)$$

The final values for $1/\tau_k = 1/\tau_{k0} + 1/\tau_{kL}$ and $1/\tau_L = 1/\tau_{L0} + 1/\tau_{LA}$, with the $1/\tau$'s in (8.30), (8.31), (8.36), and (8.37), are

$$\begin{aligned} \frac{1}{\tau_k} &= (2 n_p + 1) \left(C \frac{k_{BZ}}{2k} + C_1 \frac{2k}{k_{BZ}} \right) , && k \leq \tfrac{1}{2} k_{BZ} \\ &= (2 n_p + 1)(C + C_1) = (2.04 \times 10^{-15} \text{sec})^{-1} && k = \tfrac{1}{2} k_{BZ} \\ &= (2 n_p + 1)(C + C_1) \, k_B^3/(2k)^3 && k \geq \tfrac{1}{2} k_{BZ} \end{aligned} \qquad (8.38)$$

and

$$\frac{1}{\tau_L} = 2C\,\frac{k_{BZ}}{2k}\,\ell n\left(\frac{2k}{k_{BZ}}\right) + C_1\,\frac{2k}{k_{BZ}} \qquad k \le \tfrac{1}{2}k_{BZ}$$

$$= 2C\,\ell n\left(\frac{k_{BZ}}{k_p}\right) + C_1 = (1.35\times10^{-15}\,\text{sec})^{-1} \qquad k = \tfrac{1}{2}k_{BZ}$$

$$= \left[C\ell n\left(\frac{2k\,k_{BZ}}{k_p^2}\right) + C_1\right]\frac{k_{BZ}}{2k} \qquad k \ge \tfrac{1}{2}k_{BZ} \quad . \quad \underline{(8.39)}$$

These results for $1/\tau_k$ and $1/\tau_L$ are sketched in Fig. 7.

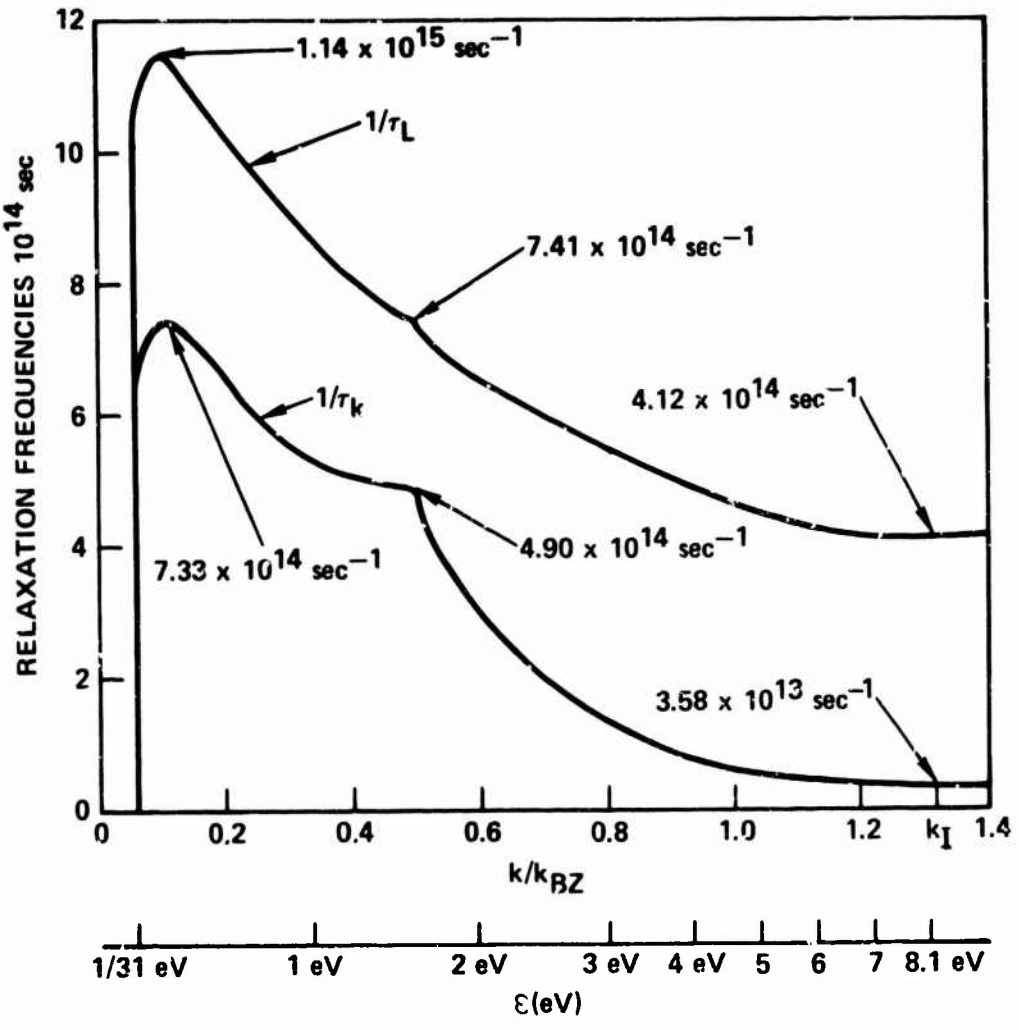

Fig. 7. Energy dependence of the relaxation frequencies from the calculated values of $1/\tau_k$ and $1/\tau_L$.

IX. HOLSTEIN PROCESS

The Holstein process is a second-order process in which an electron is scattered from state $\underset{\sim}{k}$ to state $\underset{\sim}{k}_f$, a photon is created or annihilated and a phonon is created and annihilated, as illustrated in Fig. 1. This process, which was considered by Holstein[6] in 1954 in the context of visible and infrared absorption in semiconductors and metals, has been overlooked in the electron avalanche problem. For the present purpose, Holstein's calculations must be extended to include the optical-mode process as well as the deformation-potential process (acoustical modes) and to include the case of large k's, that is, $k > \frac{1}{2} k_{BZ}$, where k_{BZ} is the wave vector at the edge of the first Brillouin zone as before.

The transition probability per unit time, ω_H, for the Holstein process can be obtained from the standard second-order perturbation-theory result

$$\omega_H = \frac{2\pi}{\hbar} \sum_{k_f} \sum_{q} \left| \sum_{k_I} \frac{\langle k_f | \mathcal{H} | k_I \rangle \langle k_I | \mathcal{H} | k \rangle}{\mathcal{E}_k - \mathcal{E}_{kI}} \right|^2 \delta(\mathcal{E}) \tag{9.1}$$

where phonon (q) and photon (Q) indices on the matrix elements are suppressed for simplicity and $\delta(\mathcal{E})$ is the appropriate energy-conserving δ function.

The Hamiltonian for the electron-photon interaction is

$$\mathcal{H}_{ep} = (e/mc) \underset{\sim}{p} \cdot \underset{\sim}{A} \quad .$$

Treating the electromagnetic field semiclassically by setting $\underset{\sim}{A}/c = \underset{\sim}{E}/i\omega$ gives

$$\mathcal{H}_{ep} = (\hbar e E / i m \omega)\, e^{i \underset{\sim}{Q} \cdot \underset{\sim}{r}}\, \hat{E} \cdot (-i\nabla) \quad . \tag{9.2}$$

The semiclassical approximation is well satisfied since $n_Q + 1 \cong n_Q$. The small photon wave vector Q is negligible, but $\hbar\omega$ must be retained in the energy conservation relations. The Hamiltonian for the deformation-potential electron-phonon process is

$$\mathcal{H}_{dp} = \mathcal{E}_1 \nabla \cdot \underset{\sim}{u} \tag{9.3}$$

as discussed in Secs. VIII and XIII.

The energy denominators $\Delta\mathcal{E} \equiv \mathcal{E}_k - \mathcal{E}_I$ in (9.1) for the four processes in Fig. 1 are equal to $\hbar\omega$, $-\hbar\omega$, $\hbar\omega$ and $-\hbar\omega$, respectively, where the small phonon energy $\hbar\omega_q$ and the small photon wave vector Q were neglected. The operator $\hat{E} \cdot (-i\nabla)$ in (9.2) generates the terms $\hat{E} \cdot \underset{\sim}{k}$ and $\hat{E} \cdot (\underset{\sim}{k} - \underset{\sim}{q})$ for the (a) and (b) processes, respectively, in Fig. 1. Thus, the two terms in (9.1) for (a) and (b) are

$$\frac{\hat{E} \cdot \underset{\sim}{k}}{\hbar\omega} + \frac{\hat{E} \cdot (\underset{\sim}{k} - \underset{\sim}{q})}{(-\hbar\omega)} = \frac{u_{Eq}\, q}{\hbar\omega} \tag{9.4}$$

where $u_{Eq} \equiv \hat{E} \cdot \hat{q}$. The corresponding terms for (c) and (d) are

$$\frac{\hat{E} \cdot \underset{\sim}{k}}{\hbar\omega} + \frac{\hat{E} \cdot (\underset{\sim}{k} + \underset{\sim}{q})}{(-\hbar\omega)} = -\frac{u_{Eq}\, q}{\hbar\omega} \quad . \tag{9.5}$$

The energy $\mathcal{E}_a$ in the delta function for the process in Fig. 1a is

$$\mathcal{E}_a = \mathcal{E}_{kf} - \mathcal{E}_k = \alpha(\underset{\sim}{k} + \underset{\sim}{Q} + \underset{\sim}{q})^2 - \alpha k^2 + \hbar\omega_q - \hbar\omega$$

where

$$\alpha \equiv \hbar^2/2m \quad .$$

Neglecting the small phonon energy $\hbar\omega_q$ and the small photon wave vector Q gives, with $u_{kq} \equiv \hat{k} \cdot \hat{q}$

$$\mathcal{E}_a = \mathcal{E}_b = 2\alpha\, kq\, u_{kq} + 2q^2 - \hbar\omega \quad . \tag{9.6}$$

Similarly

$$\mathcal{E}_c = \mathcal{E}_d = -2\alpha kq\, u_{kq} + \alpha q^2 - \hbar\omega \quad . \tag{9.7}$$

In (9.1) each matrix element contains a wave-vector Kronecker delta. Thus two of the three wave vector sums are eliminated. For the phonon emission process pe in (a) and (b) of Fig. 1, substituting (9.2), (9.4), (9.5), and (8.35) into (9.1) gives

$$\omega_H^{(pe)} = \frac{2\pi e^2 E^2}{\hbar m \omega^4} \sum_q u_{Eq}^2\, q^2\, |B_q|^2 (n_q + 1)$$

$$\times\, \delta(2\alpha\, kq\, u_{kq} + \alpha^2 q^2 - \hbar\omega) \quad . \tag{9.8}$$

No factors of 2 from electron spin appear in (9.8) because the matrix elements are diagonal in the spin variable and ω_H applies to an electron k having a given spin. By using $\delta(ax) = |a|^{-1}\,\delta(x)$, the δ function can be written as

$$\delta(\mathcal{E}_a) = \frac{1}{2\alpha kq}\, \delta(u_{kq} - u_a)$$

where

$$u_a \equiv (\hbar\omega - \alpha q^2)/2\alpha kq \quad . \tag{9.9}$$

The corresponding phonon absorption term $\omega_H^{(pa)}$ is obtained from (9.8) by replacing $n_q + 1$ by n_q. The delta function is the same since $\delta(-2\alpha kq\, u_{kq} + \alpha^2 q^2 - \hbar\omega) = (2\alpha kq)^{-1}\,\delta(-u_{kq} - u_a) = (2\alpha kq)^{-1}\,\delta(u_{kq} + u_a)$ [using $\delta(-x) = \delta(x)$], and the integral over du_{kq} from -1 to 1 is symmetrical about $u_{kq} = 0$. Adding $\omega_H^{(pe)}$ and $\omega_H^{(pa)}$ gives the value $\omega_H^{(a)}$ of ω_H for photon absorption

$$\omega_H^{(a,e)} = \frac{2\pi e^2 E^2}{3\hbar^3 m\omega 4k} \sum_q q\,|B_q|^2\,(2n_q + 1)\,\delta(u_{kq} - u_{a,e}) \tag{9.10}$$

where u_{Eq}^2 has been approximated by its average value 1/3. The result $\omega_H^{(e)}$ for photon emission was included in (9.10), where $u_e = (-\hbar\omega - \alpha q^2)/2\alpha\, kq$ is obtained from u_a by replacing $\hbar\omega$ by $-\hbar\omega$.

Using the standard prescription

$$\sum_q \rightarrow \frac{V}{(2\pi)^2} \int_0^{k_{BZ}} dq\, q^2 \int_{-1}^{1} du$$

reduces (9.10) to

$$\omega_H^{(a,e)} = \frac{e^2 E^2}{12\pi\hbar^2 m M_{dp} (N_+/V) k\omega^4} \int_0^{k_{BZ}} dq \int_{-1}^{1} du$$

$$\times\, q^5\, \frac{2n_q + 1}{\omega_q}\, \varepsilon_1^2\, \delta(u - u_{a,e}) \quad . \tag{9.11}$$

The z axis in $\underset{\sim}{q}$ space was chosen along k so that $u_{qk} = u$.

The integral

$$\int_{-1}^{1} du\, \delta(u - u_{a,e}) = 1 \qquad \text{for } |u_{a,e}| < 1$$
$$= 0 \qquad \text{for } |u_{a,e}| > 1 \tag{9.12}$$

determines the limits on the integral over q. From (9.12), (9.9), and the expression for u_e under (9.10), the upper (up) and lower (ℓo) limits for photon emission (e) and absorption (a) are

$$q_{\substack{e\\a}}^{(u)}/k = 1 + (1 \mp \hbar\omega/\mathcal{E})^{1/2}$$
$$q_{\substack{e\\a}}^{(\ell)}/k = \pm 1 \mp (1 \mp \hbar\omega/\mathcal{E})^{1/2} \quad . \tag{9.13}$$

In passing notice that these Holstein-process q's in (9.13) are the same as the electron-phonon q's in (8.20) with k_p^2/k^2 replaced by $\hbar\omega/\mathcal{E}$. For $q^{(u)} < k_{BZ}$, (9.13) is used, while for $q^{(u)} > k_{BZ}$, the upper limit is k_{BZ} according to the q integral in (9.11). That is

$$q_{\substack{e\\a}}^{(u)} = \text{lesser of } \frac{1}{2} k_{BZ} \text{ and } q_{\substack{e\\a}}^{(u)} \quad . \tag{9.14}$$

Since the energy gained by the electrons is $d\mathcal{E}/dt = \hbar\omega(\omega_H^{(a)} - \omega_H^{(e)})$, it is convenient to define

$$\omega_{HA} \equiv \omega_H^{(a)} - \omega_H^{(e)} \tag{9.15}$$

so that $d\mathcal{E}/dt = \hbar\omega\omega_{HA}$. From (9.15) and (9.11)

$$\omega_{HA} = \omega_{HA0}\vartheta^{(A)} \qquad (9.16)$$

where

$$\omega_{HA0} = \frac{e^2 k_{BZ}^5 (2n_{LA}+1)\mathcal{E}_1^2 E^2}{12\pi\hbar^2 m M_{dp} N_+ \omega_{LA}\omega^4}$$

$$= 2.94 \times 10^{12}\,\text{sec}^{-1}$$

and $\vartheta^{(A)} = \vartheta_a^{(A)} - \vartheta_e^{(A)}$ with

$$\vartheta_{\substack{e\\a}}^{(A)} = \frac{\omega_{LA}}{(2n_{LA}+1)k_{BZ}^5 k} \int_{q_{\substack{e\\a}}^{(\ell)}}^{q^{(u)}} dq\, q^5 \frac{2n_q+1}{\omega_q}$$

where LA denotes the value at the edge of the Brillouin zone, as discussed further below. The numerical value of $\omega_{H0} = 2.10 \times 10^{-12}\,\text{sec}^{-1}$ is for NaCl at room temperature and 1.06 μm with E = 2.0 MV/cm. For the optical mode process, $\mathcal{E}_1$ is replaced by the right-hand side of (8.35), with q^{-4} inserted in the integral, of course.

The rest of the present section is concerned with the equation of the integrals in ϑ for several cases of interest. First consider the case of the deformation potential. The dispersion relation for the longitudinal acoustical modes will be approximated by $\omega_q \cong (q/k_{BZ})\omega_{LA}$, where ω_{LA} is the zone-edge phonon frequency. Then in the high-temperature limit (which is satisfied for NaCl at room temperature for the low q modes but is only nominally satisfied for the zone-edge modes),

$$\frac{2n_q+1}{\omega_q} \cong \frac{k_{BZ}^2}{q^2}\,\frac{2n_{LA}+1}{\omega_{LA}} \quad .$$

With this expression, $\vartheta_{e_a}^{(A)}$ in (9.16) become

$$\vartheta_{e_a}^{(A)} = \frac{1}{k_{BZ}^3 k} \int_{q_{e_a}^{(\ell)}}^{q^{(u)}} dq\, q^3 \quad . \tag{9.17}$$

Integration gives

$$\vartheta^{(A)} = \frac{1}{4} (k/k_{BZ})^3 \left[\left(q_a^{(u)}/k\right)^4 - \left(q_a^{(\ell)}/k\right)^4 - \left(q_e^{(u)}/k\right)^4 + \left(q_e^{(\ell)}/k\right)^4 \right] . \tag{9.18}$$

The simplest procedure in numerical calculations is to use (9.18) with the q's given by (9.14) and (9.13). However, the following limiting cases of (9.18) are useful in determining the frequency and electron-energy dependence of ω_H: For sufficiently small $\mathcal{E}$, both $q_e^{(u)}$ and $q_a^{(u)}$ are less than k_{BZ}. Then, in this case of $\mathcal{E} < \frac{1}{4} (\mathcal{E}_{BZ} - \hbar\omega)^2/\mathcal{E}_{BZ}$,

$$\begin{aligned} \vartheta^{(A)} &= 4(k/k_{BZ})^3 f(\hbar\omega/\mathcal{E}) \\ &\cong 2 (\hbar\omega/\mathcal{E}_{BZ})^{3/2} && \text{for } \hbar\omega/\mathcal{E} \gg 1 \\ &\cong 8\hbar\omega\, \mathcal{E}^{1/2}/\mathcal{E}_{BZ}^{3/2} && \text{for } \hbar\omega/\mathcal{E} \ll 1 \end{aligned} \tag{9.19}$$

where

$$f(x) = (1+x)^{1/2} (1 + \tfrac{1}{2}x) - \theta(x) (1-x)^{1/2} (1 - \tfrac{1}{2}x)$$

and the unit step function $\theta(x)$ is equal to 1 for $x < 1$ of 0 for $x > 1$.

For the large $\mathcal{E}$ case of $\mathcal{E} > \frac{1}{4}(\mathcal{E}_{BZ} + \hbar\omega)^2/\mathcal{E}_{BZ}$, in which the upper limits of both integrals are equal to k_{BZ}, the value of $\mathcal{I}^{(A)}$ is

$$\mathcal{I}^{(A)} = \frac{1}{4}(k/k_{BZ})^3 f_+(\hbar\omega/\mathcal{E}) \qquad (9.20)$$

$$\cong \frac{(\hbar\omega)^5}{32\,\mathcal{E}^{5/2}\mathcal{E}_{BZ}^{3/2}} \qquad \text{for } \hbar\omega/\mathcal{E} \ll 1$$

where

$$f_+(x) = \left[\left(1 - (1-x)^{1/2}\right)^4 - \left(1 - (1+x)^{1/2}\right)^4 \right] .$$

Specific values of $f_+(\hbar\omega/\mathcal{E})$ for various values of $[\hbar\omega/\mathcal{E}]$ are: 0.971 [1]; 4.81×10^{-3} [1/2]; and 1.28×10^{-4} [1/4]. For smaller values of $\hbar\omega/\mathcal{E}$, the approximation in (9.20) is quite accurate.

Next consider the optical-mode process. From (8.35) and (9.16) with $(2n_q + 1)/\omega_q = (2n_{LO} + 1)/\omega_{LO}$ for the optical modes, the value of ω_H is given by

$$\omega_{HO} = \omega_{HOO}\,\mathcal{I}^{(0)} \qquad (9.21)$$

where

$$\omega_{HOO} \quad \frac{4\pi e^6 N_+ k_{BZ} (2n_{LO}+1) E^2}{3\hbar^2 m M \omega_{LO} \omega^4}$$

$$= 1.35 \times 10^{12}\ \text{sec}^{-1}$$

and $\mathcal{I}^{(0)} = \mathcal{I}_a^{(0)} - \mathcal{I}_e^{(0)}$, with

$$\mathcal{J}_{e_a}^{(0)} = \frac{1}{k k_{BZ}} \int_{q_{e_a}^{(\ell)}}^{q_{e_a}^{(u)}} dq\, q \quad . \tag{9.22}$$

The numerical value of $\omega_{HOC} = 1.35 \times 10^{12}\,sec^{-1}$ is for NaCl at room temperature and 1.06 μm with E = 2.0 MV/cm and $m = m_f$ and $\omega_p = 1/40\,eV$. Evaluating the integral in (9.22) gives

$$\mathcal{J}^{(0)} = \frac{1}{2}(k/k_{BZ}) \left[\left(q_a^{(u)}/k\right)^2 - \left(q_a^{(\ell)}/k\right)^2 - \left(q_e^{(u)}/k\right)^2 + \left(q_e^{(\ell)}/k\right)^2 \right] . \tag{9.23}$$

Limiting values of (9.23) are

$$\mathcal{J}^{(0)} = 2(k/k_{BZ}) \left[(1+\hbar\omega/\mathcal{E})^{1/2} - \theta(\hbar\omega/\mathcal{E})(1-\hbar\omega/\mathcal{E})^{1/2} \right]$$

$$\cong 2\, k\, \hbar\omega/k_{BZ}\, \mathcal{E} = 2\hbar\omega(\mathcal{E}\,\mathcal{E}_{BZ})^{-1/2} , \qquad \text{for } \hbar\omega/\mathcal{E} \ll 1$$

$$\cong 2(k/k_{BZ})(\hbar\omega/\mathcal{E})^{1/2} = 2(\hbar\omega/\mathcal{E}_{BZ})^{1/2}, \quad \text{for } \hbar\omega/\mathcal{E} \gg 1 \tag{9.24}$$

for $\mathcal{E} < (\mathcal{E}_{BZ} - \hbar\omega)^2/4\,\mathcal{E}_{BZ}$, and

$$\mathcal{J}^{(0)} = (k/k_{BZ}) \left[(1+\hbar\omega/\mathcal{E})^{1/2} - (1-\hbar\omega/\mathcal{E})^{1/2} - \hbar\omega/\mathcal{E} \right]$$

$$\cong \frac{(\hbar\omega)^3}{8\mathcal{E}_{BZ}^{1/2}\mathcal{E}^{5/2}} \qquad \text{for } \hbar\omega/\mathcal{E} \ll 1 \tag{9.25}$$

for $\mathcal{E} > (\mathcal{E}_{BZ} + \hbar\omega)^2/4\mathcal{E}_{BZ}$. For $\hbar\omega/\mathcal{E} = 1, 1/2, 1/3$, and $1/4$, the bracket factor in (9.25) has the values 0.414, 1.76×10^{-2}, and 2.01×10^{-3}, respectively. For $\hbar\omega/\mathcal{E} < 1/4$, the approximation in (9.25) is quite accurate.

Some useful specific values of ω_H, where

$$\omega_H = \omega_{H0} + \omega_{HA} \tag{9.26}$$

are listed in Table I.

For the conditions

$$\mathcal{E} < (\mathcal{E}_{BZ} - \hbar\omega)^2/\mathcal{E}_{BZ} \quad , \qquad \text{and } \mathcal{E} << \hbar\omega \quad , \tag{9.27}$$

which are well satisfied for 10.6, 1.06, 0.694, and 0.172 μm when $\mathcal{E} = 1/40$ eV, ω_H becomes independent of $\mathcal{E}$ and has the value

$$\omega_H(1/40\,\text{eV}) \cong \left(\frac{E}{2\,\text{MV/cm}}\right)^2 \left[1.92\times10^{11}\left(\frac{\lambda}{1.06\,\mu\text{m}}\right)^{5/2} + 1.22\times10^{12}\left(\frac{\lambda}{1.06\,\mu\text{m}}\right)^{7/2}\right] \text{sec}^{-1} \tag{9.28}$$

which is obtained from (9.16), (9.19), (9.21), and (9.24). The value 1.92×10^{11} sec^{-1} in (9.28) corresponds to $\mathcal{E} = 1/40$ eV. The corresponding value is 1.79×10^{11} sec^{-1} in the limit as $\mathcal{E}$ approaches zero. The value of 1.22×10^{12} sec^{-1} is essentially unchanged between $\mathcal{E} = 0$ and $\mathcal{E} = 1/40$ eV. This result (9.28) is useful for electrons in thermal equilibrium, since (9.27) usually is satisfied for such electrons.

Table I. Values of the rate ω_H of the Holstein photon-electron-phonon process.

λ μm	k 10^7 cm^{-1}	$\mathcal{E}$ eV	ω_{H0} $\left(\frac{E}{2\ MV/cm}\right)^2 10^{12}$ sec^{-1}	ω_{HA} $\left(\frac{E}{2\ MV/cm}\right)^2 10^{12}$ sec^{-1}	ω_H $\left(\frac{E}{2\ MV/cm}\right)^2 10^{12}$ sec^{-1}
1.06	0.653	1/31	1.23	0.192	1.42
1.06	0.923	2/31	1.25	0.203	1.45
1.06	4.14	1	1.25	1.89	2.92
1.06	4.50	1.17	1.26	1.95	3.21
1.06	5.55	1.55	0.527	1.19	1.72
1.06	6.39	1.80	0.177	0.441	0.618
1.06	6.50	2	8.2×10^{-2}	0.196	0.208
1.06	13.1	8	3.84×10^{-4}	9.04×10^{-6}	3.94×10^{-4}
0.694	0.653	1/31	0.272	5.96×10^{-2}	0.332
0.694	5.95	1.786	0.168	0.279	0.447

X. INTER-CONDUCTION-BAND PROCESS

An accurate estimate of the transition rate ω_V for the vertical inter-conduction-band process, that was illustrated schematically in Fig. 5, would require accurate values of the electron energies and wave vectors. Since these are not available, the following rough estimate will be used.

The standard perturbation-theory result for the transition probability per unit time is

$$\omega_{HV} = (2\pi/\hbar) \sum_{k_f} |\langle k_f | \mathcal{H} | k \rangle|^2 \delta(\mathcal{E}_f - \mathcal{E} - \hbar\omega) \Delta(\underset{\sim}{k}_f - \underset{\sim}{k} - \underset{\sim}{K}) \qquad (10.1)$$

where k_f is the final state of the electron, Δ is the Kronecker delta, and $\underset{\sim}{K}$ is a reciprocal lattice vector. Since the sum on $\underset{\sim}{k}_f$ is eliminated by the Kronecker delta, the energy delta function must be replaced by a line-shape factor of width $\Delta\mathcal{E}$ as usual

$$\delta(\mathcal{E}_f - \mathcal{E} - \hbar\omega) \rightarrow G(\mathcal{E})/\Delta\mathcal{E} \qquad (10.2)$$

where $\int d\mathcal{E}\, G(\mathcal{E})/\Delta\mathcal{E} = 1$ and $G(\mathcal{E}) \cong 1$ at the maximum.

The Hamiltonian is given by (9.2). The momentum matrix element can be written in terms of an oscillator strength f_k as[12]

$$|\langle k_f | \hat{E} \cdot \hbar\nabla | k \rangle|^2 = \frac{3}{2} f_k m\hbar\omega \quad . \qquad (10.3)$$

Substituting (10.2) and (10.3) into (10.1) gives

$$\omega_V = \frac{3\pi e^2 f E^2 G(\mathcal{E})}{m\omega\Delta\mathcal{E}} \qquad (10.4)$$

$$= f\left(\frac{m_f}{m}\right)\left(\frac{0.1\,\mathrm{eV}}{\Delta\mathcal{E}}\right)\left(\frac{\lambda}{1.06\,\mu\mathrm{m}}\right)\left(\frac{E}{2\,\mathrm{MV\,cm^{-1}}}\right)^2 G(\mathcal{E})\, 3.85\times 10^{14}\,\mathrm{sec}^{-1}\ .$$

This large value of ω_V suggests that the interband transitions may be sufficiently rapid to increase the electron energy from ~3eV to $\mathcal{E}_I$ as required in the theory. However, this result is not certain, and an analysis will be given in a subsequent report. In the interim, the following considerations are useful.

For an arbitrary point in the reduced Brillouin zone, the value $G(\mathcal{E})$ will be small because there is no neighboring band $\mathcal{E}_i$ such that $\mathcal{E}_i - \mathcal{E} \cong \hbar\omega$. Scattering processes must change the wave vector $\underset{\sim}{k}$ until

$$|\mathcal{E}_i - \mathcal{E} - \hbar\omega| \lesssim \Delta\mathcal{E} \qquad (10.5)$$

is satisfied, as shown schematically in Fig. 5. Large-angle scattering (with time constant τ_k) changes the position of $\underset{\sim}{k}$ in the Brillouin zone by large amounts, while small-angle scattering (with time constant $\tau_\Lambda \cong \tau_L/2.16$) changes $\underset{\sim}{k}$ by smaller amounts, thus providing both coarse and fine tuning, so to speak. The value of ω_V in (10.4) is sufficiently great that the interband transitions should have near unity probability of occurring during the time that $\mathcal{E}$ satisfies (10.5). The electron-phonon collision processes are sufficiently rapid that there are approximately 100 collisions (with relaxation time $\tau_\Lambda \cong 9.85\times10^{-16}$ sec) in the time $t \cong (\hbar\omega/\hbar\omega_{LO})\tau_L = 9.97\times10^{-14}$ sec required

for the electron to lose the energy $\hbar\omega = 1.17\,\mathrm{eV}$ that it gains, on the average, in a Holstein collision. In other words, the phonon collisions must bring $\underset{\sim}{k}$ to a position in the Brillouin zone at which (10.5) is satisfied in approximately 100 collisions or less. In the estimate of the effect of the inter-conduction-band transition on the ionization frequency in Sec. V, a value of 50 collisions was chosen as reasonable.

XI. HEATING TO THE DAMAGE THRESHOLD

In the present theory, conduction electrons are generated by one of several mechanisms. The absorption of energy by these electrons from the field then causes sufficient temperature rise to damage the crystal. The exact condition for damage is difficult to determine. Here it will be assumed simply that the temperature must be raised to the melting temperature T_m. It has been argued that this condition is reasonable.[21] Ordinary Joule (σE^2) heating is the familiar case of free-carrier absorption. However, it will be shown that the heating from the Holstein process is even greater at 10.6 μm and 1.06 μm. In Sec. D, failure mechanisms other than heating to the point of irreversible damage in the bulk of the material are considered. These mechanisms, which may have lower damage thresholds than those corresponding to $T = T_m$, include defocusing by the generated conduction electrons or by temperature gradients, multiphoton absorption, and fracture, particularly at surfaces or imperfections.

For Joule heating, the rate of change of energy per unit volume dW/dt is equal to σE^2. Thus, with $W = CT$, where C is the heat capacity per unit volume,

$$\frac{dT}{dt} = \frac{\sigma_1}{C} E^2 n_c \tag{11.1}$$

where σ has been written as $\sigma_1 n_c$, with

$$\sigma_1 = \sigma_{1mx}\, g(\omega\tau) \quad , \qquad g(\omega\tau) = 2\omega\tau_k (1+\omega^2\tau_k^2)^{-1}$$

$$\sigma_{1mx} = \frac{e^2}{2m\omega} = \frac{r_0 \lambda c}{4\pi}\left(\frac{m_f}{m}\right) = \frac{\lambda}{1.06\,\mu m}\ \frac{m_f}{m}\ 7.14\times 10^{-8}\,cm^3/sec \tag{11.2}$$

where $r_0 \equiv e^2/mc^2 = 2.82 \times 10^{-13}$ cm. The maximum value $g_{max} = 1$ of g occurs at $\omega\tau = 1$.

For the conduction-electron generation processes at 10.6 and 1.06 μm, $n_c = n_{c0}\exp(\omega_c t)$. Substitution into (11.1) and integration gives

$$T_a = \frac{\sigma_1 E^2 n_{c0}}{C\omega_c}\left(e^{\omega_c t} - 1\right) \qquad (11.3)$$

where T_a is measured with respect to the ambient temperature ($T_a = 0$ at $t = 0$). Taking the logarithm of (11.3) gives the required value of ω_c

$$\omega_c = t_p^{-1}\,\ell n\left(\frac{CT_a\omega_c}{n_{c0}\sigma_{tot}E^2} + 1\right) \quad . \qquad (11.4)$$

Here σ_1 was replaced by $\sigma_{tot} = \sigma_1 + \sigma_H$ in anticipation of results below. The factor 1 in the logarithm usually is negligible. A useful first approximation in interpreting (11.4) is to set $\omega_c = 10/t_p$ in the logarithm.

In passing notice that the required number of conduction electrons from (11.3) is, for the usual case in which $\exp(\omega_c t) >> 1$,

$$n_c = \frac{CT_a\omega_c}{\sigma_{tot}E^2}$$

which can be written in the convenient form, for the case of $\sigma_{tot} = \sigma_1$

$$n_c = \left(\frac{C}{1.84\,J/cm^3K}\right)\left(\frac{T_a}{770\,K}\right)\left(\frac{\omega_c}{5\times10^8\,sec^{-1}}\right)\left(\frac{1.06\,\mu m}{\lambda}\right)$$

$$\times\left(\frac{1}{g(\omega\tau)}\right)\left(\frac{2\,MV/cm}{E}\right)^2 2.23\times10^{18}\,cm^{-3} \quad .$$

This result shows that the previous damage criterion of $n_c = 10^{18}\,cm^{-3}$ is reasonable as a typical case. However, at short pulse durations ω_c becomes large and n_c can be three orders of magnitude greater than $10^{18}\,cm^{-3}$.

Also notice that if the density of starting electrons is $5 \times 10^{13}\,cm^{-3}$ and final density is $2 \times 10^{18}\,cm^{-3}$, then each starting electron generates $10^5 = 2^{17}$ final electrons. This value of 17 generations is less than the Seitz value[3] of 40, which applies to the different situation of dc breakdown in which a single electron generates 2^{40} electrons in a cylindrical volume V_c whose radius is the diffusion distance and whose length is the sample thickness. Such a process must be considered in establishing the damage criterion in the dc case as will be shown in a subsequent report. In the example of dc breakdown in Sec. III, the actual damage criterion did not have to be considered since the sample thickness was sufficiently great that breakdown was determined by the generation of the single starting electron.

In laser breakdown, the "40 generations" theory is less appropriate since the lack of electron drift in the ac field causes the volume V_c to be smaller, and the avalanche of a single electron is not expected to be sustained in general for barriers that extend to $\mathcal{E} = \mathcal{E}_I$.

The effect of the Holstein process is easily included by changing the value of σ_1. For the Holstein process $(dW/dt)_H = \hbar\omega\,\omega_H(k_BT)$, where $\omega_H(k_BT)$ is the average value of ω_H. Comparison of the right-hand side of this expression $\sigma_1 E^2 n_c$ shows that the one-electron conductivity for the Holstein process is

$$\sigma_H = \hbar\omega\,\omega_H(k_BT)/E^2 \quad . \qquad (11.5)$$

With ω_H given by (9.28), the value of σ_H from (11.5) is

$$\sigma_H(k_BT) = \left[8.07\times 10^{-9} \left(\frac{\lambda}{1.06\,\mu m} \right)^{3/2} + 5.13\times 10^{-8} \left(\frac{\lambda}{1.06\,\mu m} \right)^{5/2} \right] cm^3/sec . \qquad (11.6)$$

The value of $\sigma_H(k_BT)$ is greater than the value of σ_1 from (11.2). for λ slightly greater than $1.06\,\mu m$.

With $\sigma_{tot} = (5.94\times 10^{-8} + 1.43\times 10^{-7})\,cm^3/sec$, from (11.2) with m $= \frac{1}{2} m_f$, $\lambda = 1.06\mu m$, $t_p = \frac{1}{3} 10^{-8}$ sec, E = 2 MV/cm, and $n_{c0} = 5\times 10^{13}$ cm^{-3}, (11.4) gives

$$\omega_c = 3.48\times 10^9\ sec^{-1} \quad . \qquad (11.7)$$

XII. PROBABILITY FOR COLLISIONLESS ACCELERATION

The expression

$$P_\tau(t) = e^{-t\langle 1/\tau\rangle} \tag{12.1}$$

where

$$\langle 1/\tau\rangle = \frac{1}{t}\int_0^t dt'(1/\tau) \tag{12.2}$$

for the probability $P(t)$ that an electron does not make a collision in time t is easily derived as follows. If $1/\tau$ is the rate at which collisions occur, then the probability of no collision in time $t + \Delta t$ is

$$P_\tau(t + \Delta t) = P_\tau(t)(1 - \Delta t/\tau) \tag{12.3}$$

since $1 - \Delta t/\tau$ is the probability of no collision in time Δt. In the limit of $\Delta t \to 0$, (12.3) gives

$$dP_\tau/dt = P_\tau(t)/\tau$$

whose solution is (12.1). Notice that τ is a function of t as a result of its dependence on k.

The probability of interest is that of obtaining an electron with $k > k_{EL}$. If t in (12.2) is taken as the time t_{nc} required to accelerate an electron to $k = k_{EL}$ in the absence of collisions then $P_\tau(t)$ in (12.1) is the probability of generating the electron with $k > k_{EL}$ in this collisionless process. The electron also could be accelerated to $k > k_{EL}$ while suffering a single collision. In order

to show that the probability for this process is negligible with respect to $P_\tau(t)$ in the current case of $P_\tau(t) \ll 1$, consider the simple model in which it is assumed that $k = k_{EL}$ at time t_a and that there is one collision at time $\frac{1}{2}t_a$. This collision reduces the value of k_z by a factor of 1/e while leaving k (i.e., energy) essentially unchanged. Thus, at $t = \frac{1}{2}t_a$ where + and - superscripts denote immediately after and immediately before the collision, $k = k_1$ and $k_z = k_1/e$, where k_1 is the value of k at $t = \frac{1}{2}t_a^-$. At time t_a, $k_z = (1 + e^{-1})k_1$ and $k = k_{EL} \cong [1 + (1 + e^{-1})^2]^{1/2} k_1$, which gives $k_1 = 0.59\, k_{EL}$, or $t_a = 0.59\, t_{nc}$. Thus

$$P_2(k_{EL}) = \left(e^{-0.59\, t_{nc} \langle 1/\tau \rangle_{0, \frac{1}{2}t_a}}\right)\left(e^{-0.59\, t_{nc} \langle 1/\tau \rangle_{\frac{1}{2}t_a, t_a}}\right) .$$

Using

$$\langle 1/\tau \rangle_{0, \frac{1}{2}t_a} + \langle 1/\tau \rangle_{\frac{1}{2}t_a, t_a} = \frac{2}{t_a} \int_0^{\frac{1}{2}t_a} dt\, \frac{1}{\tau} + \frac{2}{t_a} \int_{\frac{1}{2}t_a}^{t_a} dt'\, \frac{1}{\tau} = 2 \langle 1/\tau \rangle_{0, t_a}$$

gives

$$P_2(k_{EL}) = e^{-1.18\, t_{nc} \langle 1/\tau \rangle} = P_\tau(k_{EL})^{1.18} .$$

For a typical value of $P_\tau(k_{EL}) \sim 10^{-10} = 1.58 \times 10^{-2}\, P_\tau(k_{EL})$. Thus, the single-collision process is negligible. Similarly, the two-collision and higher-order processes are negligible.

An approximation for $\langle 1/\tau \rangle$ can be obtained as follows. The solution to $\hbar\, dk_z/dt = eE$ is $k_z = \hbar^{-1} eEt + k_{z0}$, where $k_z = k_{z0}$ at time $t = 0$. For the case of current interest, $k_{z0} \leq k_0 \cong 5 \times 10^{-6}\ cm^{-1}$ is negligible with respect to the final value of $k_z \cong k = k_{EL}$. Thus, with k_{z0} neglected and $k_z \cong k$, t can be

written as $t = \hbar k / eE$ and the average over t in (12.2) can be replaced by an average over k:

$$\langle 1/\tau_k \rangle \cong \frac{1}{k_2 - k_1} \int_{k_1}^{k_2} dk \; 1/\tau_k \quad . \tag{12.4}$$

The average on the interval k_p to $\frac{1}{2}k_{BZ} \equiv k_{1/2}$ is obtained by numerically integrating $1/\tau_k$ in Fig. 7. The result is

$$\langle 1/\tau_k \rangle_{k_p - k_{1/2}} = (1.63 \times 10^{-15} \text{ sec}^{-1})^{-1} \quad , \tag{12.5}$$

which gives $R \equiv \tau_{1/2} \langle 1/\tau_k \rangle = 1.25$ for this interval, where k and $\tau_{1/2}$ are defined in (3.3). The average on the interval $\frac{1}{2}k_{BZ}$ to k_{EL} (for the case of $k_{EL} > \frac{1}{2}k_{BZ}$) is

$$\langle 1/\tau_k \rangle_{k_{1/2} - k_{EL}} = \frac{1}{k_{EL} - \frac{1}{2}k_{BZ}} \int_{\frac{1}{2}k_{BZ}}^{k_{EL}} dk \, (1/\tau_{1/2}) \left(\frac{1}{2}k_{BZ}/k \right)^3 \quad .$$

Evaluating the integral gives

$$\langle 1/\tau_k \rangle_{k_{1/2} - k_{EL}} = \frac{\frac{1}{4}k_{BZ}}{k_{EL}} \left(1 + \frac{\frac{1}{2}k_{BZ}}{k_{EL}} \right) \frac{1}{\tau_{1/2}} \tag{12.6}$$

which has the value $0.375 \, (1/\tau_{1/2})$ for $k_{EL} = k_{BZ}$. Combining (12.6) and (12.5) and using $(k_{1/2} - k_p) = 4.85 \times 10^7 \text{ cm}^{-1}$ gives

$$\left\langle \frac{1}{\tau_k} \right\rangle_{k_p - k_{EL}} = \left\{ 2.97 \times 10^{22} + \frac{1}{4} k_{BZ} \left(1 - \frac{\frac{1}{4} k_{BZ}^2}{k_{EL}^2} \right) \frac{1}{\tau_{1/2}} \right\} \left(k_{EL} - k_p \right)^{-1} \tag{12.7}$$

for this case of $k_{EL} > \frac{1}{2} k_{BZ}$. From (12.7), the average value of $1/\tau_k$ is $(2.60 \times 10^{-15} \text{sec})^{-1}$ at $k_{EL} = k_{BZ}$, which gives R = 0.785.

These results can be summarized in the form

$$\langle 1/\tau_k \rangle = R \langle 1/\tau_{1/2} \rangle \tag{12.8}$$

with R = 1.25 for $k_{EL} = \frac{1}{2} k_{BZ}$ and R = 0.785 for $k_{EL} = k_{BZ}$.

XIII. PARAMETER VALUES AND APPROXIMATIONS

For sodium chloride at room temperature, the following values of parameters are used:

$C = 1.84\ \mathrm{J/cm^3 K}$ $\qquad$ $K = 6.5\times10^{-2}\ \mathrm{W/cm K}$

$T \equiv T_m - 300\,\mathrm{K} = 770\,\mathrm{K}$ $\qquad$ $\mathcal{E}_I \cong 4.54\,\mathrm{eV}$ (estimate)

$k_{BZ} = 1.10\times10^{8}\ \mathrm{cm^{-1}}$ $\qquad$ $\mathcal{E}_{BZ} = (m_f/m)\ 4.66\,\mathrm{eV}$

$k_I = 1.46\times10^{8}\ \mathrm{cm^{-1}}$ $\qquad$ $\mathcal{E}_I = 8.1\,\mathrm{eV}$

$n_r = 1.5$

$M_r = 2.33\times10^{-23}\,\mathrm{g}$ $\qquad$ $M_\Sigma = 9.77\times10^{-23}\,\mathrm{g}$

$M_s = M_{Na} = 3.84\times10^{-23}\,\mathrm{g}$ $\qquad$ $M_g = M_{C\ell} = 5.93\times10^{-23}\,\mathrm{g}$

$a_{nn} = 2.82\times10^{-8}\,\mathrm{cm}$ $\qquad$ $N_+ = 2.23\times10^{22}\ \mathrm{cm^{-1}}$

$$I = c n_r E^2/4\pi = (E/2\,\mathrm{MV\,cm^{-1}})^2\ (n_r/1.5)\ 15.9\ \mathrm{GW/cm^2}$$

$$I/\hbar\omega = (\lambda/1.06\,\mu\mathrm{m})\,(E/2\,\mathrm{MV\,cm^{-1}})^2\ 8.51\times10^{28}\ \mathrm{photon/cm^2\ sec}$$

$$F \equiv I t_p = (E/2\ \mathrm{MV\,cm^{-1}})^2\ (t_p/10^{-8}\,\mathrm{sec})\ 1.59\ \mathrm{J/cm^2}$$

For $k \ll \frac{1}{2} k_{BZ}$, the phonons that interact with the electrons have wave vector $q \ll k_{BZ}$, as discussed below. In this case, the values of the q-dependent parameters are:

$M = M_{red} = 2.33\times10^{-23}\,\mathrm{g}$

$M_{dp} = M_\Sigma = 9.77\times10^{-23}\,\mathrm{g}$

$\omega_p = 1/31\,\mathrm{eV}$ $\qquad$ $2n_p + 1 = 1.76$

$k_p = 6.53 \times 10^6\ \text{cm}^{-1}$ $\qquad$ $m_k = \frac{1}{2} m_f$

$C = 9.60 \times 10^{13}\ \text{sec}^{-1} = (1.04 \times 10^{-14}\ \text{sec})^{-1}$

$C_1 = 3.54 \times 10^{13}\ \text{sec}^{-1} = (2.82 \times 10^{-14}\ \text{sec})^{-1}$

For $k \gtrsim k_{BZ}$, the important interacting phonons have $q \cong k_{BZ}$. Then the parameters have the values

$M = M_s = 3.84 \times 10^{-23}\ \text{g}$

$M_{cp} = M_g = 5.93 \times 10^{-23}\ \text{g}$

$\omega_p = 1/40\ \text{eV}$ $\qquad$ $2n_p + 1 = 2.16$

$k_p = 7.04 \times 10^6\ \text{cm}^{-1}$ $\qquad$ for $k = \frac{1}{2} k_{BZ}$

$k_p = 8.13 \times 10^6\ \text{cm}^{-1}$ $\qquad$ for $k \gtrsim 0.8\ k_{BZ}$

$m_k = 0.75\ m_f$ $\qquad$ for $k = \frac{1}{2} k_{BZ}$

$m_k = m_f$ $\qquad$ for $k \gtrsim 0.8\ k_{BZ}$

The value of the deformation-potential parameter $\mathcal{E}_1$ in (8.34) is unknown. It is believed that $\mathcal{E}_1$ is of the order of 10 eV for most materials. The free-electron theory of metals gives[7] $\mathcal{E}_1 = \frac{2}{3} \mathcal{E}_F$, where typical values of the Fermi energy $\mathcal{E}_F$ are a few electron volts. The expression

$$\mathcal{E}_1 = \sqrt{8/9}\ 1.7 \times 10^{-2} \theta_D \tag{13.1}$$

where $\mathcal{E}_1$ is in eV and the Debye temperature θ_D in degrees Kelvin is approximately satisfied for monovalent metals.[22] With $\theta_D = 312\ \text{K}$, (13.1) gives

$\mathcal{E}_1 = 5.14$ eV. Since the value $\mathcal{E}_1 = 4.54$ eV at which $1/\tau_{k0}$ and $1/\tau_{kA}$ are equal at the maximum of $1/\tau_{kA}$ is well within the accuracy of the rough estimate $\mathcal{E}_1 = 5.14$ eV, the value $\mathcal{E}_1 = 4.54$ eV will be used. Since there is no evidence to support this value in the alkali halides, the value of $\mathcal{E}_1^2$ could be in error by a factor of 4, or perhaps even greater.

The four-percent reflection at the front surface of a NaCl sample is neglected in calculating the intensity. For materials with large values of n_r, the correction would become important. The expression for the intensity, $I = c n_r E^2/4\pi$, is easily derived from the Poynting vector or from the relation $I = (c/n_r)(\mathcal{E}/V)$ with energy density $(\mathcal{E}/V) \equiv (\mathcal{E}/V)_H + (\mathcal{E}/V)_E = 2(\mathcal{E}/V)_E = (\epsilon/4\pi) E^2$ and $\epsilon = n_r^2$ for the transparent materials considered.

For $k \cong \frac{1}{2} k_{BZ}$, the phonon modes that contribute most to the integrals in $1/\tau$ in Sec. VIII are those at the edge of the Brillouin zone. Neutron data[23] shows that $\hbar\omega_{LO} \cong 1/40$ eV for these longitudinal-optical modes and $\hbar\omega_{LA} \cong 1/51$ eV. A one-dimensional model,[9] which is relevant for $\underset{\sim}{k}$ along (111), shows that the appropriate mass M is the smaller one M_s. Similarly, $M_{dp} = M_g$. For $k \ll k_{BZ}$, the phonon modes that contribute most to the integrals have $q \ll k_{BZ}$. Thus, $\omega_{LO} \cong (\omega_{LO})_{k=0} = 1/31$ eV and $M = M_{red}$. For the acoustical modes, $\omega_{LA} \cong 1/31$ eV and $M_{dp} = M_\Sigma$. Recent calculations[24] indicate that $m_k \cong \frac{1}{2} m_f$ at $\Gamma(k = 0)$ for several alkali halides. Since the nearly free electron model for conduction electrons in alkali halides is gaining popularity, the value $m_k = m_f$ will be used for electron wave vectors greater than $0.8 k_{BZ}$.

For the highly nonlinear process in which small changes in E give rise to great changes in ω_c, only the region near the peak of the laser pulses is effective. Thus, the value of the pulse duration t_p is taken as one third the full-width-half-maximum value.

Electron-hole recombination times and the time required to re-form an F center are much greater than the laser-pulse duration so that these effects can be neglected. On the other hand, trapping of electrons in the excited state of the F center is not negligible in some cases, as discussed in Sec. VII. Possible effects on the electron-avalanche breakdown will be considered in a subsequent report.

XIV. SUMMARY OF RESULTS

The processes by which the starting electrons are generated and the processes by which their energies are increased to the ionization value are summarized in Table II and Fig. 8. The dependence of the breakdown field strength on pulse duration at 1.06 μm is shown in Fig. 9. The agreement is excellent, especially in view of the facts that no parameters were adjusted and that previous theories with parameters adjusted disagreed with experiment by many orders of magnitude in t_p^{-1} over most of the curve, as discussed in Sec. B. Such good agreement is likely to be fortuitous, as discussed below. It is important that no parameters have been adjusted. Adjusting the value of parameters to improve agreement between theory and experiment reduces the credibility of any theory. This is especially relevant in the present case in which the results are so sensitive to small changes in the value of the electric field E.

The dc results of the sample-length dependence are included in Fig. 9. These results are conveniently compared with the laser-pulse-duration results by converting the sample length ℓ to the time t_ℓ required for the electron to drift across the sample by using the expression

$$t_\ell = \ell / \mu_{th} E$$

from (3.6). Values of t_ℓ for the curve marked "μ const" were calculated using the constant, low field experimental value of[2a] $\mu = 20\,cm^2/V\,sec$ for the mobility. For the $\mu = \mu(E)$ curve, the theoretical expression for the field dependence of mobility is given on p. 122 of Ref. 2a. In the variable-μ result used in

Table II. Summary of electron-avalanche-breakdown mechanism with a comparison of the photon energy $\hbar\omega$ with the maximum energy $\mathcal{E}_{pp}$ gained between collisions in the lucky-reversing-electron process.

λ	starting electrons	multiplication process	$(\hbar 2k_{pk})^2/2m \equiv \mathcal{E}_{pp}$	$\hbar\omega$
dc	thermionic emission from cathode	lucky electron $P_T(t_{nc})$	∞	0
10.6 μm	multiphoton ionization of F centers	10 Holstein process to $\mathcal{E}_{pp}$ = 1 eV	1 eV	0.117 eV
1.06 μm	two-photon ionization of F centers	3 Holstein plus ~5 interband to $\mathcal{E}_I \cong 8$ eV	10^{-2} eV	1.17 eV
0.694 μm	five-photon absorption across gap	2 Holstein plus ~3 interband to $\mathcal{E}_I \cong 8$ eV	4.3×10^{-3} eV	1.79 eV
0.172 μm	two-photon absorption across gap	1 Holstein plus 1 interband to $\mathcal{E}_I \cong 8$ eV	2.6×10^{-4} eV	7.21 eV

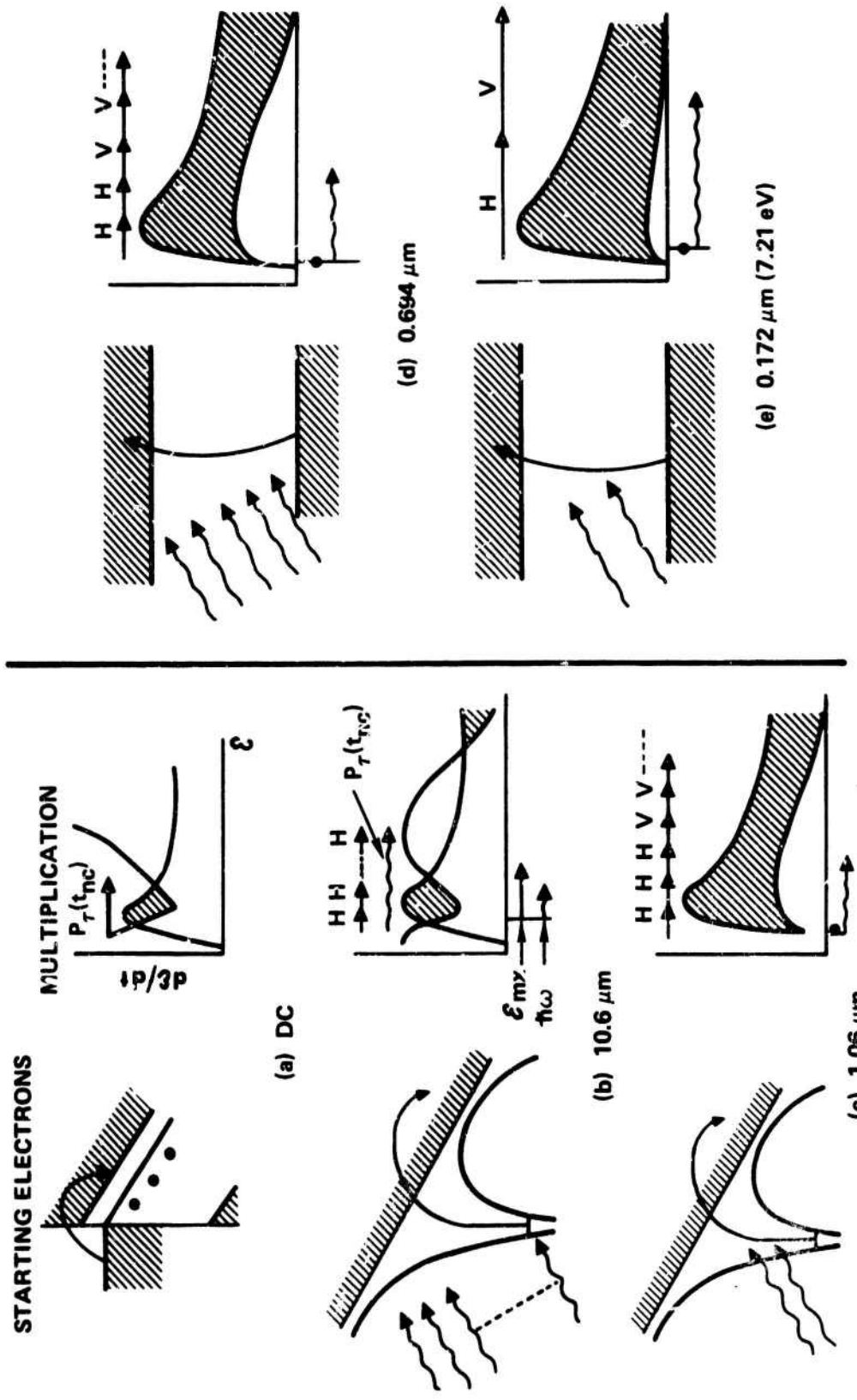

Fig. 8. Summary of the processes of generating the starting electrons and increasing their energies to the ionization value.

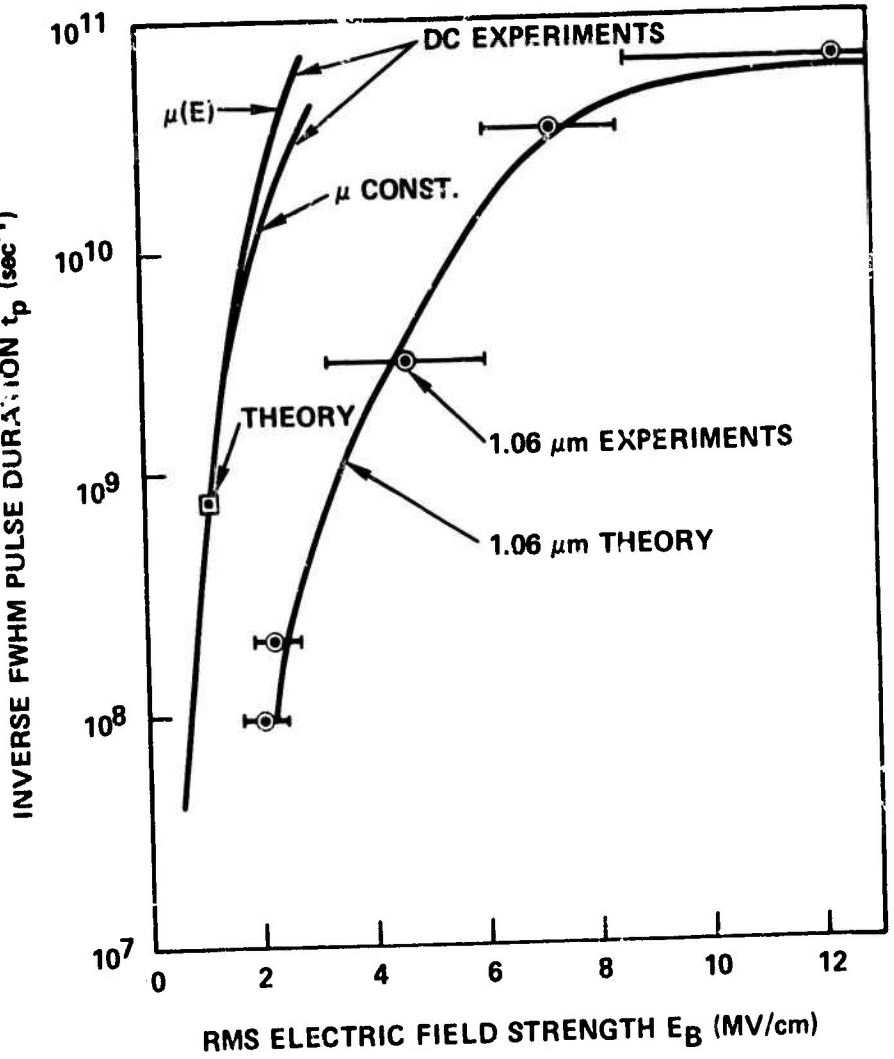

Fig. 9. Comparison of preliminary theoretical results with experimental results[14,16,10] for the dependence of the breakdown field strength on the pulse duration t_p at 1.06 μm. The dc results are displayed on the same graph by using $t_p \equiv \ell/\mu E$ where ℓ is the sample length and μ the mobility. Figs. 2, 3, and 4 of Sec. B contain previous and present theoretical results and experimental results.

Ref. 25 it was assumed that the mobility decreases with increasing field, as it should for nonpolar solids. In the theoretical result used here, the mobility increases with increasing field. The physical reason is that $\mu = e\tau_k/m$ and increasing the field increases the average value of τ_k by forcing the electrons into the higher k region in Fig. 7 where the relaxation frequency $1/\tau_k$ is smaller. Thus, the lower curve in (d) of Fig. 1 in Ref. 25 appears to be a reasonable lower limit in general, but it apparently is not approached in the alkali halides. The theoretical result for the single point calculated to date lies on the experimental curve.

The comparison between theoretical and experimental frequency dependence of the breakdown field in Fig. 10 for 10 nsec pulses shows good agreement. The experimental point at the ruby-laser frequency is the 10 nsec-pulse value of 2.1 MW/cm rather than the 4.7 nsec-pulse value of 2.3 MV/cm as in Fradin's[14] original comparison of the experimental values of E_B at different frequencies.

The agreement with experiment of all the theoretical results obtained to date is better than had been expected in view of the possible inaccuracies in the calculated values of ω_H, τ_k, and τ_L and in view of the rather gross approximations used at this early stage in the theory.

The theory presented here removes all the difficulties of previous theories discussed in Sec. B, and the tentative results obtained to date are encouraging. However, additional results from a number of other studies are needed. These include the dependence of the breakdown field on temperature, pulse duration, focal volume, impurity concentrations, and material parameters at various frequencies including the doubled-ruby frequency. Whether the measured values of

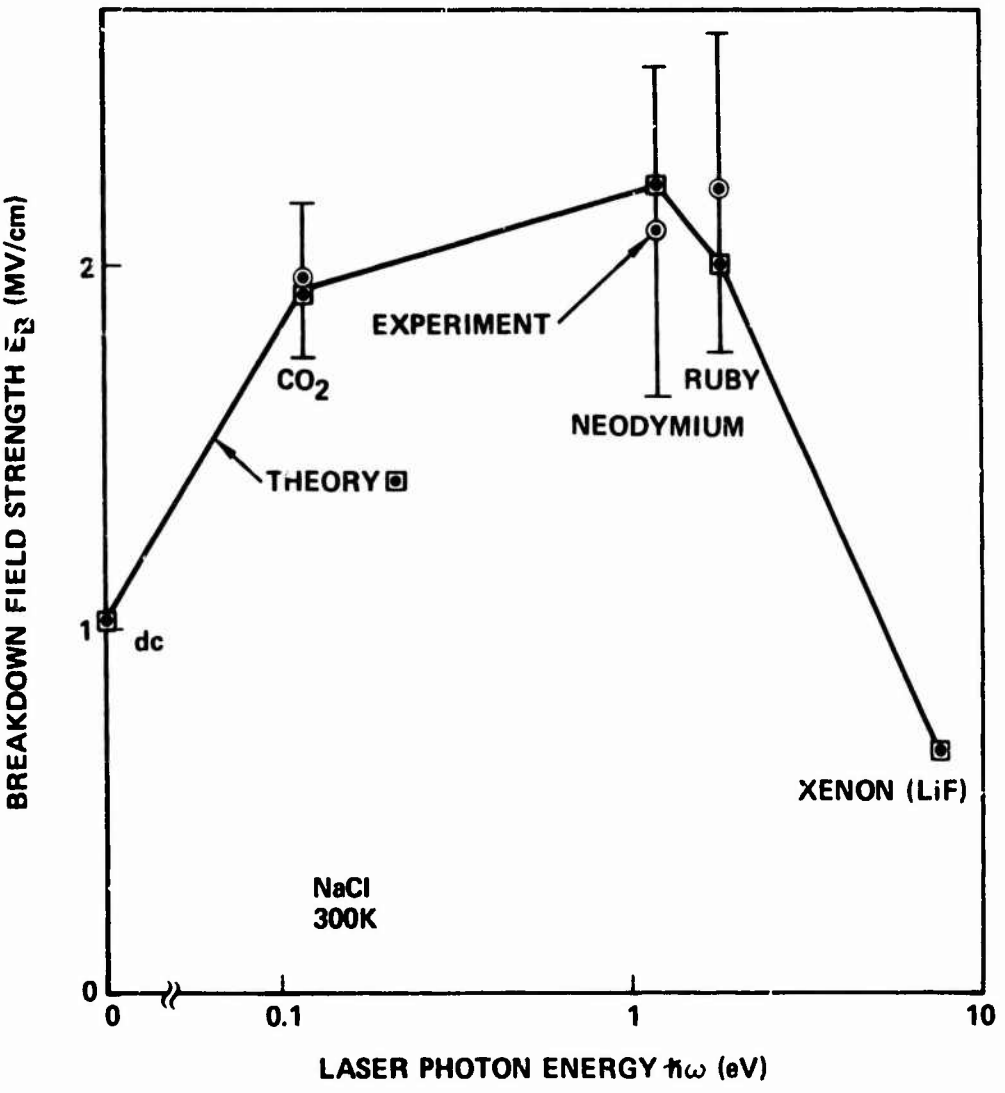

Fig. 10. Comparison of preliminary theoretical results with experimental results[10,13,14] of the dependence of the breakdown field strength E_B on the laser frequency ω showing good agreement with no adjusted parameters. Figs. 2, 3, and 4 of Sec. B contain previous and present theoretical results and experimental results.

E_B should exhibit a sharp threshold or statistical behavior must be considered for each case. Multiple-pulse effects, disorder-material effects, and possible ways of improving the damage resistance of materials must be considered. A transport theory that includes processes which change the electron energy by a large amount has been developed by Dr. T. Holstein and will be applied to the problem. A number of additional specific mechanisms that will be considered include: non-vertical inter-conduction-band transitions, multiphoton inter-conduction-band transitions, various additional processes for generating starting electrons, Umklapp processes for the Holstein process and the electron-phonon collision process at large values of $\mathcal{E}$, and space-change effects in the dc experiments.

XV. ACKNOWLEDGEMENTS

I am indebted to many people who kindly discussed electron-avalanche breakdown. It was realized that the electron-photon-optical-phonon process was one of the missing keys to the theory while discussing the Joule heating aspect of the problem with Dr. Norton Moise. Dr. Douglas Mills pointed out that the electron-photon-acoustical-phonon process had been studied by Dr. Theodore Holstein in studies of metals. Dr. Holstein subsequently became involved in the present program. He suggested that the inter-conduction-band processes should be investigated, developed a transport theory to include the effect of large-energy transfer processes, and contributed in numerous discussions. Several helpful discussions with Dr. David Fradin are gratefully acknowledged. Discussions with Drs. M. Bass, N. Boling, P. Braunlich, C. J. Duthler, F. Luty, and J. Marburger are appreciated.

REFERENCES

1. M. Van Marum, Ann. Physik 1, 68 (1799).
2. The following should lead the reader into the vast literature: (a) J. J. O'Dwyer, The Theory of Electrical Conduction and Breakdown in Solid Dielectrics, (Clarendon, Oxford, 1973); (b) N. Bloembergen, IEEE J. Quantum Elect. QE-10, 375 (1974); (c) N. Klein, Adv. in Elect. and Elect. Phys. 26, 309 (1969); (d) D.W. Fradin, Harvard Univ. Technical Report No. 643, Contract No. N00014-67-A-0298-0006, May (1973).
3. F. Seitz, Phys. Rev. 76, 1376 (1949).
4. W. Shockley, Czech. J. Phys. B11, 81 (1961) and Sol. St. Elect. 2, 35 (1961).
5. T. Holstein, Phys. Rev. 96, 535 (1954).
6. M. Bass and H. H. Barrett, IEEE J. Quantum Elect. QE-8, 338 (1971).
7. J. M. Ziman, Electrons and Phonons, edited by N. F. Mott, E. C. Bullard, and D. H. Wilkinson (Oxford, Clarendon Press, 1960).
8. K. K. Thornber and R. P. Feynman, Phys. Rev. B1, 4099 (1970).
9. C. Kittel, Introduction to Solid State Physics, 4th ed. (Wiley, New York, 1971).
10. D. B. Watson and W. Heyes, J. Phys. Chem. Solids 31, 2531 (1970); K. C. Kao and J. H. Calderwood, IEEE Trans. Elec. Insul. EI-1, 30 (1965).
11. D. H. Kleinman, Phys. Rev. 125, 87 (1962).
12. F. Wooten, Optical Properties of Solids (Academic, New York, 1972).
13. E. Yablonovitch, Appl. Phys. Lett. 19, 495 (1971).
14. D. W. Fradin, E. Yablonovitch, and M. Bass, Appl. Opt. 12, 700 (1973); D. W. Fradin, Harvard Univ. Technical Report No. 643, Contract No. N00014-67-A-0298-0006, May (1973).

15. D. W. Fradin, N. Bloembergen, and J. P. Letellier, Appl. Phys. Lett. 22, 635 (1973).

16. W. L. Smith, J. H. Bechtel, and N. Bloembergen, Phys. Rev., in press.

17. P. F. Braunlich, Bendix Research Laboratories Final Report, Contract No. F19628-73-C-0032, August (1974); P. Braunlich, A. Schmid, and P. Kelly, Appl. Phys. Lett. 26, 150 (1975).

18. I. M. Catalano, A. Cingolani, and A. N. Minafra, Phys. Rev. 55, 1629 (1972).

19. H. Frölich and N. F. Mott, Proc. Roy. Soc. A171, 496 (1939); H. Frölich, Proc. Roy. Soc. A160, 230 (1937).

20. F. Seitz, Phys. Rev. 73, 549 (1948).

21. M. Sparks and C. J. Duthler, J. Appl. Phys. 44, 3038 (1973).

22. A. H. Wilson, The Theory of Metals, 2nd ed. (Cambridge University Press, 1953).

23. G. Raunio, L. Almquist, and R. Stedman, Phys. Rev. 178, 1496 (1969).

24. D. J. Mickish. A. B. Kunz, and T. C. Collins, Phys. Rev. B9, 4461 (1974).

25. E. Yablonovitch and N. Bloembergen, Phys. Rev. Lett. 29, 907 (1972).

D. VUV WINDOW FAILURE BY MULTIPHOTON ABSORPTION AND ELECTRON DEFOCUSING, AVALANCHE, AND ABSORPTION

M. Sparks
Xonics, Incorporated, Van Nuys, California 91406

Calculated values of the intensities at which a window material fails at the xenon-laser frequency are 60 MW/cm^2 to 140 MW/cm^2 for electron-plasma defocusing, 740 MW/cm^2 for fracture, and 1.6 GW/cm^2 for melting. The lower value of 60 MW/cm^2, from impurity absorption, applies only if the quantum efficiency for generating conduction electrons is high and the impurity absorption does not saturate. The Joule heating by the conduction electrons that are generated by the two-photon-absorption and the electron-avalanche processes is greater than the direct heating by the two-photon-absorption process. Electron-plasma-induced optical distortion by these conduction electrons is greater than thermally induced optical distortion for the cases considered. Electron-avalanche multiplication increases the conduction-electron density above the two-photon value, the effect being greater at the higher intensities. Ordinary F-center absorption and a new F-center heating process are shown to be negligible here, but important at other frequencies and at higher F-center concentrations.

I. INTRODUCTION

Electron-avalanche breakdown has been studied previously in many of the alkali halides for frequencies ranging from dc through the ruby-laser frequency. The original purpose of the present investigation was to determine the effect of electron-avalanche breakdown at the xenon-laser frequency ($\hbar\omega = 7.21\,eV$). However, it was discovered that reasonable predictions could not be made with the existing theories. A discussion of the current status of theories of electron-avalanche breakdown is given in Sec. B of this report, and preliminary results of new theories of electron-avalanche breakdown applied at dc, 10.6 μm, 1.06 μm, and 0.69 μm are discussed in Sec. C of the present report. In the present section, electron-avalanche breakdown and other effects involving conduction electrons are considered for the case of 10 nsec pulses of 7.21 eV radiation in LiF. The general results are of wider applicability than this special case. In Sec. E, optical distortion by the enhanced nonlinear refractive index are considered. Other failure mechanisms were considered in the Third Technical Report.[1]

A study of the fundamental and practical limitations of transparent materials for use as high-power optical components at 7.21 eV is currently of interest as a result of the recent development of the xenon laser.[2-4] The output power of the first xenon vuv lasers was limited by the materials problem of the melting of the cavity mirror.[3] Since orders of magnitude greater power would be feasible if suitable materials were available, there is great interest in obtaining improved materials. The research reported here is part of a theoretical program

to understand the absorption and effects of high-intensity vacuum ultraviolet radiation. Such understanding is expected to be invaluable in materials-improvement programs.

The central results obtained in the present section are as follows: The Joule heating by the conduction electrons that are generated by the two-photon absorption process is greater than the direct heating by the two-photon-absorption and the electron-avalanche processes. Electron-plasma-induced optical distortion by the conduction electrons generated in the two-photon-absorption process is greater than thermally induced optical distortion for the cases considered, in which approximately one conduction electron is generated for each photon absorbed. Electron-avalanche multiplication increases the conduction-electron density n_c above the two-photon value. The effect is rather large for the cases of melting and fracture, but is almost negligible for electron-plasma optical distortion. In addition to the primary results for the values of the failure intensities I_f with all of the effects discussed above included, values of I_f for individual mechanisms are calculated to illustrate the relative importance of the various effects.

In electron-plasma optical distortion, the conduction electrons generated by the two-photon process and possibly other processes cause a change in the index of refraction which in turn distorts the optical beam. This effect is believed to have been responsible for "defocusing" observed in electron-avalanche breakdown investigations at lower frequencies. Hellwarth[5] suggested that defocusing might be responsible for repeated focal regions observed along a beam.

Yablonovitch and Bloembergen[6] proposed that the diameter of self-focused beams may be limited by this electron-plasma-defocusing mechanism.

The results for the values of the intensity I_f at which a sample fails by various mechanisms must be viewed as tentative since the values of a number of parameters that appear in the theory are unknown and it is necessary to use estimates for these values. This lack of needed information suggests a number of experimental and theoretical investigations that would be useful, as discussed in Sec. C. The present estimates indicate that the lowest intrinsic failure intensity $I_f = 0.14$ GW/cm^2 is that for optical distortion by the electron plasma generated by two-photon absorption. The electron-avalanche process does not contribute significantly to this threshold. Thermally induced optical distortion, which is negligible here as already mentioned, has been considered previously[7] for a number of materials and frequencies. Values of I_f listed in Table 1 for the various processes range between 0.14 GW/cm^2 and 20 GW/cm^2.

Other effects that are considered and shown to be negligible for the present case of LiF at 7.21 eV include F-center absorption and a new absorption process in which an electron in an excited F-center state absorbs a photon. For impure crystals or for other experimental conditions, both of these processes can be important.

Important results are denoted by underlined equation numbers.

Table I. List of values of the intensities I_f at which a LiF crystal fails by various mechanisms for a single square 7.21 eV pulse of width $t_p = 10^{-8}$ sec.

Failure Mechanism	Failure Intensity I_f in GW/cm^2		
	two-photon + Joule + electron avalanche	Joule, with n_c from two-photon	two-photon only (total conversion to heat)
Electron-Plasma Optical Distortion ($\delta n_r = \lambda/8\ell = 2.15 \times 10^{-6}$)	0.144†	DNA	0.170*
Thermally Induced Optical Distortion (T = 0.3 K)	0.34*	0.42*	0.39*
Fracture (T = 7 K)	0.74	1.0*	1.9*
Melting (T = 843 K)	1.6	5.6*	20*

*These values, which are listed for comparison only, cannot be achieved in practice because other mechanisms give lower values of I_f.

†This lowest intrinsic value of I_f = 144 MW/cm^2 applies to systems with strict optical tolerances. A possible lower extrinsic value of 60 MW/cm^2 is discussed in Sec. VI.

II. TWO-PHOTON-PLUS-JOULE HEATING

The two-photon absorption generates conduction electrons at the rate

$$dn_c/dt = \beta_2 I/2\hbar\omega \qquad (2.1)$$

where β_2 is the two-photon absorption coefficient. This expression (2.1) follows from the rate of energy absorption $\beta_2 I$ and the fact that one conduction electron is generated for unit $2\hbar\omega$ of energy absorbed. Writing β_2 as

$$\beta_2 = \left(\frac{I}{I_\beta}\right) 1.0\ \text{cm}^{-1} \quad , \qquad I_\beta = 1.2\ \text{GW/cm}^2 \quad , \qquad (2.2)$$

according to an estimate[1] for LiF at 7.21 eV, and integrating (2.1) with $n_c \cong 0$ at $t = 0$ gives

$$n_c = \left(\frac{I}{I_\beta}\right)^2 \frac{7.21\,\text{eV}}{\hbar\omega} \frac{t}{10^{-8}\,\text{sec}} 5.21\times10^{18}\,\text{cm}^{-3} \quad . \qquad (2.3)$$

The second factor of $1/I_\beta$ was introduced in (2.3) for convenience in displaying the numerical value of n_c. It should be emphasized that an experimental value of I_β is not available, and the estimated value in (2.2) could be in error by a factor of 10 or perhaps even more.

Consider the Joule heating of the crystal by these conduction electrons. The holes will be neglected since in the alkali halides the hole mass is large and the holes become self trapped to form V_k centers at low temperatures. The Joule heating by these conduction electrons gives the temperature-rise equation

$$dT/dt = \sigma E^2/C \qquad (2.4)$$

where C is the heat capacity per unit volume. The conductivity $(n_c e^2 \tau/m)(1+\omega^2\tau^2)^{-1}$ can be written in the convenient form

$$\sigma = \sigma_1 n_c \equiv \sigma_{1\,mx}\, g(\omega\tau)\, n_c \tag{2.5}$$

$$\sigma_{1\,mx} = \frac{r_0 c \lambda}{4\pi}\left(\frac{m_f}{m}\right), \qquad g(\omega\tau) = 2\omega\tau\,(1+\omega^2\tau^2)^{-1}$$

$$\sigma_1 = \frac{7.21\,eV}{\hbar\omega}\;\frac{\frac{1}{2}m_f}{m}\;\frac{g(\omega\tau)}{0.134}\;3.10\times10^{-9}\,cm^3\,sec^{-1}$$

where $r_0 = e^2/mc = 2.82\times10^{-13}$ cm and m_f is the free-electron mass. The electron-relaxation frequency τ was written as τ_k in previous sections. The value of σ_H (see Sec. C-XI) is negligible with respect to σ_1 in the present case. The value of $\sigma_H = \hbar\omega\,\omega_H(k_B T)/E^2 = 1.71\times10^{-9}\,cm^3/sec^{-1}$ obtained from (11.5) must be reduced by a factor of approximately ten since only a fraction of the energy $\hbar\omega$ appears as heat, the rest of the energy being supplied to elevate a valence electron to the conduction band. By contrast, in the cases of the previous sections, only a small fraction of the electrons excited in the first Holstein transition reached $\mathcal{E} = \mathcal{E}_I$.

A number of simplifying assumptions will be made. The actual pulse shape will be replaced by a square pulse of width $t_p = 10$ nsec. For the nonlinear processes considered, the appropriate value of t_p is less than the full-width-half-power value t_{fw} since the higher values of the electric field are much more effective than the lower values in nonlinear processes. A reasonable choice is $t_p \cong \frac{1}{3} t_{fw}$, which implies that $t_{fw} \cong 30$ nsec in the examples. The temperature dependence of all parameters is neglected. Trapping of the

conduction electrons will be neglected. For relatively pure samples there should be fewer than $\sim 5 \times 10^{15}$ negative-ion vacancies per cubic centimeter. Thus, even if every negative-ion vacancy trapped an electron, the number of trapped electrons would be a small fraction of the number generated according to (2.3) with reasonable values of I. Calculations will be made for LiF, ambient temperature T = 300 K, and $\hbar\omega = 7.21$ eV. The small reflection of 3% at the front surface is neglected, as are local field corrections. Other assumptions will be discussed as introduced.

Substituting (2.5) and (2.3) into (2.4), integrating from t = 0 to t = t_p, where t_p is the laser-pulse duration discussed above, and using $E^2 = 4\pi I / n_r c$ gives

$$T_J = \pi \sigma_{1\,m} \, g(\omega\tau) \, t_p^2 \, \beta_2 \, I^2 / n_r c \, C\hbar\omega$$

which can be written as

$$T_J = \frac{g(\omega\tau)}{0.134} \, \frac{\frac{1}{2} m_f}{m} \, \frac{1.44}{n_r} \, \frac{4.12\,\mathrm{J/cm^3K}}{C} \left(\frac{7.21\,\mathrm{eV}}{\hbar\omega}\right)^2 \left(\frac{t_p}{10^{-8}\,\mathrm{sec}}\right)^2 \left(\frac{I}{I_\beta}\right)^3 6.90\,\mathrm{K} \qquad (2.6)$$

for the temperature rise T_J from Joule heating.

In passing, it is mentioned that the relation between E^2 and I given above can be obtained from the Poynting vector or from the relation $I = (\mathcal{E}/V)v$ with $v = c/n_r$ and $\mathcal{E}/V = (n_r^2 E^2 + H^2)/8\pi$ where $H = n_r E$. For LiF, with $n_r = 1.44$, the value of E at $I = I_\beta = 1.2\,\mathrm{GW/cm^2}$ is $E = 0.560\,\mathrm{MV/cm}$.

The value of $g(\omega\tau) = 0.134$ used in (2.6) corresponds to $\omega = 1.095 \times 10^{16}$ sec^{-1} and $\tau = 1.36 \times 10^{-15}$ sec. There is no experimental value of τ, and the calculated value from Sec. C could be in error by a factor of 5 or so.

In the absence of Joule heating, the temperature rise would be smaller than the value given in (2.6). If all the absorbed energy in the two-photon process appeared instantaneously as heat, the temperature rise would be given by

$$T_2 = \beta_2 I t_p / C$$

$$T_2 = \left(\frac{I}{I_\beta}\right)^2 \left(\frac{t_p}{10^{-8}\,\text{sec}}\right) \left(\frac{4.12\,\text{J/cm}^3\,\text{K}}{C}\right) \; 2.91\,\text{K} \qquad (2.7)$$

The assumption of instantaneous heating apparently is not satisfied, as discussed in Sec. VIII.

The ratio of T_J to T_2 is proportional to the fluence $t_p I$. For $t_p = 10^{-8}$ sec, $T_J = T_2 = 0.518\,\text{K}$ at $I = 0.506\,\text{GW/cm}^2$. For smaller values of I, $T_J < T_2$.

III. FAILURE-INTENSITY THRESHOLDS

The intensity at which a system will fail as a result of the temperature rise discussed in Sec. III and as a result of the conduction-electron defocusing in Sec. IV depend strongly on the details of the particular system of interest. If strict optical tolerances must be maintained, the failure intensity I_f will be limited to values well below the values at which the material thermally fractures or melts. If the beam is focused in a small volume, thermal diffusion will reduce the temperature. For $t_p = 10^{-8}$ sec, $C = 4.12$ J/cm^{3}K, and $K = 0.11$ W/cm K, the characteristic thermal diffusion length is $\ell_D \cong (K t_p/C)^{1/2} = 1.6\,\mu$m. For thermally induced optical distortion, the value of dn/dt must be taken at constant strain (constant lattice spacing) if $t_p \ll \ell/v_s$ where ℓ is a sample dimension, while in other cases dn/dt at constant stress must be taken. For $t_p = 10^{-8}$ sec and $v_s = 5 \times 10^5$ cm/sec, the corresponding value of ℓ is $\ell = 50\,\mu$m. The effect of non-instantaneous heating by two-photon absorption, as discussed in Sec. VIII, has different consequences for different experimental conditions. In addition to affecting the value of I_f, these effects must be considered carefully when testing a material under different conditions from those of the application. Using a small focal volume and short pulse duration to obtain high power and high intensity with small test lasers is an example.

In view of these considerations which make I_f depend on the system parameters, it is not possible to give universal values of I_f, and values for specific systems will have to be calculated individually. Nevertheless, it is desirable to obtain an idea of the relative importance of the different effects. Thus, values of I_f will be calculated for a set of conditions, which are a single square pulse

of width $t_p = 10^{-8}$ sec, $\hbar\omega = 7.21$ eV, and negligible thermal diffusion. Furthermore, T_2 will be neglected when considering optical distortion, under the assumption that the heating of the lattice occurs after the pulse has passed. For melting or fracture T_2 will be included. The threshold for irreversible failure, such as caused by melting or fracture, will be taken formally as the value of I_f required to bring T up to the melting temperature T_m or fracture temperature T_{fr}. It has been argued that $T = T_m$ is a reasonable criterion for the case of focusing inside the sample.[8] However, under certain conditions, including high intensities at the sample surface, the material can fracture at the much lower temperature $T_{fr} \cong 2\sigma/\alpha E = 7\,K$, where $\sigma = 1.6 \times 10^3$ psi is the strength of the material, $E = 1.5 \times 10^7$ psi is the Young's modulus, and $\alpha = 3.23 \times 10^{-5}\,K^{-1}$ is the linear thermal expansion coefficient. Values of I_f will be calculated for the three cases of $T = T_m$, T_{fr}, and T_o (for optical distortion), which are called melting, fracture, and thermally induced optical distortion, respectively.

For $T = T_J + T_2$, the value of I_f can be obtained from (2.8) with T_J and T_2 given by (2.6) and (2.7). The result can be written as

$$I = 4.75\, I_\beta \left(\frac{T/843}{1 + 0.369\, I_\beta / I} \right)^{1/3} . \qquad (3.1)$$

For melting, setting $T = T_m = 843\,K$ in (3.1) and solving for $I = I_f$ gives $I_f = 4.63\, I_\beta$, or

$$I_f = 5.6\ GW/cm^2 \qquad \text{(melting)} . \qquad \underline{(3.2)}$$

For $T = T_f = 7\,K$, (3.1) gives $I_f = 0.85\, I_\beta$, or

$$I_f = 1.0\ GW/cm \qquad (T = T_{fr}) . \qquad \underline{(3.3)}$$

Without the Joule heating, substituting T_m and T_f into (2.7) and solving for I_f gives 20 GW/cm^2 and 1.9 GW/cm^2, respectively, which are factors of ~2 and ~4 greater than the values in (3.2) and (3.3). [The value of 1.9 GW/cm^2 is more accurate than the previous estimate[1] of 0.6 GW/cm^2, although both are rough estimates.]

Next consider the value I_f of intensity at which thermally induced optical distortion becomes intolerable. The value of T (in the center of a beam truncated at $1/e^2$) corresponding very roughly to halving the target intensity is

$$T = \lambda / 8\ell \left| \partial_n T \right|$$

where $\partial_n T \equiv \partial_{nr}/\partial T$ plus other terms corresponding to bulging from thermal expansion and stress-optic effects. With λ = 174 nm, ℓ = 1 cm, and[7] $\partial_n T = 8 \times 10^{-6}\ \mathrm{K}^{-1}$, this gives

$$T_\circlearrowleft = 0.3\ \mathrm{K} \quad . \tag{3.4}$$

Substituting (3.4) into (2.6) and solving for I gives $I_f = 0.352\ I_\beta$, or

$$I_f = 0.42\ \mathrm{GW/cm^2} \quad . \tag{3.5}$$

for this case of thermally induced optical distortion. For the common short-pulse case, the derivative $\partial n/\partial T$ is at constant lattice spacing as discussed above. Then the value of I_f from this source can be considerably greater than 0.42 GW/cm. This is unimportant in any event since I_f from defocusing by the electron plasma is even greater.

IV. OPTICAL DISTORTION BY THE ELECTRON PLASMA

The change δn_r in the refractive index n_r resulting from exciting conduction electrons can cause optical defocusing (as opposed to focusing, in the sense that δn_r is negative). The estimate below indicates that this process has the lowest threshold I_f of the nonlinear processes considered to date.

The magnitude of δn_r, which is unknown, can be estimated as follows: First, the holes are neglected and the free-electron gas result[9] for $\omega\tau >> 1$

$$n_r = \epsilon^{1/2} = (n_{r0}^2 - \omega_p^2/\omega^2)^{1/2} \tag{4.1}$$

is used. Here

$$\omega_p^2 = 4\pi n_c e^2/m = (6.41 \times 10^{13}\,\text{sec}^{-1})^2 \tag{4.2}$$

for $n_c = 6.46 \times 10^{17}\,\text{cm}^{-3}$ from (2.3) and (3.5) and $m = \frac{1}{2} m_f$. Expanding (4.1) for small ω_p^2/ω^2 gives $n_{r0} + \delta n_r$ with

$$\delta n_r = -\omega_p^2/\omega^2 2n_r = -\left(\frac{n_c}{6.46 \times 10^{17}\,\text{cm}^{-3}}\right) 1.19 \times 10^{-5} \quad . \tag{4.3}$$

Another convenient expression for δn_r is obtained by substituting n_c from (2.3) into (4.3):

$$\delta n_r = -\left(\frac{I}{I_\beta}\right)^2 1.07 \times 10^{-4} \tag{4.4}$$

where $I_\beta \equiv 1.2 \times 10^{\quad}\,\text{/cm}^2$ as before.

A similar value is obtained from an extreme-tight binding estimate. Conceptually, the creation of the electron-hole pair involves the transfer of an electron from a Cl^- ion to a F^+ ion, leaving neutral Cl and F ions. This excitation then must be spread throughout the lattice appropriately. Since the electronic polarizabilities of the Cl^- ion and the neutral Cl ion are different, the refractive index will change on the creation of the electron-hole pair.

As a very rough approximation, the change in the value of $n - 1$ may be of the order of $n - 1 (= 0.44)$ if all N ion pairs per cm^3 were converted to neutral atoms. Specifically, it is assumed that n_r changes by

$$\delta n_r = -0.44\, n_c / N \quad .$$

With $n_c = 6.46 \times 10^{17}\ cm^{-3}$ as above and $N = 6.12 \times 10^{22}\ cm^{-3}$, this expression $\delta n_r = -4.64 \times 10^{-6}$, in reasonable agreement with the value in (4.3).

The criterion used for failure by optical distortion will be taken as[7] $|\delta n_r| = \lambda / 8\ell = 2.15 \times 10^{-6}$. Thus, the estimated value of $|\delta n_r|$ in (4.3) is greater than the corresponding change from heating that corresponds to the failure by optical distortion considered in Sec. III. The value of n_c corresponding to $\delta n_r = -2.15 \times 10^{-6}$ is, from (4.3),

$$n_c = 1.04 \times 10^{17}\ cm^{-3} \quad . \qquad (4.5)$$

The value of I_f that gives rise to $\delta n_r = 2.5 \times 10^{-6}$ is, from (4.4),

$$I_f = 0.142\, I_\beta = 0.170\ GW/cm^2 \quad . \qquad (4.6)$$

It is of interest to compare the electron-plasma value of δn_r with the value

$$\delta n_r = n_2 E^2 \qquad \text{(self focusing)} \qquad (4.7)$$

for self focusing, where $n_2 \cong 10^{-13}$ esu. With $E^2 = 4\pi I / n_r c$, which gives $E = 0.269\,\text{MW/cm}$ for $I = I_\beta = 1.2\,\text{GW/cm}^2$, (4.7) can be written as

$$\delta n_r = \frac{l}{l_\beta}\, 3.2 \times 10^{-7} \qquad \text{(self focusing)} \quad . \qquad (4.8)$$

Comparison with (4.4) shows that at $l = l_\beta$, $|\delta n_r|$ from the electron plasma is a factor of 300 greater than that for self focusing. For small values of l, the self focusing becomes relatively more important since $\delta n_r \sim I$ for self focusing while $|\delta n_r| \sim I^2$ for electron-plasma defocusing. However, what is more important, when $\hbar\omega$ is less than twice the absorption edge, the two-photon process cannot conserve energy, and the remaining smaller absorption process generates fewer electrons. The point is that it is not to be concluded that electron-plasma defocusing would prevent self focusing in general. Finally, C. J. Duthler has suggested that there may be large enhancement in the value of n_2 that could make the self-focusing value of l_f smaller than the electron-plasma value, as discussed in Sec. E.

V. ELECTRON AVALANCHE

In this section it will be shown that electron-avalanche effects lower the values of I_f for fracture and melting, but not for electron-plasma optical distortion. However, the effect is marginal and relatively small errors in the values of parameters used could change this conclusion. In the avalanche multiplication processes considered, it is not necessary to have conduction electrons present originally. This is important since the original density apparently is so small that the probability of finding a conduction electron in a small focal volume is much less than unity. The lucky-reversing electron mechanism, which also is believed to be negligible, is not used.

With avalanche electron multiplication included, (2.1) contains the extra term $\omega_c n_c$:

$$\frac{dn_c}{dt} = \dot{n}_2 + \omega_c n_c \tag{5.1}$$

where ω_c is the electron-avalanche frequency to be discussed below and, from (2.3)

$$\dot{n}_2 = \left(\frac{I}{I_\beta}\right)^2 \frac{7.21\,eV}{\hbar\omega}\, 5.21\times10^{26}\,cm^{-3}\,sec^{-1} \quad . \tag{5.2}$$

At small times, for which n_c is small, the avalanche term $\omega_c n_c$ in (5.1) is negligible with respect to the constant term $\dot{n}_2$, and n_c increases linearly in time. If the pulse is sufficiently long for n_c to reach the value $\dot{n}_2/\omega_c$, the avalanche term $\omega_c n_c$ dominates and n_c increases exponentially. Thus it is seen that electron avalanche is negligible if

$$n_c < \dot{n}_2/\omega_c \equiv n_{cx} \quad . \tag{5.3}$$

An estimate of the value of ω_c can be obtained as follows. It is easy to show by the agreement of Sec. B that previous electron-avalanche mechanisms give extremely small values of ω_c. The strongest conduction-electron-generation process seems to be the Holstein photon-electron-phonon process, which increases $\mathcal{E}$ from the small equilibrium value to $\hbar\omega = 7.21\,\text{eV}$, followed by a vertical, one-photon, inter-conduction-band transition. The Holstein process, which is discussed in Sec. C-IX, allows the electron to absorb the full energy $\hbar\omega$ of the photon in a single process since the phonon can take up the excess momentum. The value of the frequency $\omega_H(k_BT)$ of the Holstein process for electrons of energy k_BT is obtained from (9.26), (9.16), (9.19b), (9.21), and (9.29c) of Sec. C-IX, from which the scaling factors from NaCl to LiF are

$$\omega_{H0} \sim \frac{(2n_{L0}+1)\lambda^{7/2}}{a_{nn}^3 M_r \omega_p} , \tag{5.4}$$

$$\omega_{HA} \sim \frac{a_{nn}\theta_D^2 \lambda^{5/2}}{M_\Sigma \omega_p^2} . \tag{5.5}$$

It was assumed that the deformation-potential parameter $\mathcal{E}_1$ scales as the Debye temperature θ_D and that $2n_{LA}+1 \cong 2k_BT/\hbar\omega_{LA}$ for the longitudinal-acoustical modes. Relative values of the parameters in (5.4) and (5.5) for LiF/NaCl are: $a_{nn} \sim 2.014/2.820$; $\omega_p \sim \omega_{L0} = 662/264$; $M_r = 5.08/13.9$; $2n_{L0}+1 \sim 1.09/1.79$; $M_\Sigma \sim 25.95/58.45$; and $\theta_D \sim 732/321$. With these values, the equations listed above give

$$\omega_c = \omega_H(k_BT) = \frac{I}{I_\beta}\, 5.15 \times 10^8\,\text{sec}^{-1} . \tag{5.6}$$

Substituting (5.2) and (5.6) into (5.3) gives

$$n_{cx} = (I/I_\beta)\ 1.01 \times 10^{18}\ cm^{-3} \quad . \qquad (5.7)$$

From (4.3) with $\delta n_r = -2.15 \times 10^{-6}$ the value of n_c is $1.16 \times 10^{17}\ cm^{-3}$. From (5.7) with $I = 0.2\ GW/cm^2$, $n_{cx} = 1.69 \times 10^{17}\ cm^{-3}$. Thus n_c is only slightly less than n_{cx}, and avalanche multiplication is not entirely negligible for electron-plasma optical distortion.

The same comparison of n_c with n_{cx} for the cases of fracture and melting show that electron avalanche cannot be neglected for these cases either. For example, for fracture, (2.3) and (5.7) with $I = 1.0\ GW/cm^2$ give $n_c = 3.62 \times 10^{18}\ cm^{-3}$ and $n_{cx} = 8.43 \times 10^{17}\ cm^{-3}$. The corresponding values for melting are $n_c = 1.13 \times 10^{20}\ cm^{-3}$ and $n_{cx} = 4.66 \times 10^{18}\ cm^{-3}$. In both cases $n_c > n_{cx}$.

Including electron avalanche reduces the values of I_f as follows. Substituting the solution to (5.1),

$$n_c = (\dot{n}_2/\omega_c)[\exp(\omega_c t) - 1] \qquad (5.8)$$

into (2.4), using (2.5), and integrating gives

$$T = \frac{4\pi\sigma_1 \dot{n}_2 I}{C\omega_c^2 n_r c}\left(e^{\omega_c t} - 1 - \omega_c t\right) \quad .$$

Setting $t = t_p$ and taking the logarithm gives

$$\omega_c t_p = \ell n\left(\frac{CT n_r c \omega_c^2}{4\pi \dot{n}_2 \sigma_1 I} + 1 + \omega_c t_p\right) \qquad (5.9)$$

which can be written in the convenient form

$$\frac{I}{I_\beta} = \frac{1}{5.15} \ln \left(1.47 \times 10^3 \frac{T}{843} \frac{I_\beta}{I} + 1 + 5.15 \frac{I}{I_\beta} \right) \quad . \tag{5.10}$$

where (5.6) has been used.

The value of I can now be found by solving (5.10) numerically, which gives $I_f = 1.6\ \mathrm{GW/cm^2}$ for $T = T_m = 843\,\mathrm{K}$. This value is smaller than the value of $5.6\ \mathrm{GW/cm^2}$ calculated with avalanche neglected and is an order of magnitude smaller than $I_f = 20\,\mathrm{GW/cm^2}$ for two-photon absorption only. The value of E corresponding to $I = 1.6\ \mathrm{GW/cm^2}$ is $E = (4\pi I/cn_r)^{1/2} = 0.65\,\mathrm{MV/cm}$.

For $T = T_{fr} = 7\,\mathrm{K}$, the solution of (5.10) is $I = 0.617\ I_\beta = 0.74\,\mathrm{GW/cm^2}$, which is only slightly smaller than the value $1.0\,\mathrm{GW/cm^2}$ obtained by neglecting electron avalanche. For $T = 0.3\,\mathrm{K}$, (5.10) gives $I = 0.284\ I_\beta = 0.34\,\mathrm{GW/cm^2}$, compared with $I = 0.352\ I_\beta = 0.42\,\mathrm{GW/cm^2}$ without avalanche breakdown.

For the case of electron-plasma defocusing, where the failure criterion is $n_c = 1.04 \times 10^{17}\,\mathrm{cm^{-3}}$ from (4.5) rather than $T = T_m$ or T_{fr} Thus (5.8) is written as

$$\omega_c t_p = \ln \left(\frac{n_c \omega_c}{\dot{n}_2} + 1 \right) \quad . \tag{5.11}$$

With n_c from (4.5), ω_c from (5.6), and $\dot{n}_2$ from (5.2), this result (5.11) becomes

$$\frac{I}{I_\beta} = \frac{1}{5.15} \ln \left(0.103 \frac{I_\beta}{I} + 1 \right)$$

which is easily solved to give

$$I_f = 0.120\ I_\beta = 0.144\ \text{GW/cm}^2 \qquad (5.12)$$

as the threshold for the electron-plasma defocusing with all effects included.

VI. CONDUCTION-ELECTRON GENERATION AND HEATING BY EXTRINSIC LINEAR ABSORPTION

It will be shown that the generation of electrons by one-photon absorption, the multiplication by the electron-avalanche process, and the resulting electron-plasma defocusing can give the lowest failure threshold, $I_f = 60\,MW/cm^2$, of any of the processes considered to date. However, such a low threshold would require nearly one conduction electron generated for each photon absorbed and no bleaching of the absorption centers for 10^{17} photons per cubic centimeter absorbed. For impurity absorption, this value of $10^{17}\,cm^{-3}$ corresponds to 1.3 parts per million of the impurity, which may well exist in the samples.

Tomiki and Miyata[10] have reported values of β for LiF, as well as for NaF, CaF_2, BaF_2, and SrF_2, between 0.1 and $1\,cm^{-1}$ at 7.21 eV. The origin of such strong absorption is not known, but it is surely extrinsic and is expected to vary from sample to sample. At such a high photon energy as 7.21 eV, the process must be electronic. It is likely that conduction electrons are generated in this absorption process, but this is by no means certain. For example, transitions between electrons in the valence bands and imperfection states in the gap could be involved. The consequences of assuming that conduction electrons are generated will now be considered.

For η electrons generated by each photon, the rate of conduction-electron generation $\dot{n}_1$ is

$$\dot{n}_1 = \eta \frac{\beta I}{\hbar\omega} = \eta \frac{\beta}{1\,cm^{-1}} \frac{I}{I_\beta} 1.04 \times 10^{27}\,cm^{-3}\,sec^{-1} \quad . \qquad (6.1)$$

Comparison with (5.2) shows that for the observed value of $\beta = 0.15\,\mathrm{cm}^{-1}$ and $\eta = 1$, the one-photon and two-photon generation rates are equal at $I = 0.36$ $\mathrm{GW/cm}^2$, and that $\dot{n}_1 > \dot{n}_2$ for smaller values of I. Thus $\dot{n}_1$ is not negligible in general.

The corresponding value of I_f for electron-plasma defocusing is easily obtained from (5.11) with ω_c given by (5.6) and $\dot{n}_2$ replaced by $\dot{n}_2 + \dot{n}_1$. This gives

$$\frac{I}{I_\beta} = \frac{1}{5.15}\,\ell n\left(\frac{0.343}{1 + 3.34\,(I/I_\beta)^2} + 1\right) \quad .$$

The solution is

$$I_f = 5.00 \times 10^{-2}\, I_\beta = 60\,\mathrm{MW/cm}^2 \quad . \qquad (6.2)$$

From (5.4) the value n_c corresponding to (6.2) is

$$n_c = 1.04 \times 10^{17}\,\mathrm{cm}^{-3} \quad . \qquad (6.3)$$

In order to generate this electron density, there must be a sufficiently great density of imperfections. Some of the $10^{17}\,\mathrm{cm}^{-3}$ electrons in (6.3) are generated by the avalanche process, some by two-photon ionization, and some by ionizing the imperfections. The density from imperfections is, neglecting saturation

$$n_{imp} \cong \dot{n}_1 t_p = 7.8 \times 10^{16}\,\mathrm{cm}^{-3} \quad .$$

Thus, most of the electrons come directly from the imperfections in this case. The corresponding imperfection concentration is $7.8 \times 10^{16} / 6.09 \times 10^{22}$, or 1.3 parts per million.

This value appears to be reasonable, and it is consistent with the following rough estimate. A typical absorption cross section σ_{xc} is

$$\sigma_{xc} = \beta / N \cong 10^{5}\,\mathrm{cm}^{-1} / 6 \times 10^{22}\,\mathrm{cm}^{-3} = 1.7 \times 10^{-18}\,\mathrm{cm}^{2} \quad .$$

Thus,

$$n_{imp} = \beta / \sigma_{xc} \cong 0.15\ \mathrm{cm}^{-1} / 1.17 \times 10^{-18}\,\mathrm{cm}^{2} = 9 \times 10^{16}\,\mathrm{cm}^{-1} \quad .$$

The estimate indicates that the imperfection density n_{imp} corresponding to the measured value of β is marginally sufficient to furnish the required number of electrons.

Next, consider the ordinary linear heating by one-photon absorption. The rate of energy absorption by the sample is $d\mathcal{E}_a / dt = \beta I V$, which can be integrated to give

$$\mathcal{E}_a / V = \beta I t_p \quad . \tag{6.4}$$

If the absorbed energy were converted to heat, the temperature rise would be

$$T = \frac{\beta}{1\,\mathrm{cm}^{-1}} \; \frac{I}{I_\beta} \; \frac{t_p}{10^{-8}\,\mathrm{sec}} \left(\frac{4.21\,\mathrm{J/cm^3\,K}}{C} \right) 2.85\,\mathrm{K} \tag{6.2}$$

Thus, the observed value of $\beta \cong 0.15\,\mathrm{cm}^{-1}$ gives $T = 0.43\,\mathrm{K}$ at $I = I_\beta = 1.2$ $\mathrm{GW/cm^2}$, which is sufficient to cause thermally induced optical distortion, assuming that the value of $T_o = 0.3\,\mathrm{K}$ for constant stress is appropriate.

The thermally induced optical distortion is negligible with respect to the electron-plasma defocusing unless the quantum efficiency η is quite low. Furthermore, the value of $T = 0.43\,K$ may be reduced, possibly by a factor of 10 or more in some cases, by incomplete conversion of the absorbed energy to heat, as discussed in Sec. VIII. Finally, the absorption may saturate as above. For example, in the present case if transitions from (or to) impurity levels are involved in the absorption, all of the levels may be emptied (or filled) before $\mathcal{E}_a$ reaches the value in (6.4).

VII. F-CENTER EFFECTS

It will be shown that the well known F-center absorption in "uncolored" LiF crystals at 7.21 eV and $t_p = 10^{-8}$ sec is negligible. A new electron-avalanche and heating mechanism involving trapping of electrons by negative-ion vacancies is found to be unimportant in uncolored crystals at 7.21 eV, although it can be important at other frequencies.

Consider the density n_F of F centers and the density n_- of negative-ion vacancies, which are needed in the calculation of both effects. The value of the absorption coefficient β in the F-center absorption band has been well studied for many alkali halides. The results are often related to Smakula's equation,[11] which gives

$$\beta \cong 2 \times 10^{-16} n_F \, \text{cm}^{-1} \tag{7.1}$$

where n_F is the number of F centers per unit volume, for NaCl or KCl at 300 K at the absorption peak. The value for LiF at 300 K should be approximately the same. The room-temperature absorption peak for LiF occurs at 5.0 eV. The value of β at 7.21 eV is much smaller than the peak value in (7.1) of course. Absorption on the high-frequency side of the F-center absorption band (in the H, K, L, and V bands and nearer the absorption edge in the α and β bands, for example), has been studied in detail in a number of materials, but apparently not in LiF.

For the chloride crystals LiCl, NaCl, KCl, RbCl, and CsCl, the F-center absorption occurs in the visible; thus the presence of F centers manifests itself as coloration of the crystals, which are water-white when pure. One simple criterion for detectability of absorption is that $\beta > 10^{-2} \text{cm}^{-1}$. Then for $\ell = 1$ cm

one percent of the radiation is absorbed. This criterion, which will be denoted "uncolored," will be used in estimating the number of F centers in high-quality LiF, where the F-center absorption is in the ultraviolet, rather than visible, region.

According to (7.1) with $\beta > 10^{-2}\,cm^{-1}$,

$$n_F \lesssim 5 \times 10^{13}\,cm^{-3}$$

for an uncolored crystal. Even if every electron were excited from the F centers into the conduction band, the resulting value of $n_c = 5 \times 10^{13}\,cm^{-3}$ is much less than the value of $1.5 \times 10^{17}\,cm^{-3}$ generated by two-photon absorption according to (2.3) with $I = 0.2\,GW/cm^2$. In fact, $1.5 \times 10^{17}\,cm^{-3}$ would be large concentration of F centers. The maximum F-center concentration that we have found in the literature, which was $5 \times 10^{19}\,cm^{-3}$ in a <u>thin film</u> at the surface of a NaCl sample generated by electrons and measured at 90 K, is several orders of magnitude higher than densities normally encountered. The point is that it is likely that F-center absorption will be negligible with respect to two-photon absorption at 7.21 eV and 10 nsec unless the crystals are very heavily colored.

It should be mentioned that in a single 10 nsec pulse there will be very few F centers formed by trapping the generated electrons at existing chlorine vacancies since the time constant for this process is $\sim 10^{-6}$ sec. Direct F-center formation by the two-photon absorption process is believed to be small since $2\hbar\omega$ is not near the exciton absorption peak. However, the effect of high transient absorption recently observed[12] at the Naval Research Laboratories will be considered in a later report.

Consider the second F-center effect associated with the excited state. It is known that conduction electrons are readily trapped by negative-ion vacancies to form the excited state F^* of an F center. The subsequent transition to the ground state F_g is slow ($\sim 10^6$ sec at room temperature in NaCl). Since the F^* state is localized, it is not necessary to conserve momentum in the process of absorbing a photon. Thus, the photon energy $\hbar\omega$ can be absorbed by the electron, as it can in the Holstein process.

In the cF^*c^* process, a low-energy conduction electron c is trapped in the F^* state and then absorbs a photon $\hbar\omega$ and ends in the conduction-band state c^* with energy $\hbar\omega - \varepsilon_{F^*}$. Very briefly, the estimate that this process is negligible in the current case of uncolored crystals at 7.21 eV uses the value $\omega_{cF^*} = 8.25 \times 10^9 \times (n_-/5\times 10^{15}\,\mathrm{cm}^{-3})\,\mathrm{sec}^{-1}$, which is an estimated[13] value for NaCl, and

$$\omega_{F^*c^*} = \frac{I}{I_\beta}\,\frac{7.21\,\mathrm{eV}}{\hbar\omega}\,G(\omega)\,1.04\times 10^{11}\,\mathrm{sec}^{-1} \quad . \qquad (7.2)$$

In (7.2), the peak value (at G = 1) was estimated by using the cross section corresponding to Smakula's equation. For $\hbar\omega \gg \varepsilon_{ph}$, where ε_{ph} is the value of $\hbar\omega$ at which the maximum absorption occurs, $G(\omega)$ should not be greater than

$$G(\omega) = \frac{2\,\omega_{pk}^2}{\omega^2 + \omega_{pk}^2} \cong 2\,(0.22/7.21)^2 = 1.86\times 10^{-3} \quad .$$

where ω_{pk} is the value of ω at the absorption peak. With (7.2) this gives $\omega_{F^*c^*} \cong 1.9\times 10^8\,\mathrm{sec}^{-1}$, and the contribution $\dot{n}_{F^*}$ of cF^*c^* to dn_c/dt is

$$\dot{n}_{F^*} = \frac{I}{I_\beta} \frac{7.21\,eV}{\hbar\omega} \frac{n_{F^*}}{5\times10^{15}cm^{-3}} \frac{G(\omega)}{1.9\times10^{-3}} 9.50\times10^{23}cm^{-3}sec^{-1} \qquad (7.3)$$

after all n_- traps have been filled. It was tacitly assumed that the c^* electrons are in turn given energy $\mathcal{E} \geq \mathcal{E}_I$ by the one-photon absorption process so that another conduction electron is generated. Comparison of (7.3) with (5.2) gives $\dot{n}_{F^*} = \dot{n}_2$ at $I = 2.16\times10^{-3}\,GW/cm^2$ for $n_{F^*} = 5\times10^{15}cm^{-3}$, or at $0.216\,GW/cm^2$ at $5\times10^{17}cm^{-3}$, which shows that the effect is negligible except perhaps at high negative-ion concentrations or low intensities.

Since the absorption is so far in the wings of the assumed bound-state to bound-state process, the frequency for the bound state to free-electron state was calculated, but found to be negligible. Using the golden-rule result for the transition probability $TP = (2\pi/\hbar) \sum_k \left| M_{F^*c^*} \right|^2 \delta(\mathcal{E})$, a parabolic conduction band, $\phi \sim \exp(-\kappa r)$, with κ^{-1} of the order of a few tens of angstroms, for the F^* wave function, the $\underset{\sim}{A}\cdot\underset{\sim}{p}$ interaction Hamiltonian, and free electrons in the conduction band gives

$$\omega_{F^*c^*} = TP = \frac{I}{I_\beta} \frac{16\mathcal{E}^{3/2}\mathcal{E}_\kappa^{5/2}}{(\mathcal{E}+\mathcal{E}_\kappa)^4} \left(\frac{1.44}{n_r}\right)\left(\frac{7.21\,eV}{\hbar\omega}\right) 1.56\times10^{7}sec^{-1}$$

which is smaller even at the peak at $\mathcal{E} \cong \mathcal{E}_\kappa$ than the value $1.9\times10^{9}\,sec^{-1}$ used above.

The cF^*c^* process can be important in other cases as a heating mechanism when the c^* electrons relax back to thermal equilibrium, rather than being further accelerated to $\mathcal{E} \geq \mathcal{E}_I$. Finally, it should be pointed out that some process such as two-photon absorption is necessary to supply the c electrons to start the cF^*c^* process.

VIII. TWO-PHOTON-HEATING TIME DELAY

The final effect considered here is that the energy $2\hbar\omega$ absorbed by the crystal when the two photons are absorbed does not appear as heat in the crystal during the pulse duration. This effect is less important than the δn_r effect above since the Joule heating dominates the straight β absorption heating even under the assumption that the $2\hbar\omega$ of energy appears as heat instantaneously. This is fortunate since the conversion to heat is not completely understood.

The following brief comments illustrate the types of problems involved. The central effects are that the time constants involved in the relaxation of the electronic energy to heat may be longer than the laser pulse duration (so that the heating occurs after the pulse is over) and that part of the $2\hbar\omega$ energy may never appear as heat since it can be radiated in the luminescence process or carried off by photoelectric electrons.

The excess energy of the electron above the conduction band minimun (at $\underset{\sim}{k} = 0$) is converted to heat rapidly, in a time of the order of the electron-relaxation frequency $\tau = 10^{-15}$ sec. The time for the mechanical movement of the ions involved in forming the V_k center, that is the self trapping of the hole, is of the order of a phonon vibrational frequency, or $\sim 10^{-13}$ sec. Thus, at least of the order of half the energy $2\hbar\omega$ is converted to heat within the pulse duration of 10^{-8} sec.

The fate of the remainder of the energy is less clear. At low temperature (77 K) a large fraction of the energy may be carried off by the luminescence photons. At room temperature the luminescence is negligible. The competing

recombination processes that dominate the luminescence process surely involve phonons, that is, heat generation. These room-temperature recombination times surely are longer than the pulse duration. Typical values of the luminescence lifetimes at 4 K are microseconds althouth variation by plus and minus three orders of magnitude occur. The luminescence of the F center in KCl goes to zero at -50 C.

REFERENCES

1. M. Sparks and C. J. Duthler, Xonics, Inc. Third Technical Report, Contract No. DAHC15-73-C-0127, 30 June 1974.
2. N. Basov, V. Denilychev, and Y. Popov, Sov. J. Quantum Electron. 1, 18 (1971).
3. P. W. Hoff, J. C. Swingle, and C. K. Rhodes, Appl. Phys. Lett. 23, 245 (1973).
4. J. B. Gerardo and A. W. Johnson, J. Appl. Phys. 44, 4120 (1973).
5. R. W. Hellwarth, National Bureau of Standards Special Publication No. 341, p. 67 (1970).
6. E. Yablonovitch and N. Bloembergen, Phys. Rev. Lett. 29, 907 (1972).
7. M. Sparks, J. Appl. Phys. 42, 5029 (1971).
8. M. Sparks and C. J. Duthler, J. Appl. Phys. 44, 3038 (1973).
9. C. Kittel, Introduction to Solid State Physics, 4th ed. (Wiley, New York, 1971).
10. T. Tomiki and T. Miyata, J. Phys. Soc. Japan 27, 658 (1969).
11. J. J. Markham, F-Centers in Alkali Halides, ed. by F. Seitz and D. Turnbull (Academic, New York, 1966).
12. R. T. Williams, J. N. Bradford, and W. L. Faust, Proc. Conference of Optical Properties of Transparent Solids, Waterville Valley, New Hampshire, Febr. 1975 (to be published); J. N. Bradford, R. T. Williams, and W. L. Faust, Phys. Rev. Lett., in press.
13. P. F. Braunlich, Bendix Research Laboratories Final Report, Contract No. F19628-73-C-0032, August (1974).

E. OPTICAL DISTORTION FROM THE NONLINEAR REFRACTIVE INDEX

C. J. Duthler

Xonics, Incorporated, Van Nuys, California 91406

I. INTRODUCTION

One of the major factors limiting the power of high-intensity, short-pulse lasers in the visible and near infrared spectral regions (e.g., Nd-glass laser) is self focusing arising from intensity dependence of the refractive index

$$n = n_0 + n_2 \langle E^2 \rangle \quad . \tag{1}$$

In Eq. (1), n_0 is the usual linear refractive index, n_2 is the nonlinear refractive index, and $\langle E^2 \rangle$ is the mean-squared value of the electric field. When an intense beam having a higher intensity at the beam center than at the beam edge is incident on a sample of optical material, the refractive index of the sample is slightly increased with the increase being greater at the center of the beam than at the edge. Consequently the optical path length through the center of the sample is greater than at the edge with the result that a sample with plane-parallel faces will behave as a lens. At very high intensities, self focusing and permanent damage occurs within the material. At lower intensities, undesirable optical distortion of the beam occurs.

For a passive optical component having plane-parallel faces and thickness z, our criterion for the threshold of optical distortion is that the change in the optical path length at the center of the beam be 1/8 wave:

$$\lambda/8 = (\delta n)z = n_2 \langle E^2 \rangle z \quad . \tag{2}$$

Using $I = cn_0\langle E^2\rangle/4\pi$, the intensity threshold for optical distortion is

$$I_{th} = cn_0\lambda/32\pi n_2 \quad , \tag{3}$$

where a sample thickness of 1 cm has been assumed.

In this section, we are concerned with nonlinear changes in the refractive index that arise from intensity dependent changes in the susceptibility of bound electrons in the solid. The electronic susceptibility makes the dominant contribution to the nonlinear index in the visible and ultraviolet, with lattice vibrations making a small contribution in the near infrared.[1] Two-photon absorption results in the creation of mobile electron-hole pairs which in turn yield a nonlinear index. This additional nonlinear index from free carriers is expected to be dominant at 7.2 eV in LiF and is considered in Sec. D.

A typical value of $n_2 = 10^{-13}$ esu is observed in the visible and near infrared. If this value along with $n_0 = 1.44$ and $\lambda = 174$ nm is used in Eq. (3), the distortion threshold $I_{th} = 7.5\ \mathrm{GW/cm^2}$ is obtained. As is shown in the following, the nonlinear index may be considerably enhanced in the vacuum ultraviolet if the wavelength is near a two-photon absorption band. The degree of enhancement depends on the strength and width of the two-photon absorption band and is not expected to be severe in LiF because of the expected broad-band nature of the two-photon absorption in this material.

The frequency dependence of the nonlinear index has not been studied experimentally. However, enhancement has been observed experimentally in other nonlinear susceptibilities that have similar theoretical frequency dependences.

Levenson et. al.[2] have observed a factor of 100 enhancement in the three-wave mixing intensity in diamond when the difference frequency was resonant with the infrared absorption band. Braunstein and Ockman[3] speculate that the factor of 100 larger frequency doubling coefficient that they observe in GaAs as compared to KDP may be a result of being in a two-photon absorption band in GaAs.

II. CALCULATION OF THE NONLINEAR INDEX

To calculate the frequency dependence of n_2 for materials in the vacuum ultraviolet, the response of the electronic susceptibility to an intense monochromatic perturbation is considered. First-order perturbation theory gives the usual linear susceptibility and refractive index. The second-order response has twice the applied frequency (hence frequency doubling) and vanishes in crystals having a center of inversion as with alkali halides and alkaline-earth halides (most candidate 7.2 eV window materials). Third-order perturbation theory yields a response at the applied frequency and at three times the applied frequency. The third-order susceptibility $\chi_{\omega}^{(3)}$ at the applied frequency yields the nonlinear index while the response at three times the applied frequency yields frequency tripling.

The third-order polarizability of isolated molecules without a permanent dipole moment has been calculated to be:[4]

$$\alpha_{\omega}^{(3)} = -\frac{1}{2}\frac{e^4}{\hbar^3}\sum_k{}'\sum_\ell{}' |x_{0k}|^2 |x_{0\ell}|^2 [2\omega_{\ell 0}(\omega_{k0} \pm \omega)^{-2}(\omega_{\ell 0}^2 - \omega^2)^{-1}$$

$$+ (\omega_{\ell 0} \pm \omega)^{-1}(\omega_{k0}^2 - \omega^2)^{-1} + 2\omega_{k0}(\omega_{k0}^2 - \omega^2)^{-1}(\omega_{\ell 0}^2 - \omega^2)^{-1}$$

$$+ 2\omega_{k0}(\omega_{k0}^2 - \omega^2)^{-1}(\omega_{\ell 0} \pm \omega)^{-2}]$$

$$+ \frac{e^4}{\hbar^3}\sum_k{}'\sum_\ell{}'\sum_m{}' [x_{0k}x_{k\ell}x_{\ell m}x_{m0}][(\omega_{k0} \pm \omega)^{-1}(\omega_{\ell 0} \pm 2\omega)^{-1}(\omega_{m0} \pm \omega)^{-1}$$

$$+ 2(\omega_{k0} \pm \omega)^{-1}\omega_{m0}\omega_{\ell 0}^{-1}(\omega_{m0}^2 - \omega^2)^{-1}] \quad , \tag{4}$$

where e is the electronic charge and x_{0k} and $\hbar\omega_{0k}$ are the dipole matrix element and energy difference between the ground state and k^{th} excited state, respectively. The sums run over all excited states and the notation $\pm$ implies summation over both + and - terms.

A simple case that still contains the essential physics is a molecule with three electronic levels: a ground state 0 and two excited states 1 and 2 with allowed dipole matrix elements between 0 and 1 and between 1 and 2.[5] Looking forward to the application of this model system to LiF, the excited state 1 can be associated with the exciton level and the level 2 with the conduction band. Alternatively, the excited state 1 could be associated with a higher level conduction band or with a lower valence band. The present state of knowledge of the band structure of LiF is not sufficient to predict which choice will be dominant. However, the various choices result in only slightly different frequency dependences with the resonant enhancement near $\frac{1}{2}$ the band gap, derived below, being common to all choices. Taking $\omega_{01} \cong \omega_{02} = \omega_0$ with $\omega_{02} - \omega_{01} = \omega_{12} \ll \omega_0$ and writing the dipole matrix element in terms of the oscillator strength $|x_{01}|^2 = \hbar f_{01}/2m\omega_0$ yields:

$$\alpha_\omega^{(3)} = -4\,\frac{e^4}{\hbar^3}\left(\frac{\hbar}{2m}\right)^2 f_{01}^2\,\frac{(3\omega_0^2+\omega^2)}{\omega_0(\omega_0^2-\omega^2)^3}$$

$$+\,2\,\frac{4}{\hbar^3}\left(\frac{\hbar}{2m}\right)^2 f_{01}f_{12}\,\frac{1}{\omega_{12}(\omega_0^2-\omega^2)^2}\left[\frac{(\omega_0^2+5\omega^2)}{(\omega_0^2-4\omega^2)}+2\right]. \quad (5)$$

At low frequencies and for frequencies near one-half the resonant frequency, the second (positive) term is dominant with the ratio of the two terms at low frequencies being ω_0/ω_{12}.[5] Hence the first term is neglected in the following.

The frequency dependence of the polarizability can be calculated more accurately than the magnitude. Therefore the polarizability is written in terms of the low-frequency limit $\alpha_0^{(3)}$ where $\alpha_0^{(3)}$ can be obtained from experiments in the visible or from a separate calculation. Methods for obtaining $\alpha_0^{(3)}$ from linear optical constants have been proposed.[5,6] The low-frequency limit of Eq. (5) is

$$\alpha_0^{(3)} = 6 \frac{e^4}{\hbar^3} \left(\frac{\hbar}{2m}\right)^2 f_{01} f_{12} \frac{1}{\omega_{12} \omega_0^4}$$

which is used to write Eq. (5) in the form:

$$\alpha_\omega^{(3)} = \frac{1}{3} \alpha_0^{(3)} \frac{\omega_0^4}{(\omega^2 - \omega_0^2)^2} \left[\frac{(\omega_0^2 + 5\omega^2)}{(\omega_0^2 - 4\omega^2)} + 2 \right] . \qquad (6)$$

This is plotted in Fig. 1 where, in the absence of damping, the nonlinear polarizability diverges at $\omega_0/2$. Damping via two-photon absorption can be included in Eq. (6) by adding a small imaginary part to $\omega_0 \rightarrow \omega_0 + i\Gamma$, where Γ^{-1} is the lifetime of the excited state. For narrow lines, this will result in $(\omega_0^2 - 4\omega^2)^{-1}$ being replaced by $(\omega_0^2 - 4\omega^2)^{-1} + (i\pi/4\omega)\,\delta(2\omega - \omega_0)$.

For a solid consisting of N molecules per unit volume, the susceptibility corresponding to the polarizability in Eq. (5) is

$$\chi_\omega^{(3)} = 2\left(\frac{n_0+1}{3}\right)^4 \frac{e^4}{\hbar^3} \left(\frac{\hbar}{2m}\right)^2 \sum_k \frac{f_{01} f_{12}}{\omega_{12}(\omega^2 - \omega_k^2)^2} \left[\frac{(\omega_k^2 + 5\omega^2)}{(\omega_k^2 - 4\omega^2)} + 2 \right] . \qquad (7)$$

The sum runs over oscillators distributed throughout the Brillouin zone with resonant frequencies ω_k. A local-field correction factor has been added.

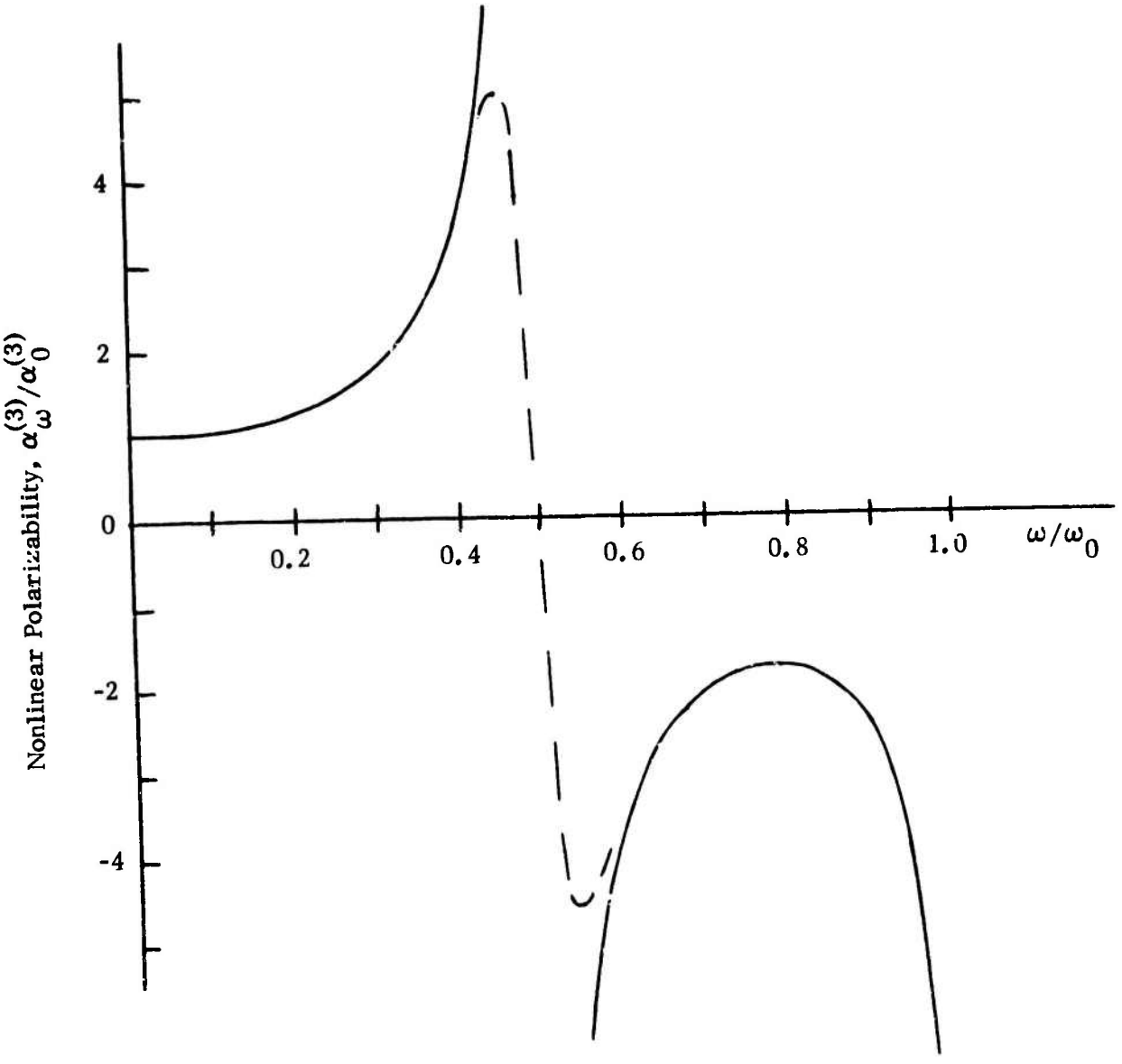

Fig. 1. Dependence of the nonlinear polarizability on frequency. Dashed line indicates the effect of damping.

Neglecting the frequency dependence of the f-numbers, ω_{12}, and n_0, Eq. (7) can be written in terms of the low-frequency susceptibility $\chi_0^{(3)}$:

$$\chi_\omega^{(3)} = \frac{1}{3N}\chi_0^{(3)} \sum_k \frac{\omega_k^4}{(\omega^2 - \omega_k^2)^2} \left[\frac{(\omega_k^2 + 5\omega^2)}{(\omega_k^2 - 4\omega^2)} + 2 \right] . \tag{8}$$

Using $n_2 = 2\pi\chi_\omega^{(3)}/n_0$ yields the frequency dependence of the nonlinear refractive index:

$$n_2 = \frac{1}{3N} n_{20} \sum_k \frac{\omega_k^4}{(\omega^2 - \omega_k^2)^2} \left[\frac{(\omega_k^2 + 5\omega^2)}{(\omega_k^2 - 4\omega^2)} + 2 \right] . \tag{9}$$

The sum in Eq. (9) is replaced by an integral using the well-known relations:

$$\frac{1}{N}\sum_k \rightarrow \frac{1}{N} \int_{BZ} \frac{k^2\,dk}{\pi} \rightarrow \frac{3}{2(\omega_m - \omega_g)^{3/2}} \int_{\omega_g}^{\omega_m} d\omega' (\omega' - \omega_g)^{1/2} . \tag{10}$$

In writing Eq. (10), parabolic bands with $\omega_k = \omega_g + \hbar k^2/2m$ have been assumed which yield the density of states $(\omega' - \omega_g)^{1/2}$ for $\omega_g < \omega' < \omega_m$. The assumption of parabolic bands with slowly varying f-numbers is expected to be approximately valid for LiF and other direct band-gap, insulating solids. For LiF the bands are broad with $\omega_m \cong 2\omega_g$.

Using Eq. (10) yields

$$n_2 = n_{20} \frac{1}{2(\omega_m - \omega_g)^{3/2}} \int_{\omega_g}^{\omega_m} \frac{\omega'^4 (\omega' - \omega_g)^{1/2}}{(\omega^2 - \omega'^2)^2} \left[\frac{(\omega'^2 + 5\omega^2)}{(\omega'^2 - 4\omega^2)} + 2 \right] d\omega' . \tag{11}$$

For frequencies ω near $\omega_g/2$ or less, the only terms in the integrand that are strongly dependent on frequency are the denominator of the first term within the square bracket and the density of states. In order to simplify the integral, ω' in the other terms is replaced by ω_g which yields

$$n_2 = \frac{2}{3} n_{20} \frac{\omega_g^4}{(\omega^2 - \omega_g^2)^2} + \frac{1}{2} n_{20} \frac{\omega_g^4 (\omega_g^2 + 5\omega^2)}{(\omega_m - \omega_g)^{3/2} (\omega^2 - \omega_g^2)^2} \int_{\omega_g}^{\omega_m} \frac{(\omega' - \omega_g)^{1/2} d\omega'}{(\omega'^2 - 4\omega^2)} \quad . \tag{12}$$

The value of the integral is

$$\vartheta(\omega < \omega_g/2) = \frac{1}{2\omega} (\omega_g + 2\omega)^{1/2} \tan^{-1} \left[\frac{(\omega_m - \omega_g)^{1/2}}{(\omega_g + 2\omega)^{1/2}} \right]$$

$$- \frac{1}{2\omega} (\omega_g - 2\omega)^{1/2} \tan^{-1} \left[\frac{(\omega_m - \omega_g)^{1/2}}{(\omega_g - 2\omega)^{1/2}} \right]$$

and

$$\vartheta(\omega_g/2 < \omega < \omega_g) = \frac{1}{2\omega} (\omega_g + 2\omega)^{1/2} \tan^{-1} \left[\frac{(\omega_m - \omega_g)^{1/2}}{(\omega_g + 2\omega)^{1/2}} \right]$$

$$- \frac{1}{2\omega} (2\omega - \omega_g)^{1/2} \ln \left| \frac{(2\omega - \omega_g)^{1/2} + (\omega_m - \omega_g)^{1/2}}{(2\omega - \omega_g)^{1/2} - (\omega_m - \omega_g)^{1/2}} \right| \quad . \tag{13}$$

The nonlinear index from Eqs. (12) and (13) is plotted as a function of frequency in Fig. 2 where the value $\omega_m = 2\omega_g$ has been assumed. Notice that although the polarizabilities of the individual oscillators in Eq. (6) and Fig. 1 diverge, the integral over the oscillators remains finite except near $\omega_m/2 \cong \omega_g$

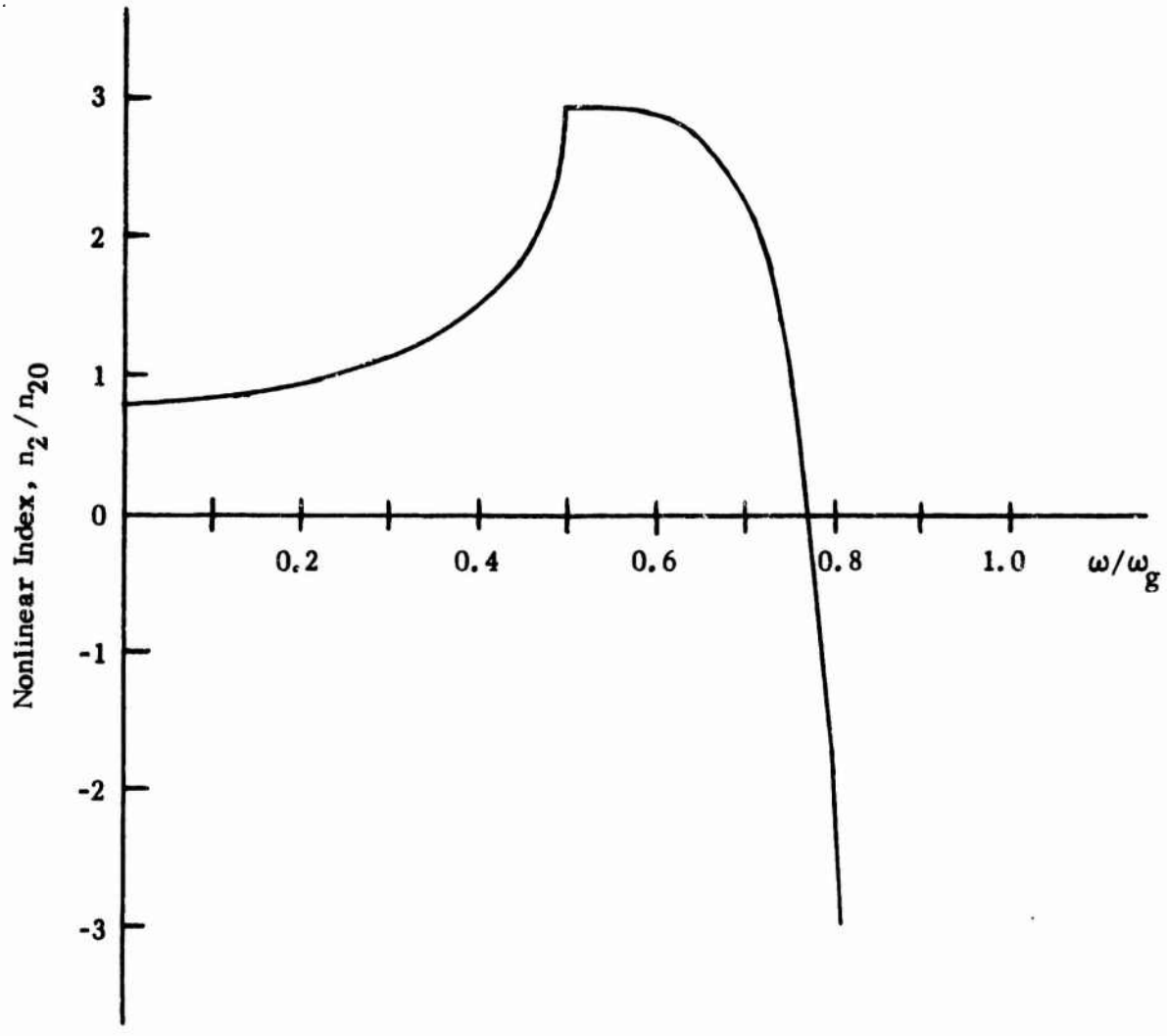

Fig. 2. Dependence of the nonlinear refractive index on frequency.

where the integral diverges logarithmically. This infinity in the integral can be removed if the density of states is not truncated abruptly at ω_m. Near $\omega_m/2 \approx \omega_g$ the nonlinear index n_2 goes to minus infinity more strongly than the integral due to the terms outside the integral. For LiF, the region near ω_g is outside the frequency range of interest with optical effects in this region being dominated by one-photon effects. The low-frequency value of $n_2 = 0.8\, n_{20}$ rather than n_{20} is a result of the approximations made in simplifying the integral.

It is seen from Fig. 2 that the maximum value of $n_2 \cong 3\, n_{20}$ occurs at $\omega \cong \omega_g/2$ increases with decreasing width of the density of states:

$$n_2(\omega_g/2)/n_{20} = \frac{32}{27} + \frac{2\sqrt{2}\,(\omega_g)^{3/2}}{(\omega_m - \omega_g)^{3/2}} \tan^{-1}\left[\frac{(\omega_m - \omega_g)^{1/2}}{(2\omega_g)^{1/2}}\right]$$

$$\cong \frac{32}{27} + \frac{2\omega_g}{(\omega_m - \omega_g)} \quad . \tag{14}$$

This could result in n_2 being very strongly enhanced for solids with narrow bands or with rapidly varying f-numbers. In this case the frequency dependence of n_2 could be approximated by the molecular model in Fig. 1.

III. KRAMERS-KRONIG RELATION BETWEEN NONLINEAR INDEX AND TWO-PHOTON ABSORPTION

Since there have been no direct measurements of the nonlinear refractive index as a function of frequency, it is desirable to relate the resonant enhancement of the nonlinear index to other quantities that can be measured experimentally. The Kramers-Kronig relations connect the real and imaginary parts of the dielectric constant and are used to relate the nonlinear index to the two-photon absorption coefficient.

The Kramers-Kronig relation for calculating the real part of the dielectric constant ϵ_R from the imaginary part ϵ_I is

$$\epsilon_R(\omega) = 1 + \frac{2}{\pi} \int_0^\infty \frac{\omega' \epsilon_I(\omega')\, d\omega'}{(\omega'^2 - \omega^2)} \quad . \tag{15}$$

If the dielectric constant is separated into linear and nonlinear parts $\epsilon = \epsilon^L + \epsilon^{NL}$, the relation for the nonlinear parts is

$$\epsilon_R^{NL}(\omega) = \frac{2}{\pi} \int_0^\infty \frac{\omega' \epsilon_I^{NL}(\omega')\, d\omega'}{(\omega'^2 - \omega^2)} \quad . \tag{16}$$

Using $n_2 = \epsilon_R^{NL}/2n_0^2$ and $\beta_2 = \frac{\omega}{n_0 c} \epsilon_I^{NL}$, where β_2 is the intensity-dependent, two-photon absorption coefficient, yields

$$n_2 = \frac{2 n_0 c}{\pi} \int_0^\infty \frac{\beta_2(\omega')\, d\omega'}{(\omega'^2 - \omega^2)} \quad . \tag{17}$$

The two-photon absorption coefficient has not been measured in LiF. However on the basis of experiments by Hopfield et. al.[7] and by Frölich and Staginnus[8] in other alkali halides, the two-photon absorption coefficient in LiF is expected to have the approximate frequency dependence $\beta_2(\omega) \cong \beta_{20}(\omega - \omega_g/2)^{1/2}$ for $\omega_g/2 < \omega < \omega_m/2$. This approximate frequency dependence is expected theoretically if the f-numbers are not strongly frequency dependent and if other weakly frequency dependent terms are taken as constants. Substitution in Eq. (17) gives

$$n_2(\omega) = \text{const.} + \frac{2n_0 c\beta_{20}}{\pi} \int_{\omega_g/2}^{\omega_m/2} \frac{(\omega' - \omega_g/2)^{1/2} d\omega'}{(\omega'^2 - \omega^2)} , \qquad (18)$$

where the constant comes from higher-frequency, two-photon absorption. Changing variables to $\omega'' = 2\omega'$ yields

$$n_2(\omega) = \text{const.} + \frac{4n_0 c\beta_{20}}{\sqrt{2}\,\pi} \int_{\omega_g}^{\omega_m} \frac{(\omega'' - \omega_g)^{1/2} d\omega''}{(\omega''^2 - 4\omega^2)} . \qquad (19)$$

Notice that Eq. (19) has the same frequency dependence as Eq. (12), which was derived from perturbation theory, except for weakly frequency dependent terms outside of the integrals. The additional frequency dependent terms are expected to change the resonant enhancement of n_2 by less than a factor of two. This difference is within the uncertainty in the functional form of the experimental two-photon absorption coefficient. The frequency dependence of the theoretical equations will also vary by about a factor of two depending on the

intermediate state chosen in the perturbation theory. The factors outside of the integrals in Eqs. (12) and (19) could be used to relate the magnitudes of the low-frequency nonlinear index n_{20} and the two-phcton absorption coefficient β_{20}. It is noted in passing that replacing $(\omega_0^2 - 4\omega^2)^{-1}$ by $(\omega_0^2 - 4\omega^2)^{-1}$ $+ (i\pi/4\omega)\,\delta(2\omega - \omega_0)$ in Eq. (6) will simultaneously give the two-photon absorption coefficient and nonlinear index al ıg with automatically satisfying the Kramers-Kronig relations.

IV. CONCLUSIONS

The xenon-laser frequency is above one-half the band gap for all crystals. In this frequency region the optical properties of materials suffer deleterious effects from both two-photon absorption and from a resonantly enhanced nonlinear refractive index. The two effects are not independent since they arise from the real and imaginary parts of the third-order susceptibility and are connected by the Kramers-Kronig relations.

For solids with broad two-photon absorption bands (as is expected for LiF), the nonlinear index in most of the two-photon frequency region is only slightly enhanced from the low-frequency value. At the xenon-laser frequency of $\omega = 0.55\ \omega_g$ in LiF, Fig. 2 indicates $n_2 \cong 3n_{20}$. Estimating $n_{20} \cong 10^{-13}$ esu, Eq. (3) gives the threshold intensity value of $I_{th} = 2\ GW/cm^2$ for optical distortion from the nonlinear index. This threshold is comparable to the threshold for fracture from two-photon heating and at least a factor of 10 greater than the threshold for optical distortion from free electron-hole pairs created by two-photon absorption.

In other cases nonlinear optical distortion may be the dominant intrinsic mechanism for material failure. Obviously with other lasers having frequencies less than one-half the band gap, two-photon absorption will not occur but resonant enhancement of the nonlinear index will occur if the laser frequency is near one-half the band gap. A similar situation may occur with the xenon laser in materials having a strongly peaked two-photon absorption spectrum. In this case the nonlinear index will be dominant if the laser frequency is adjacent to,

but not within, the two-photon absorption peak since the nonlinear index will be strongly enhanced by the sharp peak but absorption will not occur. If the laser frequency is within a sharp peak in the two-photon absorption, the two-photon absorption and nonlinear index are both enhanced with the result that two-photon absorption is expected to be dominant in this case.

Materials having band gaps only slightly greater than the xenon-laser frequency may have a large negative value of n_2 as is shown in Fig. 2. However until more is known about the band structure or two-photon absorption spectrum of insulating crystals, it cannot be predicted whether any material will actually have this behavior.

REFERENCES

1. R. Hellwarth, J. Cheriow, and T. Yang, Phys. Rev. B11, 964 (1975).
2. M. D. Levenson, C. Flytzanis, and N. Bloembergen, Phys. Rev. B6, 3962 (1972).
3. R. Braunstein and N. Ockman, "Interaction of Coherent Optical Radiation with Solids," RCA Laboratories Final Report, Contract No. NONR-4128(00), August (1964).
4. P. W. Langhoff, S. T. Epstein, and M. Karplus, Rev. Mod. Phys. 44, 602 (1972).
5. J. T. Fournier and E. Snitzer, IEEE J. Quant. Elect. QE10, 473 (1974).
6. C. C. Wang, Phys. Rev. B 2, 2045 (1970).
7. J. J. Hopfield and J. M. Worlock, Phys. Rev. 137, A1455 (1965); J. J. Hopfield, J. M. Worlock, and K. Park, Phys. Rev. Lett. 11, 414 (1963); J. M. Worlock in Laser Handbook, Vol. 2, edited by F. T. Arecchi and E. O. Schulz-DuBois (North Holland, 1972).
8. D. Frölich and B. Staginnus, Phys. Rev. Lett. 19, 496 (1967).

F. STUDIES OF OPTICAL PROPERTIES OF ALKALI HALIDE CRYSTALS†

D. L. Mills and A. A. Maradudin
Department of Physics
University of California
Irvine, California 92664

and

Xonics, Incorporated
Van Nuys, California 91406

†Research supported by Contract No. DAHC15-73-C-0127 of the Advanced Research Projects Agency of the Department of Defense, Washington, D. C.

I. INTRODUCTION

We have underway a series of studies of the optical properties of alkali-halide crystals, with emphasis on electronic absorption in the ultraviolet. From many points of view, the alkali halides represent a particularly simple group of solids, in addition to their potential role as materials for use in high-power laser applications. Indeed, most solid state physics text books use alkali halides as their first example of a crystalline solid. Yet the electronic properties of alkali halides remain poorly understood. For example, in the alkali halides (as well as in the rare gas solids), band gaps computed by means of sophisticated Hartree-Fock schemes are in very poor agreement with experiment, to the point where it is argued that there are corrections to Hartree-Fock band gaps from electron correlation effects that amount to several electron volts.[1]

To perform theoretical quantitative calculations of the properties we have under study, one requires knowledge not only of the electronic energy bands, but also the Bloch functions associated with the bands. To generate the Hartree-Fock energy bands and the associated wave functions is a complex computational task. For use in the investigations below, the wave functions are required. We plan to use an interpolation scheme based on a set of tight binding wave functions. The scheme, developed by L. J. Sham, reproduces the band structures calculated by the Hartree-Fock method, and provides in addition approximate wave functions that are simple to generate, and to apply to a variety of theoretical studies. We first describe Sham's scheme.

The electronic wave functions associated with the conduction band have their probability amplitude centered primarily on the alkali sublattice. We represent these wave functions by a tight binding approximation:

$$\psi_{c\underset{\sim}{k}}(\underset{\sim}{x}) = \sum_{\underset{\sim}{\ell}} \varphi_s(\underset{\sim}{r} - \underset{\sim}{\ell}) \exp(i\underset{\sim}{k} \cdot \underset{\sim}{\ell}) = \sum_{\underset{\sim}{\ell}} |s\underset{\sim}{\ell}\rangle e^{i\underset{\sim}{k} \cdot \underset{\sim}{\ell}} \qquad (1)$$

where $\psi_{c\underset{\sim}{k}}(\underset{\sim}{x})$ is the Bloch function associated with the conduction band, and $\varphi_s(\underset{\sim}{r} - \underset{\sim}{\ell})$ an atomic like orbital of s symmetry centered on the alkali site $\underset{\sim}{\ell}$. We generate a phenomenological Hamiltonian matrix by retaining only the overlap integrals $\langle s\underset{\sim}{\ell} + \underset{\sim}{\delta} | \mathcal{H} | s\underset{\sim}{\ell} \rangle$ between nearest and next nearest neighbor alkali sites. These overlap integrals are treated as adjustable parameters, and are fitted to the conduction band shapes generated by the full Hartree-Fock theories.

In the valence bands, the probability amplitude of the wave functions are centered predominantly on the halide sublattice. We introduce a similar tight binding scheme to describe the wave functions and energies associated with these bands. With each halide site, we have three atomic orbitals $|P_x, \underset{\sim}{\ell}\rangle$, $|P_y, \underset{\sim}{\ell}\rangle$, and $|P_z, \underset{\sim}{\ell}\rangle$. The Bloch functions associated with the valence bands then assume the form

$$\psi^{(\alpha)}_{v\underset{\sim}{k}}(x) = \sum_{\beta} c_{\alpha\beta}(\underset{\sim}{k}) |P_\beta, \underset{\sim}{\ell}\rangle \exp[i\underset{\sim}{k} \cdot \underset{\sim}{\ell}] \quad . \qquad (2)$$

There are three valence bands degenerate at the Γ' point, and $\alpha = 1, 2$ or 3 is a band label. As in our description of the conduction band, we generate an effective Hamiltonian matrix by retaining in the description the nearest and next nearest neighbor overlap integrals $\langle P_\alpha, \underset{\sim}{\ell} + \underset{\sim}{\delta} | \mathcal{H} | P_\rho, \underset{\sim}{\ell} \rangle$. Because there are

three atomic orbitals associated with each halide site, there are many more overlap integrals than in the description of the conduction band. Nonetheless, many vanish identically from symmetry considerations, and we are left with a small number of non-zero overlap integrals which once again may be fitted to band structures calculated from first principles.

In this approach, the conduction band position and shape are described by three parameters. If $E_c(\underset{\sim}{k})$ is the energy of an electron with wave vector $\underset{\sim}{k}$ in the conduction band, then in terms of the nearest neighbor overlap integral α_1, and the next nearest neighbor overlap integral β_1, we have

$$E_c(\underset{\sim}{k}) = \mathcal{E}_1 + 4\alpha_1 (\cos k_x a \cos k_y a + \cos k_y a \cos k_z a + \cos k_z a \cos k_x a) + 2\beta_1 (\cos 2ak_x + \cos 2ak_y + \cos 2ak_z)$$

where a is the distance between the alkali site and the nearest halide.

To generate the eigenvalues and Bloch functions of the valence bands, one must find the eigenvalues and eigenfunctions of a 3×3 Hamiltonian matrix. In terms of the non-vanishing nearest and next nearest neighbor overlap integrals, we have for the matrix elements

$$\mathcal{H}_{xx}(\underset{\sim}{k}) = \mathcal{E} + 4\alpha \cos k_x a (\cos k_y a + \cos k_z a) + 4\gamma \cos k_y a \cos k_z a + 2\delta \cos 2k_x a + 2\eta (\cos 2k_y a + \cos 2k_z a) \quad ,$$

$$\mathcal{H}_{xy}(\underset{\sim}{k}) = -4\beta \sin k_x a \sin k_y a \quad ,$$

and the remaining matrix elements may be generated from these two by permutation operations. The parameter $\mathcal{E}$ fixes the position of the valence band, and an illustration of the non-vanishing nearest and next nearest neighbor overlap integrals is given in Fig. 1 through Fig. 3.

This scheme provides a very good fit to the Hartree-Fock energy bands. Sham has obtained numerical values for the parameters that appear above by fitting the energy bands calculated by Mickish et al., and by Chaney et al. The parameters obtained by this means are presented in Table I.

With the approximate wave functions and method of generating the band structure described above, we are in a position to investigate a number of questions in a quantitative manner. We describe two projects currently underway. While these two projects are not yet completed, time has been expended on them during the past contractual period, and they should be completed before the next report is due.

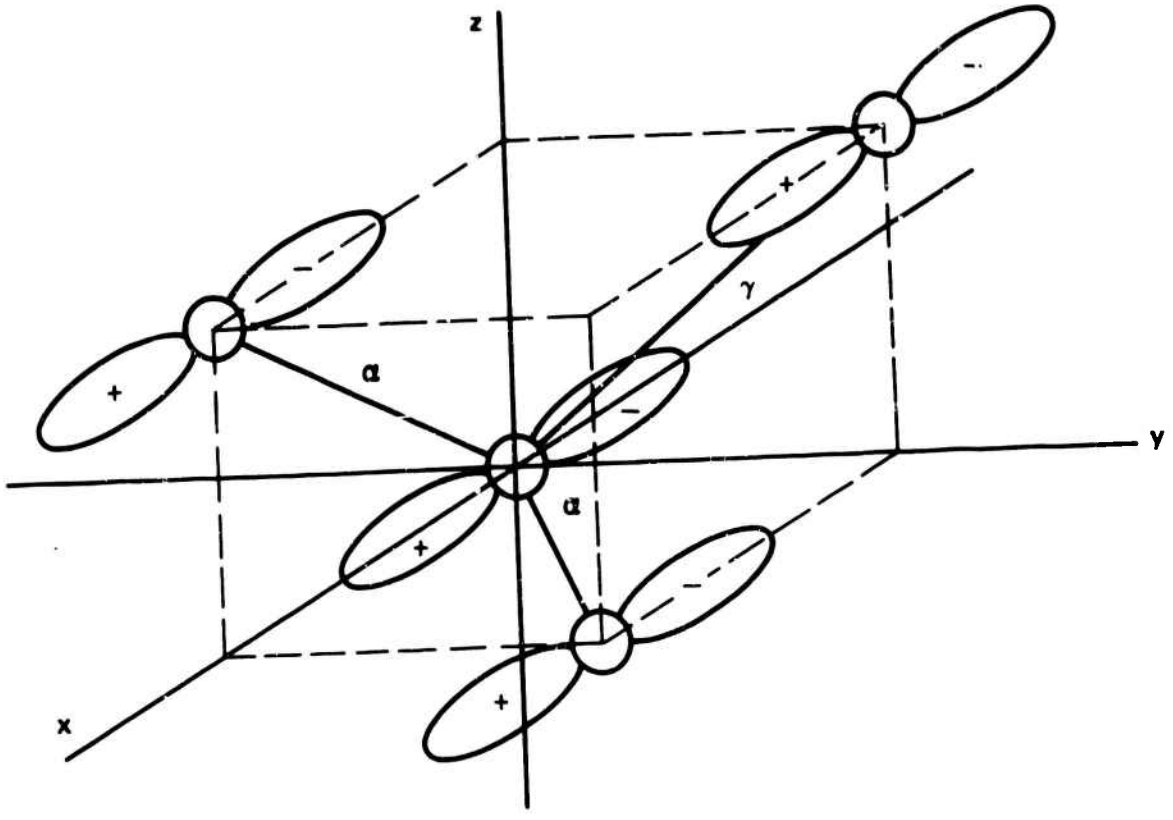

α: OVERLAP BETWEEN $|P_x>$ AT (0,0,0) AND $|P_x>$ AT a_0 (1,1,0) + EQUIVALENT SITES

γ: OVERLAP BETWEEN $|P_x>$ AT (0,0,0) AND $|P_x>$ AT a_0 (0,1,1) + EQUIVALENT SITES

Fig. 1. The overlap integrals α and γ which contribute to the matrix element $\mathcal{H}_{xx}(\underset{\sim}{k})$ in the tight binding band structure scheme.

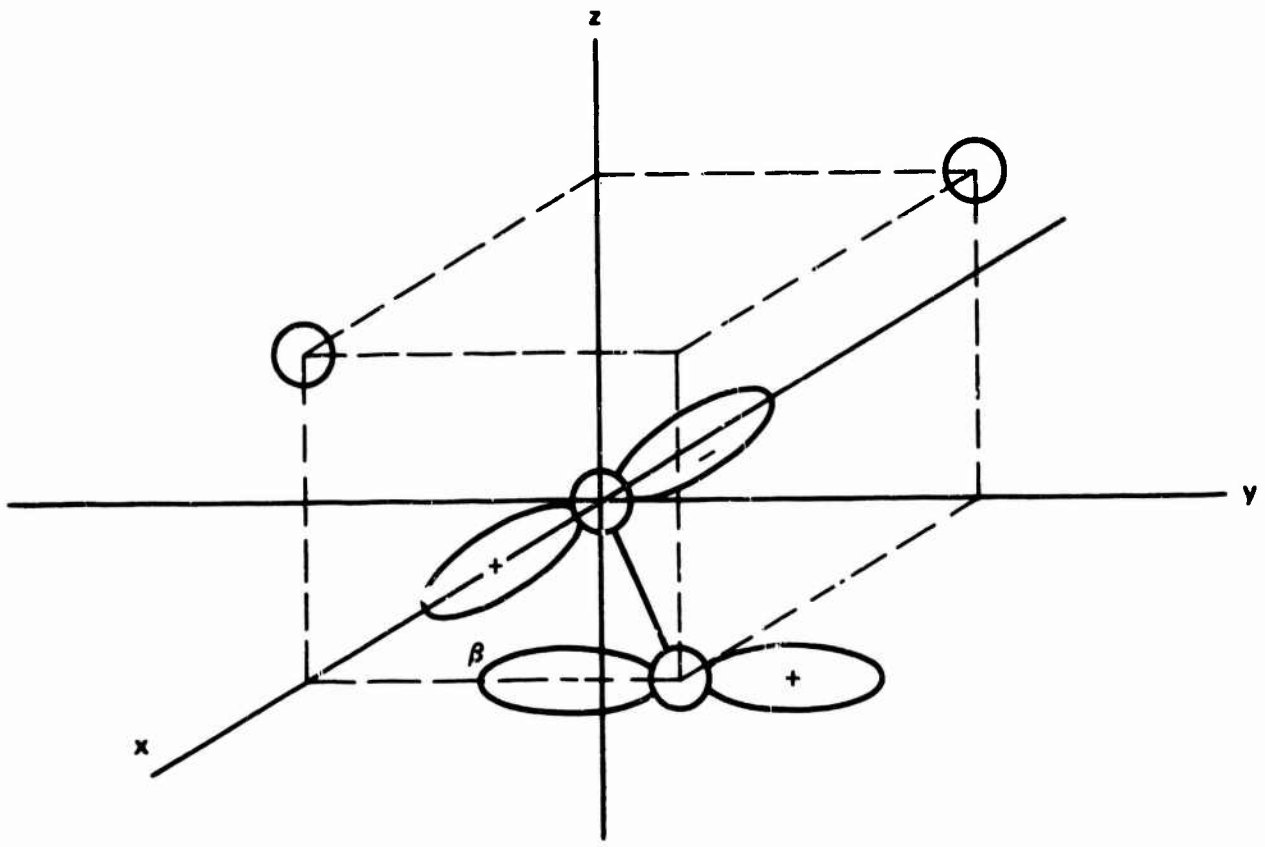

β: OVERLAP BETWEEN $|P_x>$ AT (0,0,0) AND $|P_y>$ AT a_0 (1,1,0) + THREE EQUIVALENT SITES

Fig. 2. The overlap integral β which contributes to $\mathcal{K}_{xy}(\underset{\sim}{k})$ in the tight binding band structure scheme.

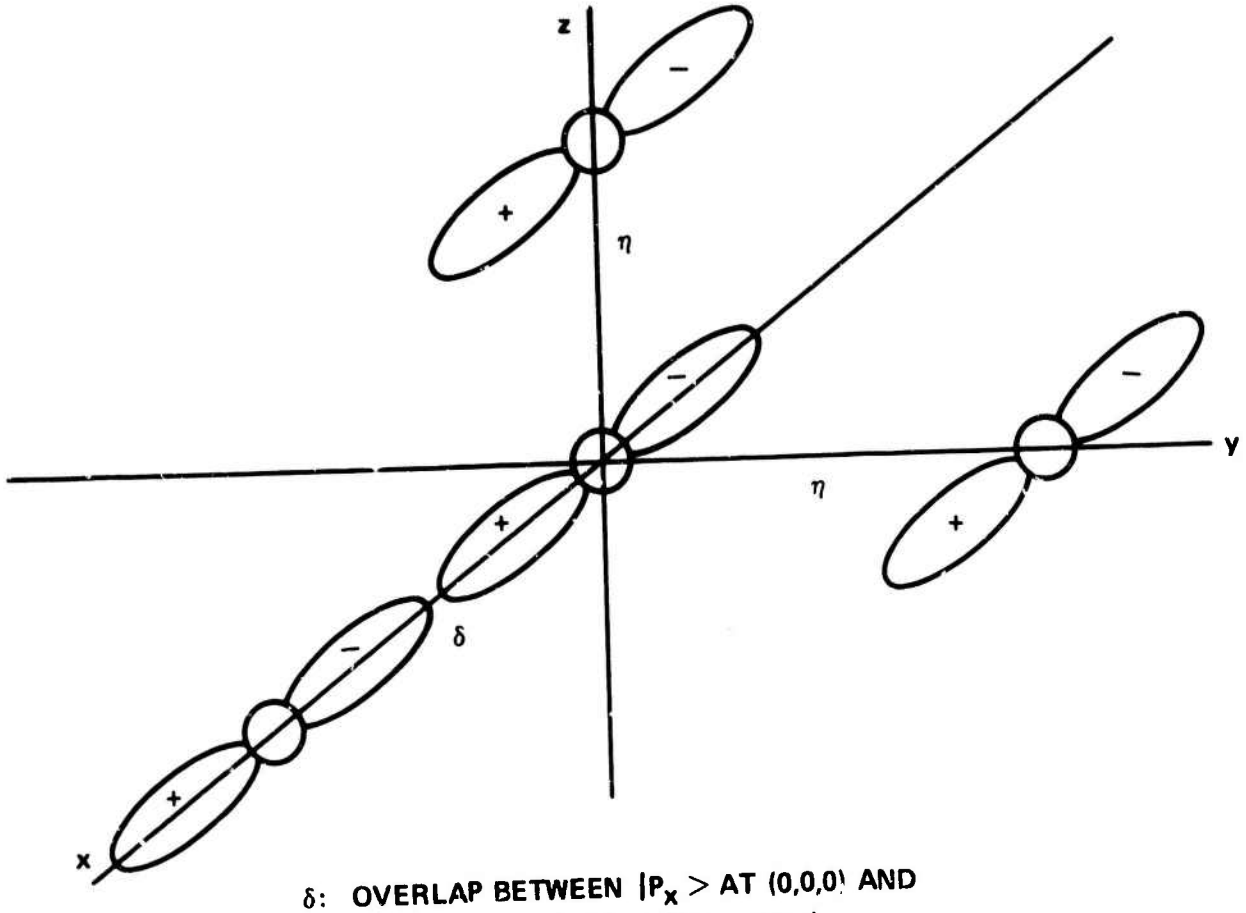

δ: OVERLAP BETWEEN $|P_x>$ AT (0,0,0) AND $|P_x>$ AT a_0 (2,0,0) AND a_0 (-2,0,0)

η: OVERLAP BETWEEN $|P_x>$ AT (0,0,0) AND $|P_x>$ AT a_0 (0,2,0) AND a_0 (0,0,2)

Fig. 3. The second neighbor overlap integrals δ and η which contribute to $\mathcal{H}_{xx}(\underset{\sim}{k})$.

Table I. The parameters which enter the tight binding scheme used to fit the energy bands calculated from first principals. The values listed in column 1 are fitted to the results of D. J. Mickish, A. B. Kunz, and T. C. Collins, Phys. Rev. B9, 4461 (1974), and the values in column 2 have been fitted to R. C. Chaney, T. E. Lafon, and C. C. Lin, Phys. Rev. B 4, 2734 (1971).

ξ	-4.73×10^{-2} Ryd.	-3.33×10^{-2} Ryd.
α	6.56×10^{-3}	5.44×10^{-3}
β	7.92×10^{-3}	5.83×10^{-3}
γ	-1.5×10^{-3}	-1.81×10^{-3}
δ	1.27×10^{-2}	1.48×10^{-3}
η	-6.13×10^{-3}	0
ϵ_1	7.09×10^{-1}	5.26×10^{-1}
α_1	-2.52×10^{-2}	-1.24×10^{-2}
β_1	1.85×10^{-2}	3.02×10^{-3}

II. A STUDY OF THE ROLE OF ELECTRONIC CORRELATIONS ON THE MAGNITUDE OF THE ENERGY GAP

As remarked earlier, very sophisticated Hartree-Fock schemes have been applied to the calculation of the electron band structures. These calculations produce values for the electronic energy gaps which are larger than the measured gaps by several electron volts.[1] This is an enormous discrepancy, and there are two possibilities for its origin. Either the Hartree-Fock calculations are in error, possibly through use of an approximate form for the exchange term in the Hartree-Fock calculations, or a physical effect not included in the Hartree-Fock description of the electron motion plays an important role in controlling the magnitude of the fundamental gap.

The researchers engaged in the band structure calculations[1] argue that the Hartree-Fock (HF) equations have indeed been accurately solved, and a many body effect not included in the HF description plays a crucial role in controlling the magnitude of the energy gap.

The physical picture of this many body effect, whose importance was first stressed a number of years ago by Fowler,[2] is the following. If an electron moves through the crystal, its coulomb field polarizes the material in its near vicinity. The polarized region that surrounds the electron creates a potential well within which the electron sits. As a result, the energy of the electron is lowered relative to its value in the absence of the polarization effect. The HF theory does not include this effect, and as a consequence overestimates the energy of the electron in the conduction band. The depth of the well is estimated to be about 2 eV.[2] The energy of the hole must be corrected in a similar

manner, to produce a second correction of roughly 2 eV. Overall, then, it is argued that through its neglect of the polarization effect, the HF theory overestimates the band gap by roughly 4 eV. If we subtract this correction from the calculated HF gap, one obtains a renormalized gap in good accord with the data.

The correction to the band gap described above is a many body correction to the HF prediction. It is a very large correction, and must be calculated with care and accuracy if we are to trust our present level of understanding of the most elementary electronic property of alkali halides: the value of the electronic energy gap.

Two methods of computing the polarization correction to the energy gap may be found in the literature. The first, described in the work of Fowler,[2] treats the electron (or hole) as a classical point charge which induces dipole moments in the surrounding polarizable ions. The field set up by the array of polarized ions gives rise to the potential well which lowers the energy of the electron.

The second method presumes the electron (or hole) interacts with a well defined exciton level. The electron-exciton interaction is mathematically isomorphic to the Frölich interaction of polaron theory, and the apparatus of polaron theory may be brought to bear on the problem.

Neither method is a satisfactory way of calculating the self-energy corrections, in our view. Fowler's method replaces the quantum mechanical description of the electron by a classical one. In addition, the self-energy effects which shift the band edge must also change the shape of the bands. It is difficult, indeed impossible, to study such effects reliably with this method.

The electronic polaron model treats the electron motion quantum mechanically and is capable in principle of evaluating the change in shape of the bands. However, this model is naive in its representation of the particle-hole excitations with which the free carrier interacts. There are excitonic contributions to the optical absorption spectrum of the alkali halides, but these exciton levels are responsible for only a small fraction of the integrated oscillator strength associated with valence band-conduction band transition.

We have made considerable progress on what we believe should be a quantitatively reliable method of assessing the importance of the polarization effect described above. In principle, our calculation is straightforward. From a many body point of view, the HF theory emerges when one includes in the proper self energy of the electron (or hole) only the lowest-order term in the electron-electron interaction. To evaluate corrections to the HF theory, one must evaluate the next order (second order) corrections to the self energy.

These second-order corrections include a description of the polarization effect described above. This may be seen in Fig. 4. In Fig. 4(a), we show the lowest-order contribution to the proper self energy in the "electronic polaron" model. If one were to compute this diagram via a proper microscopic model, the wavy line that represents the exciton in Fig. 4(a) should be replaced by a particle-hole ladder series, as illustrated in Fig. 4(b). Fig. 4(b) contains the contribution from the exciton level, and from the electron-hole continuum as well. (As remarked above, the continuum contribution is ignored in the "electronic polaron" model, and it should be quantitatively important.) In Fig. 4(c) and Fig. 4(d), the second-order contribution to the self energy is illustrated.

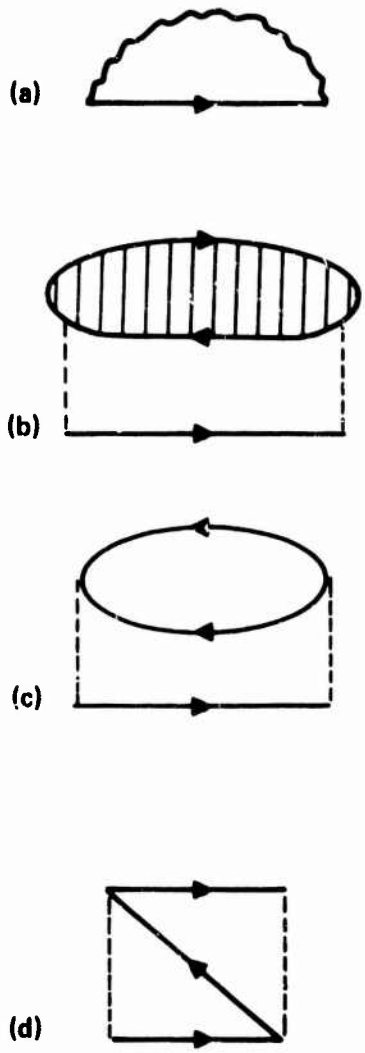

Fig. 4. (a) The lowest order proper self energy of an electron in the "electronic polaron" model. The wavy line represents an exciton, and the straight line an electron. (b) A microscopic version of (a), where the exciton is represented by a particle-hole ladder series. (c) and (d). The second order contribution to the proper self energy in the present approach.

Figure 4(c) is the lowest order description of the polarization effect, while Fig. 4(d) is an exchange diagram omitted from the "electron polaron" model. This exchange diagram should be important, and we wish to investigate its sign and magnitude quantitatively. One can not trust the estimate of the validity of the HF scheme until this is done.

We have developed a method of systematically generating corrections to the HF theory,[3] and when this method is applied to the present problem, the form of the corrections may be obtained. We then plan a series of numerical calculations which will study the self-energy induced shifts of band edges, as well as changes in the shape of the bands from these effects.

The numerical studies remain to be carried out. They will be quite arduous, since integrations over the 3D Brillouin zone are required. However, the calculations are made feasible by the availability of the phenomenological description of the band structure described earlier in this section. While the calculations will prove difficult, they would be quite impossible to contemplate without the phenomenological description of the band structure.

III. THE ELECTRONIC CONTRIBUTION TO THE INTRINSIC SURFACE ABSORPTION IN THE ALKALI HALIDES

In an ideal, infinitely extended solid, the amount of energy extracted from a beam of radiation which traverses the material is proportional to the length of travel of the beam in the material.[4] In the presence of boundaries, such as the two surfaces of a film, additional surface-induced absorption may be present. To the experimentalist, this surface absorption manifests itself as a contribution to the total energy absorption independent of the film thickness.

There are two basic physical origins of surface-induced absorption. There are extrinsic sources of absorption with origin in species adsorbed on the surface with absorption bands in the spectral regime of interest, impurities near the surface which diffuse into the material after contact with an external atmosphere, surface roughness induced absorption, and a host of other possibilities.

Even in an absolutely perfect film, with atomically smooth surface planes there will be surface-induced absorption of an intrinsic nature. Beyond the fundamental absorption edge, such intrinsic surface absorption has its physical origin in the modification of the bulk Bloch functions in the near vicinity of the surface. In addition, a much more interesting possibility is intrinsic surface-induced absorption below the fundamental absorption edge by virtue of surface states present within the gap between the valence and the conduction bands.

We have underway an investigation of the effect of a (100) surface on the electronic states of an alkali-halide film. In addition, for such films we plan to calculate the magnitude of the intrinsic surface-induced absorption.

The investigation makes heavy use of the approximate wave functions and band structure fitting scheme described earlier in this section. It is quite difficult to carry out an analysis of the effect of a surface on the electronic structure of the material, within the framework of the elegant Hartree-Fock scheme used to generate theoretical band structures for the bulk material. While this can be done with today's computational facilities, the cost in computer time and in man hours would be extensive.

However, the possibility that surface states exist in the gap is readily explored within the framework of the tight binding model of the bulk band structure described above. For example, one may construct a thin film with N atomic layers, where N may range from 10 to 20. For the conduction bands, the Bloch functions become of the form

$$\Phi^{(\alpha)}_{\underset{\sim}{k}_{\parallel}}(\underset{\sim}{r}_{\parallel}, z) = \sum_{\underset{\sim}{\ell}_{\parallel}} \sum_{\ell_z} \exp\left[i \underset{\sim}{k}_{\parallel} \cdot \underset{\sim}{\ell}_{\parallel} \right] c^{(\alpha)}_{\underset{\sim}{k}_{\parallel}}(\ell_z)\, \varphi_s(\underset{\sim}{r} - \underset{\sim}{\ell}) \qquad (3)$$

where the subscript $\parallel$ appended to a vector denotes its projection onto a plane parallel to the film surfaces. Equation (3) contains the statement that since the two directions parallel to the surface retain translational invariance, the wave functions have the Bloch character with respect to translations in these two directions. However, translational invariance normal to the surface is broken.

If the film has N layers, the Ansatz for the wave function in Eq. (3) leads one to an N x N Hamiltonian matrix. The eigenvectors and eigenvalues of this matrix lead one to the coefficients $c^{(\alpha)}_{k_{\parallel}}(\ell_z)$ and the electron energy levels of the finite film. If surface states are present, they may be readily identified.

A similar treatment applied to the tight binding valence bands leads to a 3N x 3N matrix. Since matrices up to 100 x 100 and larger are readily handled by modern computers, there is no difficulty in applying this scheme to films as thick as 30 or 40 atomic layers, although for our purposes we may confine our attention to thinner films.

At this point, we have completed the analysis which sets up the Hamiltonian matrix for the finite film, and we are ready to proceed with the numerical computations. The initial set of numerical calculations should be completed shortly.

REFERENCES

1. D. J. Mickish and A. Barry Kunz, J. Phys. C. 6, 1723 (1973).

2. W. Beall Fowler, Phys. Rev. 151, 657 (1966).

3. In a different physical context, this ladder series has been discussed by D. L. Mills and E. Burstein, Phys. Rev. 188, 1465 (1969).

4. This presumes the crystal is sufficiently transparent that only a small fraction of the energy is absorbed from the beam as it passes through.

G. A POSSIBLE MECHANISM FOR EXTRINSIC ABSORPTION IN INSULATORS BELOW THE FUNDAMENTAL ABSORPTION EDGE†

D. L. Mills
Department of Physics
University of California
Irvine, California 92664

and

Xonics, Incorporated
Van Nuys, California 91406

†Research supported by Contract No. DAHC15-73-C-0127 of the Advanced Research Projects Agency of the Department of Defense, Washington, D. C.

In principal, below the fundamental absorption edge of wide band gap insulators, absorption of electromagnetic radiation by one-photon processes should be extremely weak, provided the photon energy is far enough below the absorption edge for phonon assisted transitions to be negligible. However, experimental studies of alkaline earth fluorides show that below the fundamental absorption edge, appreciable absorption exists.[1] The absorption constant β is indeed five or six orders of magnitude smaller below the gap than above, but below the gap β assumes values in the range of 10^{-1} to 10^{-2} cm^{-1}, and is only weakly dependent on frequency. While this absorption is indeed weak by conventional standards, if the materials are to be used for fabrication of optical components in high-powered ultraviolet lasers, then the presence of this absorption will become a matter of concern.

The component of the absorption below the gap reported in Ref. 1 appears to be extrinsic, and becomes weaker as the quality of the material is improved. One may then wish to presume the absorption has its origin in point defects or impurities. Point defects and impurities give rise to localized electronic levels and sharp absorption lines. It is hard to reconcile this with the observation that β levels off below the absorption edge to a value rather insensitive to the frequency. Of course, such impurity levels may be broadened considerably by a variety of mechanisms, and one may have many overlapping levels with origin in small residual concentrations of distinct kinds of impurities and defects. If this is so, one would expect structure of some kind to show through nonetheless.

Here we explore a mechanism which in principle can give rise to broad absorption bands. This is absorption via electron states localized near dislocation

lines. It is well known that in both ionic and semiconducting materials, electrons (and holes, may be trapped in localized levels associated with dislocation lines. Since the dislocation line is a one-dimensional structure, these states necessarily form one-dimensional energy bands, since the electron or hole is free to run along the core of the dislocation line. Such bands will extend into the forbidden energy gap, possibly overlapping the bulk conduction or valence band, and they will give rise to broad absorption bands with a width controlled by that of the valence band, and the width of the band of levels localized to the dislocation line. (We consider a process where a photon is absorbed by a transition which lifts an electron from a valence band state to an empty state localized on the dislocation line, for example.)

It is difficult to make a quantitative theory of this absorption process, primarily because very little is known about the detailed nature of these states. There is considerable literature on the influence of carriers trapped on dislocation lines on a number of macroscopic crystal properties, but it is difficult to extract information about the nature of the localized levels from the data. There also are a few theoretical studies of the levels, but they tend to be rather schematic, and confined to rather special configurations. As a result we have rather few guidelines to follow, and the estimate below will necessarily be very crude. The conclusions are somewhat speculative as a consequence.

Indeed, the study of the absorption of photons by dislocation-induced transitions in a crystal which contains controlled dislocation arrays offers an excellent means of obtaining information about these electronic levels. We know of no systematic experimental data on this question, and a series of studies would prove

most useful. It has been pointed out[2] that crystals may be grown with well defined linear arrays of dislocations. Then for such a crystal, dislocation line-induced absorption below the absorption edge could be extracted from the background by comparison of the absorption constant for the cases of the electric field parallel and perpendicular to the dislocation array. If such experiments could be carried out, they would play a key role in assessing the importance of the effects described here.

We now proceed with a very crude estimate. We have in mind transitions from the filled valence band to an empty band of electronic levels localized on the core of a dislocation line.

Let us begin with a grossly oversimplified picture, which we shall subsequently extend. Suppose a linear dislocation line gives rise to a linear array of localized electronic transitions, each of which absorbs at the frequency ω_0. The contribution to the absorption constant $\beta(\omega)$ from such an array of levels is given by an elementary formula:

$$\beta(\omega) = \frac{2\pi^2 N e^2 f}{c m n} \delta(\omega - \omega_0) \quad , \tag{1}$$

where n is the index of refraction of the material, m and c the mass of the electron and vacuum velocity of light, with e the electron charge. The two remaining quantities f and N are the oscillator strength of the transition and the number of levels/unit volume, respectively. If there are n_d dislocation lines/unit area, then we expect

$$N = \frac{n_d}{a_0} \quad , \tag{2}$$

where a_0 is the distance between adjacent unit cells.

If we take account of the band like character of the states localized on the dislocation line, and of the states in the valence band which form the initial state, then we do not get an absorption line as in Eq. (1), but an absorption band of width W. The transitions described by Eq. (1) are spread over this band, and we account for this by the replacement

$$f\,\delta(\omega - \omega_0) \rightarrow \frac{\langle f\rangle \hbar}{W} \tag{3}$$

where $\langle f\rangle$ is the oscillator strength averaged over the band. Then we find for the absorption constant

$$\beta \cong \frac{2\pi^2 n_d e^2 \langle f\rangle \hbar}{c m n W a_0} \quad . \tag{4}$$

It is a straightforward matter to make crude estimates of all quantities which enter Eq. (4) save for one: the average value of the oscillator strength. We shall retain it in the formulas that follow.

We now inquire about the dislocation density n_d required for β to assume the value 10^{-2} cm. If we choose $W \cong 3$ eV, $a_0 = 3 \times 10^{-8}$ and $n \approx 2$, then β will equal 10^{-2} where the product $n_d\langle f\rangle$ is given by

$$n_d\langle f\rangle \approx 3\times 10^{7}\ \mathrm{cm}^{-2} \quad . \tag{5}$$

If we assume the transitions are strong, so $\langle f\rangle$ is near unity, then a dislocation line density in the range of $10^{8}\mathrm{cm}^{2}$ may lead to appreciable contributions to β below the fundamental absorption edge of the crystal.

The primary uncertainty in the above estimate is the value of the oscillator strength $\langle f \rangle$. To estimate this quantity will require detailed knowledge of the electron wave functions that enter the transition. As remarked earlier in this section, very little is known of these functions at the present time. Thus, the estimates above will have to be regarded as conjectural in nature at this time.

The estimate above, with the qualification expressed in the preceding paragraph in mind, suggests the possibility that the presence of dislocation lines may lead to weak broad band absorption in transparent materials, for frequencies below the fundamental absorption edge. It would be most interesting to see experimental studies which explore this possibility.

REFERENCES

1. T. Tomiki and T. Miyata, J. Phys. Soc. Japan 27, 658 (1969).

2. M. Hass, private communication to D. L. Mills.

H. MULTIPHONON ABSORPTION OF ALKALI HALIDES AND QUASISELECTION RULES

J. A. Harrington
University of Alabama in Huntsville, Huntsville, Alabama 35807

C. J. Duthler*
Xonics, Incorporated, Van Nuys, California 91406

F. W. Patten and M. Hass†
U. S. Naval Research Laboratory, Washington, D. C. 20375

A well-defined band has been observed in the low temperature infrared spectrum of KI, KBr, NaI, and RbCl in the region corresponding to the sum of three optical branch phonons and no corresponding band in the two- and four-phonon regions. These results can be accounted for by deducing an odd-even quasiselection rule for crystals having a gap between the optical and acoustical branches of the vibration spectrum.

The infrared absorption spectrum of alkali halides in the multiphonon region has received a great deal of experimental and theoretical attention in the past few years. For all alkali halide crystals which have been studied previously, the experimental results consist of an exponentially decreasing absorption as a function of frequency which contains no resolved structure in the three-phonon and higher multiphonon regions.[1] The theoretical interpretation of these results has been accounted for by a number of different approaches which have generally assumed that anharmonic

coupling of the phonons to the reststrahl mode is the main source of the multiphonon absorption.[2-8] The present experimental results provide the first evidence for structure in the multiphonon absorption of alkali halides. A well-defined band has been observed in the low-temperature infrared spectrum of KI, KBr, NaI, and RbCl in the frequency region corresponding to the sum of three optical branch phonons. No corresponding bands have been observed in the two- and four-phonon regions.

Boyer et al. predicted structured absorption in these crystals for both even and odd sums of optical branch phonons. This structure arises from peaks that occur in the multiphonon density of states of these crystals which have a gap or near gap between the optical and acoustical branches of the phonon spectrum.[8] To account for the missing even sum bands observed experimentally, one must use a theory that takes proper account of transition matrix elements rather than simply using an average matrix element along with the multiphonon density of states.

A general theory of multiphonon absorption based on actual phonon interactions and dispersion relations has been presented by Sparks and Sham.[2] By proceeding along the lines of Sparks and Sham for the two-phonon case, Duthler and Sparks calculated the two-phonon absorption of NaI, which has a gap, to deduce a quasi-selection rule.[9] This rule states that the two-phonon band associated with the sum of two optical branch phonons would be expected to be much weaker than the sum involving one optical and one acoustical branch phonon. The extension of a calculation of this nature and the generalization of the quasiselection rule to higher sum bands is presented here and can be applied to explain the present experimental results.

The experimental results for the infrared multiphonon spectrum for KI, KBr, RbCl, and NaCl are shown in Fig. 1 along with a comparison with the theory of Boyer et al.[8] and the results for NaI are shown in Fig. 2 along with a comparison with the present theory. Results have been taken on different crystals with different spectrometers and a correction for low temperature emittance of the sample was employed. Consequently, it is believed that the observed spectral structure is indicative of the bulk crystal and not associated with impurities or with the instruments. Some difficulty in reproducibility was found at lower absorption coefficients which is believed to be associated with surface effects, but spectra in this region are not essential to our argument.

The results for NaCl are typical of many crystals which have been studied previously in that the absorption coefficient decreases exponentially as a function of frequency with little or no structure in the three- and higher n-phonon regions, even at lower temperatures.[10] The calculations of Boyer suggest that some slight structure might be present at low temperatures for NaCl even beyond the two-phonon region. While the experimental results might be regarded as showing some structure, this would be difficult to confirm without additional measurements.

On the other hand, for KI, RbCl, NaI, and KBr, a definite band appears at low temperatures and some trace of this may exist at room temperature. The position of this band is in quite good agreement with an approach based upon a multiphonon density of states with a position for these gap crystals corresponding to the sum of three optical branch phonons. Furthermore, no corresponding band appears in the frequency range corresponding to two- and four- optical branch phonons. It can be seen in Fig. 2 for NaI that theoretical calculation by the approach to be described

succeeds in reproducing the main features of the experimental data of NaI and is in accord with the quasiselection rule deduced from these calculations. As is evident from the data, the quasiselection rule appears to hold for the other gap and near gap crystals studied here.

In calculating the absorption coefficient, we include only the anharmonic contribution to the absorption in which a photon is absorbed by virtual excitation of the fundamental reststrahl mode which decays by emission of n final-state phonons. The contributions to the absorption from higher-order dipole moments is neglected, although there have been recent estimates that this contribution may be large.[11] As the transition matrix elements for both mechanisms are similar, the quasiselection rule and general shape of the absorption may have many common features using either mechanism.

In the following, we present a new form for the Sparks and Sham expression for the absorption from n-phonon absorption processes. At least for crystals having a gap, it is possible to show the existence of an n-phonon quasiselection rule which states that the splitting of the fundamental reststrahl phonon into an odd number of optical phonons is a strong process, while the splitting into an even number is a weak process.

Using the results and notation of Sparks and Sham, the "anharmonic" contribution to the absorption coefficient β as a function of frequency ω is

$$\beta(\omega) = \frac{4\pi N e^{*2}}{c\, m_r n_r \Omega} \quad \frac{\omega \omega_f \Gamma(\omega)}{(\omega^2 - \omega_i^2)^2 + [\omega_f \Gamma(\omega)]^2} \quad , \tag{1}$$

where N is the number of unit cells in a crystal of volume Ω, e^* is the Born effective charge, c is the speed of light, m_r is the reduced mass of the two ions in the

unit cell, n_r is the refractive index at frequency ω, ω_f is the frequency of the fundamental mode, and $\Gamma(\omega)$ is the relaxation frequency of the fundamental mode. The contribution of the n-phonon summation process to the relaxation frequency Γ is obtained in Ref. 2 from straightforward perturbation theory which yields

$$\Gamma_n(\omega) = \frac{2\pi}{\hbar^2}\,\frac{1}{n!}\left(\frac{\hbar}{2m_<}\right)^{n+1}\left(\frac{m_<}{m_r}\right)\omega^{-1}(n_\omega+1)^{-1}\left(\phi^{(n+1)}\right)^2\Lambda_n^2\,\Sigma_n \quad , \tag{2}$$

where

$$\Sigma_n = N^{-n}\sum_{Q_1\cdots Q_n} N\Delta\left(\sum_{j=1}^{n}\vec{q}_j\right)\;\delta\left(\omega-\sum_{j=1}^{n}\omega_{Q_j}\right)$$

$$\times\prod_{j=1}^{n} 2\left|U_x(Q_j)\right|^2\,\frac{\left[n(\omega_{Q_j})+1\right]}{\omega_{Q_j}}\left[1+(-1)^{n+1}\cos\left(2\sum_{j=1}^{n}\varphi_{Q_j}\right)\right] \quad , \tag{3}$$

and where

$$U_x(Q_j) = w_{<Q_jx} - (m_</m_>)^{1/2}\,w_{>Q_jx}\,e^{iq_x a_{nn}} = \left|U_x(Q_j)\right|e^{i\varphi(Q_j)} \quad . \tag{4}$$

In Eqs. (2)-(4), $m_<$ and $m_>$ are the smaller and greater ionic masses; $n(\omega_{Q_j})$ is the Bose-Einstein occupation number of the phonon mode Q_j having wave vector $\vec{q}_j$, branch b_j, and frequency ω_{Q_j}; $w_{<Q_jx}$ and $w_{>Q_jx}$ are the x-components of the polarization vectors representing the displacements of the smaller and greater ions; a_{nn} is the spacing between nearest-neighbor ions; and $\phi^{(n+1)}$ is the $(n+1)$th derivative of the assumed nearest-neighbor, central-force potential. In Eq. (2), Λ_n is a vertex correction factor to the simple vertex where the fundamental mode splits directly into n final-state phonons which is considered explicitly in writing Eqs. (3) and (4). The sum over phonon modes Q_j in Eq. (3) is unrestricted.

We have chosen to write the Fourier transform of the x-component of the relative displacement $U_x(Q_j)$ in Eq. (4) in terms of a magnitude and a phase φ_{Q_j}, which is slightly different than in Ref. 2 where Σ_n was incorrectly written into terms of the two products of the real and imaginary parts of the U_x term. The principal term involved in deduction of the quasiselection rule is the phase factor φ_{Q_j}. For a given branch, the phase factor φ_{Q_j} tends to remain constant through the Brillouin zone with $\varphi_{Q_j} \cong 0°$ for optical branches and $\varphi_{Q_j} \cong 90°$ for acoustical branches. This result has been calculated directly for the simple case of the linear diatomic chain with nearest-neighbor interactions. In the present calculations, the values of φ_{Q_j} were taken from lattice-vibration calculations for NaI using the deformation dipole model of Karo and Hardy[12] where the mean value of φ_{Q_j} was found to be 3°, 3°, and 4° for the three optical branches of NaI and 71°, 106°, and 115° for the three acoustical branches. By approximating the phase factor by 0° for optical branches and by 90° for acoustical branches, it is possible to arrive at the odd-even quasiselection rule for sums of optical branch phonons in gap crystals by insertion in Eq. (3). The slight departure from an exact value of 0° or 90° will result in a weakening of this selection rule for higher multiphonon processes. In the case of NaI, it would be expected to hold to about seven optical phonons.

Another simplification results from the realization that the magnitudes of $U_x(Q_j)$ for a given type of branch (optical or acoustical) are fairly constant throughout the Brillouin zone, at least for gap crystals, except for the relatively unimportant case of acoustical phonons near the zone center. This result is obtained using either a one-dimensional diatomic chain, or using the Karo and Hardy polarization vectors for NaI. If this approximation is made, the complicated $\vec{q}$ dependent sum in Eq. (3)

is reduced to a thermally weighted density of states in which the branches are kept distinct. These approximations also allow one to easily calculate vertex corrections, which are found to be negligible for NaI.

Details of the multiphonon absorption calculation using the quasiselection rule will be published elsewhere.[13] In the present calculation, it has been assumed that the width of the final-state phonons is less than the width of the histogram bins used in Fig. 3. This is a fairly good approximation at 80 K, but there is experimental evidence from inelastic neutron scattering data indicating that the phonons are broadened at room temperature, especially for the longitudinal optical branch where there is considerable broadening. Consequently, the room temperature theoretical curve is much sharper than the experimental curve where no distinct three-phonon peak is observed.[14] Incorporating a phonon linewidth in the present theory would improve the agreement.

In conclusion, the first experimental evidence for a well-defined band in the three-phonon region of an alkali halide has been found in KI, RbCl, KBr, and NaI, all of which have a gap or near gap between the optical and acoustical branches. This band, which corresponds to the sum of three optical branch phonons, can be accounted for by a generalization of a quasiselection rule which states that the odd sum band of optical branch phonons in the multiphonon spectrum is much stronger than the even sum. This quasiselection rule has been deduced for a crystal having a gap, but is believed to apply to some extent to all of the alkali halides.

We should like to thank L. L. Boyer for permission to use his unpublished calculated spectrum of RbCl, and M. Sparks for discussions concerning the theory of multiphonon absorption.

REFERENCES

*Research supported by the Advanced Research Projects Agency of the Department of Defense and monitored by the Defense Supply Service, Washington, D. C.

†Visiting Associate, California Institute of Technology, 1974-1975.

1. T. F. Deutsch, J. Phys. Chem. Solids 34, 2091 (1973).
2. M. Sparks and L. J. Sham, Phys. Rev. B 8, 3037 (1973).
3. D. L. Mills and A. A. Maradudin, Phys. Rev. B 8, 1617 (1973).
4. (a) T. C. McGill, R. W. Hellwarth, M. Mangir, and H. V. Winston, J. Phys. Chem. Solids 34, 2105 (1973); (b) T. C. McGill in "Proceedings of the International Conference on the Optical Properties of Highly Transparent Solids, 1975," edited by B. Bendow and S. S. Mitra (Plenum, New York, to be published).
5. A. K. Nedoluha in "Proceedings of the International Conference on the Optical Properties of Highly Transparent Solids, 1975," edited by B. Bendow and S. S. Mitra (Plenum, New York, to be published).
6. B. Bendow, S. C. Ying, and S. P. Yukon, Phys. Rev. B 8, 1679 (1973).
7. K. V. Namjoshi and S. S. Mitra, Phys. Rev. B 9, 815 (1974).
8. L. L. Boyer, J. A. Harrington, M. Hass, and H. B. Rosenstock, Phys. Rev. B 11, 1665 (1975) review the experimental data as well.
9. C. J. Duthler and M. Sparks, Phys. Rev. B 9, 830 (1974).
10. R. W. Pohl in "Proceedings of the Internaticnal Conference on the Optical Properties of Highly Transparent Solids, 1975," edited by B. Bendow and S. S. Mitra (Plenum, New York, to be published) reports results for the gapless crystal NaF at low temperature.

11. See references cited in Refs. 4(b) and 8.

12. A. M. Karo and J. R. Hardy, Phys. Rev. 129, 2024 (1963).

13. C. J. Duthler (to be published).

14. A. D. B. Woods, B. N. Brockhouse, R. A. Cowley, and W. Cochran, Phys. Rev. 131, 1025 (1963); E. R. Cowley and R. A. Cowley, Proc. Roy. Soc. London Ser. A287, 259 (1965).

Figure Captions

FIG. 1. Absorption coefficient as a function of frequency for some alkali halides compared with calculations of Boyer, et al. For crystals with a gap or near gap (KI, KBr, and RbCl), the band corresponds to the sum of three optical branch phonons. For NaCl, which lacks a gap, no well-defined structure is observed at low temperature.

FIG. 2. Absorption coefficient as a function of frequency for NaI compared with present calculations. The band corresponds to the sum of three optical branch phonons.

FIG. 3. Contributions to the relaxation frequency of NaI as a function of frequency for quasiallowed combinations of phonons. The relatively small contribution made by the quasiunallowed sum of two optical phonons is shown by a dashed line to illustrate the validity of the quasiselection rule.

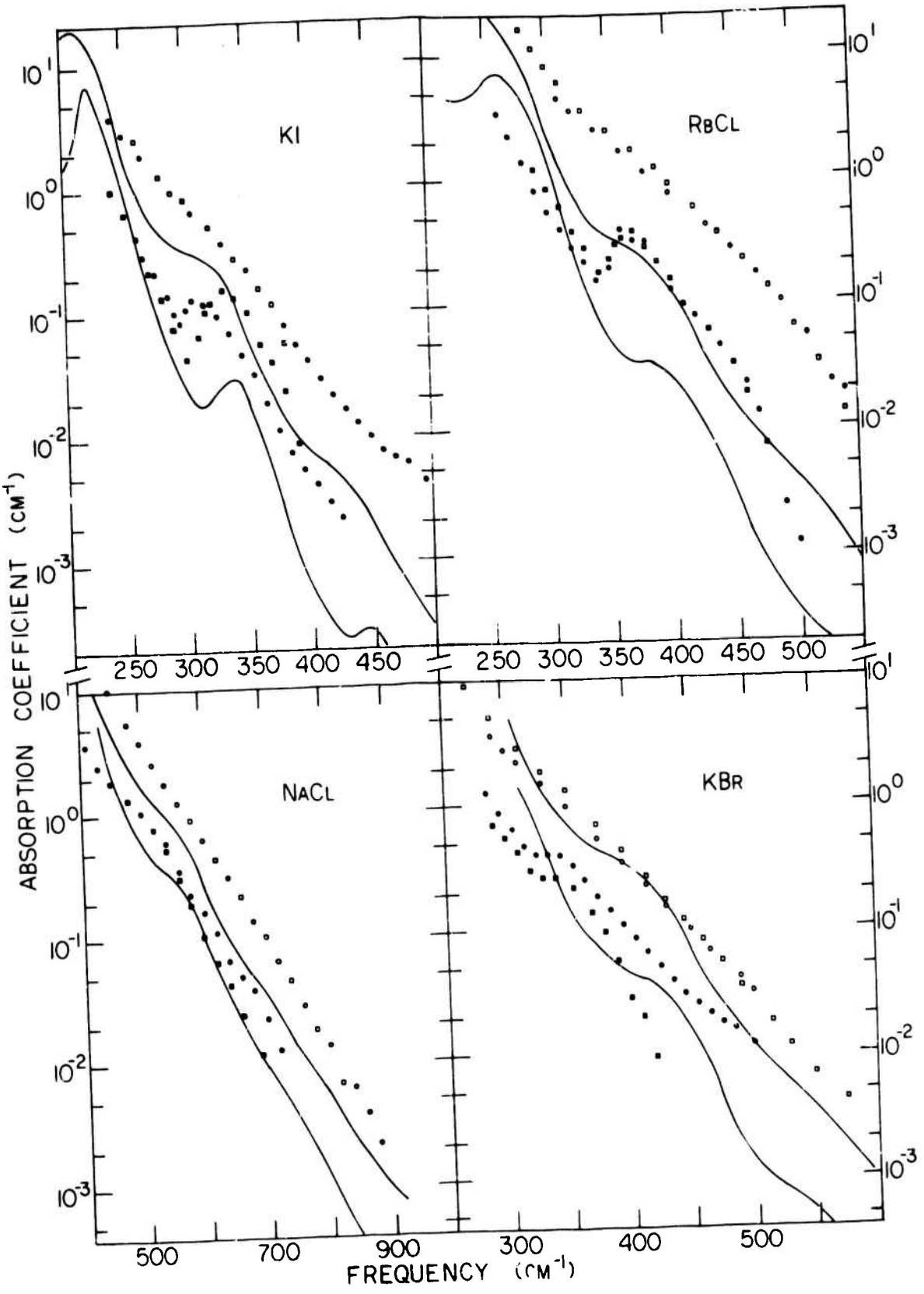
KI
RbCl
NaCl
KBr
ABSORPTION COEFFICIENT (cm⁻¹)
FREQUENCY (cm⁻¹)
250 300 350 400 450
250 300 350 400 450 500
500 700 900
300 400 500
10¹
10⁰
10⁻¹
10⁻²
10⁻³

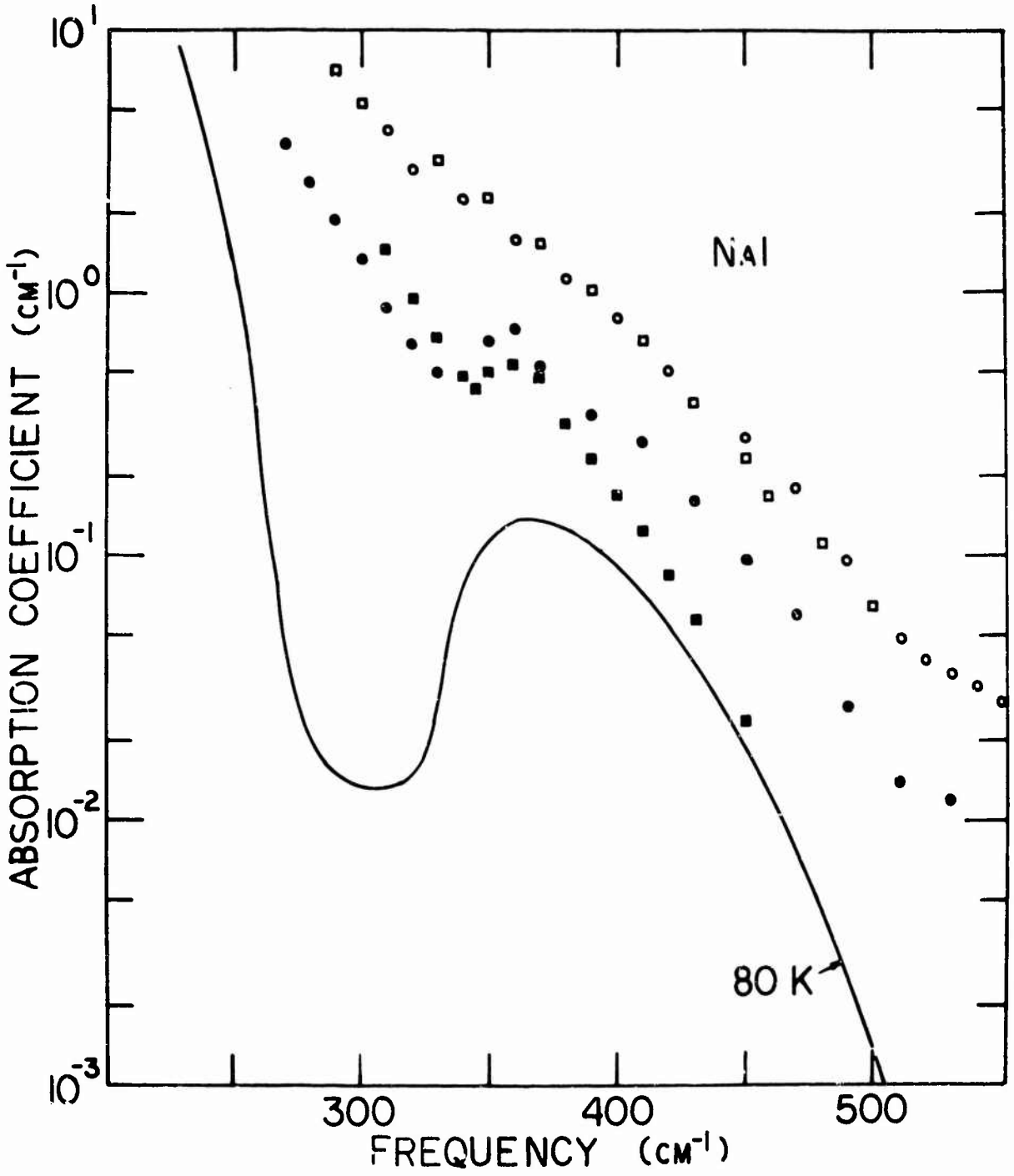
ABSORPTION COEFFICIENT (cm⁻¹)
10¹
10⁰
10⁻¹
10⁻²
10⁻³
NaI
80 K
300
400
500
FREQUENCY (cm⁻¹)

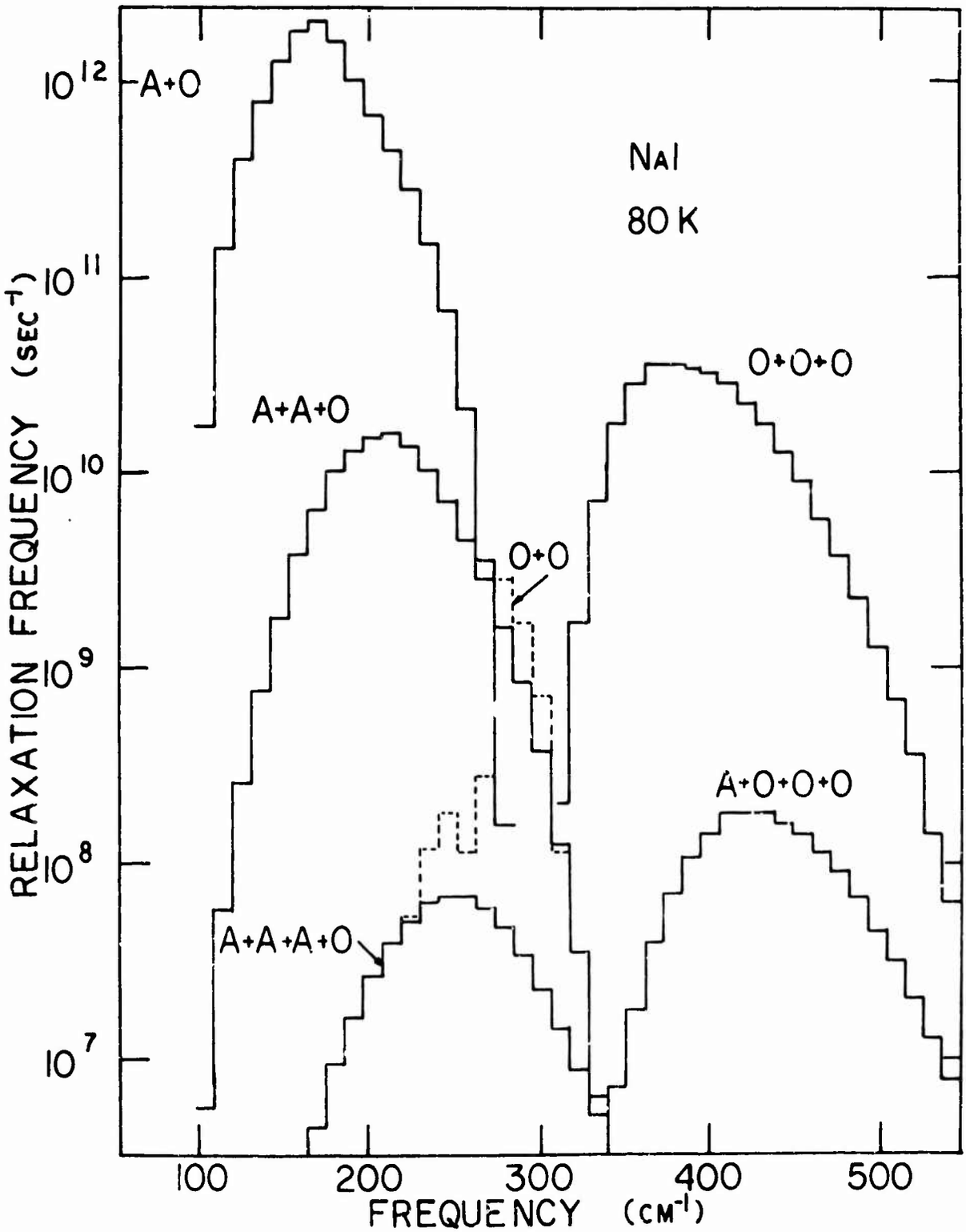
A+O
NaI
80 K
A+A+O
O+O+O
O+O
A+O+O+O
A+A+A+O
RELAXATION FREQUENCY (sec⁻¹)
10¹²
10¹¹
10¹⁰
10⁹
10⁸
10⁷
100
200
300
400
500
FREQUENCY (cm⁻¹)

I. ENHANCED STIMULATED RAMAN SCATTERING AND GENERAL THREE-BOSON PARAMETRIC INSTABILITIES*

M. Sparks and J. H. Wilson
Xonics, Incorporated, Van Nuys, California 91406

A recent theory of stimulated Raman scattering explained a Stokes-intensity enhanced gain that had been observed but that was not predicted by earlier theories. It is shown that in the earlier golden-rule analyses (perturbation theory treatment of occupation numbers n) the enhancement was lost by neglecting the increase of the vibrational amplitudes above their thermal equilibrium values. Even though the probability of an individual ion or molecule being excited is small, the occupation number of the phonon in the Raman process is large. In the previous mode-amplitude analyses, the enhancement was lost in the method of linearizing the nonlinear differential equations. By solving these same mode-amplitude equations for the n's without using the previous linearization scheme, the enhancement is obtained and the equivalence of the mode-amplitude and golden-rule Boson-occupation-number results is demonstrated explicitly. The analysis shows explicitly that the loss of phase information in using the Boson occupation numbers does not cause the loss of enhancement. The results are applicable to other three-Boson splitting processes that are important in ferromagnetism, phonon interactions, plasma instabilities, and device physics.

I. INTRODUCTION

Stimulated Raman scattering was first observed[1] and analyzed[2,3] in 1962. It was recently realized[4] that a parametric instability in the Raman Stokes process causes a Stokes-intensity gain enhancement that explains a number of observed anomalies including a nearly discontinuous increase, or "jump," in the Stokes intensity I_S as a function of the laser intensity I_L in the absence of self focusing and feedback. The purpose of the present investigation is to resolve the discrepancy between early theories[2,3] that did not give the gain enhancement and the later theory[4] that did. In addition to identifying the assumptions in both types of the early theories that led to the loss of enhancement, the equivalence of the results of the occupation number (n) rate-equation analysis and the mode amplitude (a and $a^\dagger$) analysis is demonstrated, and it is shown that the loss of phase information in the occupation-number analysis does not affect the enhancement results. The results are of interest in the general three-Boson splitting problem, which arises in a number of fields of physics, as discussed below.

The characteristic feature of a parametric instability is that as the amplitude n_0 of some mode 0 increases, the amplitude n_k of a mode k that is coupled to 0 first increases slowly, then increases rapidly to a great value as n_0 approaches a critical value. For example, in the Raman process a laser photon is annihilated, a Stokes photon is created, and a fundamental (Reststrahl) phonon is created. As the laser-photon occupation number n_L approaches a critical value n_R, the occupation numbers n_f and n_S of the fundamental-phonon

and Stokes-photon modes become very large. This increase in the value of n_S is the gain enhancement and "jump" already mentioned.

Any three-Boson splitting process is potentially unstable parametrically. There are analogies between the instability in the Raman process and previously studied instabilities in ferromagnetic resonance[5-7] (premature saturation of the main resonance, subsidiary absorption below the main resonance, and parallel-pumping absorption), plasma physics,[8] and electronic devices.[9]

The physical interpretation of these instabilities is rather simple. The balance of energy put into the f phonons by the Raman process against that removed from the f phonons by relaxation is a key to the explanation. The power out by relaxation (by interaction with impurities or other phonons, for example) increases linearly with the number of phonons n_f, which is just the condition that a relaxation time exists. On the other hand, the power into the f phonons increases nonlinearly with increasing n_f since the Raman process is a three-Boson process (which results in products of Boson occupation numbers in the expression for the power). Thus, at a critical value of the laser intensity, the amplitude n_f becomes very large.

Previous analyses of stimulated Raman scattering and other parametric processes used either the equations of motion of the Boson occupation numbers obtained from perturbation theory (the golden rule) or the equations of motion of the mode amplitudes (creation and annihilation operators or Fourier components and their complex conjugates of the electric field, for example). In the case of stimulated Raman scattering, the previous results from the mode-amplitude analysis do not give the enhancement obtained by the recent occupation-number analysis.

In the present paper the relation between the two approaches is demonstrated explicitly, and the points in the previous analyses at which the enhancement was lost are identified. In the previous golden-rule type analyses, the enhancement was lost by neglecting the deviation of the vibrational amplitude from the thermal equilibrium value. Even though n_f becomes large, the probability of an individual ion or molecule being excited is small, roughly speaking. Specifically, $n_f / N << 1$ is usually satisfied, where N is the number of unit cells or molecules. It was this fact that the individual ions or molecules are not highly excited that led to the assumption that the thermal equilibrium values were maintained in the previous analyses. There are similar results for other three-Boson processes. For example, in ferromagnetism, magnon occupation numbers are large at the threshold, while the probability of an individual electron spin being in the reversed-spin state is small.

In the previous mode-amplitude analyses, the enhancement was lost in the method of linearizing and decoupling the nonlinear differential equations for the mode amplitudes a_L, a_S, a_f, and their complex conjugates (or Hermitian conjugates in the quantum-mechanical solution). It is shown specifically that reducing the nonlinear equations to parametric linear equations (that is, linear equations with time-dependent coefficients) by assuming that the laser-field amplitude $a_L = b_L \exp(-i\omega_L t)$, where b_L is a constant, results in the loss of the enhancement. The same linearization scheme applied to well known magnon or phonon parametric instabilities results in the loss of the steady-state solution, even though damping is included and a steady-state solution is expected on the basis of simple physical arguments. By solving the same mode-amplitude equations

for the n's without using this linearization scheme, the difficulties are removed and the equivalence of the mode-amplitude and golden-rule results is demonstrated explicitly for the stimulated-Raman-scattering and magnon problems.

The central features of enhanced stimulated Raman scattering are classical. In the classical analyses, care has been exercised to keep the order of the a and $a^{\dagger}$ correct so that the equations can be easily converted to quantum equations in Sec. IV. The present analysis is concerned only with the steady-state solution.

In Sec. IV several points that are not apposite to the central results, but are of general interest, are discussed. These include a ferromagnetic instability, purely quantum mechanical effects, resolution of a difficulty in the quantum treatment when dissipation is included, and the problem of phases mentioned above. Important results are indicated by underscored equation numbers.

II. MODE-AMPLITUDE ANALYSIS OF ENHANCED STIMULATED RAMAN SCATTERING

In this section the same mode-amplitude equations for stimulated Raman scattering that were previously solved by a common linearization approximation to obtain gain without enhancement are solved without making this linearization approximation. The present solution gives the gain enhancement and agrees with the results of the golden-rule analysis, as discussed in the following section.

The mode-amplitude equations have been obtained classically from Maxwell's equations with terms added to account for the coupling of the electromagnetic and elastic waves.[3,10,11] Specifically, an interaction Lagrangian was added to the sum of the electromagnetic and elastic Lagrangians and the field-amplitude equations were obtained from the Lagrangian. The resulting second-order partial differential equations were reduced by standard methods to the following first-order partial differential equations[10,11]

$$\frac{\partial a_f}{\partial t} = -i\omega_f a_f - V a_L a_S^{\dagger} - \frac{1}{2}\Gamma a_f \tag{2.1}$$

$$\frac{\partial a_S}{\partial t} = -i\omega_S a_S - V a_L a_f^{\dagger} - c_S \frac{\partial a_S}{\partial x} \tag{2.2}$$

$$\frac{\partial a_L}{\partial t} = -i\omega_L a_L + V^* a_f a_S - c_L \frac{\partial a_L}{\partial x} \tag{2.3}$$

where the a's are the Fourier components of the fundamental phonon field f, the laser field L, and the Stokes field S, the $a^{\dagger}$'s are the complex conjugates of the a's, V is the coupling coefficient for the coupling of the three fields, and V^* is the complex conjugate of V. Equations (2.1)-(2.3) and the complete treatment

of Secs. II and III are classical. If (2.1)-(2.3) are to be interpreted as quantum-mechanical operator equations, a noise source must be added to preserve the commutation relations since damping has been added in these equations. The quantum treatment will be considered in Sec. VI.

The previous solutions were obtained by linearizing these equations by assuming that $a_L = a_{L0}\exp(-i\omega t)$ where a_{L0} is a constant, as discussed in Sec. I. There are several possible ways of solving these equations without using this linearization method, as discussed in Sec. IV. The simplest method, which also best illustrates the relation to the golden-rule results, is to convert equations (2.1)-(2.3) to rate equations for $n_f \equiv a_f^\dagger a_f$, $n_L = a_L^\dagger a_L$, and $n_S = a_S^\dagger a_S$, which will be solved for the steady-state solution. This is easily accomplished by using $\partial n_f/\partial t = a_f^\dagger \partial a_f/dt$ + cc and similar equations for n_S and n_L, which gives

$$\frac{\partial n_f}{\partial t} = F - \Gamma n_f \qquad (2.4)$$

$$\frac{\partial n_S}{\partial t} = F - c_S \frac{\partial n_S}{\partial x} \qquad (2.5)$$

$$\frac{\partial n_L}{\partial t} = -F - c_L \frac{\partial n_L}{\partial x} \qquad (2.6)$$

$$\frac{\partial F}{\partial t} = 2|V|^2 [n_L(n_f + n_S) - n_S n_f] - \frac{1}{2}\Gamma F \qquad (2.7)$$

$$F \equiv -V a_L a_f^\dagger a_S^\dagger + cc \ . \qquad (2.8)$$

Equation (2.7) was obtained by substituting (2.1)-(2.3) into $-\partial F/\partial t$ $= V(\partial a_L/\partial t) a_f^\dagger a_S^\dagger + V a_L (\partial a_f^\dagger/\partial t) a_S^\dagger + V a_L a_f^\dagger \partial a_S^\dagger/\partial t + cc$. The term $Vc_L(\partial a_L/\partial x) a_f^\dagger a_S^\dagger + Vc_S a_L a_f^\dagger \partial a_S^\dagger/\partial x + cc$ vanishes since a Stokes photon

is created for every laser photon annihilated and the propagation of the two photons is the same for $c_S \cong c_L$.

Setting the time derivatives of n_f, n_S, and F equal to zero, as discussed in Sec. IV, gives the steady-state solution

$$c_S \frac{\partial n_S}{\partial x} = 4|V|^2 \Gamma^{-1} [n_L(n_f + n_S) - n_S n_f] \qquad (2.9)$$

and

$$n_R^{-1} [n_L(n_f + n_S) - n_S n_f] - n_f = 0 \qquad (2.10)$$

where $n_R \equiv \Gamma^2/4|V|^2$. Neglecting the saturation term $n_S n_f$ in (2.10), which has been considered elsewhere[12] and not apposite to the argument, and solving for n_f gives

$$n_f = \frac{(n_L/n_R) n_S}{1 - n_L/n_R} \quad . \qquad (2.11)$$

The results (2.11) and (2.9) with $n_S n_f$ neglected give the enhanced stimulated Raman scattering result

$$n_S = +n_S(0) \exp \beta_{g\,new} x \quad , \qquad (2.12)$$

where $\beta_{g\,new} = (\Gamma/c_S)\, n_L/n_R\, (1 - n_L/n_R)^{-1}$. The results (2.9)-(2.12) are identical to the results derived previously[4] using the golden rule. In passing, notice that n_L can be considered as a constant in (2.7).

III. LOSS OF ENHANCEMENT IN PREVIOUS ANALYSES

Previous treatments[2,3] of stimulated Raman scattering did not yield the enhancement obtained in the previous section. These analyses either specifically assumed no increase in the vibrational energy above the thermal equilibrium value or solved equations (2.1) and (2.2) or their equivalents by a method equivalent to that described below. In the former case, (2.11) (or (4.19) in the following section) is replaced by

$$n_f = \bar{n}_f \ .$$

Substituting this expression into (2.9), neglecting the saturation term $n_S n_f$, and solving for n_S gives

$$n_S = \bar{n}_f \left(e^{\beta_{old} x} - 1\right) + n_S(0)\, e^{\beta_{old} x} \tag{3.1}$$

where $\beta_{old} = 4|V|^2 n_L/\Gamma c_S = (\Gamma/c_S)(n_L/n_R)$. This is just the previous Raman gain factor with no enhancement.

In the latter of these two previous types of analyses, the nonlinear equations (2.1) and (2.2), which were treated as <u>classical</u> equations, were linearized and decoupled from (2.3) by assuming that

$$a_L \equiv b_L e^{-i\omega_L t} \tag{3.2}$$

where b_L is independent of time. Then substituting $a_f = b_f \exp(-i\omega_f t)$ and $a_S^\dagger = b_S^\dagger \exp(i\omega_S t)$ into (2.1) and the Hermitian conjugate of (3.2) gives

$$\frac{\partial b_f}{\partial t} = V b_L b_S^\dagger - \frac{1}{2}\Gamma b_f \tag{3.3a}$$

$$\frac{\partial b_S^\dagger}{\partial t} = V^* b_L^\dagger b_f - c_S \frac{\partial b_S^\dagger}{\partial x} \tag{3.3b}$$

for the case of resonance, that is $\omega_L = \omega_S + \omega_f$. Setting the time derivatives equal to zero and eliminating b_f from the two equations gives

$$c_S \frac{\partial b_S}{\partial x} = 2|V|^2 n_L b_S/\Gamma$$

which has the solution

$$b_S(x) = b_S(0)\, e^{\beta x} \tag{3.4}$$

where $\beta = 2|V|^2 n_L/c_S\Gamma$, which shows no gain enhancement. A nonzero steady-state solution (3.4) was obtained in this previous analysis because the pump b_L acts as a source. This is particularly clear in the analogous problems of a parametrically pumped pendulum or moving-plate capacitor problem where the energy is supplied by the mechanism that changes the length of the pendulum or moves the capacitor plates.

In order to further show how the assumption (3.2) causes the loss of enhancement, (3.3) with b_L independent of time will be solved by another method, in direct analogy with the solution of Sec. II where the time dependence of b_L was retained. By the same method used in Sec. II, (3.3a) and (3.3b) give

$$\frac{\partial n_f}{\partial t} = F - \Gamma n_f \tag{3.5}$$

$$\frac{\partial n_S}{\partial t} = F - c_S \frac{\partial n_S}{\partial x} \tag{3.6}$$

$$\frac{\partial F}{\partial t} = 2|V|^2 n_L(n_f + n_S) - \frac{1}{2}\Gamma F - (c_S V b_L b_f \frac{\partial b_S}{\partial x} + cc) \ . \tag{3.7}$$

By neglecting the time dependence of b_L, the nonlinear term $-2|V|^2 n_f n_S$ in (2.7) is lost and the last term in (3.7), which did not appear in (2.7), is gained. The former makes the solution incorrect in the saturation region and the latter eliminates the enhancement. Neglecting the time dependence of b_L is equivalent to neglecting the last two terms in (2.3) for da_L/dt. By so neglecting the last term $c_L \partial a_L/\partial x$ in (2.3), the cancellation of the similar term $c_S \partial a_S/\partial x$ from (2.2) does not occur in the equation for $\partial F/\partial t$; thus, the last term in (3.7) is present. Neglecting the other term $V^* a_f a_S$ in (2.3) corresponds directly to the absence of the term $2|V|^2 n_S n_f$ in (3.7). This discussion indicates that the physical significance of the linearization by using (3.2) is that the effect of increases in the amplitudes a_f and a_S on the amplitude a_L is neglected and the spatial rate of change of a_L is neglected while a comparable term of a_S is retained.

Stated differently, it is tempting to neglect the time derivative of b_L when b_L is large so that the fractional change in b_L is small. However, db_L/dt must be retained since it is of comparable magnitude to other terms such as db_S/dt that are retained. It makes no difference that the fraction change in b_S is large while that in b_L is small.

Finally, the loss of enhancement in (3.5)-(3.7) can be seen by setting the time derivatives equal to zero, $\partial n_S/\partial x = \beta n_S$, and $\partial b_S/\partial x = \frac{1}{2}\beta b_S$ in (3.5)-(3.7) and eliminating F. This gives

$$2|V|^2 n_L(n_f + n_S) - \tfrac{1}{2}(\Gamma + c_S\beta)\, c_S \beta n_S = 0$$

$$c_S \beta n_S = \Gamma n_f \ .$$

Eliminating n_f gives

$$2|V|^2 \Gamma^{-1} n_L (c_S\beta + \Gamma) - \frac{1}{2}(c_S\beta + \Gamma) c_S\beta = 0 \quad .$$

Dividing by $\frac{1}{2} c_S (c_S \beta + \Gamma)$ gives

$$\beta = \beta_{old} \equiv 4|V|^2/c_S\Gamma$$

in agreement with (3.4).

IV. FERROMAGNETIC INSTABILITIES, QUANTUM MECHANICAL EFFECTS, AND PHASES

The considerations of this section are not essential to the explanation of differences in the three types of treatment of enhanced Raman scattering, but are of general interest. First consider the parametric instability in the simplest three-Boson process, illustrated in Fig. 1, where one Boson 0 is annihilated and two Bosons having equal frequencies and damping are created. The propagation of all three Bosons is negligible. As specific examples, in the case of ferromagnetic subsidiary-resonance absorption,[5-7] Boson 0 is a uniform precession (wave vector $\underset{\sim}{k} = 0$) magnon, and in parallel pumping, Boson 0 is a photon in the microwave cavity. In both cases, the output Bosons are magnons having wave vectors $\underset{\sim}{k}$ and $-\underset{\sim}{k}$. Propagation effects are negligible since the magnons cannot propagate out of the sample and the sample is small with respect to the electromagnetic wavelength. The process also represents phonon processes[12] and other Boson processes.

It will be demonstrated that the equations of motion of the mode amplitudes can be solved to give the golden-rule results directly. The same mode-amplitude equations will be solved by an approximate method of converting nonlinear differential equations into linear differential equations with time-dependent coefficients, or so called parametric equations. This approximate method, which is the same method used in the early treatments of the stimulated Raman scattering, gives incorrect results in the present magnon problem as it did in the stimulated Raman scattering problem.

The equations of motion of the Fourier components a's of the $k = 0$ and the $+\underset{\sim}{k}$ and $-\underset{\sim}{k}$ modes, denoted 0, +, and -, and the complex conjugates are[5,7]

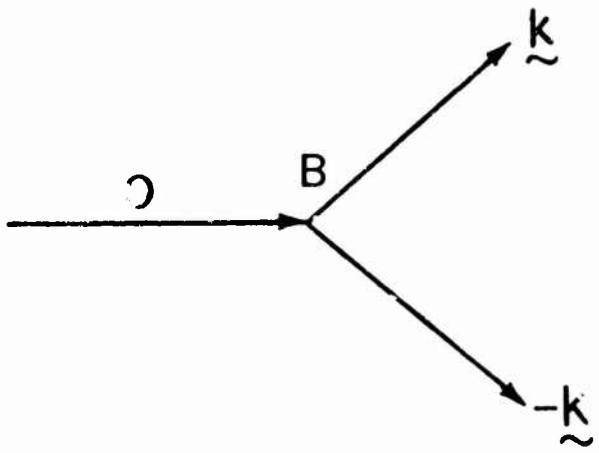

Fig. 1. Three-Boson splitting process that exhibits a parametric instability.

$$da_+/dt = -i\omega_+ a_+ - Ba_0 a_-^\dagger - \gamma a_+ \quad , \tag{4.1}$$

$$da_-^\dagger/dt = -i\omega_- a_-^\dagger - B^* a_0^\dagger a_+ - \gamma a_-^\dagger \quad , \tag{4.2}$$

$$da_0/dt = -i\omega_0 a_0 + B^* a_+ a_- \quad , \tag{4.3}$$

where B is the coupling constant. This set of equations (4.1)-(4.3) and the Hermitian conjugate equations is a set of six nonlinear classical differential equations for the six variable a_i and $a_i^\dagger$ with $i = 0, +, -$.

A previous classical method of solution was to linearize the equations by formally assuming that $a_0 = b_0 e^{-i\omega_0 t}$ and $a_0^\dagger = b_0^\dagger e^{i\omega_0 t}$ where b_0 and $b_0^\dagger$ are constants, as in Sec. II. Then (4.1) and (4.2) are a set of two parametric differential equations for a_+ and $a_-^\dagger$. Substituting these expressions for a_0 and $a_0^\dagger$ along with $a_+ = b_+ \exp(-i\omega_+ t)$ and $a_-^\dagger = b_-^\dagger \exp(i\omega_- t)$ into (4.2) and (4.3) and taking the derivatives gives

$$db_+/dt = Bb_0 b_-^\dagger - \gamma b_+ \tag{4.4}$$

$$db_-^\dagger/dt = B^* b_0^\dagger b_+ - \gamma b_-^\dagger \quad . \tag{4.5}$$

The time-dependent coefficients were eliminated by assuming that the resonance condition $\omega_0 = \omega_+ + \omega_-$ is satisfied. Since these two equations are linear with constant coefficients, their solution is simple. Taking the derivative of (4.4), using (4.5) to eliminate b_-, and substituting the trial solution $b_+ = b_{+0} \exp(\lambda t)$ into the resulting equation gives

$$a_+ = e^{-i\omega_+ t} e^{-\gamma t} \left[b_+^{(+)} e^{|Bb_0| t} + b_+^{(-)} e^{-|Bb_0| t} \right] \quad . \tag{4.6}$$

There is no non-zero steady-state solution except in the singular case of $|Bb_0| = \gamma$. The common expression "parametric instability" arises from the fact that a_+ becomes infinite as $t \to \infty$ when the amplitude $|b_0|$ of the zero mode is sufficiently great; that is, when

$$|b_0|^2 > \gamma^2/|B|^2 \quad . \tag{4.7}$$

The classical effect of neglecting the time dependence of b_0 is somewhat less dramatic in the present case of the magnon instability than in the Raman scattering case since the correct steady-state solution for small values of b_0 is $a_+ = 0$ even when the time dependence of b_0 is retained. In the case of large values of b_0, the difference between the zero steady-state solution obtained for the case of b_0 independent of time and the non-zero steady-state solutions (4.13) and (4.14) for the case of time dependence included is of course more significant. In passing it is mentioned that in parametric equations the terms such as $Bb_0 b_-^\dagger$ and its complex conjugate in (4.4) and (4.5) are source terms, which give rise to the energy flow from the $\underset{\sim}{k} = 0$ to the $\pm\underset{\sim}{k}$ modes. Thus, the steady-state solution is not $b_+ = b_- = 0$ in general.

To resolve the difficulty of no classical steady-state solution, a method of solution other than the parametric linearization used above is needed. One approach would be to linearize (4.1) simply by considering $a_0 a_-^\dagger$ as a single variable. Since $a_0 a_-^\dagger$ is coupled to a_+ according to (4.1), the standard procedure is to consider the equation of motion for $a_0 a_-^\dagger$. If this equation contains only a_+ and $a_0 a_-^\dagger$ (and no product $a_+ a_0 a_-^\dagger$), then the two linear differential equations could be easily

solved. Unfortunately the equations do not uncouple at this step. Furthermore, taking the derivatives of the additional variables that appear in the $a_0 a_-^\dagger$ equation couples in still more variables, and the chain of equations becomes large. Nevertheless, this method, along with several other powerful and elegant methods, afford useful tools for attacking the problem. As already noted in Sec. II, a simpler method is to start with the operator $a_+^\dagger a_+ \equiv n_+$, rather than a_+. Just as in Sec. II, it is found that

$$dn_+/dt = F_+ - \Gamma(n_+ - \bar{n}_+) \qquad (4.8)$$

$$dn_-/dt = F_+ - \Gamma(n_- + \bar{n}_-) \qquad (4.9)$$

$$dn_0/dt = -F_+ \qquad (4.10)$$

$$dF_+/dt = 2|B|^2 \left[n_0(n_+ + n_-) - n_+ n_- \right] - \Gamma F_+ \quad , \qquad (4.11)$$

where $F_+ = -Ba_0 a_+^\dagger a_-^\dagger + cc$ and $\Gamma \equiv 2\gamma$, the factor of two arising as usual from the fact that $a \sim \exp(-\gamma t)$ implies that $|a|^2 \sim \exp(-2\gamma t)$. The terms $\Gamma\bar{n}_+$ and $\Gamma\bar{n}_-$ were added formally to make n_+ and n_- relax to their thermal equilibrium values $\bar{n}_+$ and $\bar{n}_-$. As in the previous cases, the treatment is classical. If the usual commutation relations for the $a^\dagger$ and a are used formally, then $n_+ + n_-$ in (4.11) is replaced by $n_+ + n_- + 1$. The considerations of the commutation relations and of adding damping, noise sources, and thermal equilibrium values that are addressed below for the case of Raman scattering are not considered here since this would carry us too far afield.

There are several physical situations for which the solutions to (4.8)-(4.11) are of interest. The first is that to which the golden rule is commonly applied.

That is, at time t = 0 the system is in the state in which n_L is very large and all other modes are in thermal equilibrium, roughly speaking. The perturbation $-i\hbar B a_0 a_+^\dagger a_-^\dagger + c.c.$ is then applied for a time short with respect to the time for n_0 to change substantially, but sufficiently long for energy conservation to be well satisfied. The case in which n_0 is maintained at a constant value by the microwave field in the cavity also is of interest. In both of these cases, n_0 is constant, or approximately constant. However, dn_0/dt in (4.10) is not zero because (4.10) is only the contribution to the rate of change of n_0 from the coupling to the $\pm k$ modes. Stated differently, $\hbar\omega_0 dn_0/dt$ from (4.10) gives the power from the zero mode to the pair $\pm\underset{\sim}{k}$, which is not zero in the steady state. The contribution to dn_0/dt from the coupling of the zero mode to the microwave field could be added, by replacing (4.10) with $dn_0/dt = \text{const.}\, n_0 - F_+$ for example, but this would carry us too far from the issue at hand. In passing, notice the physical significance of F_+ as the energy flow from the zero mode to the pair $\pm\underset{\sim}{k}$, in units of quanta per second.

The steady-state solution to (4.8)-(4.9) is obtained by setting $dF_+/dt = 0$ (i.e., constant energy flow) and $dn_+/dt = 0$ and solving for n_+ and n_-. This gives

$$n_- = n_+ = 2|B|^2 \Gamma^{-2} \left[2n_0 n_+ - n_+^2 \right] \tag{4.12}$$

which are the standard results obtained from the golden rule. For $n_0 < n_c - \epsilon$, where ϵ is very small, the solution to (4.12) is

$$n_- = n_+ = \frac{\bar{n}_+}{1 - n_0/n_c} \quad , \qquad n_c \equiv \Gamma^2/4|B|^2 \quad , \tag{4.13}$$

where $\bar{n}_- = \bar{n}_+$, for $n_0 > n_c + \epsilon$ the solution is

$$n_- = n_+ = 2(n_0 - n_c) \quad , \tag{4.14}$$

and for $n_0 = n_c$, the solution is $n_- = n_+ = (2 n_0 \bar{n}_+)^{1/2}$.

These results are obtained simply from the golden rule as follows: The standard expression $(2\pi/\hbar^2)|\langle f|\mathcal{H}|i\rangle|^2 \delta(\omega)$ for the transition rate between states $|i\rangle$ and $|f\rangle$ gives

$$dn_+/dt = (2\pi/\hbar^2) \left[|\mathcal{H}|_+^2 - |\mathcal{H}|_-^2 \right] \rho(\omega) - \Gamma(n_+ - \bar{n}_+)$$

where $|\mathcal{H}|_+^2$ is the matrix element for increasing n_+ by one, $|\mathcal{H}|_-^2$ is that for decreasing n_+ by one, $\rho(\omega)$ is the density of states, and the relaxation term $\Gamma(n_+ - \bar{n}_+)$ is added formally. For a single transition on resonance ($\omega_0 = \omega_+ + \omega_-$) the appropriate value of $\rho(\omega)$ is[7,6,4] $\rho(\omega) = 1/\pi\Gamma$. Using the usual expressions for the matrix elements of the a's and $a^\dagger$'s gives

$$dn_+/dt = 2|B|^2\Gamma^{-1} \left[(n_+ + 1)(n_- + 1) n_0 - n_+ n_- (n_0 + 1) \right] - \Gamma(n_+ - \bar{n}_+) \quad . \tag{4.15}$$

Since the bracket factors in (4.15) and (4.11) (with the replacement $n_+ + n_- \rightarrow n_+ + n_- + 1$) are equal, the steady-state solution to (4.15) is given by (4.13) and (4.14) as already mentioned. Notice that when the factor of 1 is added to (4.11), $\bar{n}_+$ in (4.13) is replaced by $\bar{n}_+ + n_0/2n_c$.

Even though only the steady-state case is considered here, it should be mentioned that the transient solutions of (4.15) and of (4.8)-(4.10) are different in

general. The simplest case of $n_+ n_-$ negligible, $n_+(0)$ = constant, and n_0 = constant can be solved trivially to illustrate this point.

In the quantum mechanical treatment it is well known[9b,9c,13,14] that formally adding the term $-\frac{1}{2}\Gamma a_f$ to the equation (2.1) for da_f/dt is inconsistent with the commutation relation $[a_f, a_f^\dagger] = 1$. The difficulties with the commutation relations and with relaxation to zero have been the subjects of numerous previous investigations.[5,9,13,14] In the magnon problem, relaxation to thermal equilibrium has been treated classically by formally adding a noise source.[5] Both the commutation-relation problem and that of relaxing to zero can be treated by enlarging the system to include the modes that are responsible for the damping, that is, by including a damping reservoir explicitly.[9c,13,14] Since noise problems are not addressed in the present study, it is not surprising that the phenomenological damping used above can be justified within the usual enlarged-system approach as follows.

The simplest damping mechanism is that of two-Boson damping induced by a localized imperfection such as a void or impurity ion. (For nonlocalized imperfections, wave vector is conserved and the sum on j below is reduced to a single term.[7]) Even though this damping mechanism is not often the actual dominant mechanism, we follow the standard practice of using it in order to illustrate how including the damping reservoir resolves the commutator difficulty and gives relaxation to thermal equilibrium. The reservoir is taken as a set of Bosons, say phonons to be concrete, with creation and annihilation operators $a_j^\dagger$ and a_j. Then the Hamiltonian for the interaction with the reservoir is

$$\mathcal{H}_i = \sum_j \hbar \Omega_j a_f a_j^\dagger + \text{cc}$$

where cc denotes hermitian conjugate. The Heisenberg equation of motion of a_f, with this interaction included, is (2.1) with $-\frac{1}{2}\Gamma a_f$ replaced by $G'_{af} \equiv -i\sum_j \Omega_j a_j$. By writing the Heisenberg equations of motion of a_j and $a_j^\dagger$ as integral equations which are substituted into G'_{af}, taking the Laplace transform of G'_{af}, using the approximation $[s - i(\omega_f - \omega_j)]^{-1} \cong \pi\delta(\omega_f - \omega_j) + i\mathcal{P}(\omega_f - \omega_j)^{-1}$ (since the pole of interest is near $s = 0$ in the perturbation-theory limit[15]) with $\mathcal{P}$ denoting the principal part and s the transform variable, and inverting the transform gives

$$G'_{af} \equiv -i\sum_j \Omega_j a_j \cong -\frac{1}{2}\Gamma a_f + G_{af} \tag{4.16}$$

where

$$G_{af} = -i\sum_j \Omega_j a_j(0)\, e^{-i\omega_j t}$$

is the noise source and

$$\Gamma = 2\pi\sum_j |\Omega_j|^2\, \delta(\omega_j - \omega_f)$$

is the golden-rule result for the relaxation frequency. The real parts of the frequency shifts arising from $\mathcal{P}$ are ignored for simplicity.

The equations of motion for the n's and F can be obtained directly from the Heisenberg equations or from the equations for the a's, with $-\frac{1}{2}\Gamma a_f$ replaced by the right-hand side of (4.16). In either case, using $\langle G_{nf}(t)\rangle \equiv \langle -\sum_j \Omega_j a_j(0)\, a_f^\dagger(t)\, e^{-i\omega_j t} + cc\rangle \cong \Gamma\bar{n}_f$, which is not difficult to derive,[9c] gives

$$dn_f/dt = F - \Gamma(n_f - \bar{n}_f) + g_{nf}(t) \tag{4.17}$$

where

$$g_{nf}(t) = G_{nf}(t) - \langle G_{nf}(t)\rangle$$

and similar equations for n_S, n_L, and F. Taking the averages over the reservoir (the phonon-bath mode) of all terms in (4.22) and using $\langle g_{nf} \rangle = \langle G_{nf} \rangle - \langle G_{nf} \rangle = 0$ gives

$$\frac{d\langle n_f \rangle}{dt} = \langle F \rangle - \Gamma(\langle n_f \rangle - \bar{n}_f) \tag{4.18}$$

and similar equations of $\langle n_S \rangle$, $\langle n_L \rangle$, and $\langle F \rangle$. Thus, (2.4)-(2.7) with the $\bar{n}_f$ term added as above are valid when the operators n_f, etc. are interpreted as averages over the reservoir. Recall that $\bar{n}_f$ is the thermal equilibrium value of n_f, that is the average over the complete ensemble, while $\langle n_f \rangle$ is the average over the reservoir only (phonons in thermal equilibrium). Notice that in the absence of the source, $\langle a_f \rangle$ relaxes to zero while $\langle a_f^\dagger a_f \rangle$ relaxes to the thermal equilibrium value $\bar{n}_f$.

The following physical description of the damping and noise term is useful in visualizing these effects even though the explanation is oversimplified. The energy flow from the f phonons to the phonons in the bath is not a smooth function of time. For example, if the energy transfer is visualized as the interchange of quanta of energy between the f phonons and the bath, then in the time interval $0 - t_1$, there may be 10 net quanta of energy entering the bath. In the interval t_1 to $2t_1$ there may be 8, in the interval $2t_1$ to $3t_1$ there may be 12, and so forth. The average value of, say, 10 quanta per time t_1 corresponds to Γ, and the fluctuations of, say, 2 quanta per time t_1 corresponds to the noise term that averages to zero. There are also fluctuations in the energy flow F from the laser photons L to the Stokes photons S and phonons f since F depends on the fluctuating amplitude of the f modes.

This visualization explains why it is not rigorously correct to set the various time derivatives equal to zero in the "steady state." That is, the fluctuations are still present when average values have reached constant values. Since the interest here is in the average values rather than the fluctuations, the time derivatives can be set equal to zero, or, mathematically, the reservoir averages can be used in order to eliminate the fluctuation terms.

Consider the purely quantum mechanical effects in the Raman-scattering problem. When the mode amplitudes in (2.1)-(2.3) are operators with the usual commutation relation $[a_i, a_i^\dagger] = 1$, the factors $n_f + n_S$ in (2.7), (2.9), and (2.10) are replaced by $n_f + n_S + 1$. Replacing Γn_f by $\Gamma(n_f - \bar{n}_f)$ formally in the relaxation terms in (2.4) and (2.10) gives a relaxation of n_f to its thermal equilibrium value $\bar{n}_f$. The complete expression $\Gamma(n_f - \bar{n}_f)$ is of course obtained in standard quantum mechanical calculations of relaxation.[9,7] With these two additions, (2.11) and (2.12) become

$$n_f = \frac{\bar{n}_f + (n_L/n_R)(n_S + 1)}{1 - n_L/n_R} \tag{4.19}$$

$$n_S = (\bar{n}_f + 1)[\exp(\beta_{g\,new}\, x) - 1] + n_S(0) \exp \beta_{g\,new}\, x \quad . \tag{4.20}$$

Thus, comparison of (4.20) with (2.12) shows that the quantum-mechanical effect is that the zero-point oscillation is amplified ($\exp \beta_{g\,new}\, x - 1$ term), and the effect of including $\bar{n}_f$ is that the term $\bar{n}_f(\exp \beta_{g\,new} x - 1)$ accounts for "amplification of the thermal equilibrium value of n_f."

Finally, consider the physical explanation of the result that the loss of phase information in using the golden rule does not affect the final result in view of the

fact that the phases are important in some sense. Specifically, a parametric process which increases the amplitude of a given phase will decrease the amplitude of a mode that is π radians out of phase with the increasing mode. The reason that the loss of phase information in using occupation numbers is not important in the final result is that the modes in the original thermal distribution that have the correct phase are the ones that are amplified. A similar situation exists in the simple case of a classical harmonic oscillator responding to an applied harmonic force. The phase of the oscillator is important since it determines whether energy is extracted from or delivered to the driving force. This does not imply that energy-conservation arguments, which suffer from an analogous loss of phase information, are not valid. It should be mentioned that wave vector and frequency phase matching are included in the occupation number approach. Wave vector phase matching arises from Kronecker deltas in sums over wave vectors, and frequency phase matching arises from the energy-conserving delta function. The present calculation settles the question of the importance of phases in obtaining the enhancement by showing explicitly that the phases are unimportant in the result.

REFERENCES

*A preliminary version of the present section was included in the previous technical report. In the quantum treatment in the present version, the non-trivial questions of damping, relaxation to thermal equilibrium, and preservation of commutation relations are addressed.

1. E. J. Woodbury and W. K. Ng, Proc. IRE 50, 2367 (1962).
2. R. W. Hellwarth, Phys. Rev. 130, 1850 (1963).
3. Y. R. Shen and N. Bloembergen, Phys. Rev. 137, A1787 (1965); N. Bloembergen, Am. J. Phys. 35, 989 (1967); F. De Martini, Phys. Rev. B4, 4556 (1971).
4. M. Sparks, Phys. Rev. Lett. 32, 450 (1974), and Phys. Rev. A 11, 595 (1975). In an erratum to the letter, the effect of optical dispersion was overlooked. Thus, the reservations expressed in the erratum are not appropriate.
5. H. Suhl, J. Phys. Chem. Solids 1, 209 (1959).
6. H. B. Callen, Fluctuation, Relaxation and Resonance in Magnetic Systems, edited by D. ter Haas (Oliver and Boyd, Edinburgh, 1962); R. M. White and M. Sparks, Phys. Rev. 130, 623 (1963).
7. M. Sparks, Ferromagnetic Relaxation Theory (McGraw-Hill, New York, 1964).
8. S. V. Silin, Sov. Phys. JETP 21, 1127 (1965); D. F. DuBois and M. V. Goldman, Phys. Rev. Lett. 14, 544 (1965).
9. a. W. H. Louisell, Coupled Modes and Parametric Electronics (Wiley, New York, 1960); b. Radiation and Noise in Quantum Electronics (McGraw-Hill, New York, 1964); c. Quantum Statistical Properties of Radiation (Wiley, New York, 1973).
10. N. M. Kroll, J. Appl. Phys. 36, 34 (1965).
11. C. S. Wang, Phys. Rev. 182, 482 (1969).

12. M. Sparks and H. C. Chow, Phys. Rev. B10, 1699 (1974).

13. I. R. Senitzky, Phys. Rev. 115, 227 (1959).

14. M. Lax, Phys. Rev. 145, 110 (1966).

15. The reader with explicit interest in this reservoir approach should transform the complete differential equation.[9c] The results are unchanged.

J. LIST OF PUBLICATIONS

New publications and those whose status has changed since the Fourth Technical Report of 6 December 1974 are included in the following list:

1. M. Sparks, "Stimulated Raman Scattering: Enhanced Stokes Gain and Effects of Anti-Stokes and Parametric Phonon Processes," Phys. Rev. A11, 595 (1975).

2. A. A. Maradudin and D. L. Mills, "The Scattering and Absorption of Electromagnetic Radiation by a Semi-Infinite Crystal in the Presence of Surface Roughness," Phys. Rev. B11, 1392 (1975).

3. M. Sparks and C. J. Duthler, "Materials Damage Threshoids for Vacuum-Ultraviolet Optics," to be published.

4. M. Sparks and J. H. Wilson, "Enhanced Stimulated Raman Scattering and General Three-Boson Parametric Instabilities," Phys. Rev., in press.

5. H. C. Chow and M. Sparks, "Calculated Reflectance of Aluminum in the Vacuum Ultraviolet," J. Appl. Phys. 46, 1307 (1975).

6. M. Sparks, "Theory of Laser-Materials Damage by Enhanced Stimulated Raman Scattering," J. Appl. Phys. 46, 2134 (1975).

7. M. Sparks, "Theory of Laser Heating of Solids: Metals," J. Appl. Phys., in press.

8. D. L. Mills and A. A. Maradudin, "Surface Roughness and the Optical Properties of a Semi-Infinite Material: The Effect of a Dielectric Overlayer," Phys. Rev., in press.

9. J. A. Harrington, C. J. Duthler, F. W. Patten, and M. Hass, "Multiphonon Absorption of Alkali Halides and Quasiselection Rules," submitted to Phys. Rev. Lett.

10. M. Sparks, "Current Status of Electron-Avalanche-Breakdown Theories," paper presented at 7th NBS-ONR-ASTM Symposium on Damage in Laser Materials, Boulder, Colo., July 1975.

11. C. J. Duthler and M. Sparks, "Intensity Limits for Materials Damage in the Vacuum Ultraviolet," paper presented at 7th NBS-ONR-ASTM Symposium on Damage in Laser Materials, Boulder, Colo., July 1975.